#345 SPECIAL ISSUE
NOVEMBER 2018

ICES REPORT ON OCEAN CLIMATE 2017

Prepared by the Working Group on Oceanic Hydrography

ICES COOPERATIVE RESEARCH REPORT

RAPPORT
DES RECHERCHES
COLLECTIVES

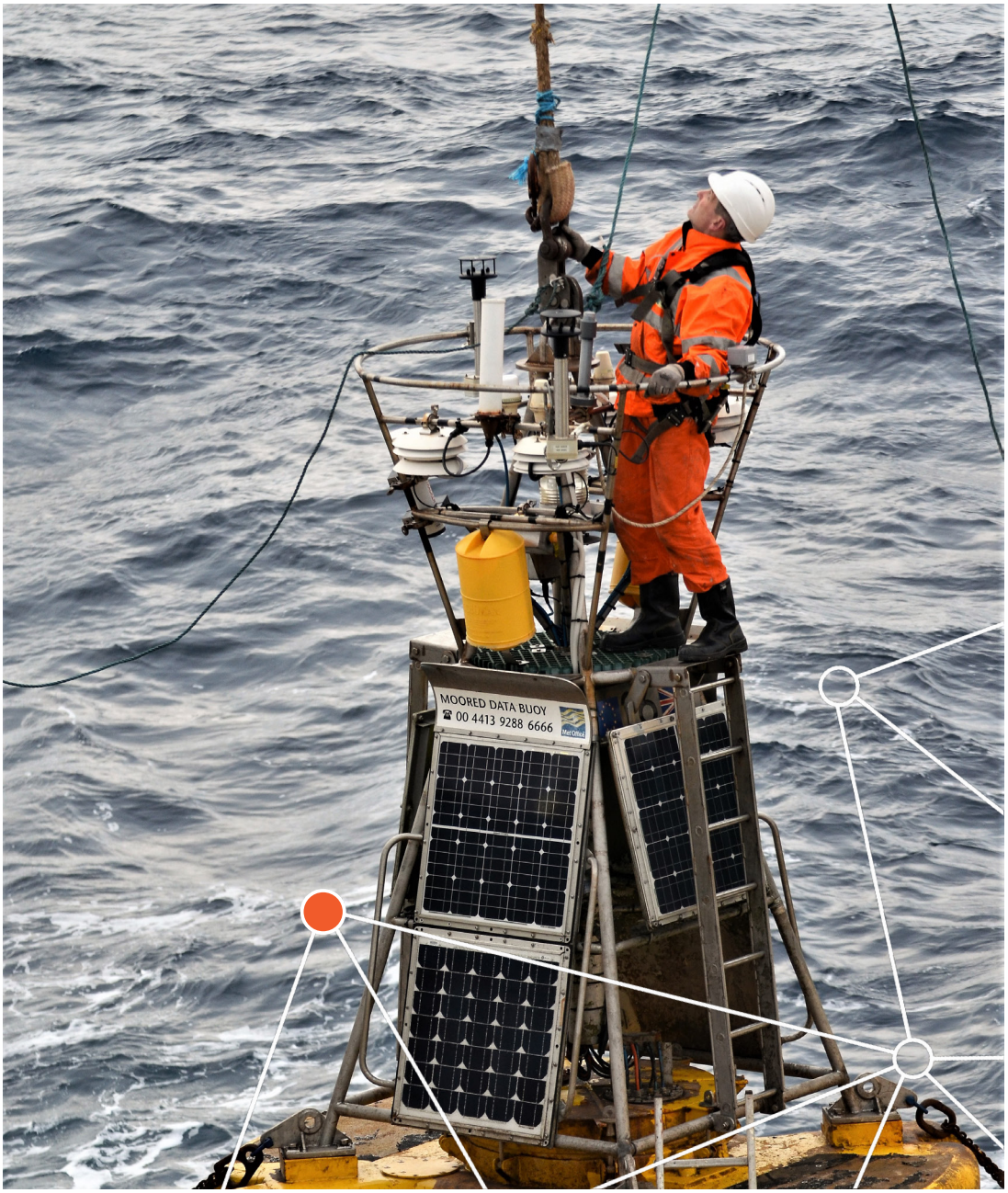

ICES INTERNATIONAL COUNCIL FOR THE EXPLORATION OF THE SEA
CIEM CONSEIL INTERNATIONAL POUR L'EXPLORATION DE LA MER

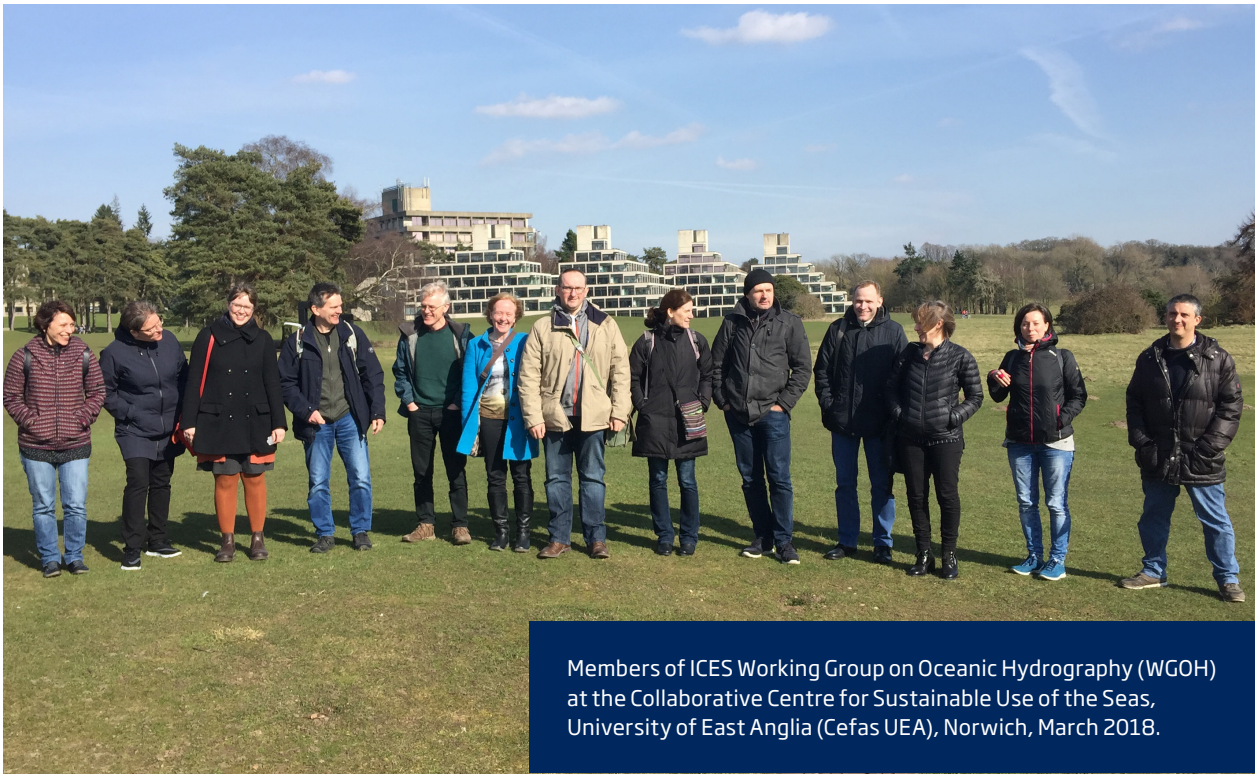

Members of ICES Working Group on Oceanic Hydrography (WGOH) at the Collaborative Centre for Sustainable Use of the Seas, University of East Anglia (Cefas UEA), Norwich, March 2018.

International Council for the Exploration of the Sea
Conseil International pour l'Exploration de la Mer
H. C. Andersens Boulevard 44–46
DK-1553 Copenhagen V
Denmark
Telephone (+45) 33 38 67 00
Telefax (+45) 33 93 42 15
www.ices.dk
info@ices.dk

Recommended format for purposes of citation:
González-Pola, C., Larsen, K. M. H., Fratantoni, P., and Beszczynska-Möller, A. (Eds). 2018. ICES Report on Ocean Climate 2017. ICES Cooperative Research Report No. 345. 119 pp. http://doi.org/10.17895/ices.pub.4625

Series Editor: Emory D. Anderson

Cover image: Weather buoy M6 – preparation for deployment. Tomasz Szumski, Marine Institute, Ireland.

DOI: http://doi.org/10.17895/ices.pub.4625
ISBN 978-87-7482-221-9
ISSN 2707-7144

ICES COOPERATIVE RESEARCH REPORT
RAPPORT DES RECHERCHES COLLECTIVES

ICES REPORT ON OCEAN CLIMATE 2017

#345 SPECIAL ISSUE
NOVEMBER 2018

Prepared by the Working Group on Oceanic Hydrography

A SPECIAL ACKNOWLEDGEMENT TO SARAH HUGHES

The members of ICES Working Group on Oceanic Hydrography (WGOH) would like to dedicate this report to our colleague and friend Sarah Hughes, from Marine Scotland Science in Aberdeen, who has left oceanography to pursue other professional goals.

Sarah joined WGOH in 2003 and immediately became an integral member of the working group. In her first year, she assumed a leading role as editor of the group's main product, ICES Report on Ocean Climate (IROC), then in its fourth edition. Sarah attended almost every annual meeting, served as editor for 13 of the 15 IROCs released during her tenure, co-organized the decadal variability symposium in Santander in 2011, and acted as co-chair of the group from 2015 to 2017. Sarah advocated strongly for the adoption of common procedures aimed at standardizing the collection of time-series provided by a long list of international contributors, shaping the continuous improvement and evolution of the IROC. Sarah's positive contributions are clearly reflected in the layout and quality of the present IROC.

Within WGOH, Sarah was known for the energy she put into encouraging partnership and collaboration among the group's diverse membership, enthusiastically promoting and inspiring fruitful discussions and supporting WGOHs engagement with the broader international community. We acknowledge Sarah`s commitment to WGOH and promise to build on her legacy in the future evolution of the group. We wish her the best in her new professional endeavors.

Drawing samples for salinity analysis on RRS Discovery.
Photo: Penny Holliday, National Oceanography Centre, UK.

1. INTRODUCTION

Long time-series of ocean properties are rare in the surface ocean and even more uncommon in the deep ocean. The North Atlantic region is unique in having a relatively large number of locations where oceanographic data have been collected repeatedly for multiple years or decades; the longest records extend back more than a century.

ICES Report on Ocean Climate (IROC) combines decades of ocean observations across the North Atlantic ICES region to describe the current status of sea temperature and salinity and atmospheric conditions, as well as observed trends and recent variability.

The focus of the IROC is the observed variability of the upper ocean (the upper 1000 m). Information from the longest time-series is synthesized into an overview of changes across the ICES areas of the North Atlantic and Nordic seas. The introductory sections contain gridded fields constructed by optimal analysis of the Argo float data distributed by the Coriolis Data Centre in France. In addition to the temperature and salinity measurements, complementary datasets are included, such as sea level pressure (SLP), air temperature, and ice cover. An estimate of the Subpolar Gyre Index, included for the first time in 2016, is also provided. The main body of the report consists of short summaries of the variability in the intermediate and deep waters of the North Atlantic across regions.

The data presented here represent an accumulation of knowledge collected by many individuals and institutions over decades of observations. A list of contacts for each dataset is provided at the end of the report, including email addresses for the individuals who provided information and the data centres at which full archives are maintained. Much of the data included in this report are available to download at http://ocean.ices.dk/iroc, where additional data may also be found.

For a more detailed overview of a particular region, a full description of some of the datasets that are used to develop the time-series presented in this report can be found in the annual meeting reports of ICES Working Group on Oceanic Hydrography (WGOH) at http://www.ices.dk/community/groups/Pages/WGOH.aspx

ICES WGOH met 21–23 March 2018 in Norwich, UK to review oceanographic conditions in the North Atlantic in 2017. The joint analysis of the existing hydrographical time-series provided the following highlights.

1.1 HIGHLIGHTS FOR THE NORTH ATLANTIC 2017

- Accelerated freshening in the upper ocean, first observed in the eastern subpolar North Atlantic in 2016, persisted into 2017, and expanded to include the southern Norwegian Sea. Notably, the freshening was accompanied by above-average temperatures.
- Air and sea surface temperatures were higher than normal across most of the region, with the exception of the central subpolar North Atlantic and Baltic Sea.
- Ice cover in the Barents Sea remained very low.
- Following a five-year period of increasing heat content, the upper layer of the Norwegian Sea reached a new record-high value.
- The gradual freshening of upper waters (100–400 m), first observed in the northeast Subtropical Gyre, is now widespread, having reached western Iberian waters and the Canaries.
- In the western North Atlantic, ocean temperatures were near normal or slightly cooler than normal in the north (the Labrador and Newfoundland shelves) and warmer than normal in the south (along the Northeast US shelf).

1.2 HIGHLIGHTS FOR THE NORTH ATLANTIC ATMOSPHERE IN WINTER 2016/2017

- The winter North Atlantic Oscillation (NAO) index was positive (+1.47) for the fourth consecutive winter, the first such positive run since 1992–1995.
- The anomaly in sea level pressure (SLP) did not resemble a typical NAO pattern. Instead, the high-pressure anomaly shifted east, centred over the North Sea, and the low-pressure anomaly over the Arctic was split to the southeast and southwest of Iceland and the Nordic seas.
- Winds were more northerly over the Labrador Sea and southerly across the Northeast Atlantic and into the Nordic seas.
- Winter air temperatures were near average (1981–2010) over the Subpolar Gyre and central North Atlantic, whereas temperatures were generally higher than normal elsewhere around the margins, particularly over the northern Barents Sea.

1.3 BEYOND 2017: INITIAL ASSESSMENT OF THE NORTH ATLANTIC ATMOSPHERE IN WINTER 2017/2018

An initial assessment of the North Atlantic atmosphere at the end of the IROC year is included. Atmospheric conditions during winter are a determining factor of oceanic conditions for the following year; therefore, this outlook offers some predictive capability for spring–autumn 2018.

The SLP pattern for December 2017–March 2018 suggests a weak, near-neutral NAO index winter. This ends the run of strong positive NAO winters with what was almost certainly the weakest NAO winter (either positive or negative) this decade.

Air temperatures were cold over Iberia, Norway, and the Subpolar Gyre, including over the Irminger Sea and Iceland Basin. Warmer-than-average conditions were evident southwest of the Subpolar Gyre and in the Greenland Sea. Experimental forecasts from the US (over seasonal periods) and the UK (over 1–5 years) suggest a warmer outlook for the Subpolar Gyre region more typical of the long-term average (1981–2010).

Rough sea seen from the bridge of RV Celtic Explorer, Rockall survey 2017. Photo: Tomasz Szumski, Marine Institute, Ireland.

NORTH ATLANTIC UPPER OCEAN TEMPERATURE: OVERVIEW

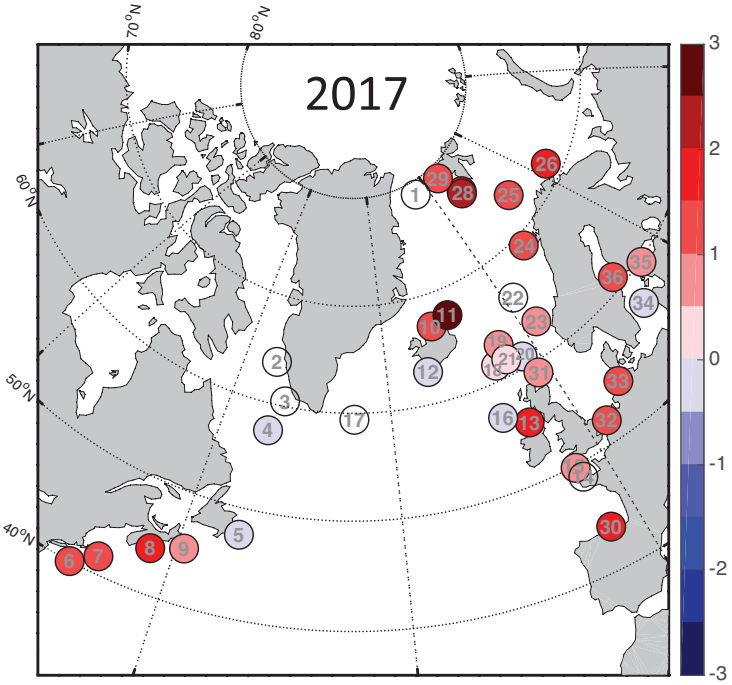

FIGURE 1.
Upper ocean temperature anomalies at selected locations across the North Atlantic. The anomalies are normalized with respect to the standard deviation (s.d.; e.g. a value of +2 indicates 2 s.d. above normal). Upper panel: map of conditions in 2017. Lower panels: time-series of normalized anomalies at each of the selected stations. Colour intervals 0.5 s.d.; reds = positive/warm; blues = negative/cool. More details can be found in Section 4.

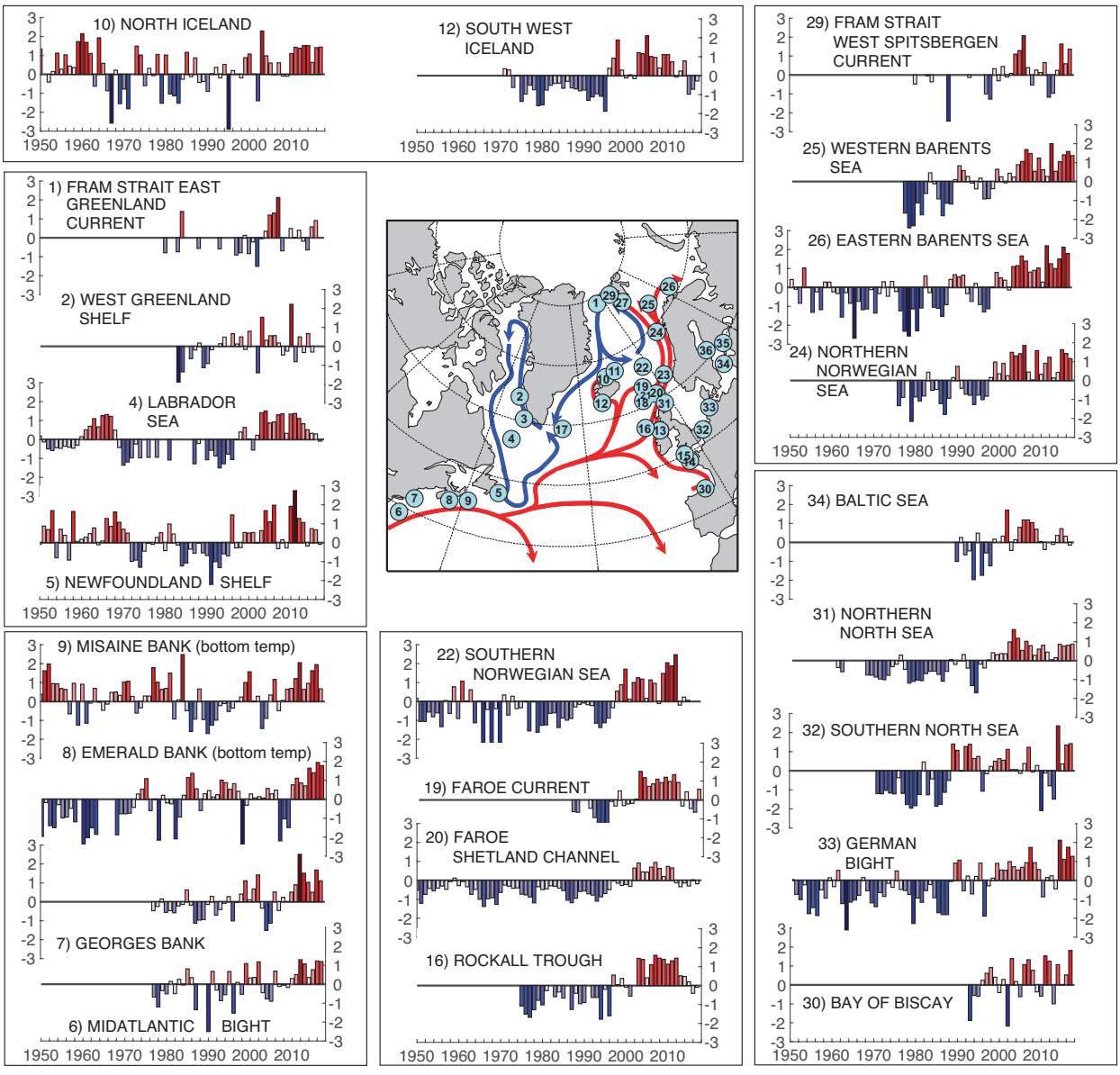

NORTH ATLANTIC UPPER OCEAN SALINITY: OVERVIEW

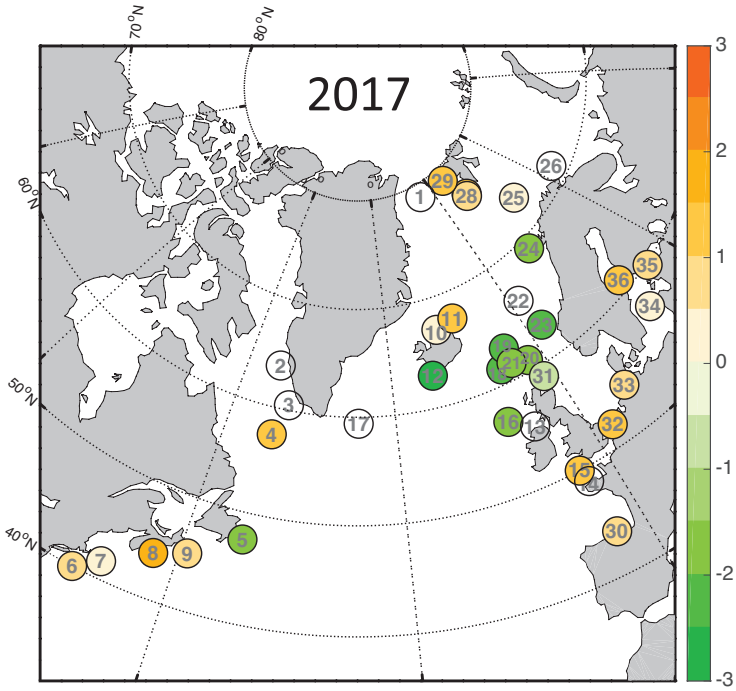

FIGURE 2.
Upper ocean salinity anomalies at selected locations across the North Atlantic. The anomalies are calculated relative to a long-term mean and normalized with respect to the s.d. (e.g. a value of +2 indicates 2 s.d. above normal). Upper panel: map of conditions in 2017. Lower panels: time-series of normalized anomalies at each of the selected stations. Colour intervals 0.5 s.d.; oranges = positive/saline; greens = negative/fresh. More details can be found in Section 4.

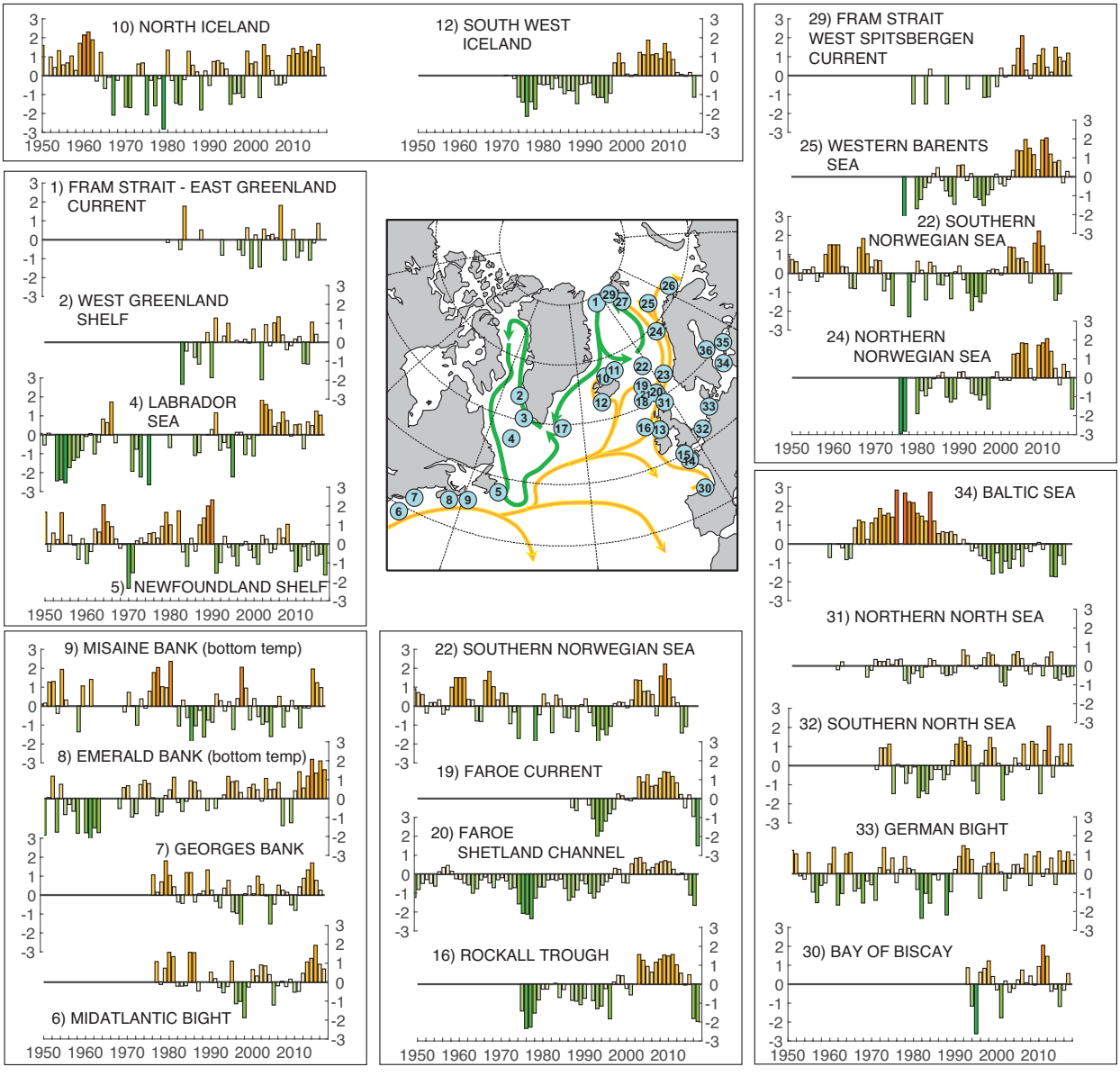

Hydrographic works and mooring service from the most recent Scotia cruise. Photo: Helen Smith, Marine Scotland Science (MSS, Aberdeen), UK.

2. SUMMARY OF UPPER OCEAN CONDITIONS IN 2017

This section summarizes conditions in the upper layers of the North Atlantic during 2017 using data from (i) a selected set of sustained observations, (ii) gridded sea surface temperature (SST) data, and (iii) gridded vertical profiles of temperature and salinity from Argo floats.

2.1 *IN SITU* STATIONS AND SECTIONS

Where *in situ* section and station data are presented in the summary tables and figures, normalized anomalies have been provided to allow better comparison of trends across regions (Figures 1–3; Tables 1 and 2). The anomalies have been normalized by dividing the values by the s.d. of the data during 1981–2010 (or the closest period available). Therefore, a value of +2 represents data (temperature or salinity) measuring 2 s.d. higher than normal.

"Sustained observations" or "time-series" are regular measurements of ocean temperature and salinity made over a long period (10-100 years). Most measurements are made 1-4 times a year, but some are made more frequently.

"Anomalies" are the mathematical differences between each individual measurement and the average value of temperature, salinity, or other variables at each location. Positive anomalies in temperature and salinity imply warm or saline conditions; negative anomalies imply cool or fresh conditions.

"Seasonal cycle" describes the short-term changes at the surface of the ocean brought about by the passing of the seasons; the ocean surface is cold in winter and warms through spring and summer. Temperature and salinity changes caused by the seasonal cycle are usually much greater than the prolonged year-to-year changes we describe here.

	2008	2009	2010	2011	2012	2013	2014	2015	2016	2017
1	-0.69		0.49	0.01	0.40	-0.18	-0.64	0.58	0.91	
2	-0.46	-0.25	2.22	-0.81	0.50	-0.33	0.67	-0.30		
3	0.06	0.70	1.15	0.57	1.28	0.18	0.83	-0.47	-0.41	
4	1.36	0.33	1.34	1.38	1.11	0.83	0.52	0.33	0.29	-0.09
5	0.15	-0.28	1.92	2.75	1.28	1.07	-0.18	0.74	0.68	-0.08
6	-0.05	-0.17	0.30	0.51	2.17	1.07	0.36	0.77	1.23	1.20
7	0.24	0.00	0.51	0.90	2.51	1.51	1.03	0.51	1.68	1.11
8	-1.04	-1.50	0.76	1.12	0.87	0.71	1.64	1.40	1.95	1.78
9	0.06	0.65	0.69	1.20	2.05	0.64	0.96	1.63	1.95	0.67
10	-0.09	-0.10	1.10	1.43	1.38	1.52	1.52	0.63	1.41	1.44
11	0.64	0.46	0.30	1.03	0.64	0.79	1.89	0.89	1.15	2.62
12	0.40	1.12	1.11	0.73	-0.07	0.24	0.77	-0.98	-0.72	-0.28
13		1.45	0.40	1.04	0.62	0.42	1.72	0.71	1.59	1.96
14	0.11	-0.80	-1.95	0.06	0.38	-0.83	1.58	1.04	0.50	
15	0.40	-0.66	0.02	0.05	0.59	-0.26	0.70	0.25	0.19	0.63
16	1.45	1.38	1.13	1.31	1.45	0.52	0.48	0.20	-0.41	-0.09
17	-0.56	-0.73	0.55	0.69	-0.29		-0.01	-0.43	-0.75	
18	1.30	1.41	0.73	1.28	-0.03	0.04	0.55	0.13	-0.04	0.21
19	0.92	1.20	0.98	1.34	0.93	-0.32	0.43	-0.45	-0.65	0.57
20	0.63	0.20	0.74	0.66	-0.13	-0.34	-0.14	-0.30	0.03	-0.18
21	0.76	0.92	1.36	0.92	0.34	0.45	0.55	0.17	-0.13	0.07
22	-0.11	1.48	2.05	1.87	2.47	-0.19	0.23	0.06		
23	0.19	1.71	0.86	1.12	0.44	0.55	0.33	0.52	0.38	0.91
24	0.03	1.58	0.33	0.91	1.23	0.14	0.43	1.63	1.43	1.16
25	0.54	1.24	0.62	0.27	2.00	0.54	1.05	1.41	1.59	1.37
26	0.81	0.90	1.02	0.28	2.20	1.25	1.00	1.50	2.12	1.79
27	-0.23	0.55	0.40	1.02	0.90	0.03	1.12	0.95	1.42	1.50
28	0.22	0.53	-0.01		0.60	-0.23	1.17		0.88	2.35
29	1.28	1.53	1.49	1.66	1.07	1.14	1.53	1.98	0.64	1.36
30	0.77	-0.37	-0.60	1.53	1.25	-1.00	1.07	0.02	0.53	1.82
31	0.28	0.61	0.81	0.45	0.04	0.15	0.86	0.77	0.81	0.87
32	-0.07	0.28	-2.08	-0.12	-0.79	-1.49	2.35	0.36	1.35	1.42
33	0.94	0.57	-0.87	0.15	0.24	-0.45	2.12	1.11	1.75	1.27
34	1.05	0.70	0.05	-0.38		-0.11	0.37	0.72	0.33	-0.14
35	1.07	1.48	0.38	-0.36	0.74	1.08	0.07	0.29	1.07	0.99
36	1.29	1.36	-0.53	-1.16	-0.17	0.02	1.46	1.42	1.60	1.16

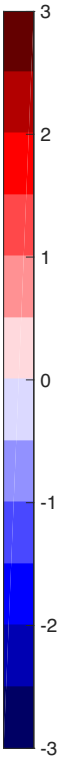

	2008	2009	2010	2011	2012	2013	2014	2015	2016	2017
1	-1.08		0.54	-0.93	-0.60		-1.08	-0.17	0.86	
2	-0.40	-0.18	0.17	0.31	-1.12	-1.15	1.07	0.42		
3	0.11	1.24	0.07	1.20	-0.14	0.80	-0.47	0.15	-1.28	
4	1.20	0.75	-0.07	0.53	0.56	-0.74	0.68	0.49	1.25	1.04
5	1.04	-0.37	-1.46	-1.17	-0.13	-0.85	0.13	-0.62	-0.54	-1.64
6	-0.23	0.16	-0.53	-0.49	0.47	1.07	1.26	1.95	0.95	0.70
7	0.26	0.15	-0.52	-0.81	0.44	0.89	1.33	1.70	0.78	0.26
8		-1.28	0.42	1.42	0.56	1.19	2.07	1.35	1.99	1.52
9	-1.11	-0.27	0.29	-0.13	-1.16	-0.09	-0.11	1.96	1.24	0.98
10	-0.39	1.07	1.43	1.16	1.54	1.24	1.34	1.01	1.65	0.44
11	1.07	0.66	0.99	1.13	1.55	1.22	-0.04	0.90	1.06	1.01
12	0.90	1.69	1.24	0.85	0.17	0.06	-0.04	0.17	-1.14	-3.22
13										
14	-0.00	-0.02	-0.11	0.87	1.17	0.11	-0.54	0.46	0.38	
15	0.39	0.75	0.46	1.31	0.76	0.79	0.46	1.43	0.85	1.37
16	1.32	1.54	1.49	1.57	1.02	0.58	-0.05	0.50	-1.82	-1.97
17	0.00	0.13	1.39	0.85	0.46		0.35	0.71	0.49	
18	1.22	1.61	1.53	1.41	0.31	0.46	-0.08	0.32	-1.53	-2.28
19	1.08	1.43	1.39	1.17	0.83	0.22	-0.49	0.20	-0.95	-2.49
20	0.54	0.65	0.71	0.66	0.26	-0.04	0.05	-0.29	-1.11	-1.65
21	0.58	1.07	1.16	0.74	0.64	0.16	-0.34	-0.36	-1.16	-1.96
22	-0.51	1.59	2.23	1.45	0.48	0.18	-1.42	-1.08		
23	0.51	2.01	1.82	1.53	0.69	0.30	-0.63	0.17	-0.97	-2.37
24	-0.12	1.73	1.85	2.07	1.40	0.49	-0.36	0.71	0.34	-1.65
25	2.61	0.86	4.29	4.58	2.70	1.73	1.92	-0.60	0.66	0.03
26	0.16	0.52	0.88	1.60	0.34	-0.02	0.16	-0.74		
27	0.33	0.64	0.95	1.74	1.71	0.98	1.57	0.67	1.02	1.02
28	0.92	0.71	0.82		1.45	1.00	1.74		1.21	0.95
29	-0.16	0.63	1.08	1.42	0.45	0.18	1.50	0.97	0.76	1.18
30	0.43	-0.04	0.93	2.05	1.47	-0.38	-0.26	-1.18	-0.32	0.56
31	0.14	0.03	-0.53	0.47	0.74	-0.65	-0.75	-0.43	-0.58	-0.55
32	1.27	1.13	-1.47	0.80	2.07	-0.60	0.47	1.13	0.13	1.13
33	0.93	1.17	-0.15	0.25	0.82	-0.58	1.21	0.67	1.15	0.70
34	-0.40	-0.08	0.08	-0.29	0.03	-1.71	-1.74	-0.61	-1.08	0.06
35	-0.04	0.87	0.78	-0.85	-1.12	0.57	0.20	-0.27	-0.04	0.76
36	0.33	0.64	2.17	2.18	1.03	0.40	1.01	-0.65	-0.20	1.33

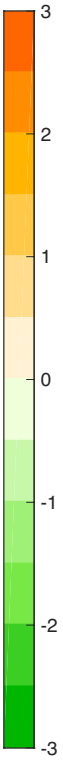

TABLES 1 AND 2.
Changes in temperature (Table 1, top) and salinity (Table 2, bottom) at selected stations in the North Atlantic region during the past decade, 2007–2017. The index numbers on the left can be used to cross-reference each point with information in Figures 1 and 2 and in Table 3. Unless specified, these are upper-layer anomalies. The anomalies are normalized with respect to the s.d. (e.g. a value of +2 indicates that the data observation of temperature or salinity for that year was 2 s.d. above normal). Blank boxes indicate that data were unavailable for a particular year at the time of publication. Note that no salinity data are available for Station 13. Colour intervals 0.5 s.d.; red = warm; blue = cold; orange = saline; green = fresh.

Index	Description	Section	Measurement depth	Reference period	Lat.	Lon.	Mean T	S.D.	Mean S	S.D.
1	Fram Strait - East Greenland Current	4.21	50-500 m	1983-2010	78.83	-6.00	0.69	0.57	34.650	0.135
2	Fylla section - Station 4 - Greenland Shelf	4.1	0-50 m	1983-2010	63.88	-53.37	2.64	1.10	33.162	0.392
3	Cape Desolation section - Station 3 - Greenland Shelf	4.1	75-200 m	1983-2010	60.47	-50.00	5.72	0.66	34.923	0.062
4	Central Labrador Sea	4.2	15-50 m	1981-2010	57.07	-50.92	4.68	0.69	34.635	0.176
5	Station 27 - Newfoundland Shelf temperature - Canada	4.3	0-175 m	1981-2010	47.55	-52.59	0.33	0.39	31.946	0.166
6	NE US continental shelf - Northern Mid Atlantic Bight	4.5	1-30 m	1981-2010	40.00	-71.00	11.36	0.94	32.710	0.430
7	NE US continental shelf - Northwest Georges Bank	4.5	1-30 m	1981-2010	41.50	-68.30	10.00	0.79	32.580	0.270
8	Emerald Basin - Central Scotian Shelf - Canada	4.4	250 m (near bottom)	1981-2010	44.00	-63.00		0.83		0.151
9	Misaine Bank - Northeast Scotian Shelf - Canada	4.4	100 m (near bottom)	1981-2010	45.00	-59.00		0.63		0.134
10	Siglunes Station 2-4 - North Iceland - North Icelandic Irminger Current - spring	4.6	50-150 m	1981-2010	67.00	-18.00	3.41	0.98	34.859	0.108
11	Langanes Station 2-6 - Northeast Iceland - East Icelandic Current - spring	4.6	0-50 m	1981-2010	67.50	-13.50	1.22	0.61	34.729	0.067
12	Selvogsbanki Station 5 - Southwest Iceland - Irminger Current - spring	4.6	0-200 m	1981-2010	63.00	-21.47	7.88	0.47	35.187	0.049
13	Point 33 - Astan	4.10	5m	1998-2010	48.78	-3.94	12.79	0.34	35.206	0.112
14	Western Channel Observatory (WCO) -E1 - UK	4.10	0-40 m	1981-2010	50.03	-4.37	12.43	0.93	35.200	0.100
15	Malin Head Weather Station	4.11	surface	1981-2010	55.37	-7.34	10.25	0.57		
16	Ellett Line - Rockall Trough - UK (section average)	4.12	30-800 m	1981-2010	56.75	-11.00	9.35	0.28	35.351	0.036
17	Central Irminger Sea subpolar-mode water	4.15	200-400 m	1991-2010	59.40	-36.80	4.35	0.53	34.900	0.031
18	Faroe Bank Channel - West Faroe Islands	4.16	Upper Layer High Salinity Core	1988-2010	61.40	-8.30	8.80	0.36	35.302	0.043
19	Faroe Current - North Faroe Islands (modified North Atlantic water)	4.16	Upper Layer High Salinity Core	1987-2010	63.00	-6.00	8.11	0.39	35.249	0.043
20	Faroe Shetland Channel - Shetland Shelf (North Atlantic water)	4.16	Upper Layer High Salinity Core	1981-2010	61.00	-3.00	9.95	0.47	35.398	0.051
21	Faroe Shetland Channel - Faroe Shelf (modified North Atlantic water)	4.16	Upper Layer High Salinity Core	1981-2010	61.50	-6.00	8.32	0.54	35.256	0.055
22	Ocean Weather Station Mike	4.19	50 m	1981-2010	66.00	2.00	7.71	0.44	35.176	0.036
23	Southern Norwegian Sea - Svinøy section - Atlantic water	4.19	50-200 m	1981-2010	63.00	3.00	8.04	0.39	35.234	0.039
24	Central Norwegian Sea - Gimsøy section - Atlantic water	4.19	50-200 m	1981-2010	69.00	12.00	6.89	0.34	35.154	0.031
25	Fugløya - Bear Island section - Western Barents Sea - Atlantic inflow	4.20	50-200m	1981-2010	73.00	20.00	5.55	0.46	35.078	0.035
26	Kola section - Eastern Barents Sea	4.20	50-200m	1981-2010	71.50	33.50	4.22	0.52	34.771	0.056
27	Greenland Sea section - West of Spitsbergen 76.5°N	4.20	0-200 m	1996-2010	76.50	10.50	3.19	0.61	35.058	0.043
28	Northern Norwegian Sea - Sørkapp section - Atlantic water	4.19	50-200 m	1981-2010	76.33	10.00	4.08	0.60	35.073	0.038
29	Fram Strait - West Spitsbergen Current	4.21	50-500 m	1983-2010	78.83	7.00	3.11	0.69	35.027	0.038
30	Santander Station 6 (shelf break) - Bay of Biscay - Spain	4.7	0-30 m	1993-2010	43.71	-3.78	15.74	0.32	35.460	0.160
31	Fair Isle Current water (waters entering North Sea from Atlantic)	4.17	0-100 m	1981-2010	59.00	-2.00	9.93	0.61	34.874	0.132
32	Section average - Felixstowe - Rotterdam - 52°N	4.17	Surface	1981-2010	52.00	3.00		0.72		0.212
33	North Sea - Helgoland Roads	4.17	Surface	1981-2010	54.18	7.90	10.26	0.75	32.096	0.568
34	Baltic Proper - east of Gotland - Baltic Sea	4.18	Surface T Surface S	1990-2010 1987-2010	57.50	19.50	9.27	1.03	7.172	0.196
35	Baltic - LL7 - Baltic Sea	4.18	70 m	1991-2010	59.51	24.50	3.97	0.73	7.961	0.666
36	Baltic - SR5 - Baltic Sea	4.18	110 m	1991-2010	61.05	19.35	3.27	0.58	6.428	0.141

TABLE 3.
Details of the datasets included in Figures 1.0.1 and 1.0.2 and in Tables 1 and 2. Blank boxes indicate that no information was available for the area at the time of publication. T = temperature, S = salinity. Some data are calculated from an average of more than one station; in such cases, the latitudes and longitudes presented here represent a nominal midpoint along that section.

2.2 SEA SURFACE TEMPERATURE

For around 40 years, satellites have been recording SSTs, and this information has led to the creation of gridded products. Figure 3 shows seasonal SST anomalies for 2017 extracted from the Optimum Interpolation SST dataset version 2 (OISST.v2) provided by NOAA–CIRES Climate Diagnostics Center in the USA. The data may be less reliable at higher latitudes where *in situ* data are sparse and cloud cover hinders satellite data. Regions with ice cover for > 50% of the averaging period appear blank.

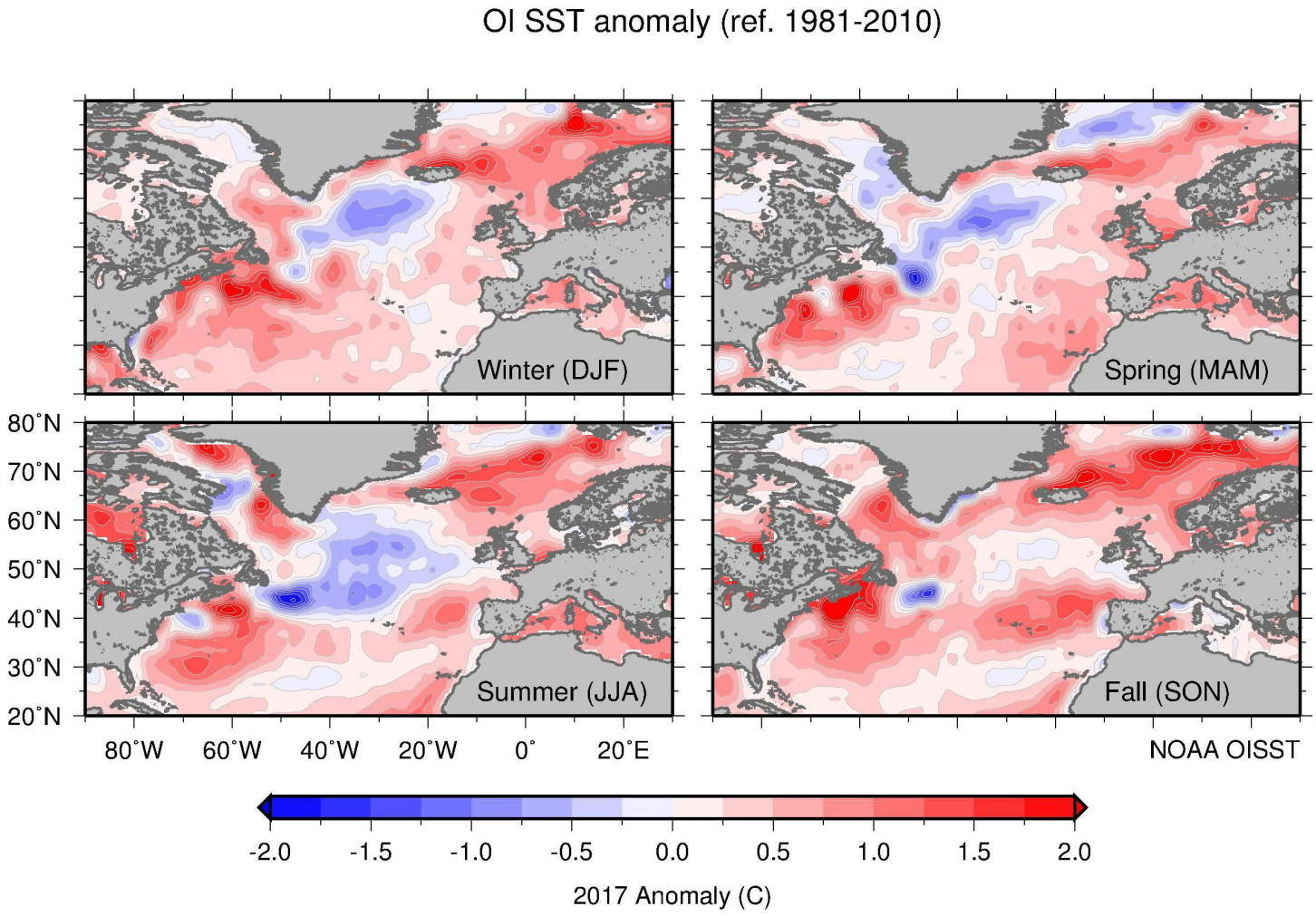

FIGURE 3.
Maps of seasonal sea surface temperature anomalies (°C) over the North Atlantic for 2017 from the NOAA OISST.v2 dataset provided by NOAA–CIRES Climate Diagnostics Center, USA. The data are produced on a 1° grid from a combination of satellite and *in situ* temperature data. The colour-coded temperature scale is the same in all panels, and the anomaly is calculated with respect to mean conditions for 1981–2010.

2.3 ARGO GRIDDED TEMPERATURE AND SALINITY FIELDS

N. Kolodziejczyk, G. Reverdin, and D. Desbruyères

The Argo[1] network of profiling floats has been set up to monitor large-scale global ocean variability. Argo data are transmitted in real-time and made available by the two Global Data Assembly Centres (Argo GDACs are located in Brest, France and Monterey, USA). Delayed-mode data undergo expert calibration processes and are delivered later. In the North Atlantic, temperature and salinity conditions of the upper 2000 m have been adequately described since 2002. This dataset is thus suitable for an overview of oceanographic conditions in the North Atlantic basin and complements the data at the repeat stations and sections collected mostly at the periphery of the basin by partners of the ICES Working Group on Ocean Hydrography (WGOH).

In subsection 2.3.1, temperature and salinity anomalies are calculated using World Ocean Atlas 2005 climatology (WOA05[2]), which mainly reflects mean oceanic conditions of the pre-Argo period, i.e. before the 2000s. Thus, temperature and salinity anomalies reflect change compared with this period.

2.3.1 ISAS: Gridded temperature and salinity fields

Temperature and salinity gridded fields are estimated on a regular half-degree grid using the *In Situ* Analysis System (ISAS; Gaillard *et al.*, 2016). The dataset used to generate ISAS gridded fields is available to download from Coriolis Argo GDAC[3]. Coriolis assembles many types of data transmitted in real-time, merging the Argo dataset with GTS data, such as mooring data, marine animals, CTDs. However, the Argo dataset remains the main contributor in the open ocean.

For the optimal interpolation procedure, the *in situ* temperature and salinity profiles are vertically interpolated on 152 standard levels between the surface and 2000 m depth. Horizontal mapping to produce gridded fields is performed at each standard level independently. The mapping method is based on optimal estimation principles and includes horizontal smoothing through specified covariance scales. The reference state was computed as the mean of a 2005–2012 analysis (using ISAS13; Gaillard *et al.*, 2016), and the *a priori* variances were computed from the same dataset.

ISAS15 constitutes the highest quality delayed mode products, including only *in situ* data that have been processed and to which quality-control protocols, tailored to the ISAS15 product, have been applied. The most recent years of the analysed series, i.e. 2016–2017, use the near real-time dataset prepared by Coriolis at the end of each month from real-time data. Over this period, data are interpolated using ISAS v6 including only real-time mode data (i.e. only from automatic QC processing). Over time, delayed-mode data are progressively incorporated, replacing the near real-time data from previous years.

2.3.2 Surface layers

Seasonal cycle

During winter 2016/2017, near-surface waters (10 m depth) in the middle of Subpolar Gyre (north of 45°N) and in the Labrador Sea were anomalously colder and fresher than the WOA05 pre-Argo (before 2002) climatological winter (Figure 4). South of 40°N, near-surface waters were extremely warm and salty in the western basin, indicating a northward shift of the Gulf Stream. A warmer-than-normal Subtropical Gyre (south of 45°N) was also observed.

The Subpolar Gyre cold anomaly persisted, but decreased throughout the year in 2017 (Figure 4, upper panel). However, during summer 2017, the Labrador and Greenland basins were warm compared with pre-Argo climatological conditions. Notably fresh salinity anomalies (Figure 4, lower panel) were reported along the northeastern and northwestern Greenland coasts in each of the four seasons, while the sea surface was saltier in the Labrador Sea along the Canadian coast and in the Greenland Sea north of Iceland.

In the Irminger Sea, winter 2017 was the coldest over the 2002–2017 period (thick red line; Figure 5, Irminger Sea) where near-surface temperatures were well below the pre-Argo seasonal climatology (thick black line). Near-surface temperatures in the Labrador Sea (Figure 5, Labrador Sea) exhibited extreme cooling. These conditions reversed the general trend of warmer conditions that have been observed over the last decade in the Irminger and Labrador seas. Near-surface temperatures were also anomalously cold during summer, cooler than any temperature measured since 2002.

1) http://www.argo.ucsd.edu
2) https://www.nodc.noaa.gov/OC5/SELECT/woaselect/woaselect.html
3) http://www.coriolis.eu.org/

In contrast, the seasonal cycle of near-surface temperatures in the Gulf Stream region (Figure 5, Gulf Stream) confirms the warm shift observed in recent years. Both winter and summer temperatures exhibited maximum values, more than 1°C above the pre-Argo period. Off the European coast in the eastern Atlantic (Figure 5, Eastern Atl.), seasonal near-surface temperatures were normal relative to the period 2002–2017 and not significantly different from the pre-Argo period.

Mixed layer depth

Atmospheric cooling during winter and freshwater fluxes drive buoyancy loss (increasing density) in the ocean surface layers and lead to winter convection in North Atlantic. The mixed-layer depth is a useful indicator of the intensity of winter convection in the North Atlantic, providing a measure of how deep vertical overturning penetrates into the water column. To allow comparison across all areas over the past decade, a definition for the mixed-layer depth is adopted based on the level at which density changes by more than 0.03 kg m^{-3} with respect to the 10-m depth. The criterion on density is more accurate because it is sensitive to the stratification of both temperature and salinity. March is selected as the common period for maximum mixed-layer depth before the onset of restratification in spring. Of course, this is not exact as the timing may vary from year to year at a single location and might not occur at the same time over the whole basin (between February and March in the North Atlantic).

In the northern basin extending from the Labrador Sea to the Irminger Sea, deep mixed layers (> 2000 m) were observed across a large area in winter 2017. Despite the exceptional winters of 2015 and 2016, the areal extent of deep mixed layers in 2017 was the third largest in the time-series (Figure 7). This increased area was a result of deeper mixed layers in the Irminger Basin during the 2015, 2016, and 2017 winters compared with 2013 and 2014. The deep mixed layers may reflect strong winter convection in both Labrador and Irminger basins.

In the eastern basin off Scotland and Ireland, shallower mixed layers (< 800 m) were observed in March 2017, contrasting to the deeper mixed layers (> 800 m) observed during 2012–2016. In the Bay of Biscay, the 2017 March mixed-layer depth remained shallower (< 600 m) than the exceptional winter 2014 and 2015 (> 600 m).

Interannual variability

In 2017, the most salient feature observed in the annual near-surface temperature anomaly maps is the persistence of a coherent cold anomaly over the Subpolar Gyre (Figure 8, upper). The subpolar cold anomaly increased in size and intensity during 2013–2015, with anomalies exceeding 2°C.

However, since 2016, this cold anomaly has diminished in intensity (1°C) and extension. In contrast, persistent warm anomalies (> 2°C) have been observed since 2012 in the Nordic seas (> 65°N) encompassing the Greenland Sea and along the eastern Greenland coast (Figure 8, upper). In the Subtropical Gyre, surface conditions remained warm in 2017, especially in the Gulf Stream region, where a northward shift of the subtropical front may explain the extreme warm anomalies (> 3°C).

Over the 2012–2017 period, the persistent large-scale, cold, near-surface temperature anomaly in the Subpolar Gyre was accompanied by a fresh near-surface salinity anomaly (about 0.4). More precisely, a fresh anomaly (0.4) was observed in 2012 in the western Atlantic basin around 45°N and subsequently observed moving across the Supolar Gyre towards the eastern North Atlantic. The fresh anomaly entered the Irminger Basin in 2016 (Figure 8, lower).

A noticeable strong negative near-surface salinity anomaly has been observed since 2014 along the Greenland coast in both the Labrador and Irminger basins. The fresh near-surface water may be explained by an increase in the freshwater flux from the atmosphere, ocean, or Greenland ice sheet melt.

2.3.3 Deep layers

At 1000 m (Figure 9, upper), the Labrador and Irminger seas in the Subpolar Gyre were warmer than pre-Argo condition until 2014 (0.4°C). However, the warming tendency has not been observed (0°C anomaly) since 2015 and temperatures have returned to pre-Argo conditions. Since 2002, the temperature time-series, averaged between 800 and 1200 m depth, confirms the trend; deep temperatures in both the Labrador and Irminger basins increased from 2002 to 2011 (+0.4°C) and 2013 (+0.3°C), subsequently cooling in 2016 and 2017 (Figure 10, Irminger Sea and Labrador Sea). This reflects colder conditions in the Subpolar Gyre water column in both basins after 2012, relative to the 2002–2012 period. Note that in the eastern Subtropical Gyre between Iceland and Ireland, persistent cold conditions (and colder than the pre-Argo period) were observed between 2002 and 2017.

The deep waters of the Greenland Sea have warmed since 2002, reaching a maximum of 0.3°C in 2017 (Figure 9, upper and Figure 10, Greenland Sea). At 1000 m, the Mediterranean outflow water was warmer and saltier south of 40°N and off the Strait of Gibraltar. From 2012 to 2017, the salty (> 0.04 pss) and warm anomaly increase seems to have extended westward into the subtropical basin (Figure 9). In contrast, a persistent cold and fresh anomaly between Iceland and Rockall Trough intensified in 2016 and 2017 (Figure 9).

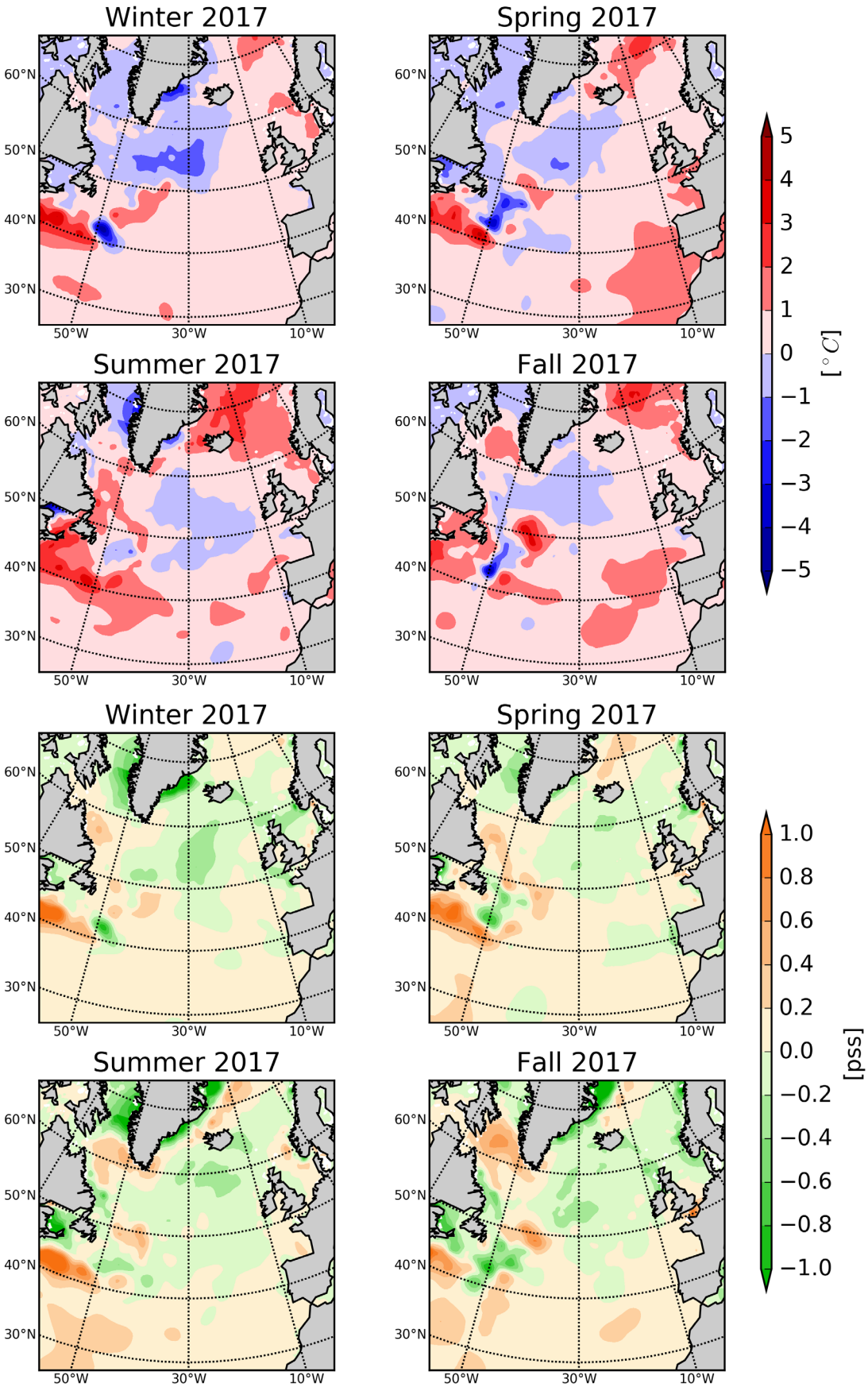

FIGURE 4.
Maps of 2017 seasonal temperature (upper) and salinity (lower) anomalies at 10 m depth in the North Atlantic. Anomalies are the differences between the ISAS monthly mean values and the reference climatology, World Ocean Atlas 05 (WOA5). The colour-coded scale is the same in all panels. Data from Coriolis, ISAS monthly analysis of Argo data.

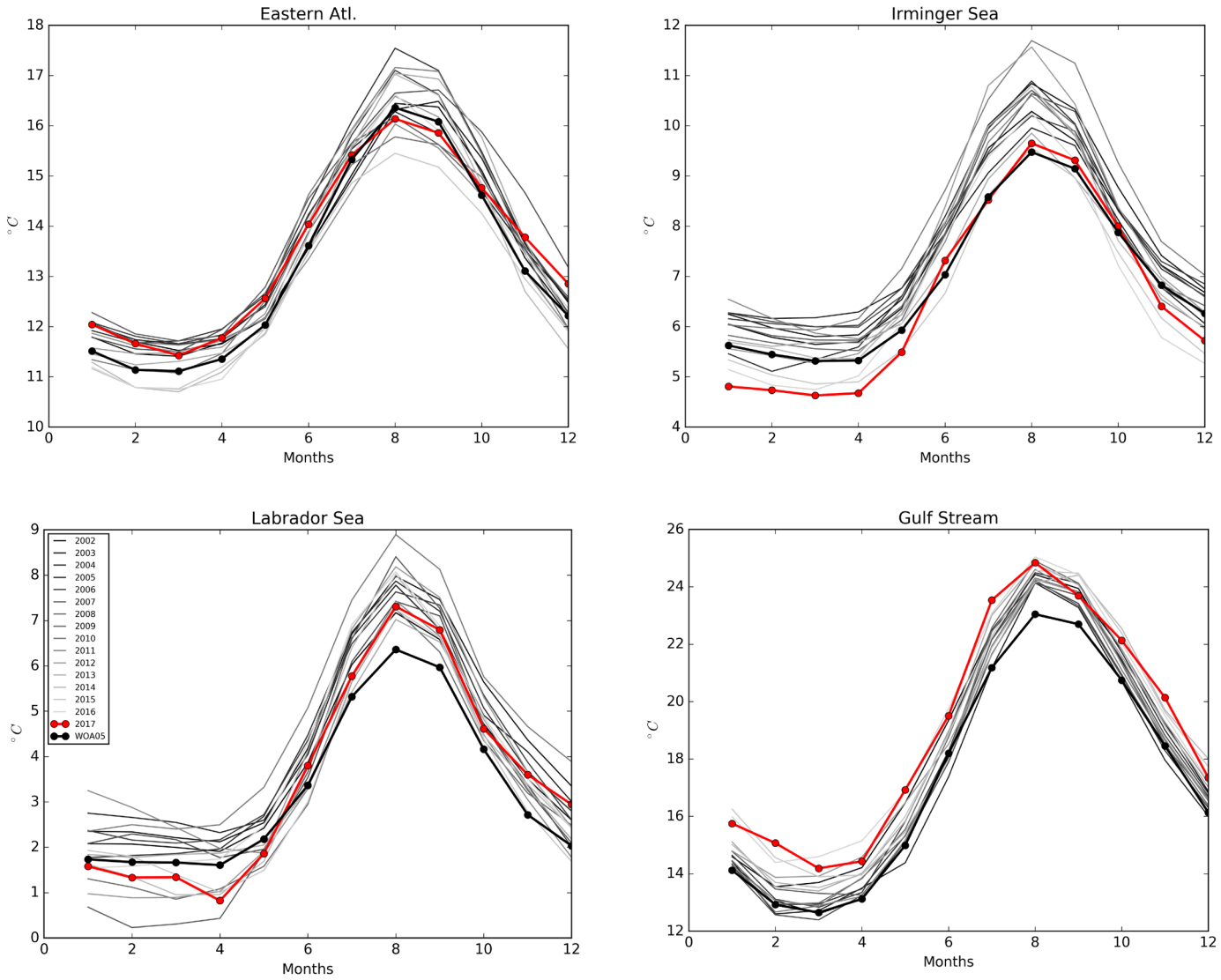

FIGURE 5.
Seasonal cycle for near-surface temperature (10 m depth) at four points in the North Atlantic basin (see position of stations in Figure 6). Eastern Atlantic (station 1 in Figure 6); Irminger Sea (station 2 in Figure 6); Labrador Sea (station 3 in Figure 6), and Gulf Stream region (station 4 in Figure 6). Thick red is 2017, thick black is the WOA05 climatology, other curves show the years 2002–2016.

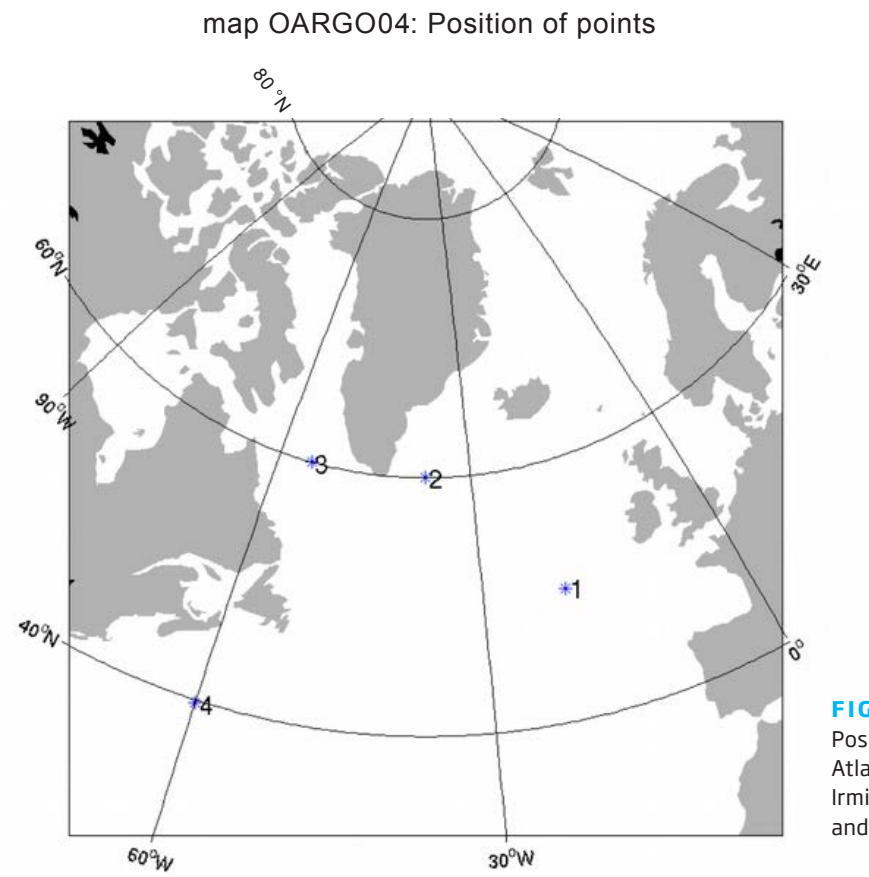

FIGURE 6.
Positions of four stations in the North Atlantic basin: Eastern Atlantic (1), Irminger Sea (2), Labrador Sea (3), and Gulf Stream region (4).

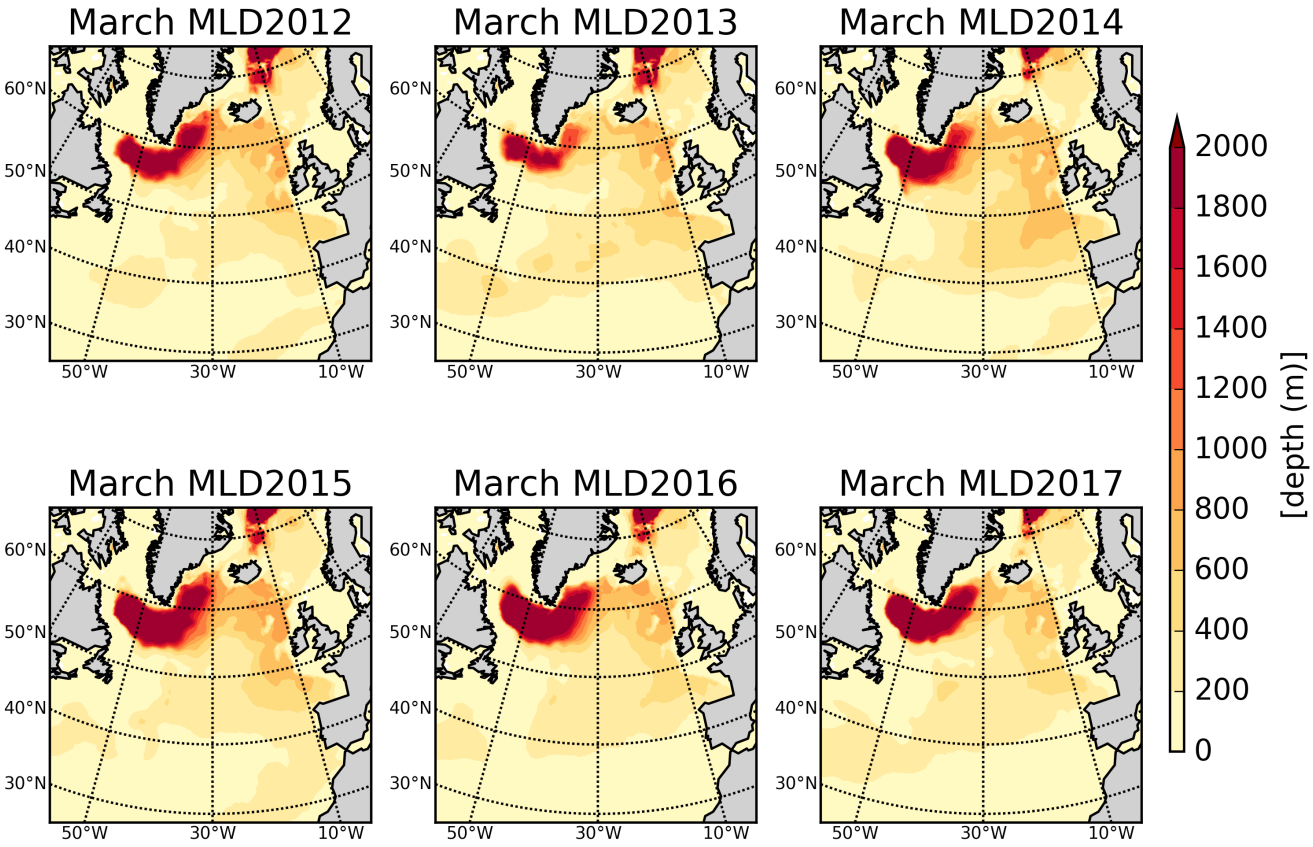

FIGURE 7.
Maps of North Atlantic winter (March) mixed-layer depths (MLD) for 2012–2017 from the ISAS monthly analysis of Argo data. Note that from 2017, the mixed-layer depth is defined as the depth at which density has increased by more than 0.03 kg m^{-3} from the density at 10 m. This criterion represents MLD in areas affected by both temperature and salinity (ice melting).

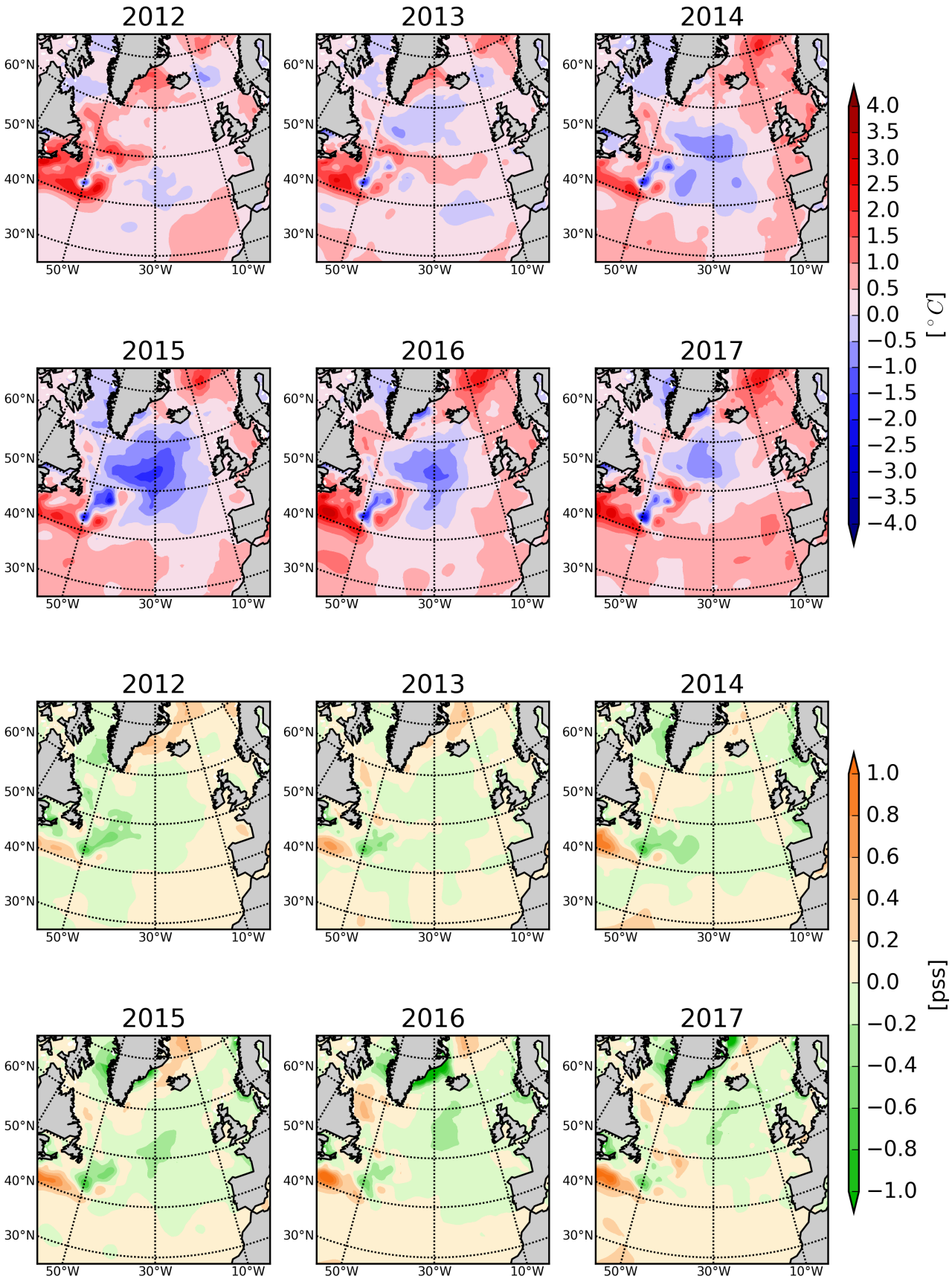

FIGURE 8.
Maps of annual temperature (upper) and salinity (lower) anomalies at 10 m in the North Atlantic for the period 2012–2017. Anomalies are the differences between the ISAS monthly mean values and the reference climatology, WOA5. The colour-coded scale is the same in all panels. Data from Coriolis, ISAS monthly analysis of Argo data.

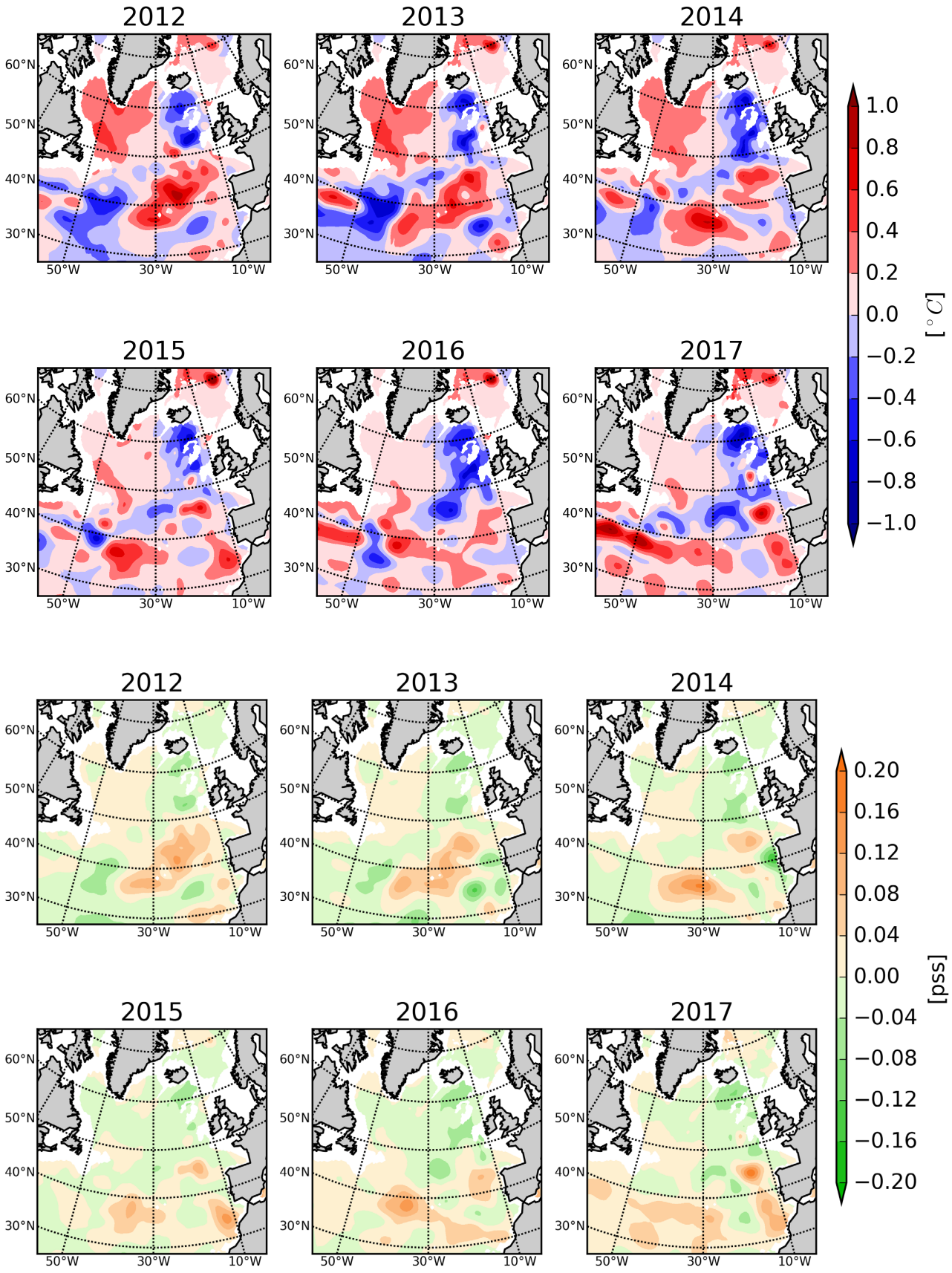

FIGURE 9,
Maps of annual temperature (upper) and salinity (lower) anomalies at 1000 m in the North Atlantic for the period 2012–2017. Anomalies are the differences between the ISAS monthly mean values and the reference climatology, WOA5. The colour-coded scale is the same in all panels. Data from Coriolis, ISAS monthly analysis of Argo data.

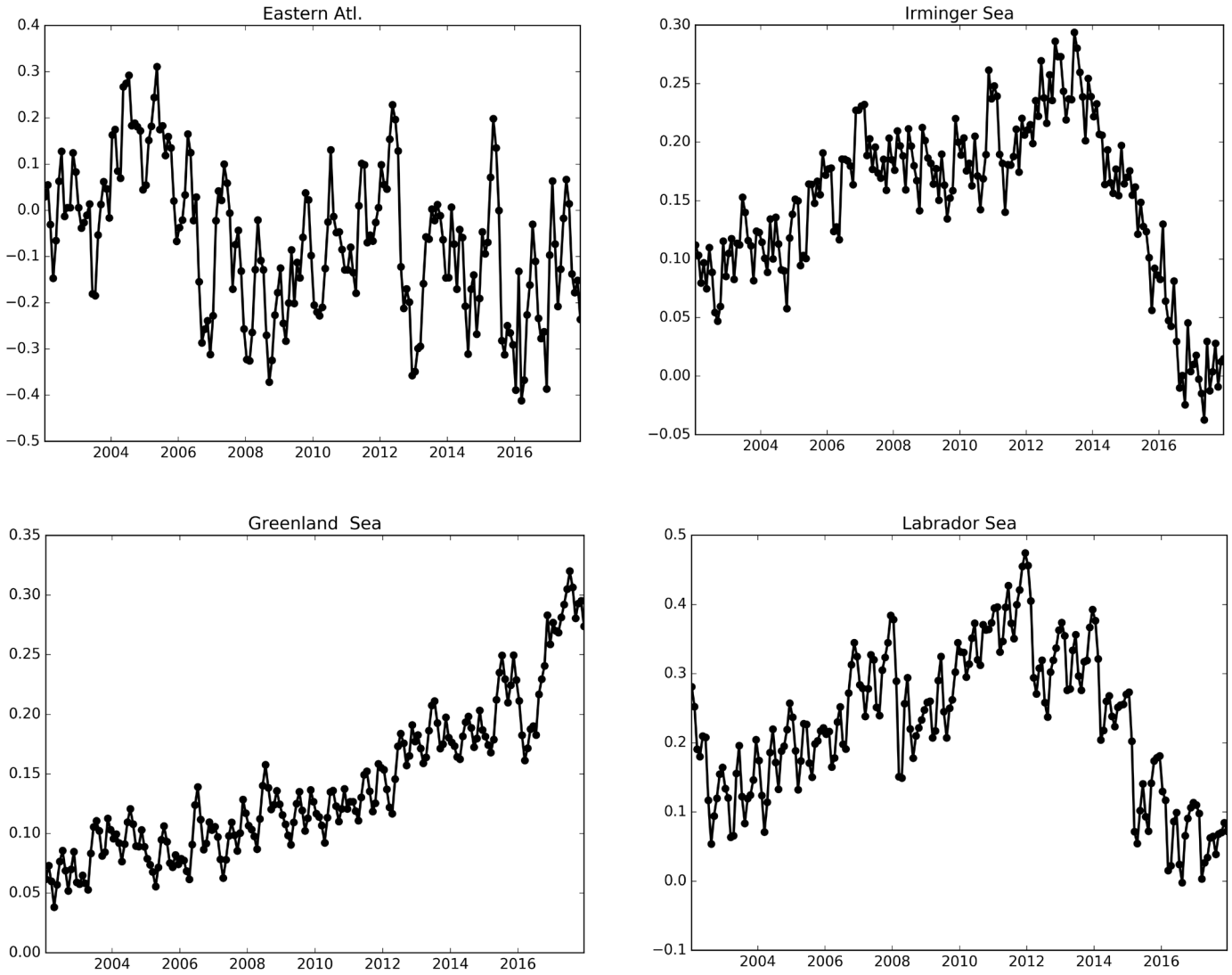

FIGURE 10,
Time-series of temperature anomalies (using WOA05 as reference) averaged over the period 2002–2017 in the 800–1200 m layer in (a) Eastern Atlantic region (25°W, 15°W, 45°N, 55°N); (b) Irminger Sea (40°W, 30°W, 55°N, 65˚N); (c) Greenland Sea (15°W, 5°W, 65°N, 75°N); and (d) Labrador Sea (60°W, 50°W, 55°N, 65°N).

2.4 SUBPOLAR GYRE INDEX

L. Chafik, H. Hátún, and B. Berx

The surface circulation of the North Atlantic is dominated by two gyres: one that circulates warmer water in a clockwise direction (Subtropical Gyre) and another that circulates cooler waters in the opposite direction (Subpolar Gyre) (Figure 17). The Subpolar Gyre encompasses the North Atlantic, East Greenland, and Labrador currents. Both gyres are driven by a combination of processes, the most important for the Subpolar Gyre being the strength and direction of surface winds, the exchange of heat between atmos-phere and ocean, and the large-scale circulation known as the overturning circulation (Berx and Payne, 2017).

The principal dynamics of the North Atlantic Subpolar Gyre are revealed using sea surface height variability over the Subpolar and Subtropical gyres. Satellite altimetry measurements are available since 1993 (Pujol ***et al.***, 2016), and applying the method of Häkkinen and Rhines (2004) to this 24-year dataset (1993–2016), we have pro-duced an updated version of the Subpolar Gyre index. The Subpolar Gyre index now appears as the second principal component and not as the first principal component as previously reported (Hátún and Chafik, 2018). The new Subpolar Gyre index, which does not include the trend associ-ated with the leading sea-surface height mode, still captures the main dynamics and intensity of the cyclonic Subpolar Gyre circulation and is recognized to have significant implications for a wide-range of climatic (Hátún *et al.*, 2005; Buck-ley and Marshall, 2016; Moffa-Sánchez and Hall, 2017), as well as ecological (Hátún *et al.*, 2009, 2016, 2017) aspects in the North Atlantic.

The Subpolar Gyre index was negative in the early 1990s, reflecting a period of strong gyre circulation (anomalously low sea surface heights, Figure 11), intensified by the anomalously strong atmospheric forcing and, in turn, represented by a very high NAO index during the late 1980s–early 1990s (Delworth *et al.*, 2016).

A rapid reversal of westerly winds that occurred during winter 1995/1996 switched the NAO index to negative in 1996, followed by a period with average or negative NAO values. As a result, the Subpolar Gyre index transitioned to a positive phase, indicating a weaker and contracted gyre circulation (anomalously high sea surface heights, Figure 11). This modified gyre shape, most notably in the eastern North Atlantic, permitted a larger contribution of warm, saline, nutrient-poor subtropical waters to Atlantic inflows towards the Arctic, which ultimately accessed the central Subpolar Gyre, further weakening its strength.

Strong atmospheric forcing and winter convection since 2014, associated with a positive NAO index (e.g. Yashayaev and Loder, 2017), has resulted in a recovery of the Subpolar Gyre and hence a return to a very strong and expanded gyre-scale circulation similar to that in the early 1990s. This is clearly illustrated by a switch to negative Subpolar Gyre index values in the past few years (Figure 11). The advantage of using the Subpolar Gyre index over the NAO index in ocean research is that it integrates the oceanic imprint of the various atmospheric forcings, and thus has more direct implications for the marine climate and ecosystems in the subpolar North Atlantic.

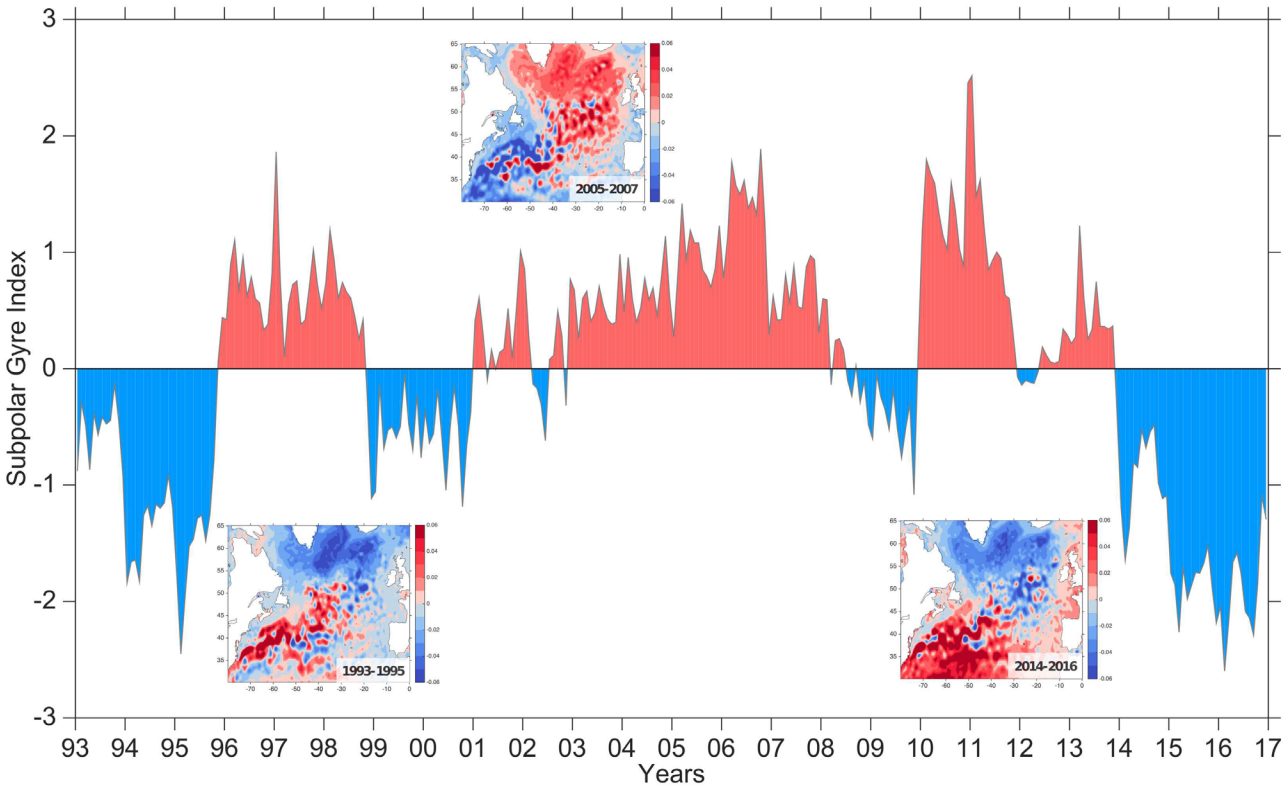

FIGURE 11.
The new monthly Subpolar Gyre index (second principal component) from January 1993 until December 2017. The insets show deseasonalized and detrended sea level anomaly averaged over the years indicated in the bottom right of each inset. Data source: altimetry data obtained through the Copernicus Marine Environment Monitoring Service (http://marine.copernicus.eu). Index source: Léon Chafik (Department of Meteorology, Stockholm University, Stockholm, Sweden) and Hjálmar Hátún (Faroe Marine Research Institute, Torshavn, Faroe Islands).

Hydrographic works and mooring service from the most recent Scotia cruise. Photo: Helen Smith. Marine Scotland Science (MSS, Aberdeen), UK.

CTD deployment from RV Celtic Explorer. Rockall survey 2018.
Photo: Tomasz Szumski, Marine Institute, Ireland.

3. NORTH ATLANTIC ATMOSPHERE

S. Dye

The North Atlantic Oscillation (NAO) is a pattern of atmospheric variability that has a significant effect on oceanic conditions. It affects windspeed, precipitation, evaporation, and the exchange of heat between ocean and atmosphere, and its effects are most strongly felt in winter. The NAO index is a simple device used to describe the state of the NAO. It is a measure of the strength of the sea level air pressure gradient between Iceland and Lisbon, Portugal. When the NAO index is positive, there is a strengthening of the Icelandic low-pressure system and the Azores high-pressure system. This produces stronger mid-latitude westerly winds, with colder and drier conditions over the western North Atlantic and warmer and wetter conditions in the eastern North Atlantic. When the NAO index is negative, there is a reduced pressure gradient, and the effects tend to be reversed.

There are several slightly different versions of the NAO index calculated by climate scientists. The Hurrell winter (December/January/February/March, or DJFM) NAO index (Hurrell *et al.*, 2013) is most commonly used and is particularly relevant to the eastern North Atlantic. Note that although we may think of winter as coming at the end of the year, the Hurrell "winter season" spans an annual boundary and precedes the year of interest; therefore, winter December 2016 to March 2017 sets up conditions for summer 2017.

The NAO is the dominant pattern of atmospheric pressure variability in the North Atlantic. However, when the NAO itself is weak (i.e. the dominant atmospheric pattern is not an NAO type pattern), this may be because a different pattern is occurring. Two other dominant atmospheric regimes have been identified as useful descriptors: (i) the Atlantic Ridge mode, when a strong anticyclonic ridge develops off western Europe (similar to the East Atlantic pattern); and (ii) the Blocking regime, when the anticyclonic ridge develops over Scandinavia. The four regimes (positive NAO, negative NAO, Atlantic Ridge, and Blocking) have all been occurring at around the same frequency (20–30% of all winter days) since 1950 (Hurrell and Deser, 2010). For this reason, we also include maps of SLP, windspeed, and air temperature, as this offers a more detailed understanding of the North Atlantic atmospheric variability than the NAO Index.

3.1 NORTH ATLANTIC OSCILLATION (NAO) INDEX

Following a long period of increase, from an extreme and persistent negative phase in the 1960s to a most extreme and persistent positive phase during the late 1980s and early 1990s, the Hurrell NAO index underwent a large and rapid decrease in winter 1995/1996. For many of the years between 1996 and 2009, the Hurrell winter NAO index was weak and a less useful descriptor of atmospheric conditions, mainly because the SLP patterns were not typical of the NAO. In winter 2009/2010, the index was strongly negative (Figure 12), and its anomaly pattern exerted a dominant influence on atmospheric conditions.

This was the strongest negative anomaly since 1969 and the second strongest negative value for the Hurrell winter NAO index on record (starting in 1864). Winter 2014/2015 saw the highest NAO index since 1995 and the fourth most positive NAO index in the last 110 years (Hurrell and National Center for Atmospheric Research Staff, 2017). In winter 2016/2017, the NAO index was strong and positive (+1.47) for the fourth consecutive winter, the first such positive run since 1992–1995.

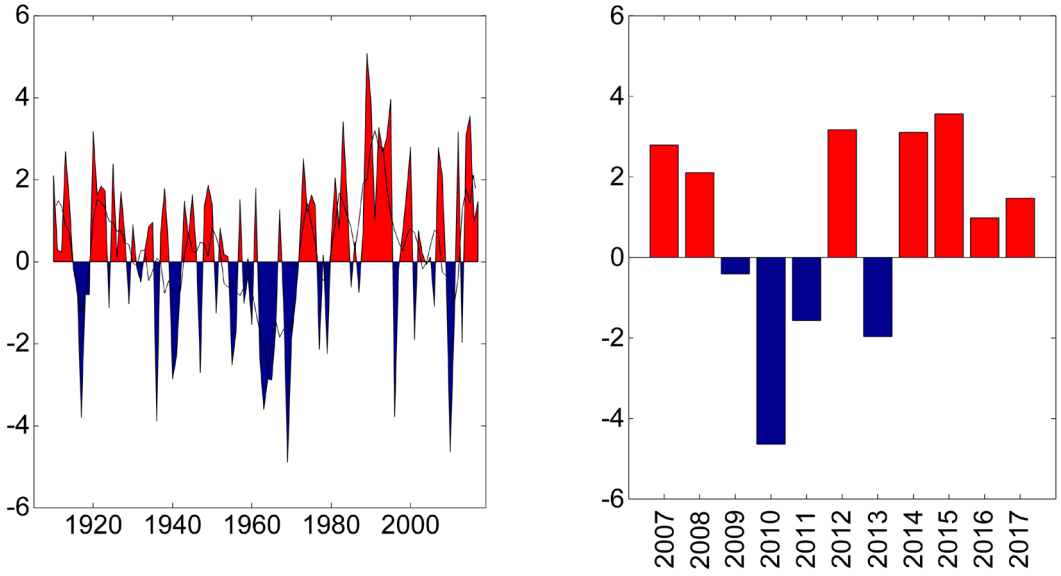

FIGURE 12.
The Hurrell winter (DJFM) NAO index for the past 100 years with a two-year running mean applied (left panel) and for the current decade (right panel). Data source: NAO Index Data provided by the Climate Analysis Section, NCAR, Boulder, CO, USA, (Hurrell and National Center for Atmospheric Research Staff, 2017).

3.2 SEA LEVEL PRESSURE AND WINDSPEED

Atmospheric conditions indicated by the NAO index are more understandable when the anomaly fields are mapped. Ocean properties are particularly dominated by winter conditions; hence, the inclusion of SLP and windspeed maps for winter (Figures 13 and 14).

The top panel of Figure 13 shows winter SLP averaged over 30 years (1981–2010). The dominant features ("action centres") are the Iceland Low, situated southwest of Iceland, and the Azores High, west of Gibraltar. The middle panel of Figure 13 shows the mean SLP for winter 2016/2017 (DJFM), and the bottom panel shows winter 2016/2017 SLP anomaly (i.e. the difference between the top and middle panels).

SLP patterns are closely related to wind patterns. The geostrophic (or "gradient") wind blows parallel with the isobars, with lower pressure to the left; the closer the isobars, the stronger the wind. The strength of the winter mean surface wind averaged over the 30-year period (1981–2010) is shown in the upper panel of Figure 14, while the middle panel shows the mean surface wind for winter 2016/2017 and the lower panel the anomaly in winter 2016/2017.

The SLP anomaly for winter 2016/2017 (Figure 13) was not a typical NAO pattern as the high pressure anomaly centred over the North Sea, and was found only east of the Azores. This ridge of high pressure extended north into the Iceland Sea, effectively curtailing the eastern extent of the Iceland Low, leading to an Arctic-centred low-pressure anomaly extending southward and splitting to the southeast and southwest of Iceland and the Nordic seas. The influence of this is seen in mixed-pattern winds (Figure 14). Winds were stronger and more northerly than usual over the Labrador Sea, while somewhat stronger southerly winds blew across the path of the North Atlantic current west of Ireland and the UK. Weaker-than-average winds were evident over the North Sea, Bay of Biscay, and Irminger Sea and along the coasts of East Greenland and North America from the Carolinas to Newfoundland.

Taking dissolved oxygen samples from CTD at 2017 GO - S3H1IP transatlantic survey. Photo: Tomasz Szumski, Marine Institute, Ireland.

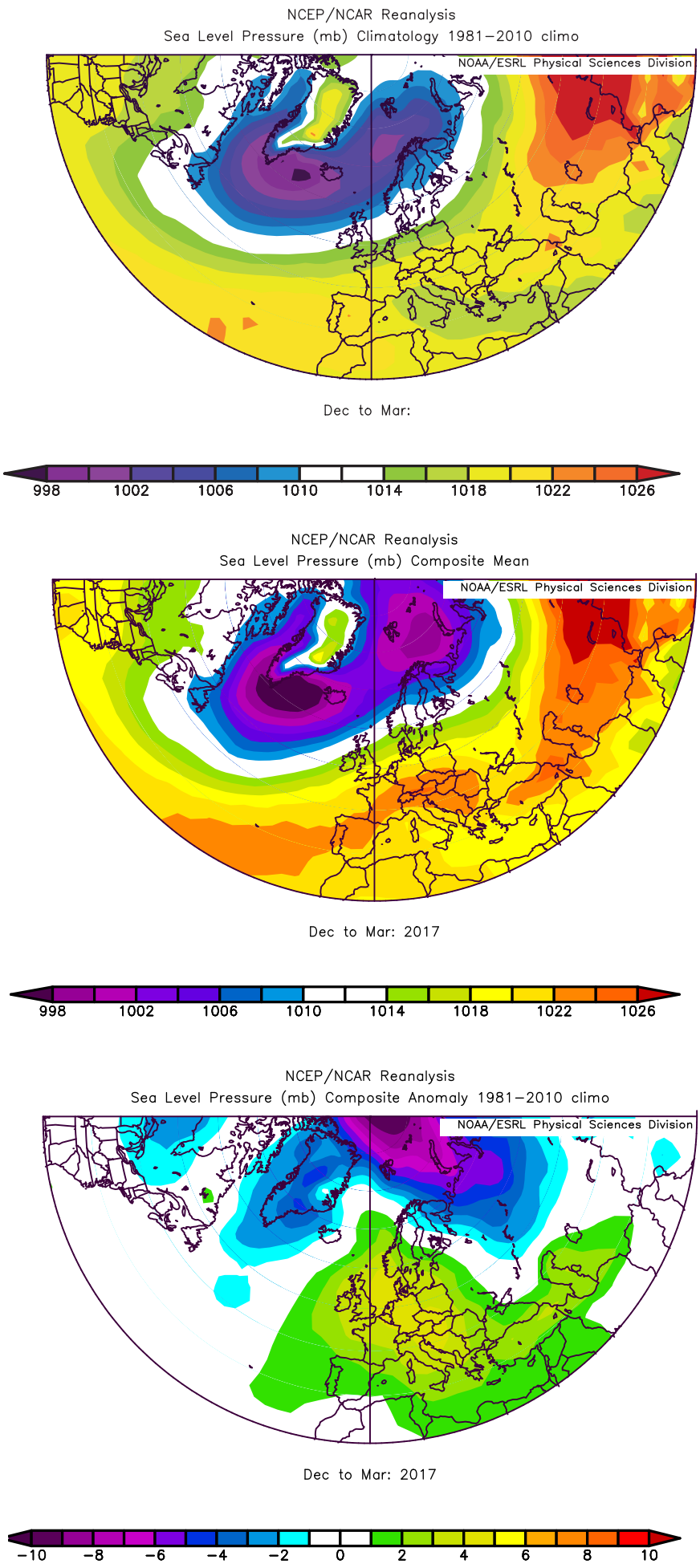

FIGURE 13.
Winter (DJFM) sea level pressure (SLP) fields. Top panel: SLP averaged over 30 years (1981–2010). Middle panel: SLP in winter 2016/2017. Bottom panel: winter 2016/2017 SLP anomaly, calculated as the difference between the top and middle panels. Images provided by the NOAA/ESRL Physical Sciences Division, Boulder, CO, USA.

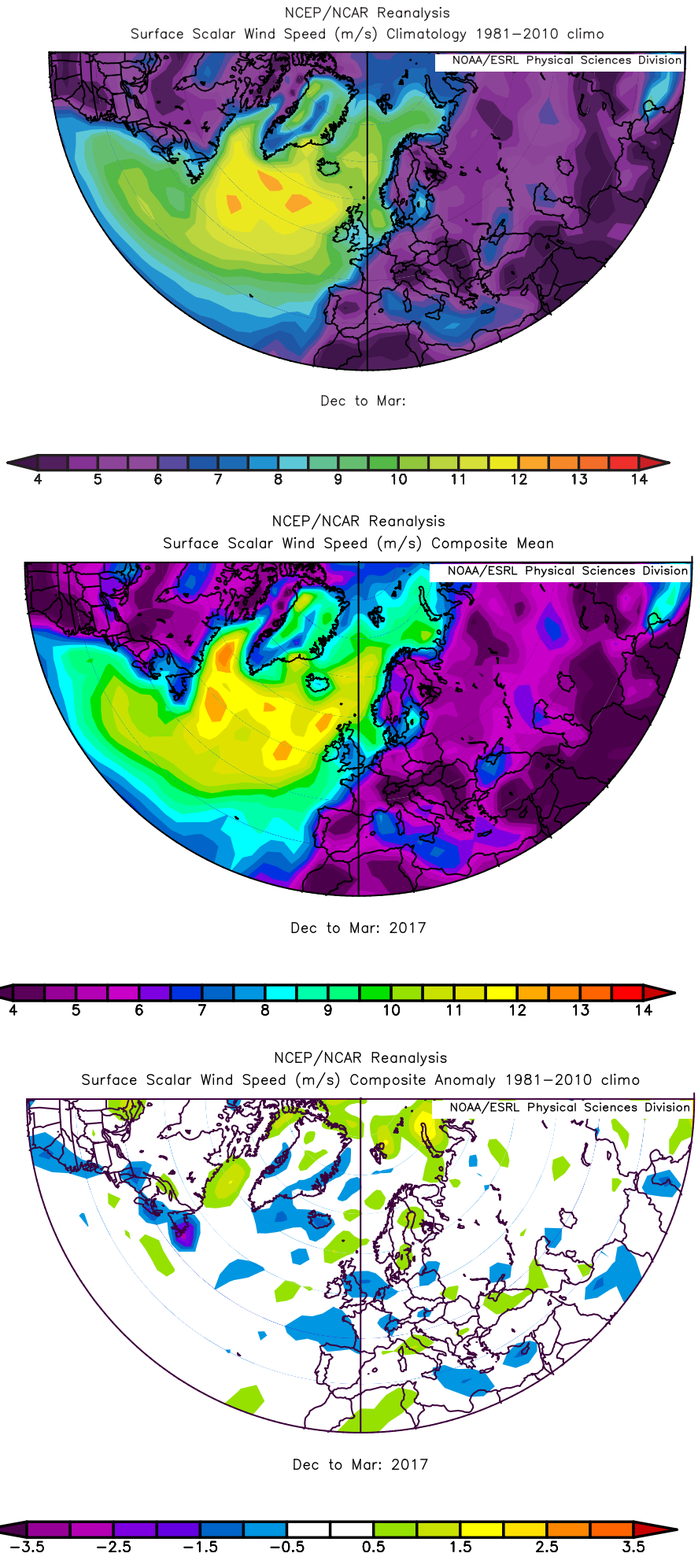

FIGURE 14.
Winter (DJFM) windspeed fields. Top panel: scalar windspeed averaged over 30 years (1981–2010). Middle panel: scalar windspeed in winter 2016/2017. Bottom panel: winter 2016/2017 scalar windspeed anomaly, calculated as the difference between the top and middle panels. Images provided by the NOAA/ESRL Physical Sciences Division, Boulder, CO, USA.

3.3 SURFACE AIR TEMPERATURE

North Atlantic winter mean surface air temperatures are shown in Figure 15 (Kalnay *et al*., 1996). The 1981–2010 mean conditions (Figure 15, top panel) show warm temperatures penetrating far to the north on the eastern side of the North Atlantic and the Nordic seas, caused by the northward movement of warm oceanic water. The middle panel of Figure 15 shows conditions in winter (DJFM) 2016/2017, and the bottom panel shows the difference between the two.

Winter air temperatures were near average (1981–2010) over the Subpolar Gyre and open North Atlantic. This pattern is consistent with the relatively cool SST anomalies observed in the Subpolar Gyre in recent years. Around the margins of the North Atlantic, temperatures were generally higher than normal. Warmer conditions were particularly noticeable over the northern Barents Sea, the northern Labrador Sea, and the East Greenland coast north of the Denmark Strait.

3.4 OUTLOOK BEYOND 2017

An initial assessment of the North Atlantic atmosphere at the end of the IROC year is included. Atmospheric conditions during winter are a determining factor of oceanic conditions for the following year; therefore, this outlook offers some predictive capability for spring–autumn 2018.

NAO

The SLP anomaly for winter 2017/2018 suggest a near-neutral NAO index winter, bringing an end to the run of strong positive NAO winters, and was almost certainly the weakest NAO index winter (either positive or negative) this decade. While the first 3 months of winter 2017/2018 experienced a broadly positive NAO pattern, negative NAO conditions in March made the full winter index weaker. The winter 2017/2018 SLP pattern is almost the reverse of that experienced the previous winter, with a cyclonic anomaly centred over the North Sea and limited to east of the Azores, while an anticyclonic anomaly over the Arctic extended southeast and southwest of Iceland. Recent advances in understanding the predictability of the NAO are showing significant skill in seasonal predictions of the European winter through predictability of the winter NAO (Scaife *et al*., 2014), Arctic Oscillation (AO), and sudden stratospheric warming (SSW) events (Scaife *et al*., 2015). Results published by the Met Office suggest that there is even significant skill in predicting the winter NAO index one year ahead (Dunstone *et al*., 2016) with a correlation coefficient (r) between observed NAO and predicted of about 0.4 for the second winter, comparing well with that of about 0.6 for the first winter, as described in Scaife *et al.* (2014).

Temperature

Air temperatures in winter 2017-2018 were cold over Iberia, Norway, and the Subpolar Gyre, including over the Irminger Sea and the Iceland Basin. Warmer-than-average conditions were evident southwest of the Subpolar Gyre and in the Greenland Sea.Experimental forecasts from the USA (seasonal periods: NOAA Climate Prediction Center - The North American Multi-Model Ensemble) and the UK (1–5 years: Met Office Decadal forecast January 2018) also suggest an outlook more typical of the long-term average (1981–2010) for temperatures in the Subpolar Gyre region than has been seen in the last few cold anomaly years. As experimental forecasts at an early stage, these are noted here so that their performance may be tracked and their utility gauged as they develop.

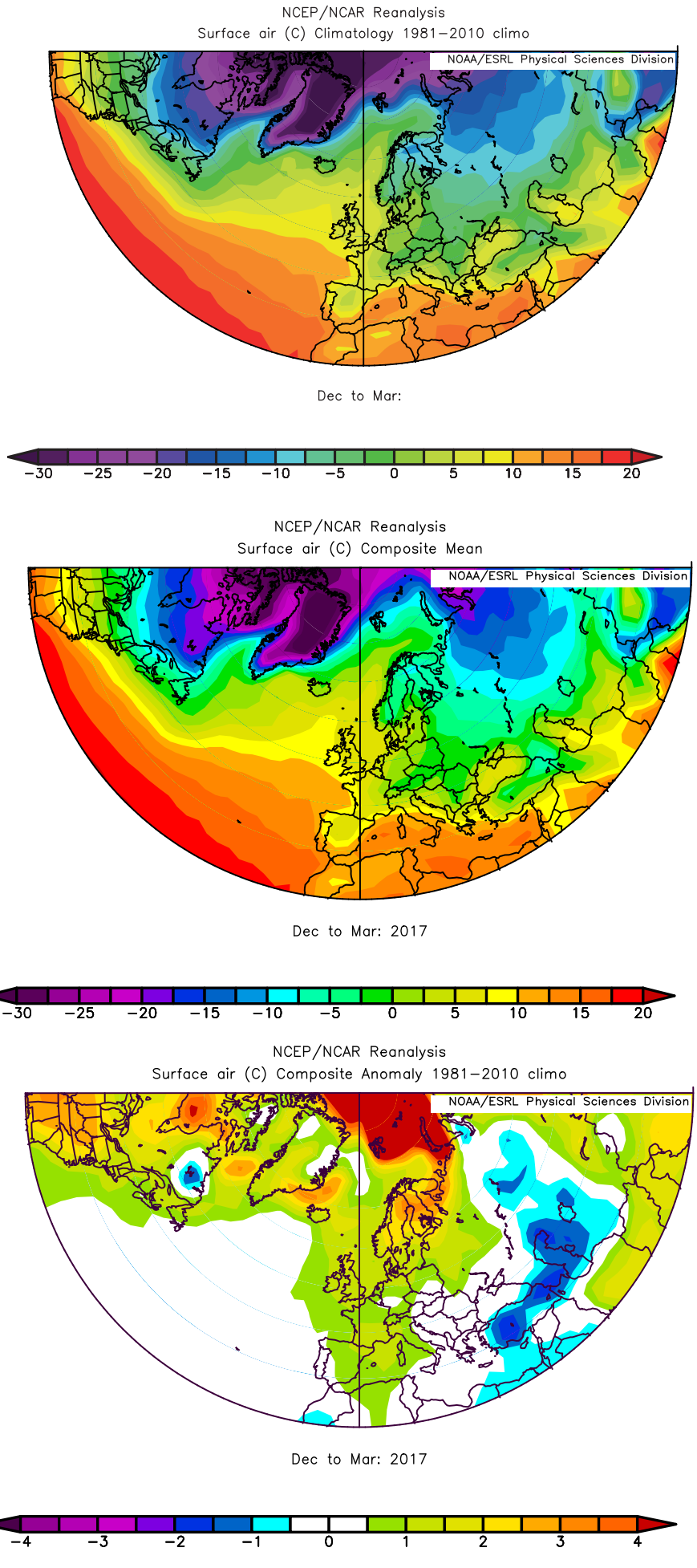

FIGURE 15.
Winter (DJFM) surface air temperature fields. Top panel: surface air temperature averaged over 30 years (1981–2010). Middle panel: surface air temperatures in winter 2016/2017. Bottom panel: winter 2016/2017 surface air temperature anomaly, calculated as the difference between the top and middle panels. Images provided by the NOAA/ESRL Physical Sciences Division, Boulder, CO (available online at http://www.cdc.noaa.gov/)

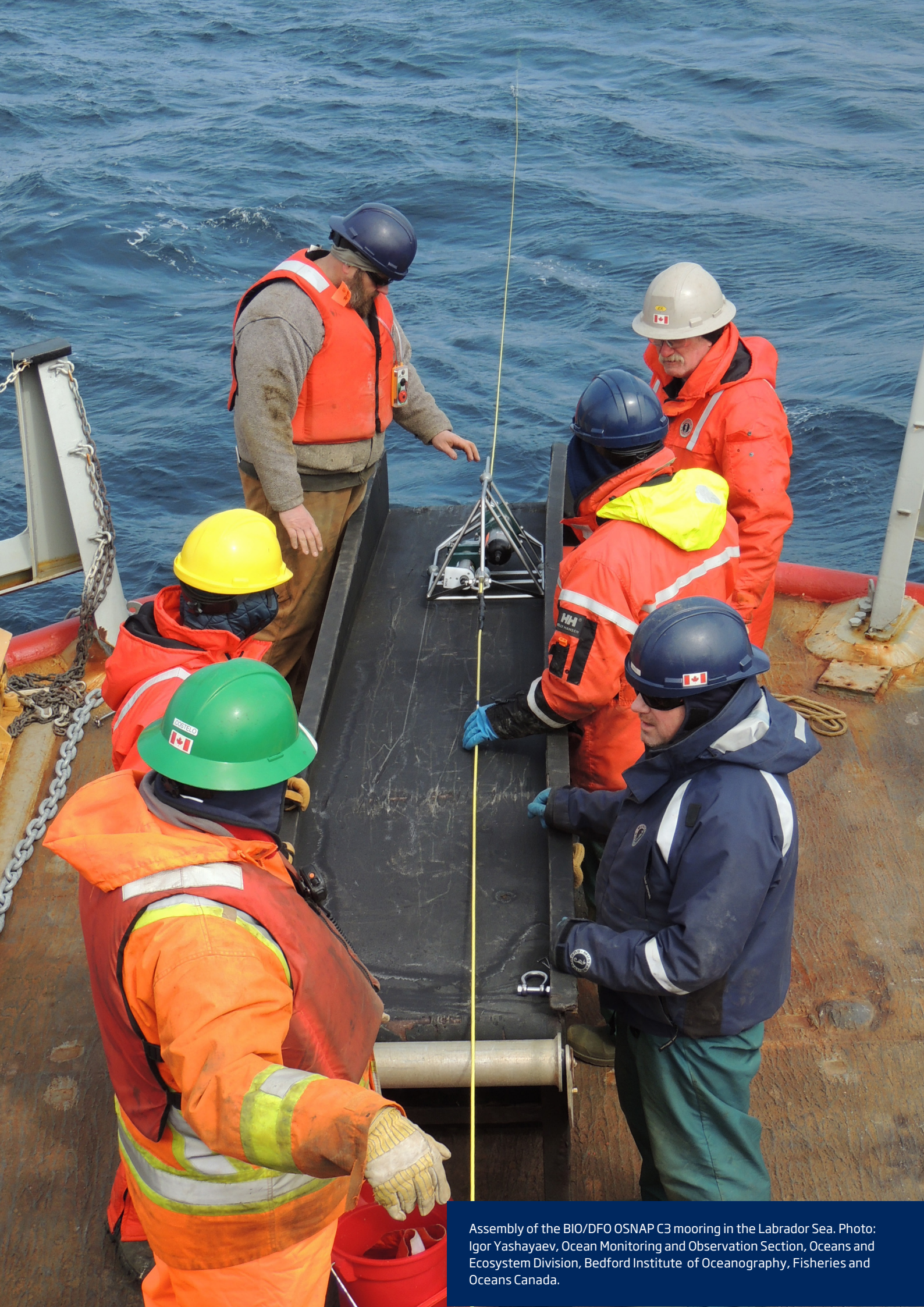

Assembly of the BIO/DFO OSNAP C3 mooring in the Labrador Sea. Photo: Igor Yashayaev, Ocean Monitoring and Observation Section, Oceans and Ecosystem Division, Bedford Institute of Oceanography, Fisheries and Oceans Canada.

4. DETAILED AREA DESCRIPTIONS, PART I: THE UPPER OCEAN

INTRODUCTION

This section presents time-series from sustained observations in each of the ICES areas shown in Figure 16. The general pattern of oceanic circulation in the upper layers of the North Atlantic, in relation to the areas described here, is shown in Figure 17. In addition to temperature and salinity, we present other indices where available, such as air temperature and sea ice extent. We summarize the regional context of the sections and stations, noting any significant changes.

Most standard sections or stations are sampled annually or more frequently. Many of the time-series presented here have been extracted from larger datasets and have been chosen as indicators of the conditions in a particular area. Where appropriate, data are presented as anomalies to demonstrate how the values compare with the average, or "normal", conditions (usually the long-term mean of each parameter during 1981–2010). For datasets that do not extend as far back as 1981, average conditions have been calculated from the start of the dataset through 2010.

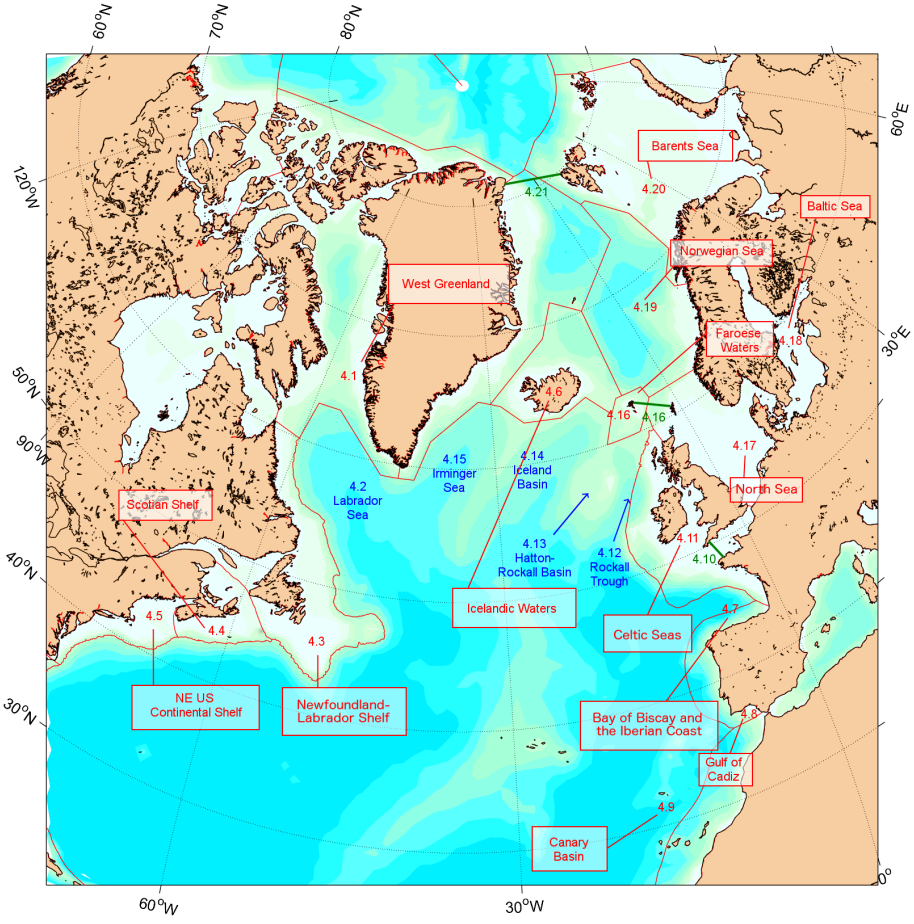

FIGURE 16.
Schematic of marine areas used to organize data presentation in this section. Numbers refer to the subsection number. Regions are labelled in red. Ocean basins are labelled in blue. Green numbers indicate straits. NOAA Large Marine Ecosystem boundaries (http://lme.edc.uri.edu/) are shown as background reference, but hydrograpic regions are loosely defined so they do not perfectly overlap.

In places, the seasonal cycle has been removed from a dataset either by calculating the average seasonal cycle during 1981–2010 or by drawing on other sources, such as regional climatology datasets. Smoothed versions of most time-series are included using a "Loess smoother", a locally weighted regression with a two- or five-year window (chosen as the most appropriate to each time-series).

In some areas, data are sampled regularly enough to allow a good description of the seasonal cycle. Where possible, monthly data from 2017 are presented and compared with average seasonal conditions and statistics.

Although there are no real boundaries in the ocean, it is the intention that the data presented will represent conditions in a particular area. In this section, datasets are grouped into areas based on existing definitions. NOAA Large Marine Ecosystems (LMEs[4]) are taken as an overall reference as they cover all regions except ICES ecoregions[5], but the bathymetry of ocean basins[6] and the general pattern of ocean circulation (Figure 17) are also taken into account.

While the data presented offer the best available indicative time-series within a region, it should be noted that, in large areas with complex circulation patterns, consideration should be given to how representative these data are of the whole ecoregion.

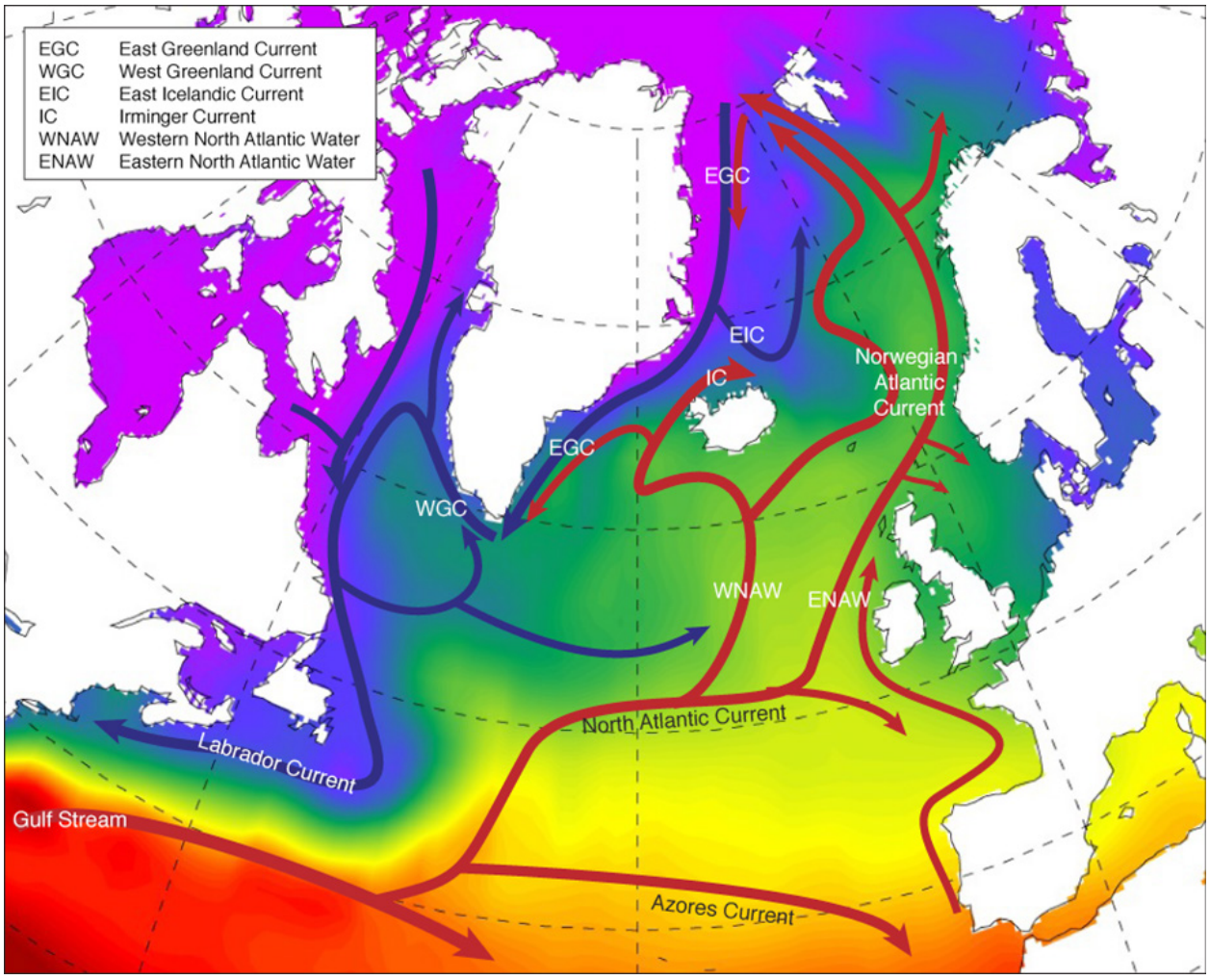

FIGURE 17.
Schematic of the general circulation of the upper ocean (0–1000 m) in the North Atlantic. Blue arrow = movement of cooler waters of the Subpolar Gyre; red arrows = movement of warmer waters of the subtropical gyre.

4) http://lme.edc.uri.edu/
5) http://www.ices.dk/community/advisory-process/Pages/ICES-ecosystems-and-advisory-areas.aspx
6) http://www.gebco.net/data_and_products/undersea_feature_names/

4.1 WEST GREENLAND

B. Cisewski

The NOAA Large Marine Ecosystem project identifies the ecosystem of the Canadian Eastern Arctic–Western Greenland as an LME. Only conditions in the West Greenland portion of the region are examined here. The hydrographic conditions presented are monitored at two oceanographic sections across the continental slope of West Greenland in the southwestern part of the ecoregion at a position that is influenced by the West Greenland Current (WGC; Figure 18). The WGC carries water northward along the west coast of Greenland and consists of two components: a cold, fresh inshore component, which is a mixture of polar water and melt water, and a warmer, saltier offshore component called Irminger Seawater. As part of the cyclonic Subpolar Gyre, the WGC is subject to hydrographic variations on a range of time-scales associated with variability of the gyre.

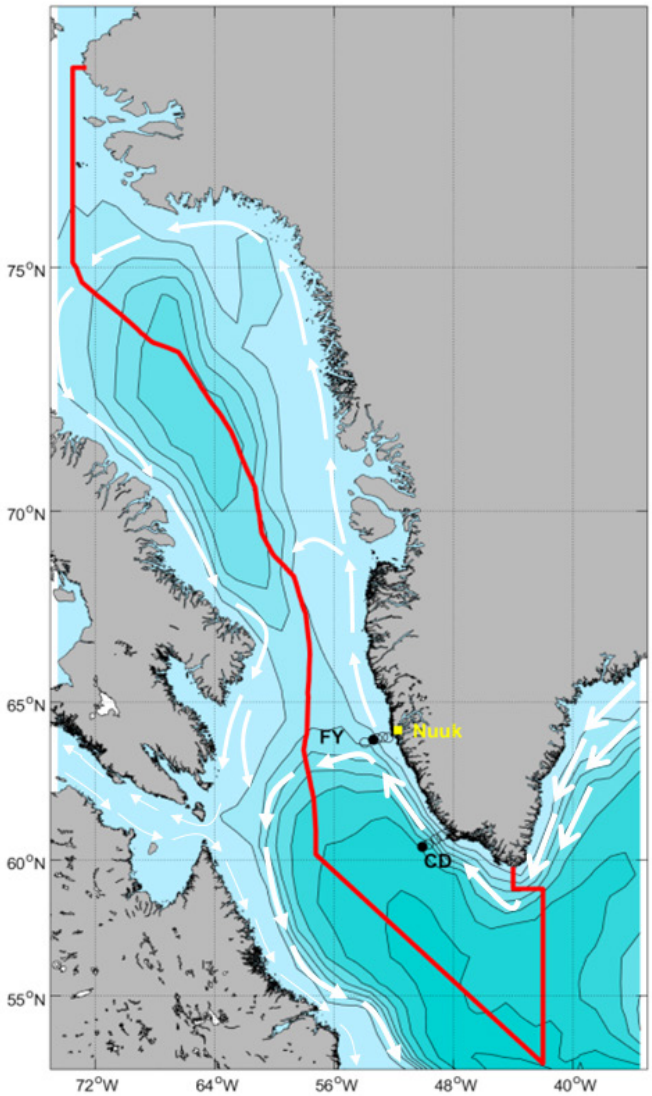

In winter 2016/2017, the NAO index was positive (1.47) for the fourth consecutive winter. The annual mean air temperature at Nuuk Weather Station in West Greenland was 0.4°C in 2017, which was 1.0°C above the long-term mean (1981–2010).

Hydrographic conditions are monitored in two oceanographic NAFO/ICES sections spanning the western shelf and continental slope of Greenland near Cape Desolation and Fyllas Bank. In each section, two offshore stations were chosen to document changes in hydrographic conditions off West Greenland. However, in autumn 2017, both the Cape Desolation and the Fyllas Bank sections were abandoned due to severe weather conditions.

FIGURE 18.
Circulation schematic for the Labrador Sea and Davis Strait. The location of Nuuk is marked in yellow. White arrows show the path of the surface circulation. The thick arrows are the West Greenland Current (WGC). The red line shows the extent of NAFO Division 1a, Western Greenland. The circles labelled "FY" are Fyllas Bank hydrographic section stations. Station 4 is marked as a black circle. The circles labelled "CD" are Cape Desolation hydrographic section stations. Station 3 is marked as a black circle.

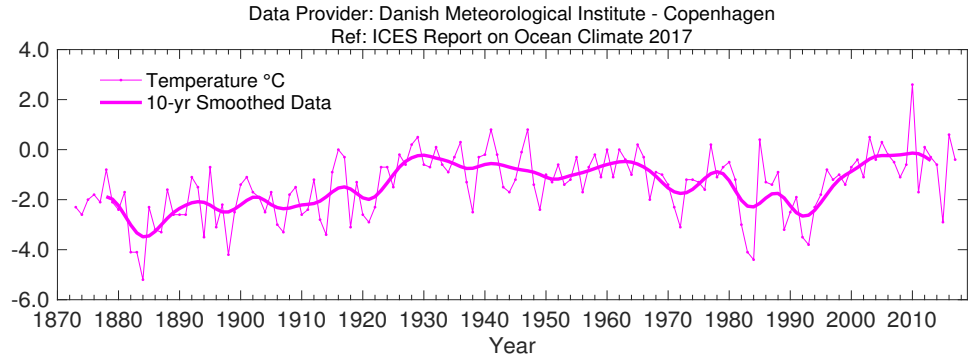

FIGURE 19.
West Greenland. Annual mean air temperature at Nuuk station (64.16°N 51.75°W). Data source: Cappelen (2018).

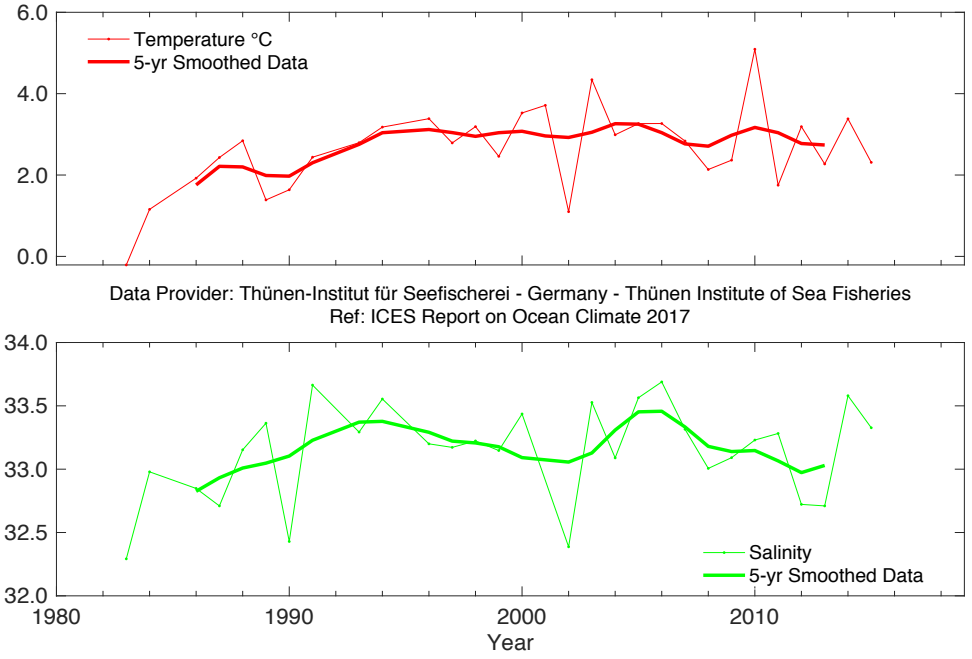

FIGURE 20.
West Greenland. Mean temperature (upper panel) and salinity (lower panel) in the 0–50 m water layer at Fyllas Bank Station 4 (63.88°N 53.37°W). Data until 2015.

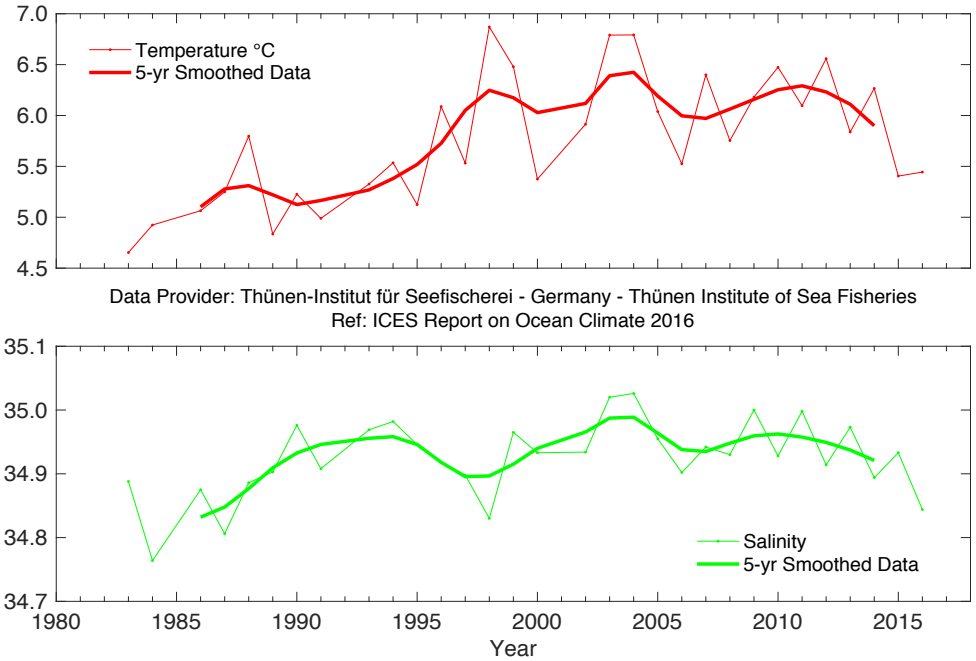

FIGURE 21.
West Greenland. Temperature (upper panel) and salinity (lower panel) in 75–200 m water layer at Cape Desolation Station 3 (60.47°N 50°W). Data until 2016.

4.2 LABRADOR SEA

I. Yashayaev

The Labrador Sea is located between Greenland and the Labrador coast of eastern Canada. The deep semi-enclosed Labrador Basin lies offshore from the West Greenland and the Newfoundland–Labrador Shelf ecoregions. Cold, low-salinity water of polar origin circles the Labrador Sea in an anticlockwise current system that includes both the north-flowing West Greenland Current on the eastern side and the south-flowing Labrador Current on the western side. Warm and saline Atlantic water (AW) originating in the subtropics flows north into the Labrador Sea on the Greenland side beneath and offshore of the West Greenland Current and becomes colder and fresher as it advances around the sea.

Interannual changes in the hydrographic conditions of the Labrador Sea depend on variable influences of heat loss to the atmosphere, heat and salt gain from AW, freshwater gain from Arctic outflow, melting sea ice, precipitation, and run-off, as well as the cumulative effect of past changes termed ocean preconditioning (Yashayaev and Loder, 2017). In the Labrador Sea, surface heat losses in winter result in the formation of dense waters. This process makes the Labrador Sea the primary region in the northern hemisphere for the atmospheric ventilation of the Atlantic Ocean's intermediate depth waters. Through winter cooling of surface and subsurface waters and their subsequent mixing and sinking to depths of 500–2500 m (depending on winter severity), a relatively dense and deep intermediate water mass, known as Labrador Sea water (LSW) is formed. This water spreads over the Atlantic Ocean, ventilating its deep layers while feeding and driving the global ocean's overturning circulation, or ocean conveyor belt.

The Atlantic Zone Off-shelf Monitoring Program (AZOMP) of Fisheries and Oceans Canada (Bedford Institute of Oceanography) provides observations of variability in ocean climate and plankton affecting regional climate and ecosystems of the North Atlantic and global climate system. An annual survey of the AR7W (Atlantic Repeat 7-West) Line in the Labrador Sea has been conducted since 1990, usually in May. Initially, this survey was part of the World Ocean Circulation Experiment, but is now the core component of AZOMP. The only year missing from the 1990–2018 record is 2017, when it was not possible for Fisheries and Oceans Canada to carry out a regular field campaign in the Labrador Sea, and no other groups sampled the region. Fortunately, the network of profiling Argo floats proved instrumental for monitoring year-round variability, and the temperature and salinity profiles received from the Argo floats were used as the basis for the 2017 assessment in the Labrador Sea.

A sequence of severe winters in the early 1990s led to deep convection, peaking in 1993–1994, that filled the upper two kilometres of the water column with cold, freshwater. Conditions have generally become milder since the mid-1990s. During 1995–2011, the upper levels of the Labrador Sea became warmer and more saline as heat losses to the atmosphere decreased and AW has become increasingly dominant. However, over the past seven years (2011–2017), the upper and intermediate layers have displayed trends of cooling and freshening.

In winter 2016/2017, as in previous winters (Yashayaev and Loder, 2017), the mid-high latitude North Atlantic experienced a more moderate cumulative surface (ocean-to-atmosphere) heat loss than in winter 2014/2015. In the context of longer-term variability, the latter was associated with the highest surface heat loss in more than two decades. Despite weaker heat losses in the following two winters (2015/2016 and 2016/2017), the water column preconditioning caused by convective mixing in the previous years led to the most significant formation of LSW (volume and depth) since 1994. Similar to 2016, the temperature and salinity profiles obtained by the

Further intensification of cooling, convective mixing, and intermediate water mass production in the Labrador Sea during winter 2016/2017.

Argo floats show that the winter mixed layer, and hence convection in the central Labrador Sea, reached 2000 m in 2017, exceeding the mixed-layer depths of 1600 and 1700 m in 2014 and 2015, respectively (Figure 22). Hence, deep-water convection from the previous years has resulted in a kind of preconditioning (of vertical stratification by previous convective events) that favoured this year's record deep convection. The 2017 vintage of LSW is associated with low temperature (< 3.3°C) and low salinity (< 34.86) between 1000 and 1700 m. The 2015/2016 and 2016/2017 winter convections are arguably the deepest since the record deep cooling of 2400 m observed in 1994, and the resulting LSW year class is one of the largest ever observed outside the early 1990s.

The strong winter convection in 2016/2017 further added to increased gas (dissolved oxygen, anthropogenic gases, and carbon dioxide) uptakes and consequently respective gas concentrations in the Labrador Sea in the lower part of the 0–2000 m layer, but as there was no cruise to the Labrador Sea in 2017, this could not be confirmed with direct ship-based measurements.

The progressive cooling of the upper 2000 m and the deep, intense winter mixing during five out of six consecutive winters (2011/2012, 2013/2014, 2014/2015, 2015/2016, and 2016/2017) have interrupted the general warming and stratification-building trend that has persisted in the Labrador Sea intermediate waters since the mid-1990s. Signifying the last five winters, through above-average regional winter cooling during 2012–2017, the depth to which cooled waters sink has progressively reached and exceeded 2000 m. Because of this intermittent recurrence of intensified LSW formation, the annual average temperature and density in the region's upper 2000 m have predominantly varied on a bidecadal time-scale, rather than having a long-term trend, as might be expected from anthropogenic climate change.

Interannual variability of the Labrador Sea's ocean heat content and cumulative surface heat loss during the cooling seasons indicates that anomalously strong winter atmospheric cooling associated with the NAO is continuing to drive the recurrent convection. In turn, recurrent deep convection is contributing to decadal-scale variability of deep-water properties and transport across and from the subpolar North Atlantic (by the ocean's western boundary and interior pathways) and potentially in the Atlantic meridional overturning circulation (AMOC).

Both upper (0–200 m) and deeper (200–2000 m) layers have been cooling since 2010. However, the freshening trend seen in the newly formed or newly ventilated LSW between 2011 and 2016 reversed in 2016, making the LSW formed in winter 2016/2017 the densest since the mid-1990s.

The surface freshening that peaked in the central Labrador Sea in 2012 reduced and reversed in the following years, making the upper layer salinity of the last two years the highest in a decade.

The intermediate waters of 400–2000 m depth experienced significant cooling after 2011, progressing in 2012 and during 2014–2017, while salinity has largely reduced since 2011 due to the intensification of deep mixing and export of freshwater from the upper layer. However, over the past two years, salinity has steadily increased in the intermediate layers. The progressive deepening of convective mixing that has occurred in the Labrador Sea during five of the recent six winters (2011/2012, 2013/2014, 2014/2015 and 2015/2016; the 2012/2013 convective event was comparable to or weaker than the one in 2011/2012) has reversed the general warming trend that was observed in the intermediate waters of the Labrador Sea during 1994–2011.

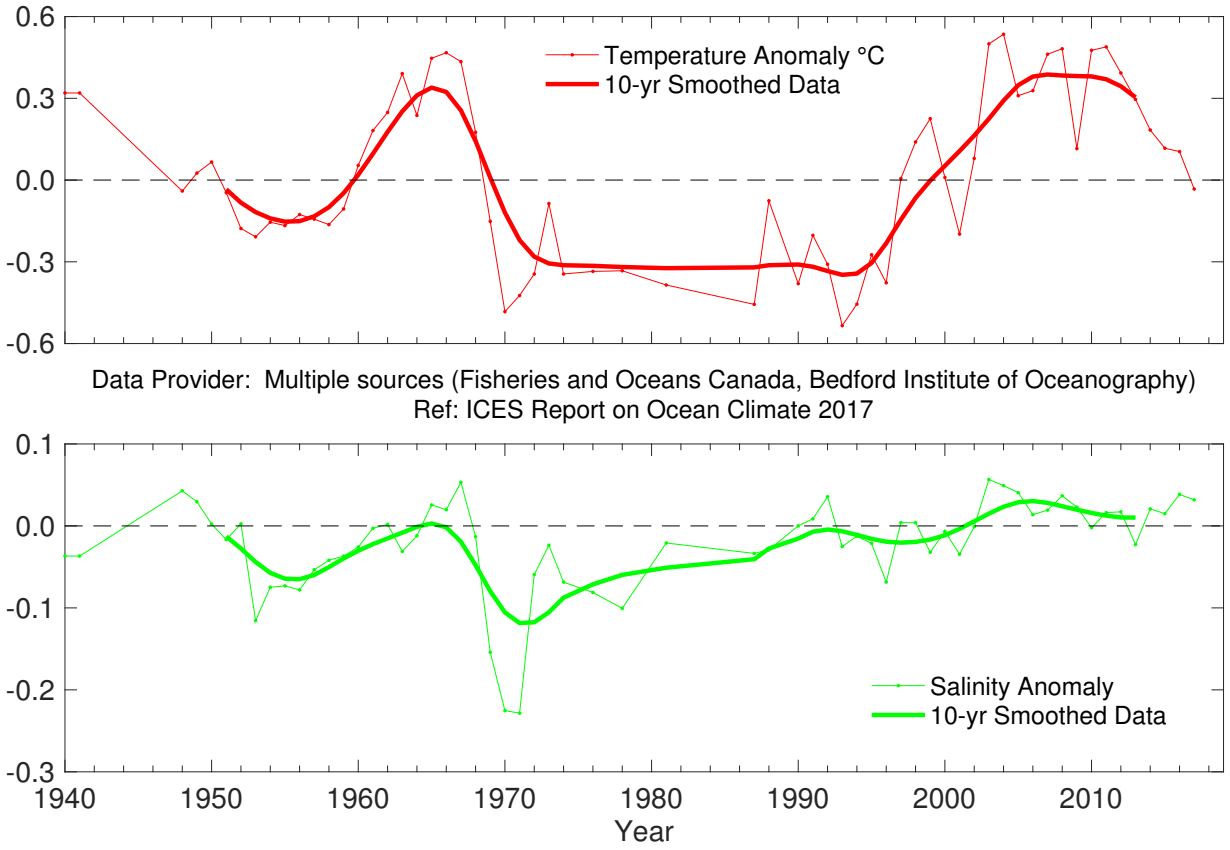

FIGURE 22.
Labrador Sea. Potential temperature (upper panel) and salinity (lower panel) anomalies at 50–200 m from CTD and Argo data in the west-central Labrador Sea (centred at 56.7°N 52.5°W). Estimates of seasonal cycle (derived from all data in the time-series) have been removed from the observations.

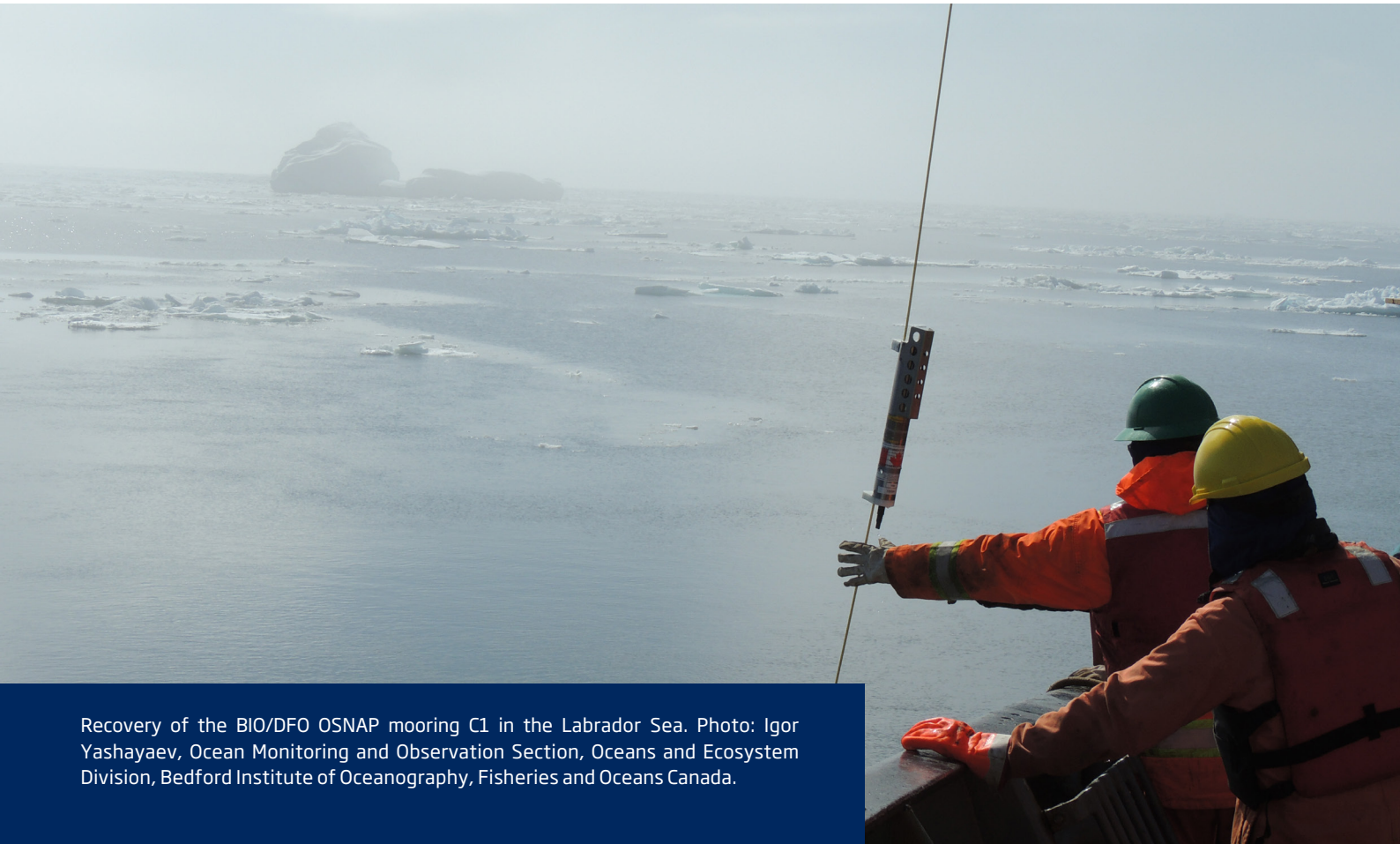

Recovery of the BIO/DFO OSNAP mooring C1 in the Labrador Sea. Photo: Igor Yashayaev, Ocean Monitoring and Observation Section, Oceans and Ecosystem Division, Bedford Institute of Oceanography, Fisheries and Oceans Canada.

4.3 NEWFOUNDLAND-LABRADOR SHELF

E. Colbourne

This region is situated on the western side of the Labrador Sea, stretching from the Hudson Strait to the southern Grand Bank, and is dominated by shallow banks, cross-shelf channels or saddles, and deep marginal troughs near the coast. Circulation is dominated by the south-flowing Labrador Current, which brings cold freshwater from the north as well as sea ice and icebergs to southern areas of the Grand Banks.

Hydrographic conditions are determined in part by the strength of winter atmospheric circulation over the Northwest Atlantic (NAO), advection by the Labrador Current, cross-shelf exchange with warmer continental slope water, and bottom topography. Superimposed are large seasonal and interannual variations in solar heat input, sea ice cover, and storm-forced mixing. The resulting water mass on the shelf exhibits large annual cycles with strong horizontal and vertical temperature and salinity gradients.

The annual NAO index (December–February, Iceland–Azores), a key indicator of climate conditions in the Northwest Atlantic, decreased from the record high of 2015, but remained in a positive phase at 0.3 s.d. above normal and, as a result, Arctic air outflow to the Northwest Atlantic decreased in most areas from the previous year. Annual air temperatures over Labrador at Cartwright (Figure 24) increased from 0.4°C (−0.3 s.d.) below normal in 2016 to 0.3°C (0.2 s.d.) above normal in 2017. Farther south at St John's, air temperature anomalies were near normal at +0.06°C (+0.1 s.d.). Sea ice extent on the Newfoundland–Labrador Shelf was lighter than normal (0.4 s.d.) in 2017 (Figure 23).

At the standard monitoring site off eastern Newfoundland (Station 27), the depth-averaged annual water temperature has experienced a decreasing trend over the past several years from a record high in 2011 when the temperature was +1.1°C (2.8 s.d.) above normal (Figure 25). In 2017, the water-column-averaged temperature at Station 27 was slightly below normal by −0.03°C (−0.1 s.d.), whereas salinity was significantly below normal by 1.6 s.d.

A robust index of ocean climate conditions in eastern Canadian waters is the extent of the cold intermediate layer (CIL; Figure 26) of < 0°C water overlying the continental shelf. This winter-cooled water remains isolated between the seasonally heated upper layer and the warmer shelf slope water throughout summer and early autumn. During the 1960s, when the NAO was well below normal and had the lowest value ever in the twentieth century, the volume of CIL water was at a minimum (warmer-than-normal conditions), and during the high NAO years of the early 1990s, the CIL volume reached near-record high values (colder-than-normal conditions). Since the late 1990s, as ocean temperatures increased, the area of CIL water experienced a downward trend that lasted until 2011. Since then, however, the CIL area has trended upwards and reached its highest level in 2015 since 1970 on the Grand Banks (2.2 s.d. above normal) during spring. In 2017, the CIL area was above normal off southern Labrador (+0.8 s.d.) and near normal (+0.07 s.d.) off eastern Newfoundland during summer.

A composite of climate data from the Northwest Atlantic, including various measures of meteorological, sea ice, water masses, and ocean temperature and salinity conditions, shows a warming trend that began in the mid-1990s, peaked in 2010, and has since decreased to mostly below normal (cold/fresh) conditions during the past four years. The 2015 value was the seventh lowest in 68 years of observations and the lowest value since 1993, while the 2017 value was the fifteenth lowest.

Ocean temperatures off Newfoundland and Labrador were near normal or slightly below normal in 2017.

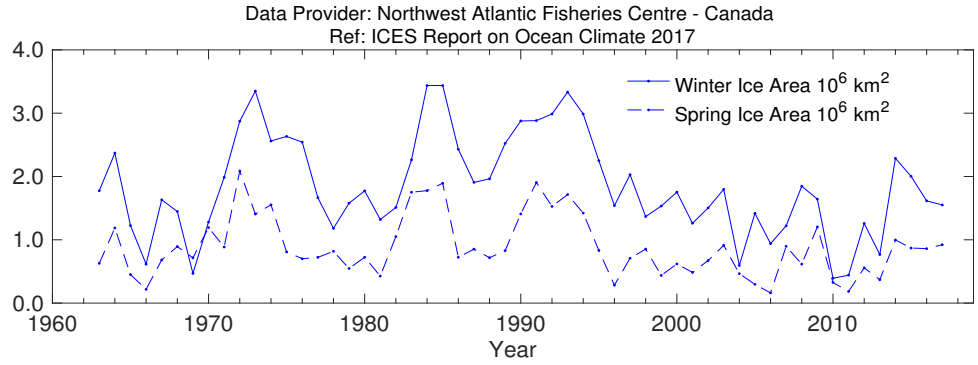

FIGURE 23.
Northwest Atlantic: Newfoundland-Labrador Shelf. Winter and spring sea ice areas off Newfoundland-Labrador between 45°N and 55°N.

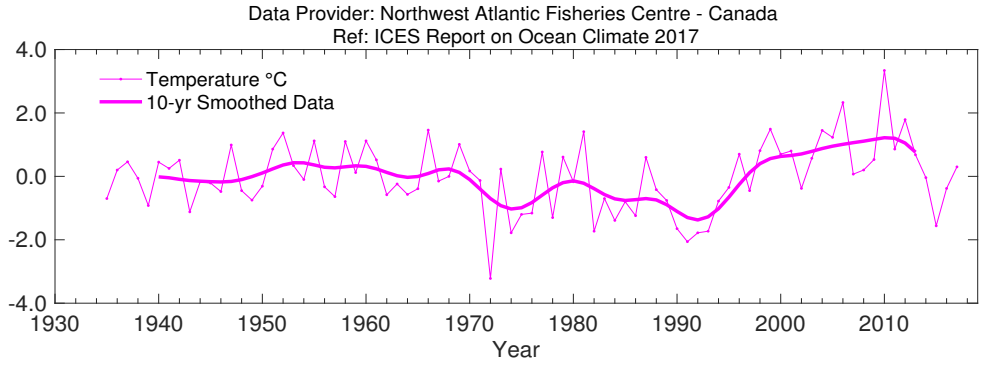

FIGURE 24.
Northwest Atlantic: Newfoundland-Labrador Shelf. Annual air temperature anomalies at Cartwright on the Labrador coast.

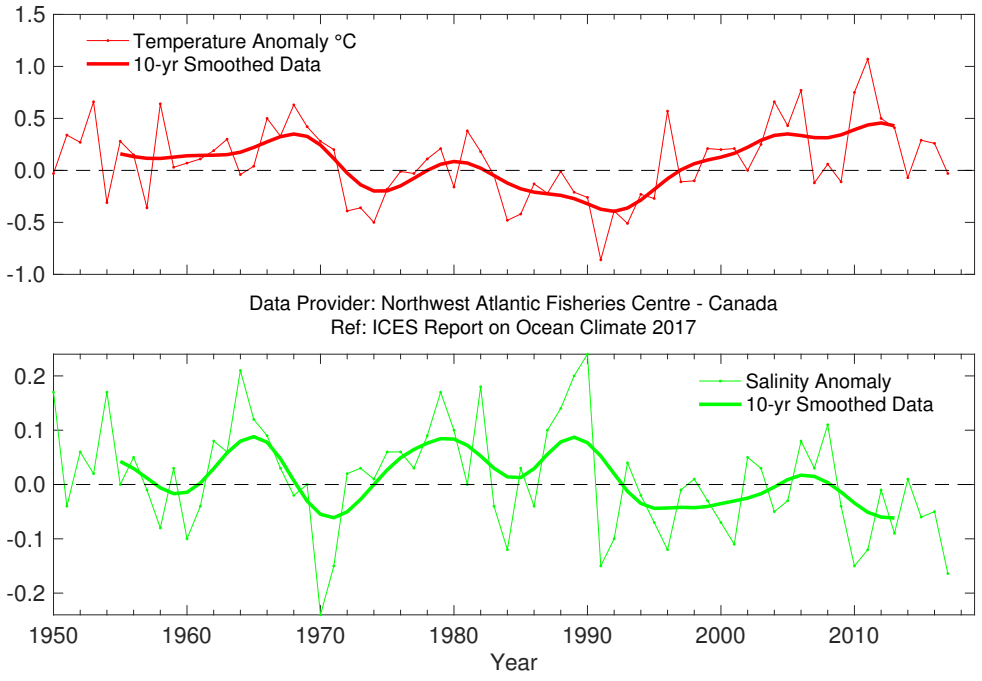

FIGURE 25.
Northwest Atlantic: Newfoundland-Labrador Shelf. Annual depth-averaged Newfoundland Shelf temperature (top panel) and salinity (middle panel) anomalies at Station 27 (47.55°N 52.59°W).

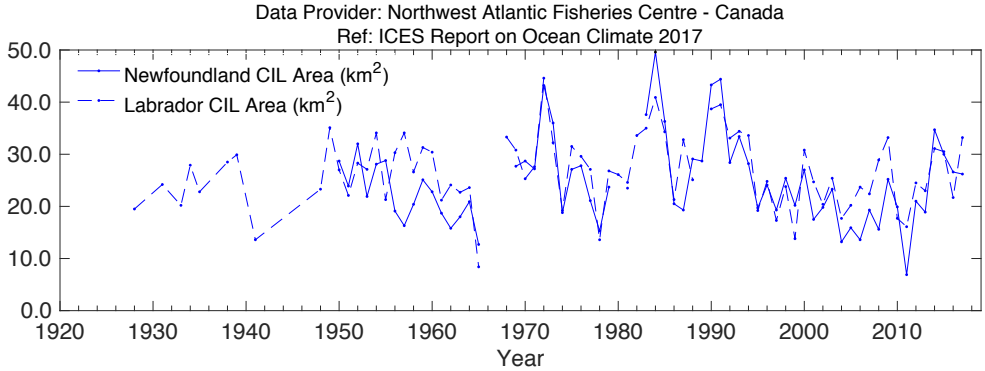

FIGURE 26.
Spatial extent of cold intermediate layer (CIL).

4.4 SCOTIAN SHELF

D. Herbert and R. Pettipas

The Scotian Shelf is the continental shelf off the coast of Nova Scotia and is identified as an LME. It is characterized by complex topography consisting of many offshore shallow banks and deep mid-shelf basins. It is separated from the Newfoundland Shelf in the northeast by the Laurentian Channel and borders the Gulf of Maine to the southwest. Surface circulation is dominated by a general flow toward the southwest, interrupted by a clockwise movement around the banks, and an anticlockwise movement around the basins, with the strengths varying seasonally.

Hydrographic conditions on the Scotian Shelf are determined by heat transfer between ocean and atmosphere, inflow from the Gulf of St Lawrence and the Newfoundland Shelf, and exchange with offshore slope waters. Water properties have large seasonal cycles and are modified by freshwater run-off, precipitation, and melting of sea ice. Temperature and salinity exhibit strong horizontal and vertical gradients that are modified by diffusion, mixing, currents, and shelf topography.

In 2017, annual mean air temperature over the Scotian Shelf (Figure 28), represented by Sable Island observations, was +0.8°C (+1.2 s.d.) above the long-term mean (1981–2010). The amount of sea ice on the Scotian Shelf in 2017, as measured by the total area of ice seaward of Cabot Strait between Nova Scotia and Newfoundland from January to April, was 5700 km^2, well below the long-term mean coverage of 32 000 km^2 (Figure 27). After an above-average year in 2015, conditions returned to those similar to the 2010–2013 period, which had extremely low coverage.

Topography separates the northeastern Scotian Shelf from the rest of the shelf. In the northeast, the bottom tends to be covered by relatively cold water (2–5°C), whereas the basins in the central and southwestern regions typically have bottom temperatures of 6–10°C. The origin of the latter is the offshore slope waters, whereas water in the northeast comes principally from the Gulf of St Lawrence. The interannual variability of the two water masses differs.

Measurements of temperatures at 100 m at the Misaine Bank Station capture the changes in the northeast (Figure 29). They revealed well above-average temperatures in 2017, +0.4°C (+0.7 s.d.), and below normal for salinity, −0.13 (−0.4 s.d.). The deep Emerald Basin anomalies represent the slope water intrusions onto the shelf that are subsequently trapped in the inner basins. In 2017, the 250 m temperature and salinity anomalies were well above normal, +1.5°C (+1.8 s.d.) and +0.23 (+1.6 s.d.), respectively, slightly less than the record in 2016 (Figure 30). Model simulations of the region showed a large flux of warm salty water from the slope region.

Ocean temperatures and salinity in the deep basins of the Scotian Shelf were well above normal in 2017, reflective of warm salty conditions in the slope region offshore.

The Vestmannaeyjar Islands, Iceland.
Photo: Penny Holliday, National Oceanography Centre, UK.

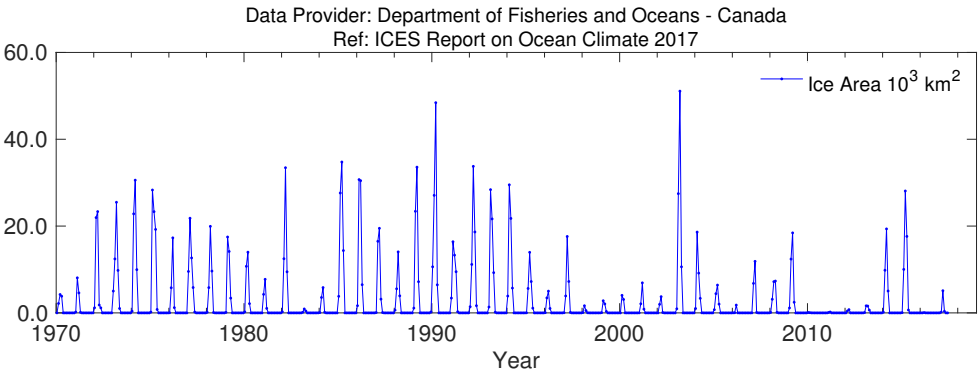

FIGURE 27.
Northwest Atlantic: Scotian Shelf. Monthly means of ice area seaward of Cabot Strait.

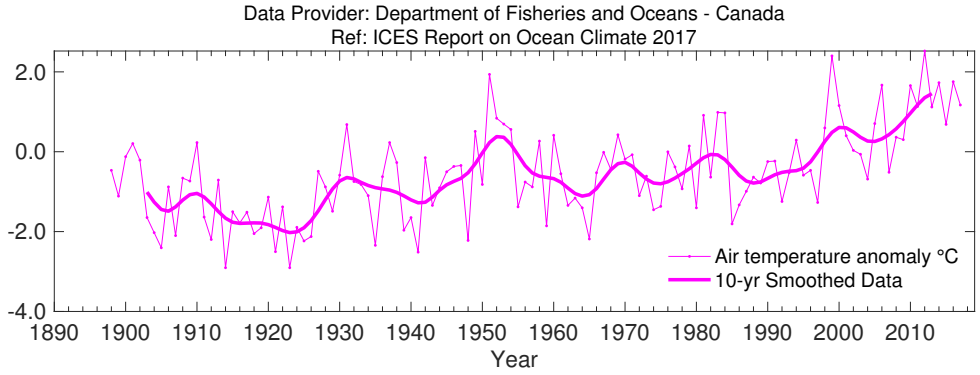

FIGURE 28.
Air temperature anomalies at Sable Island on the Scotian Shelf

Recovery of the BIO/DFO OSNAP mooring C1 in the Labrador Sea. Photo: Igor Yashayaev, Ocean Monitoring and Observation Section, Oceans and Ecosystem Division, Bedford Institute of Oceanography, Fisheries and Oceans Canada.

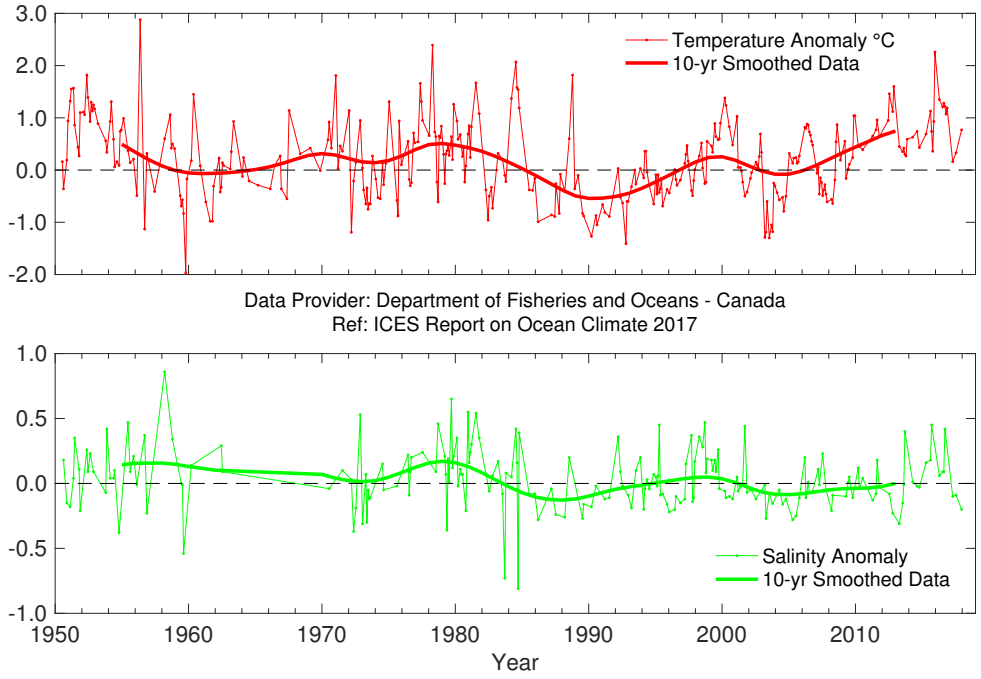

FIGURE 29.
Near-bottom temperature (upper panel) and salinity (lower panel) anomalies at Misaine Bank (100 m).

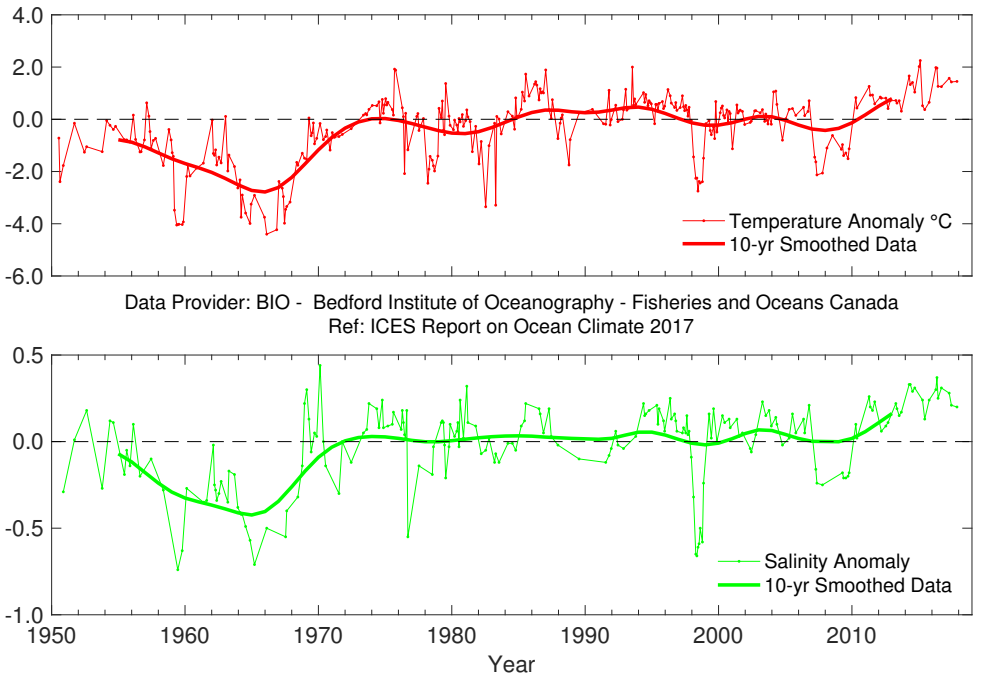

FIGURE 30.
Near-bottom temperature (upper panel) and salinity (lower panel) anomalies in the central Scotian Shelf (Emerald Basin, 250 m).

4.5 NORTHEAST US CONTINENTAL SHELF

P. Fratantoni

The Northeast US continental shelf extends from the southern tip of Nova Scotia, Canada, southwestward through the Gulf of Maine and the Mid-Atlantic Bight to Cape Hatteras, North Carolina (Figure 31). Contrasting water masses from the Subtropical and Subpolar gyres influence the hydrography in this region. Located at the downstream end of an extensive interconnected coastal boundary current system, the Northeast US continental shelf is the direct recipient of cold/fresh Arctic-origin water, accumulated coastal discharge, and ice melt that has been advected thousands of kilometers around the boundary of the subpolar North Atlantic. Likewise, subtropical water masses, advected by the Gulf Stream, slope currents, and associated eddies, also influence the composition of water masses within this shelf region. The western boundary currents of the Subpolar and Subtropical gyres respond to variations in basin-scale forcing through changes in position, volume transport, and/or water mass composition, and it is partly through these changes that basin-scale climate variability is communicated to the local Northeast US continental shelf. Shelf-wide, hydrographic conditions have been monitored annually in this region since 1977 as part of quarterly ecosystem monitoring and twice-yearly bottom-trawl surveys conducted by the US National Marine Fisheries Service, Northeast Fisheries Science Center.

Observations indicate that the entire Northeast US shelf was significantly warmer in 2017 than the mean for the period 1981–2010. Annually, 0–30 m temperatures were 0.9–1.2°C warmer than normal everywhere (Figures 33–37), with the largest anomalies observed in the Mid-Atlantic Bight (Figure 33 and Figure 34) and eastern Gulf of Maine (Figure 36). Of the seasons sampled, warming was most pronounced during autumn in the northern Mid-Atlantic Bight and Gulf of Maine and during winter on Georges Bank (e.g. Figure 38), where regional temperature anomalies exceeded 1 s.d. Extremely warm conditions were also observed near the bottom across the entire region, with anomalies exceeding those at the surface in most seasons (not shown). During autumn, the bottom temperature measured more than 1 s.d. above normal across the entire Northeast US shelf, while similarly large anomalies were observed near bottom in the eastern Gulf of Maine year-round. The exception was during March and April in the northern Mid-Atlantic Bight, where cold anomalies were observed near the bottom.

In 2017, surface waters in the upper 30 m were more saline than normal everywhere on the Northeast US shelf except in the western Gulf of Maine (Figure 35). The largest positive anomalies were observed in the northern Mid-Atlantic Bight (Figure 34). Seasonally, large positive anomalies (exceeding 1 s.d.) were observed during February and March throughout the Mid-Atlantic Bight, on Georges Bank during February and April (Figure 38), and during autumn in the eastern Gulf of Maine. Near-bottom waters in the eastern Gulf of Maine were more saline than average year-round, while freshening was observed at the bottom in the western Gulf of Maine. Bottom water conditions were more seasonally variable in the southern Mid-Atlantic Bight (not shown).

Deep waters that enter the Gulf of Maine through the Northeast Channel represent one of the dominant water mass sources to the Gulf of Maine slope waters, (Mountain, 2012). These deep waters lying between 150 and 200 m are uninfluenced by seasonal atmospheric forcing. Annually, deep inflow to the Gulf of Maine was very warm and slightly fresh in 2017 compared with the long-term mean (Figure 39). However, an exceedingly fresh (slightly cold) anomaly observed in June dominates this annual mean, whereas very warm and slightly salty conditions were observed in the deep channel throughout the remainder of the year.

Waters on the Northeast US shelf were warmer and more saline than normal during 2017.

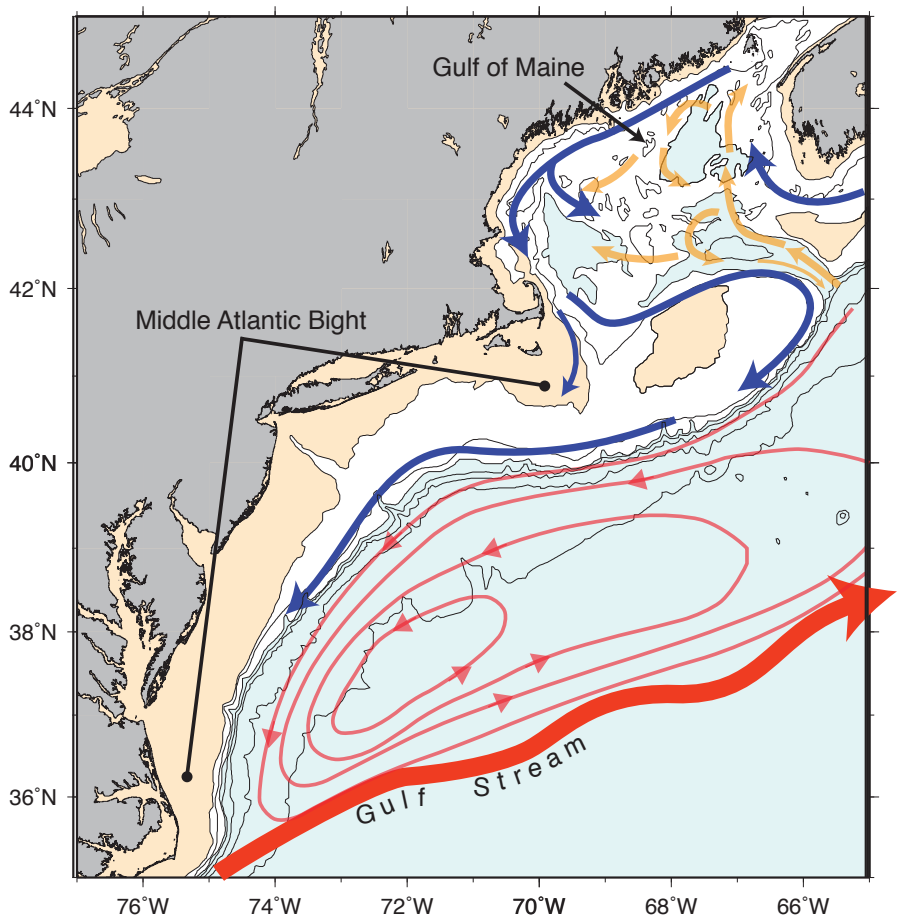

FIGURE 31.
Circulation schematic for the Northeast US shelf region. Blue arrows represent shelf water circulation and orange arrows represent deeper slope-water circulation pathways. Water depths deeper than 200 m are shaded blue. Water depths shallower than 50 m are shaded tan.

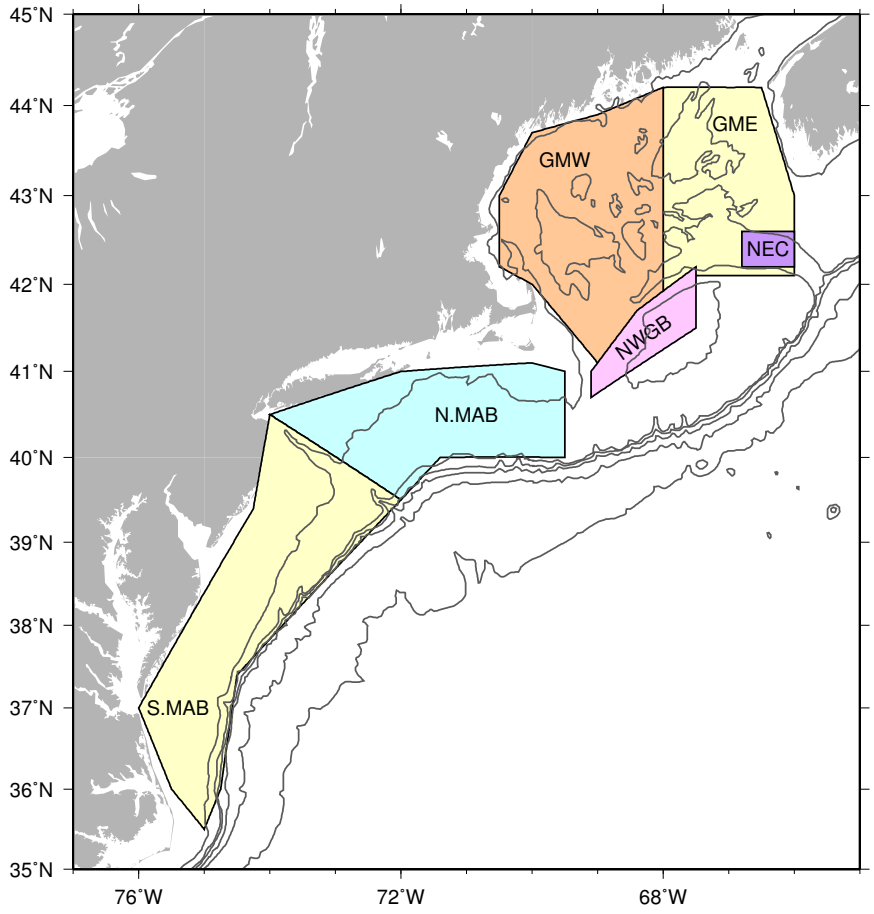

FIGURE 32.
Northeast US continental shelf. There are six regions within which CTD observations are used to compute regional average time-series: eastern and western Gulf of Maine (GME and GMW); northern and southern Mid-Atlantic Bight (N.MAB and S.MAB); Northeast Channel (NEC); Northwest Georges Bank (NWGB). The 50, 200, 500, 1000, 2000, and 3000 m isobaths are also shown.

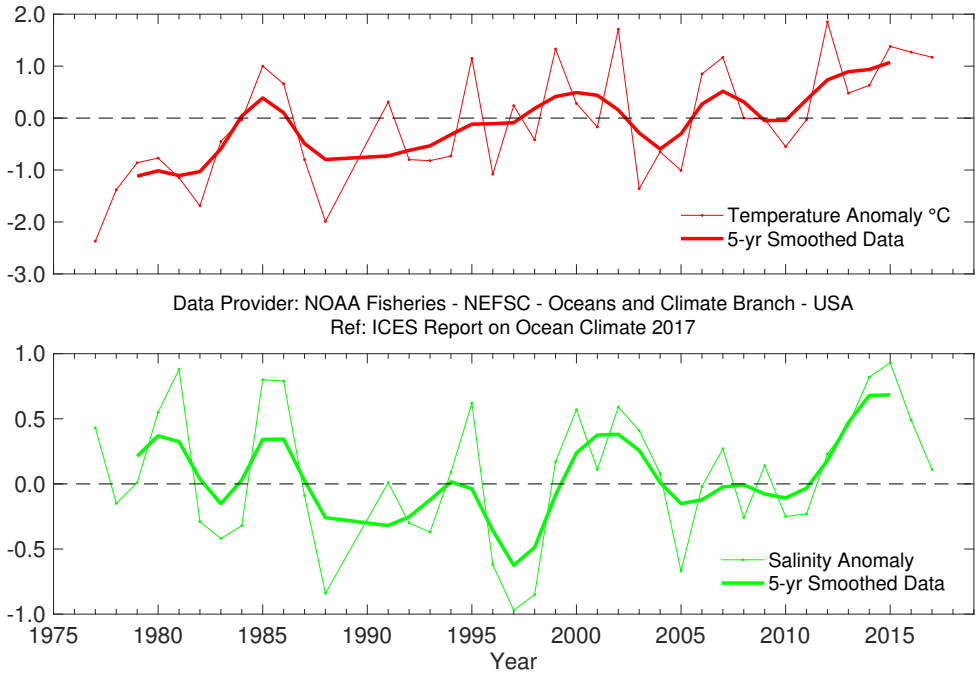

FIGURE 33.
Time-series plots of 0–30 m averaged temperature anomaly (upper panel) and salinity anomaly (lower panel) in the region between Cape Hatteras, North Carolina and Hudson Canyon. Anomalies are calculated relative to the period 1981–2010 using hydro-graphic data from shelf-wide surveys.

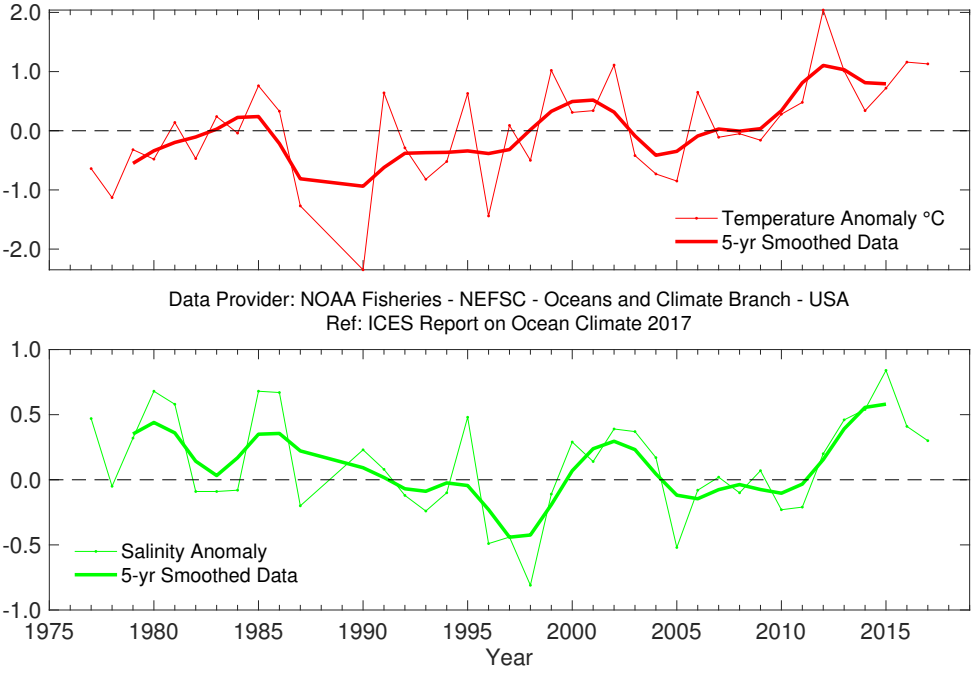

FIGURE 34.
Time-series plots of 0–30 m averaged temperature anomaly (upper panel) and salinity anomaly (lower panel) in the region between Hudson Canyon and Cape Cod, Massachusetts. Anomalies are calculated relative to the period 1981–2010 using hydrographic data from shelf-wide surveys.

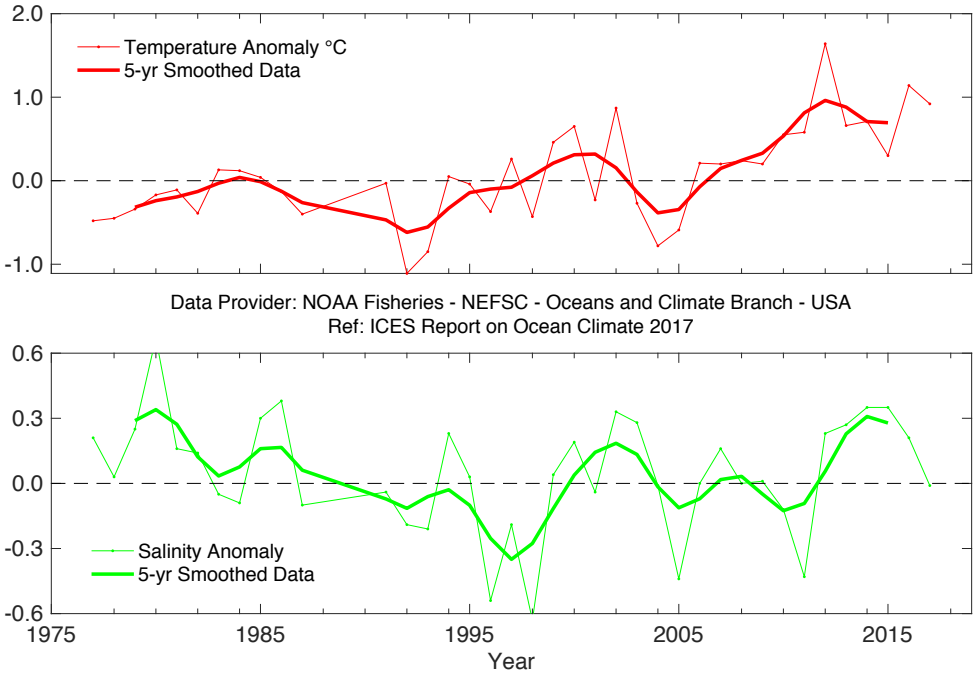

FIGURE 35.
Time-series plots of 0–30 m averaged temperature anomaly (upper panel) and salinity anomaly (lower panel) in the western Gulf of Maine. Anomalies are calculated relative to the period 1981–2010 using hydrographic data from shelf-wide surveys.

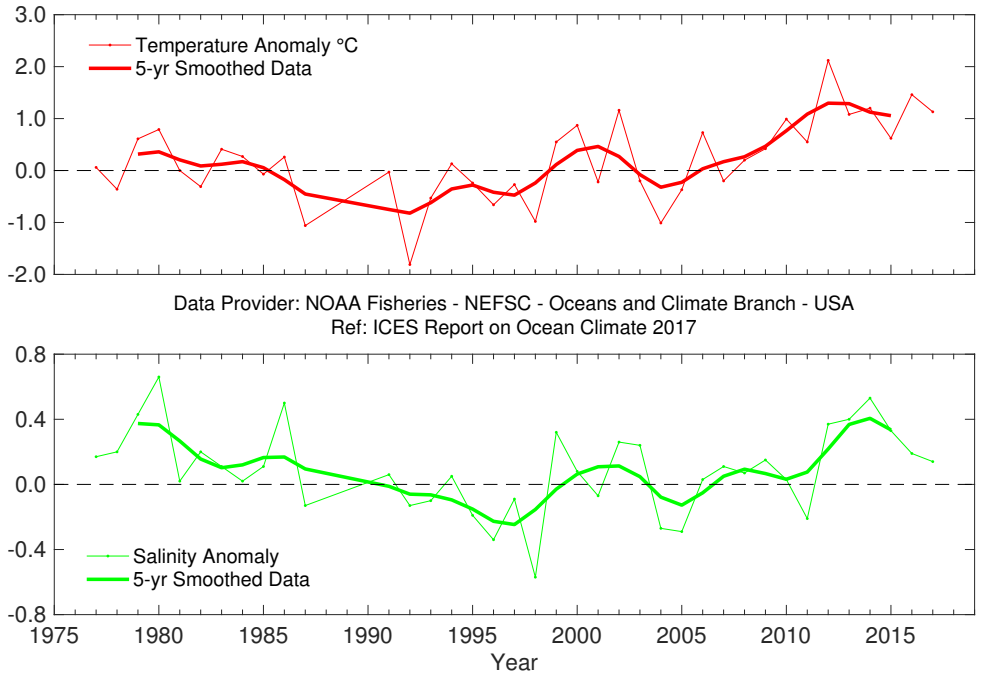

FIGURE 36.
Time-series plots of 0–30 m averaged temperature anomaly (upper panel) and salinity anomaly (lower panel) in the eastern Gulf of Maine. Anomalies are calculated relative to the period 1981–2010 using hydrographic data from shelf-wide surveys.

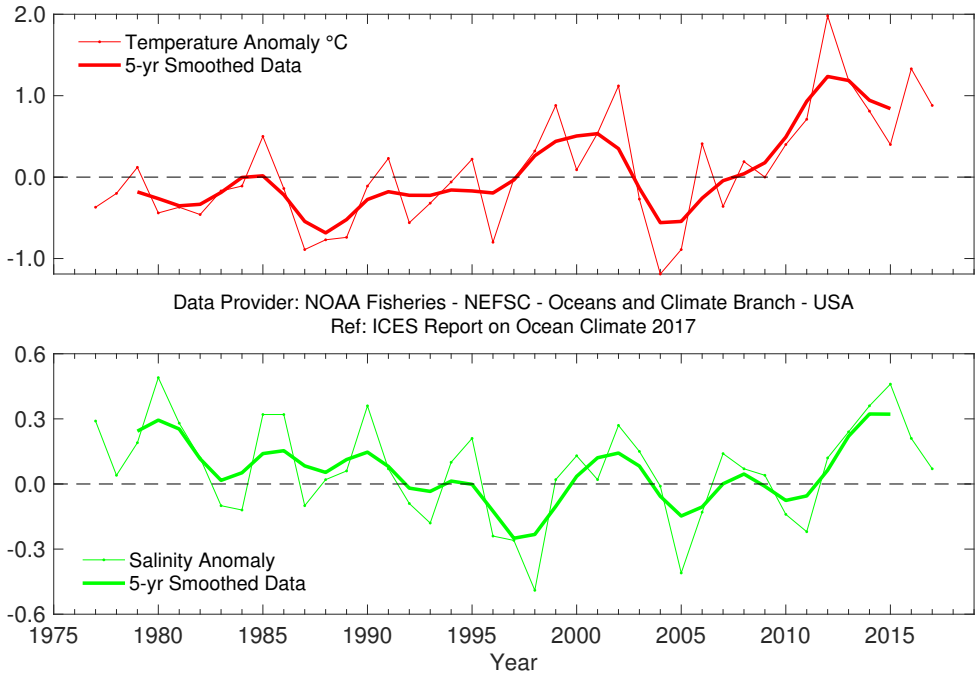

FIGURE 37.
Time-series plots of 0–30 m averaged temperature anomaly (upper panel) and salinity anomaly (lower panel) on George Bank. Anomalies are calculated relative to the period 1981–2010 using hydrographic data from shelf-wide surveys.

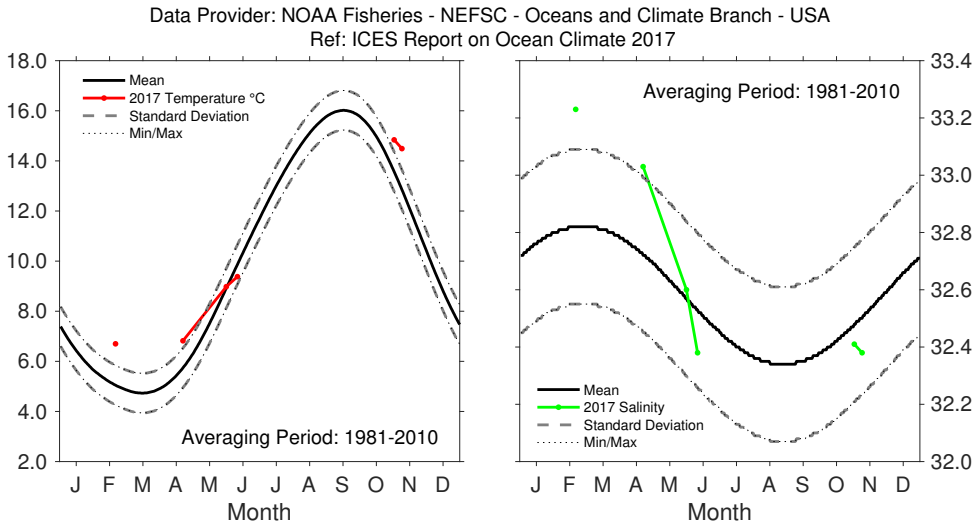

FIGURE 38.
2017 temperature (left) and salinity (right) averaged over 0–30 m at northwest Georges Bank, relative to the annual cycle calculated 1981–2010. The envelope corresponding to the monthly range and 1 s.d. are shown.

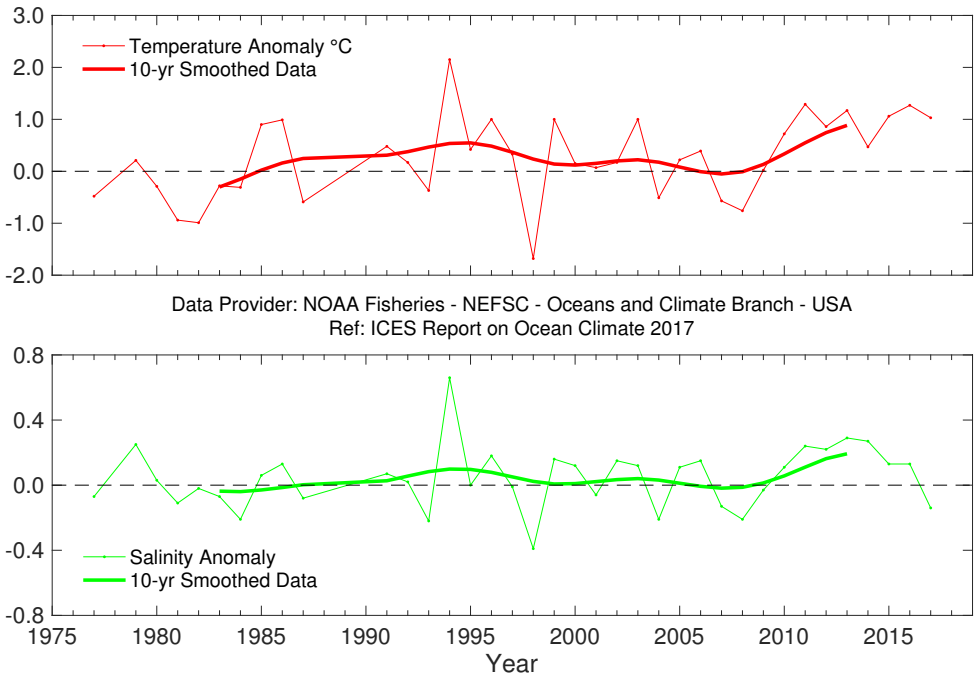

FIGURE 39.
Time-series plots of 150–200 m averaged temperature anomaly (upper panel) and salinity anomaly (lower panel) in the Northeast Channel. Anomalies are calculated relative to the period 1981–2010 using hydrographic data from shelf-wide surveys.

Recovery of the BIO/DFO OSNAP mooring C2 in the Labrador Sea. Photo: Igor Yashayaev, Ocean Monitoring and Observation Section, Oceans and Ecosystem Division, Bedford Institute of Oceanography, Fisheries and Oceans Canada.

4.6 ICELANDIC WATERS

H. Valdimarsson

The Iceland Shelf and Sea are identified as a NOAA LME and an ICES ecoregion. Iceland is at the meeting place of warm and cold currents which converge in an area of submarine ridges (Greenland-Scotland Ridge, Reykjanes Ridge, Kolbeinsey Ridge) that form natural barriers to the main ocean currents (Figure 40). The warm Irminger Current (6–8°C), a branch of the North Atlantic Current, flows from the south, and the cold East Greenland and East Icelandic currents (–1°C to 2°C) flow from the north. Deep and bottom currents in the seas around Iceland are principally the overflow of cold water from the Nordic seas and the Arctic Ocean over the submarine ridges into the North Atlantic.

Annual mean air temperatures for south (Reykjavik) and north (Akureyri) continue to be among the highest observed. The temperature of the AW to the south was lower than average, and salinity in this water was lower than it has been for over 40 years. Salinity and temperature to the north and east of Iceland were both well above average.

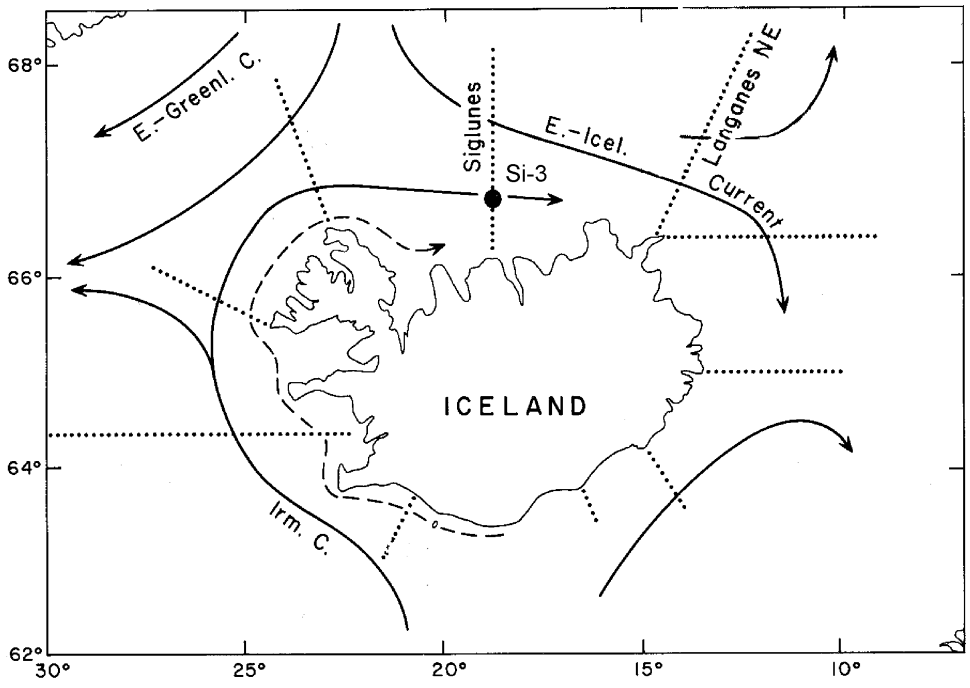

FIGURE 40.
Main currents and location of standard sections in Icelandic waters.

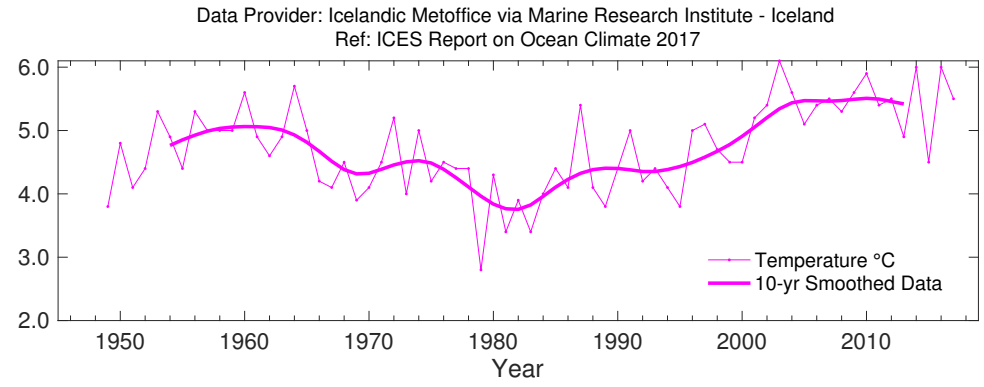

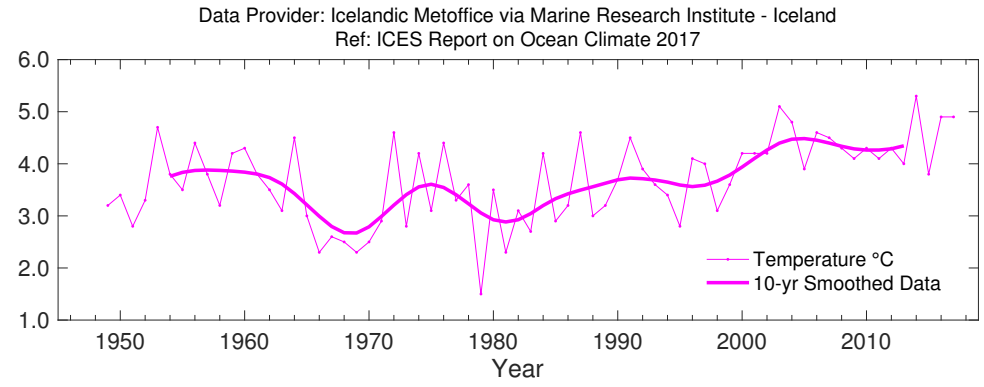

FIGURE 41.
Icelandic waters: Mean annual air temperature at Reykjavik (upper panel) and Akureyri (lower panel).

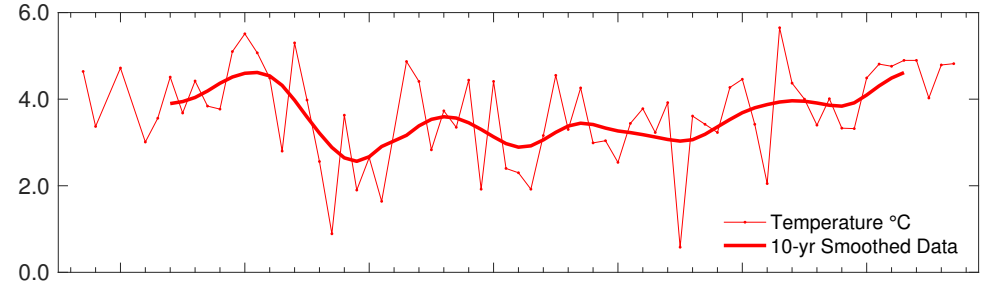

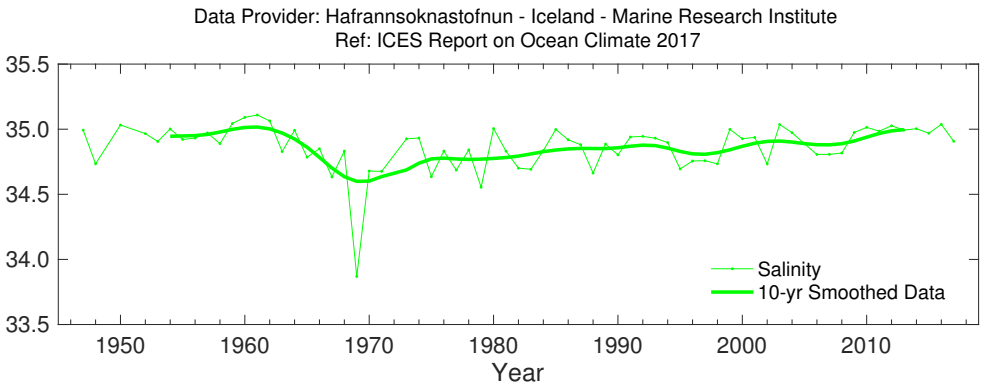

FIGURE 42.
Icelandic waters: Temperature (upper panel) and salinity (lower panel) at 50–150 m at Siglunes Stations 2–4 in northern Icelandic waters.

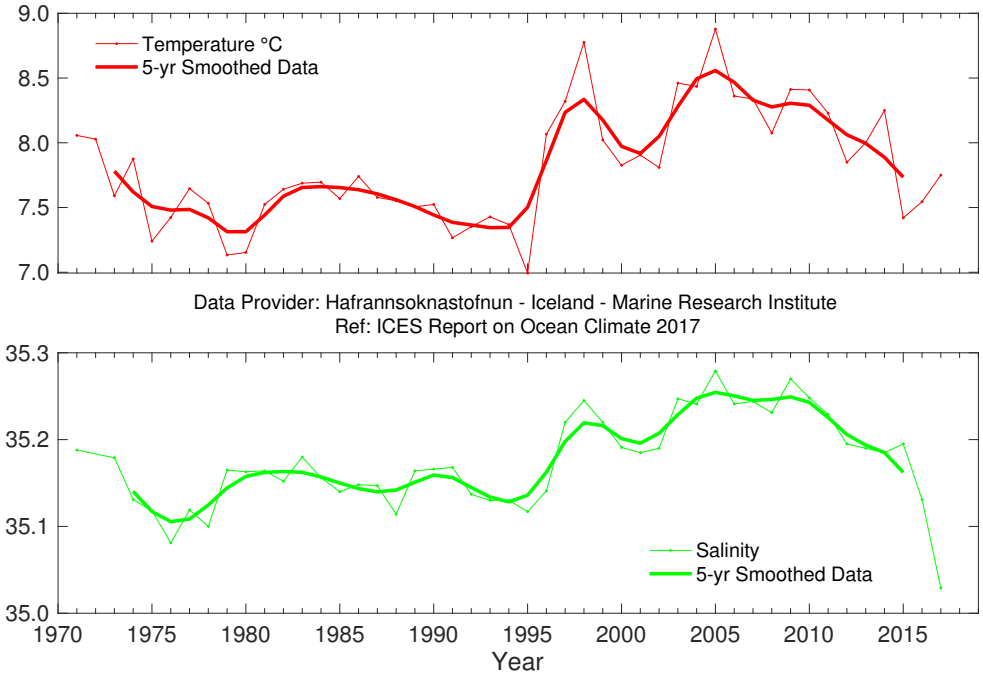

FIGURE 43.
Icelandic waters. Temperature (upper panel) and salinity (lower panel) at 0–200 m at Selvogsbanki Station 5 in southern Icelandic waters.

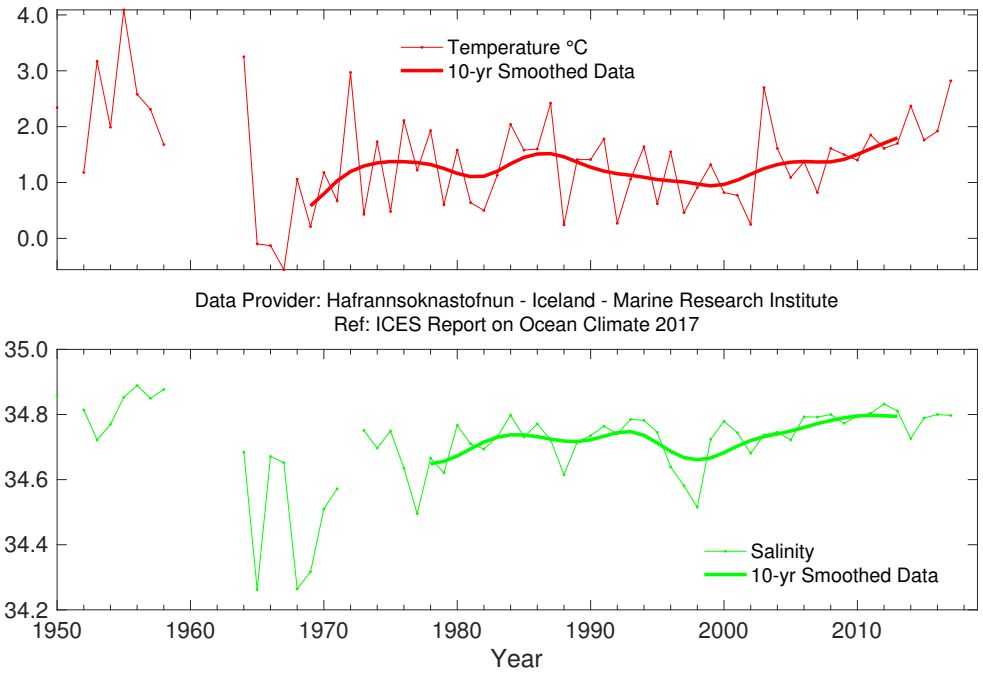

FIGURE 44.
Icelandic waters: Temperature (upper panel) and salinity (lower panel) at 0–50 m in the East Icelandic Current (Langanes Stations 2–6).

4.7 BAY OF BISCAY AND IBERIAN COAST

A. Fontán, C. González-Pola, and V. Valencia

The western Iberian coast is located at the northeastern edge of the Subtropical Anticyclonic Gyre, sometimes referred to as the intergyre region. It is characterized by weak upper ocean circulation with mean southward flow of few cm s^{-1} (e.g. Paillet and Mercier, 1997). The Bay of Biscay is considered an adjacent sea, with weak anticyclonic circulation (Pingree, 1993; van Aken, 2002). The area also encompasses the northern tip of the northwest African upwelling system. Coastal upwelling events dominate in spring and summer, and a geostrophic balanced poleward flow known as the Iberian Poleward Current develops in autumn and winter (Pingree and Le Cann, 1990). Regional modal waters that comprise the upper permanent thermocline are known as Eastern North Atlantic Central Waters (ENACW). Below this, Mediterranean Water (MW) spreads northwards from the Gulf of Cadiz, mostly as a slope current. Labrador water can be identified at ca. 1800 m, and the deep ocean is occupied by a mixture of cold polar waters known as North Atlantic Deep Water (NADW).

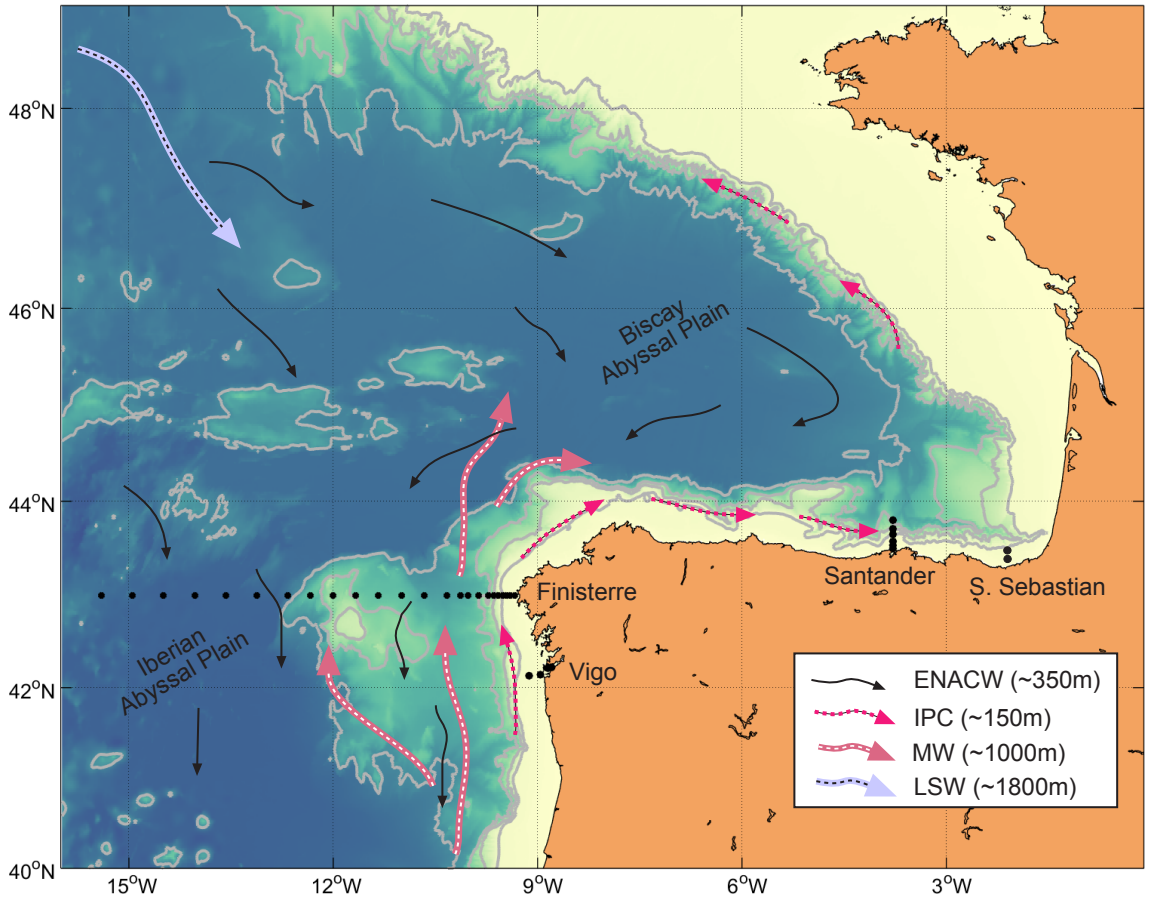

FIGURE 45.
Circulation schematic for northwest Iberian waters and the Bay of Biscay. Thin black arrows show the dominant southward flow of the upper ocean, mainly carrying Eastern North Atlantic Central Waters (ENACW). The Iberian Poleward Current (IPC) and Mediterranean Water (MW) pathways are also shown. Black dots represent the hydrographical stations, recording monthly at Vigo, Santander, and San Sebastian and 1–2 times per year in the Finisterre section.

From an atmospheric point of view, 2017 can be considered warm with respect to the long-term average in the Iberian waters and southern Bay of Biscay. Average air temperature exceeded 0.4°C relative to 1981–2010 in southern Bay of Biscay (Figure 46). The seasonal cycle was characterized by the prevalence of normal-to-warm or very warm conditions all year except for January and September, which were cold. In 2017, precipitation was normal-to-slightly dry, resulting from a combination of dry-to-normal conditions through October followed by very wet conditions during the last two months of the year. The continental run-off was exceptionally low, below the long-term average, –1 s.d. relative to 1981–2010.

SST responded to the local atmospheric forcing with the prevalence of average-to-warm or very warm conditions throughout the year. The annual SST anomaly, 0.60°C in 2017, was slightly above that of 2016 in the southern Bay of Biscay (Figure 47). The 0–30 m average at the outer station in Santander provided a similar temperature anomaly (0.52°C), which is a record high since the start of the series in 1993. Salinity from the same series was slightly above average after four consecutive years, with a negative anomaly (Figure 48). Near-surface waters, influenced by the development of winter mixed layers (up to 300 m), were saltier than in previous years, but still fresher than the long-term average, and temperatures continued to be above the long-term average. Section 5.2.6 describes the status of deeper waters in the region.

Overall ocean conditions were consistent with local atmospheric conditions (warm and normal-to-slightly dry), lacking any strong signature of influence by waters of southern origin.

Upper ocean temperatures continue to be warm, exceeding those in 2016. Fresh conditions present in 2013–2016 weakened in 2017, and salinity is now close to neutral.

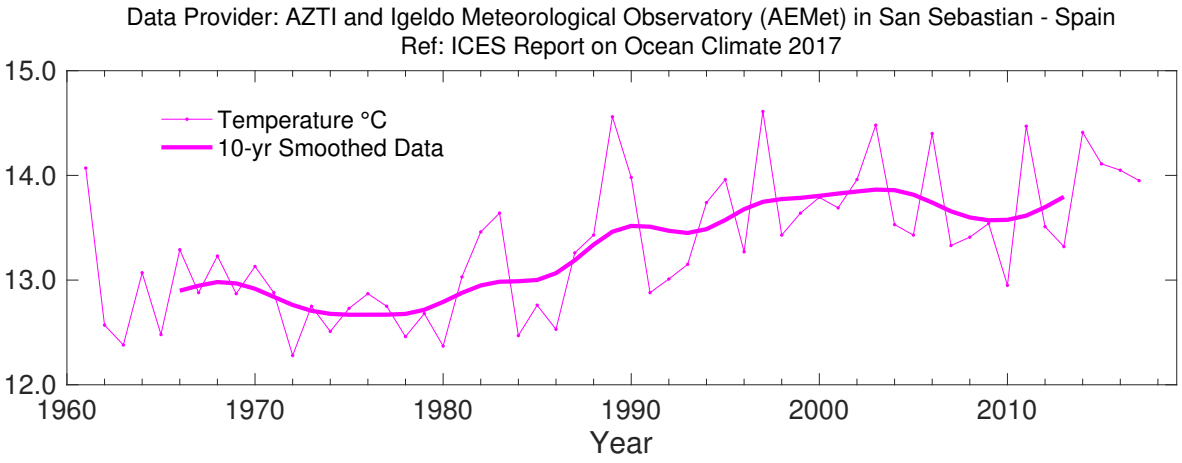

FIGURE 46.
Bay of Biscay and eastern North Atlantic. Air temperature at San Sebastian (43°18.50'N 2°2.37'W).

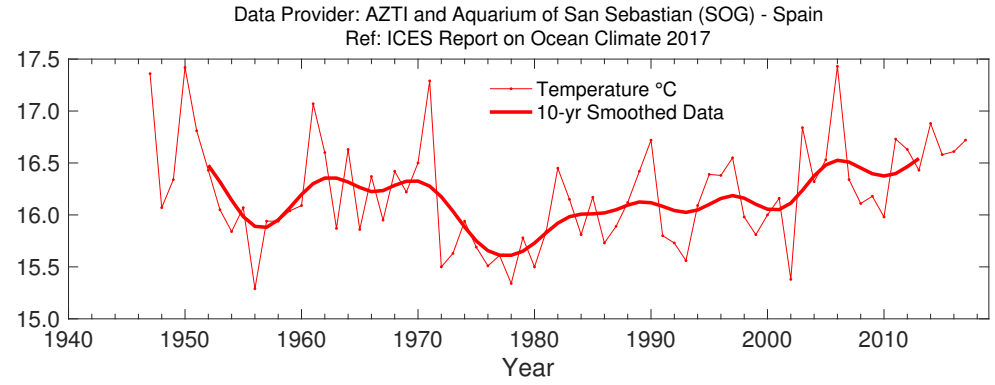

FIGURE 47.
Bay of Biscay and eastern North Atlantic. Sea surface temperature (SST) at San Sebastian (43°18.50'N 2°2.37'W).

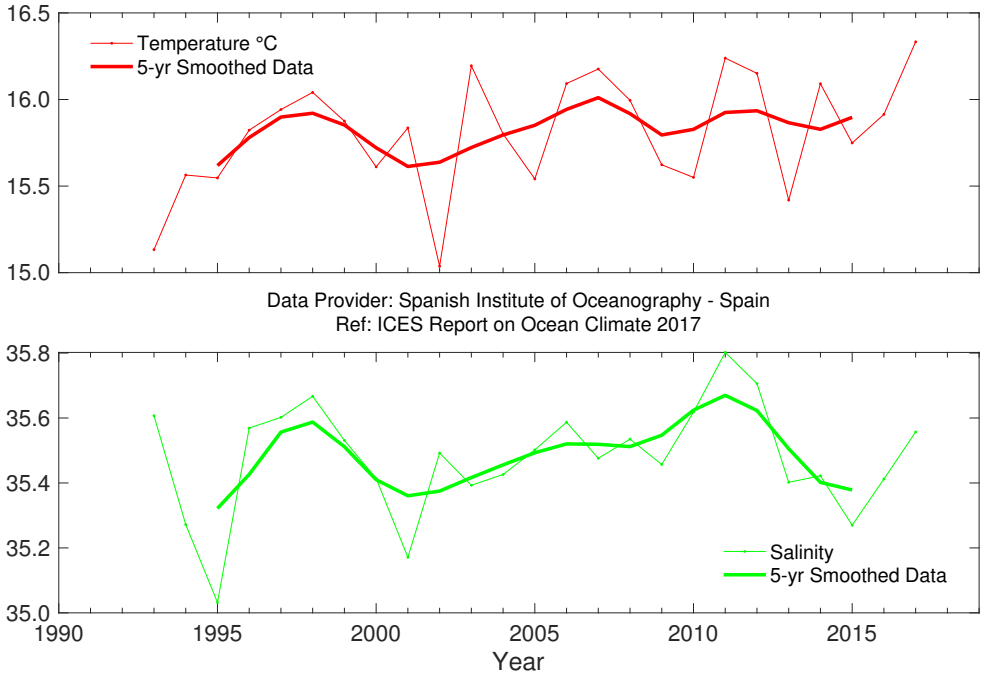

FIGURE 48.
Bay of Biscay and eastern North Atlantic. Temperature (upper panel) and salinity (lower panel) at Santander Station 6, 5-30 m (43°42.50'N 3°47.00'W).

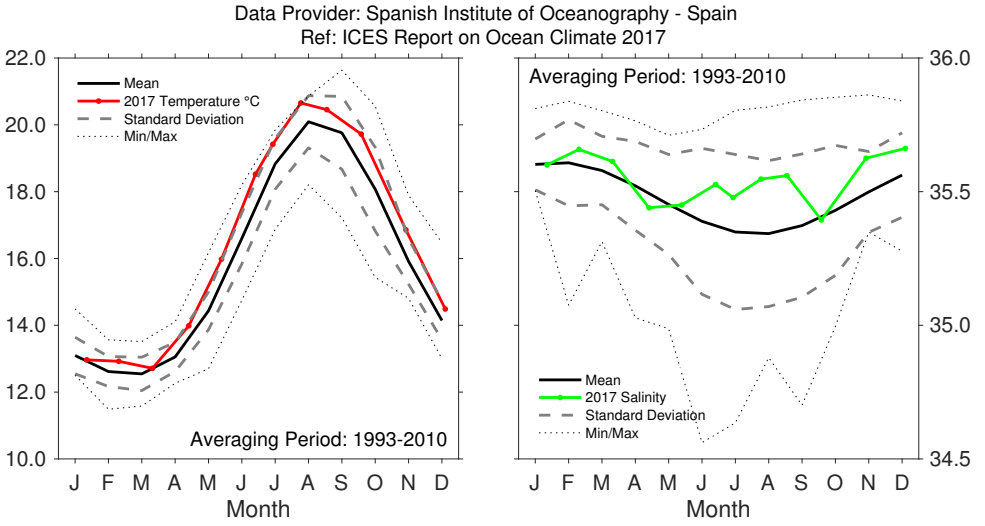

FIGURE 49,
Bay of Biscay and eastern North Atlantic. 2017 monthly temperature (left panel) and salinity (right panel) at Santander Station 6, 10 m (43°42.50'N 3°47.00'W).

4.8 GULF OF CADIZ

R. Sánchez-Leal

The Gulf of Cadiz is located southwest of the Iberian Peninsula where the Atlantic Ocean and the Mediterranean Sea connect through the Strait of Gibraltar. Here, a two-layered inverse estuarine circulation governs water exchange. Mediterranean Water (MW) flows into the Gulf of Cadiz beneath the AW that flows into the Mediterranean Sea. Surface circulation is governed by this exchange.

Dominant features include: (i) the baroclinic Gulf of Cadiz Current that advects relatively fresh and cool waters from the Portuguese Coastal Transition Zone (CTZ) to feed the Atlantic Inflow (AI) into the Mediterranean Basin; (ii) the meridional branch of the Azores Current, a largely barotropic flow that brings warmer more saline AW to supplement the AI into the Mediterranean; (iii) an inshore current system linked with coastal runoff like the Guadalquivir River plume; and (iv) the Trafalgar cyclonic cell, an upwelling hot spot generated by tidal stirring over the Trafalgar Banks.

The subsurface circulation is driven by Mediterranean Overflow Water, a branched, warm, saline, dense gravity current attached to the seabed that follows the intricate bottom topography (Figure 50).

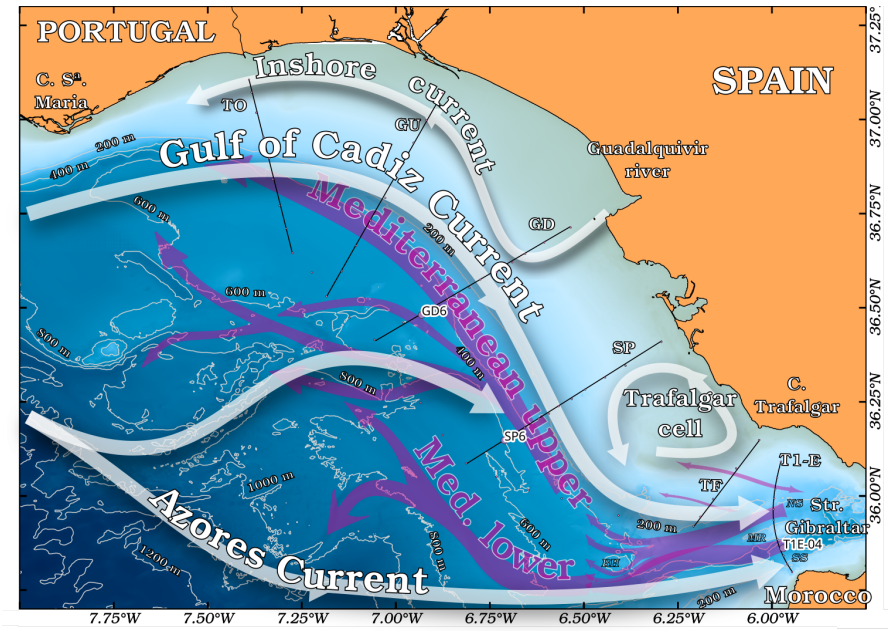

FIGURE 50.
Circulation schematic for the Gulf of Cadiz. White arrows show the surface circulation. Cyan arrows show the subsurface circulation. Also included are the STOCA project standard sections (black lines) and fixed oceanographic station under the responsibility of the Spanish Institute of Oceanography, Cadiz, whose data are presented in this report (GD6 and SP6). Puertos del Estado provides data from a weather buoy located at GD6.

Both air temperatures and SSTs in the Gulf of Cadiz show a statistically significant warming trend of about 0.31°C per decade over the last two decades. The smoothed time-series suggests the existence of interannual variability, with major departures in 2009, when temperatures were colder than average, and 2011, when these were anomalously warm. Temperatures during 2016/2017 were also higher than average. A relative maximum was observed by the end of 2016, and temperatures exhibited a slight decrease over 2017. It seems that 2018 is the first year of a cooler-than-average phase.

Apart from surface layers that are strongly influenced by fluctuations of meteorological origin, observations sug-

gest seasonal and longer-term variability patterns at all depths. In 2017, near-surface waters (0–50 m) were colder (about –0.3°C) and fresher (0.04) than the 2009–2017 mean. On the contrary, waters below 50 m were warmer than average (0.1–0.3°C). In fact, the ENACW was anomalously warm in 2017 (the warmest year of the time-series). The water column down to 350 m was less saline than the previous year (about 0.06 fresher than the mean), whereas the MOW was colder and less saline than average.

During 2009–2010, surface waters (upper 50 m of the water column) have shown significant warming. On the contrary, ENACW (50–350 m) is cooling (about 0.3°C per decade) and freshening (0.1 per decade). In the upper MOW, (350–530 m), temperature and salinity between 350–420 m and salinity between 450–540 m are increasing. Below 530 m, the deeper MOW exhibits a significant freshening with no associated significant warming.

In 2017, the Gulf of Cadiz featured cooler upper waters, warmer and more saline Eastern North Atlantic Central Waters, and colder Mediterranean Overflow Water (MOW).

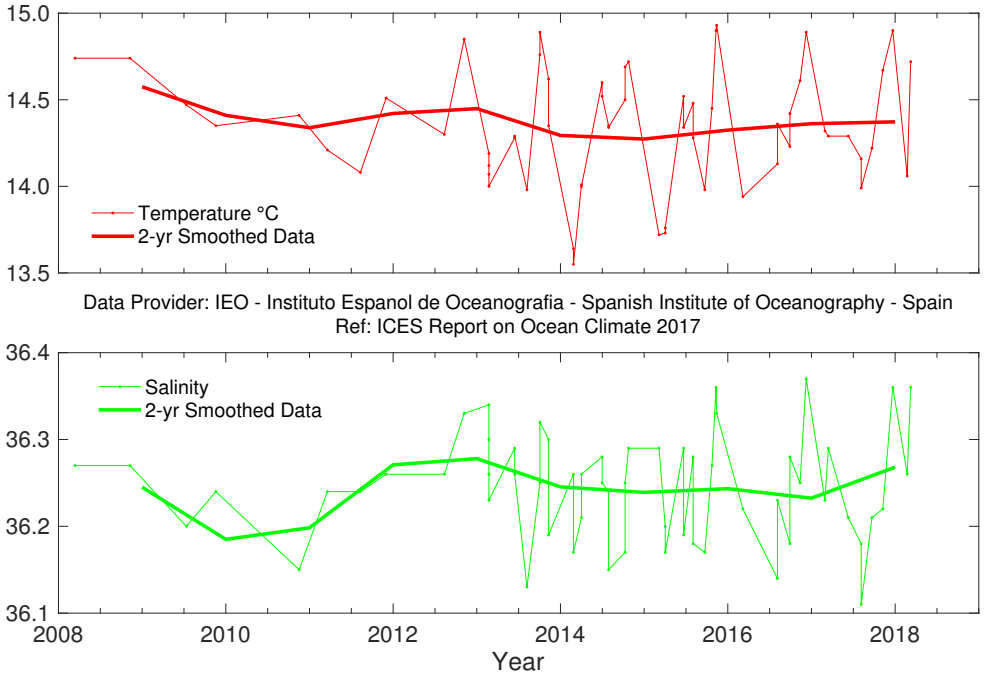

FIGURE 51.
Gulf of Cadiz. Potential temperature (upper panel) and salinity (lower panel) for the whole 600 m water column at the Station SP6 (36.14°N 6.71°W) of the STOCA program.

4.9 CANARY BASIN

P. Vèlez-Belchí

The Canary Basin sits at the boundary between the oceanic waters of the Subtropical Atlantic Gyre and the upwelling waters from the Canary Current Large Marine Ecosystem (CCLME) off the coast of northwest Africa. Since the early 2000s, the Canary Islands archipelago region has been monitored by the Spanish Institute of Oceanography (Tel *et al.*, 2016): the oceanic waters west of Lanzarote and the Coastal Transition Zone (CTZ) of the upwelling region of the Canary Current Large Marine Ecosystem (Stations 11–23 and 1–10, respectively, Figure 52).

The south-flowing Canary Current and the Canary Upwelling Current, associated with the upwelling front (Figure 50), influence the upper levels. The slowly propagating tongue of Mediterranean Water and the slope current known as the Canary Intermediate Poleward Current influence the intermediate levels (Hernández-Guerra *et al.*, 2017; Vèlez-Belchí *et al.*, 2017).

The waters above the seasonal thermocline are characterized on the θ/S diagram by scattered temperature and salinity values due to sea-sonal heating and evaporation. These waters, considered surface waters, occupy the upper 300 m in the oceanic region and the upper 100 m in the stations influenced by the coastal upwelling. Beneath the seasonal thermocline and through the permanent thermocline, roughly 300–700 m, is the North Atlantic Central Waters (NACW). These waters are character-ized on the θ/S diagram by an approximately straight-line relationship between potential temperature (11.4°C < θ < 14.9°C) and salinity (35.6 < S < 36.1). At intermediate levels, roughly 700–1200 m, two distinct water masses are found in the Canary Islands region: the fresher (S < 35.3) and slightly lighter Antarctic Interme-diate Waters (AAIW), and the saltier (S > 35.4) and heavier Mediterranean Waters (MW).

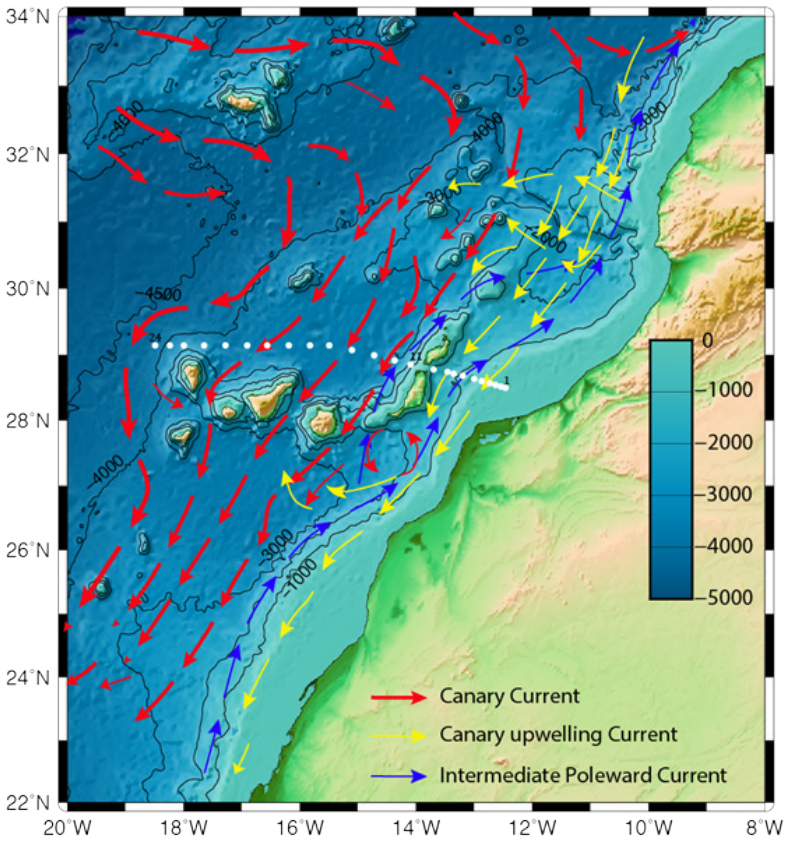

FIGURE 52.
Circulation schematic for the Canary Basin. Red arrows show the southward Canary Current carrying mainly NACW and intermediate waters. Yellow arrows show the Canary Upwelling Current that flows in the thermocline waters. The white dots represent the distribution of 24 hydrographic stations sampled in the Canary Islands archipelago region since 1997. Stations 1–10 are used to estimate changes in the CTZ and, west of Lanzarote, Stations 11–24, the oceanic waters.

Following the trend initiated in 2015, there was a slight decrease during 2017 in the warming and an increase in salinity compared to previous years.

Between the 1990s and the early 2000s, there was a decrease in temperature and salinity of all upper-layer waters. In the mid-2000s, there followed a marked increase in both temperature and salinity, which peaked in 2014 in the hottest and most saline year on record. Since 2015, both temperature and salinity have decreased; at the end of 2017, mean temperature and salinity were similar to those observed in the late 1990s (Vèlez-Belchí *et al*., 2015).

In the depth stratum that characterizes the NACW waters (200–800 dbar), there is an overall statistically significant warming of 0.12 ± 0.07°C decade^{-1} and an increase in salinity of 0.016 ± 0.012 per decade^{-1} (Figure 53). The overall increase in temperature and salinity almost compensate in density, confirming that the observed trends are due to deepening of the isoneutral surfaces rather than changes along the isoneutral surfaces. This overall increase in salinity and temperature for the NACW waters was also observed in the CTZ, although with slightly smaller values for the trend due to the influence of upwelling. There is a higher variability of the CTZ due to the proximity of the upwelling region and the frequent intrusions of upwelling filaments. For the same reason, uncertainty is higher in the trend estimates.

Surface waters in the CTZ show a non-statistically significant cooling of −0.33 ± 0.49°C decade^{-1}, and a non-statistically significant decrease in salinity of −0.059 ± 0.069 decade^{-1}, both coherent with an increase in upwelling in the CCLME. Upwelling in the CCLME continues to strengthen; 2015 was the coolest and freshest year on record for surface waters influenced by the upwelling. SSTs from satellite observations corroborate changes in the upwelling regime inferred from the *in situ* observations, with different areas showing increases in upwelling. However, the magnitude of the observed trend in the satellite SST is different, probably due to the thin layer of ocean that the satellite observes.

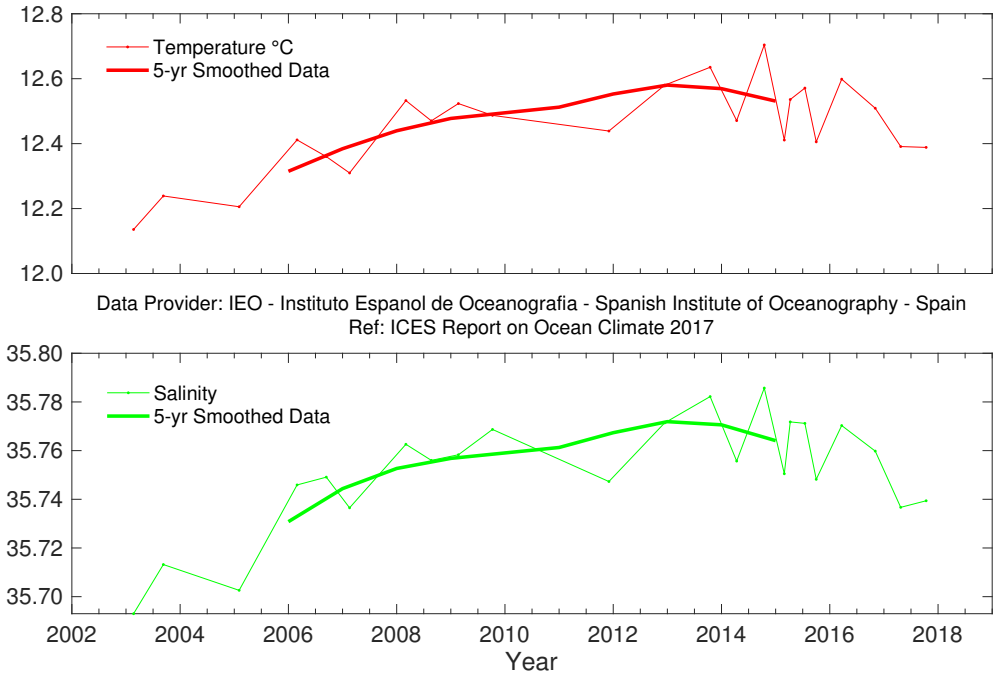

FIGURE 53.
Potential temperature (upper panel) and salinity (lower panel) for the 200–800 m layer in the oceanic waters of the Canary Basin.

4.10 SOUTHWEST APPROACHES

T. Smyth

The datasets presented here are from the western end of the English Channel and the boundary of the Celtic Sea and the Bay of Biscay ecoregions. The area is commonly referred to as the Southwest Approaches, which relates to the passage of shipping through the English Channel. As these data come from a boundary between different ecoregions, they relate to the region forming a pathway for AW enter the southern North Sea.

Station E1 (50.03°N 4.37°W) is on the south coast of England in the western English Channel. The water depth is 75 m, and the station is tidally influenced by a 1.1-knot maximum surface stream at mean spring tide. The seabed is mainly sand, resulting in a low bottom stress (1–2 ergs cm^{-2} s^{-1}). The station may be described as oceanic with the development of a seasonal thermocline; stratification typically starts in early April, persists throughout summer, and is eroded by the end of October. The typical depth of the summer thermocline is ca. 20 m. The station is greatly affected by ambient weather.

Measurements have been taken at this station since the end of the nineteenth century, with data currently available since 1903 (Figure 54). Apart from the gaps for the two world wars and a hiatus in funding between 1985 and 2002, the series is unbroken. The data takes the form of vertical profiles of temperature and salinity. Early measurements were taken with reversing mercury-in-glass thermometers and discrete salinity bottles. More recently, electronic equipment (Seabird CTD) has been utilized. The time-series demonstrates considerable interannual variability of temperature (Figure 54).

E1 was sampled on 19 occasions during 2017: approximately fortnightly in summer and monthly in winter. The temperature pattern for the last 2–3 years was broadly mirrored during 2017, with markedly warm late autumn (November) and winter (January, February) months (ca. 1–2°C); spring and summer were generally average or slightly above the long-term average (Figure 55).

The salinity values recorded during 2017 were consistently 0.1–0.2 above the long-term mean (ca. 35.2–35.3) throughout the year apart from a brief period in early spring when they were close to average (Figure 54).

The Astan Site (48.77°N 3.94°W) is located 3.5 km off the north coast of Brittany, France, in the western English Channel. Measurements began in the late 1990s and are collected twice a month at this coastal station. Properties at this site are typical of western Channel waters. Bottom depth is ca. 60 m, and the water column is well mixed for most of the surveys. There is no update for 2017.

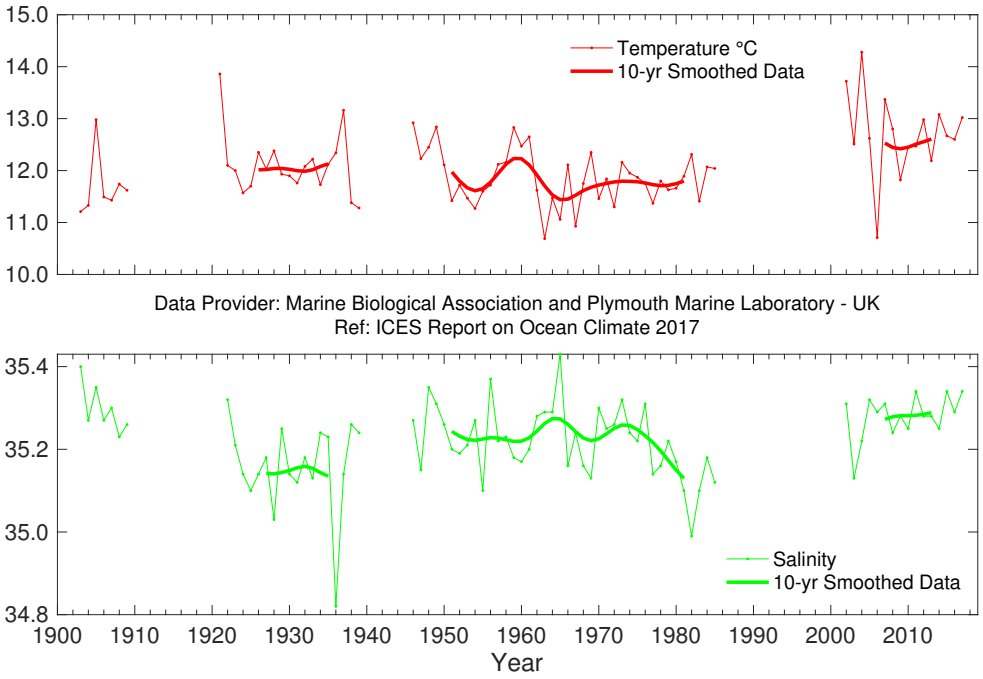

FIGURE 54.
Temperature (upper panel) and salinity (lower panel) anomalies of surface (0–40 m) water at Station E1 in the western English Channel (50.03°N 4.37°W).

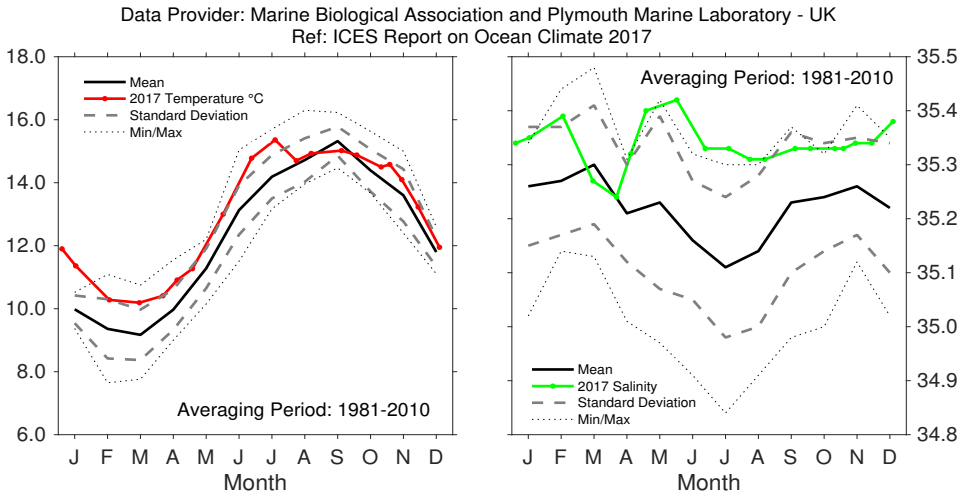

FIGURE 55.
Monthly average seasonal cycle with 2017 temperature (left panel) and salinity (right panel) observations of surface (0–40 m) water at Station E1 in the western English Channel (50.03°N 4.37°W).

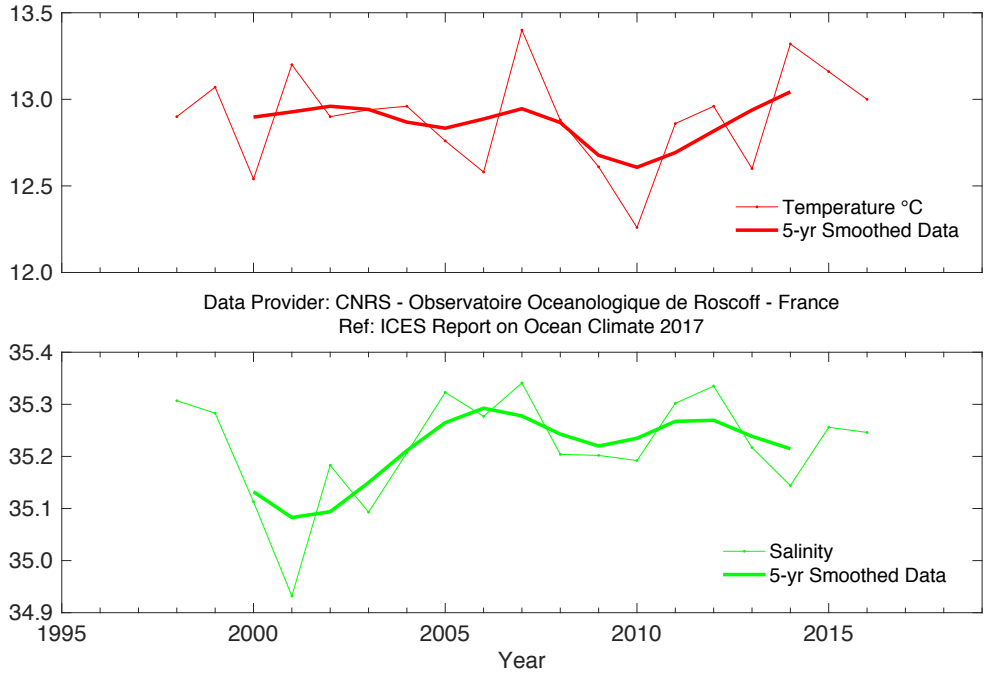

FIGURE 56.
Temperature (upper panel) and salinity (lower panel) of surface water at the Astan station (48.77°N 3.94°W) base period 1998–2010. Data until 2016.

4.11 CELTIC SEAS

K. Lyons and C. Cusack

The Celtic Seas is an ICES ecoregion and within one of NOAA's Large Marine Ecosystems; the area is included in LME 24 (Celtic-Biscay Shelf). The Celtic Seas region contains the shelf seas of northwestern Europe and part of the Rockall Trough. The shelf seas are, in the main, relatively shallow (< 100 m). The structure of the water column on the shelf is primarily driven by (i) vertical mixing due to tides and wind, and (ii) the seasonal variation of solar heating, leading to seasonal (summer) density-driven currents (e.g. Irish Coastal Current). In addition to the influence of coastal waters on the shelf, the area is strongly influenced by the poleward transport of AW as well as the continental slope current that brings water northward from the Biscay region.

The mean SST recorded at Malin Head for 2017 was the highest on record at 0.89°C above the 1981–2010 mean (Figure 58). Malin Head monthly mean temperatures for 2017 were all above the average (Figure 57).

Record sea surface temperature at Malin Head station.

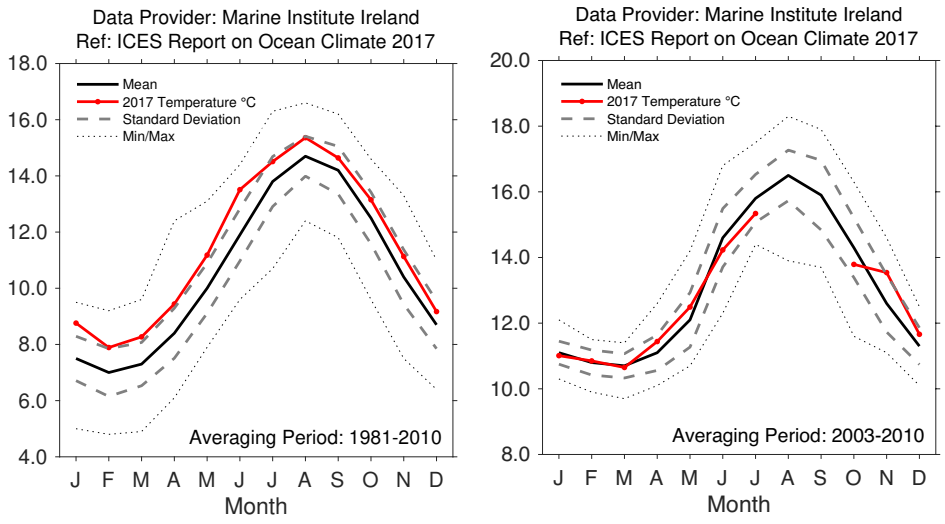

FIGURE 57.
Celtic Seas: Monthly average seasonal cycle with 2017 monthly temperature at Malin Head (left) and the M3 Weather Buoy southwest of Ireland (right; 51.22°N 10.55°W).

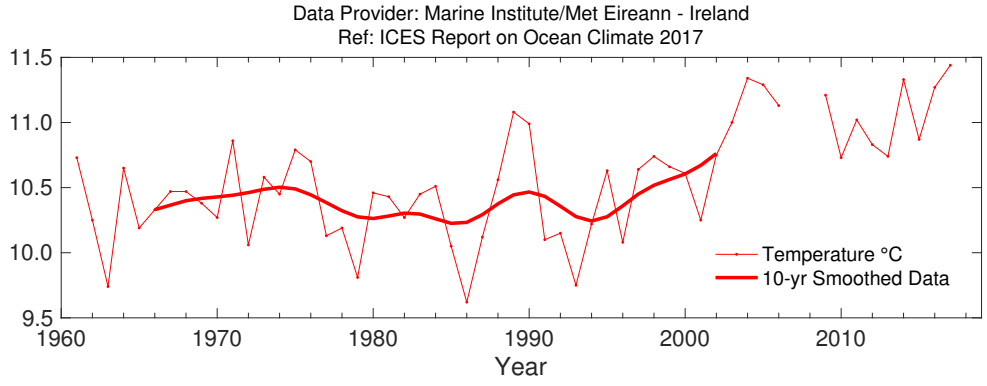

FIGURE 58.
Celtic Seas: Temperature at the Malin Head coastal station (55.39°N 7.38°W).

4.12 ROCKALL TROUGH

N. P. Holliday

Rockall Trough is a deep ocean basin situated west of Britain and Ireland and sitting within the Celtic Seas and Oceanic Northeast Atlantic ecoregions. With significantly different oceanographic characteristics than the shallower shelf sea areas, Rockall Trough is separated from the Iceland Basin by Hatton and Rockall banks and from the Norwegian Sea by the shallow (500 m) Wyville-Thomson Ridge. It is a route for warm North Atlantic upper water to reach the Norwegian Sea, where it is converted into cold, dense overflow water as part of the thermohaline overturning in the North Atlantic. The upper water column is characterized by poleward-moving eastern North Atlantic water, which is warmer and more saline than waters of the Iceland Basin that also contribute to the Norwegian Sea inflow (Figure 59).

The potential temperature of the upper 800 m was close to the 1981–2010 mean in 2017. The upper ocean has been cooling relative to a peak of 9.8°C in 2007 (Figure 60). The salinity of the upper 800 m has been decreasing since the end of the 2000s, with sharp freshening between 2015 and 2016, and persistently low salinity in 2017. Salinity in 2017 was the lowest observed in the Rockall Trough since 1978.

Warm and fresh conditions in the Rockall Trough in 2017.

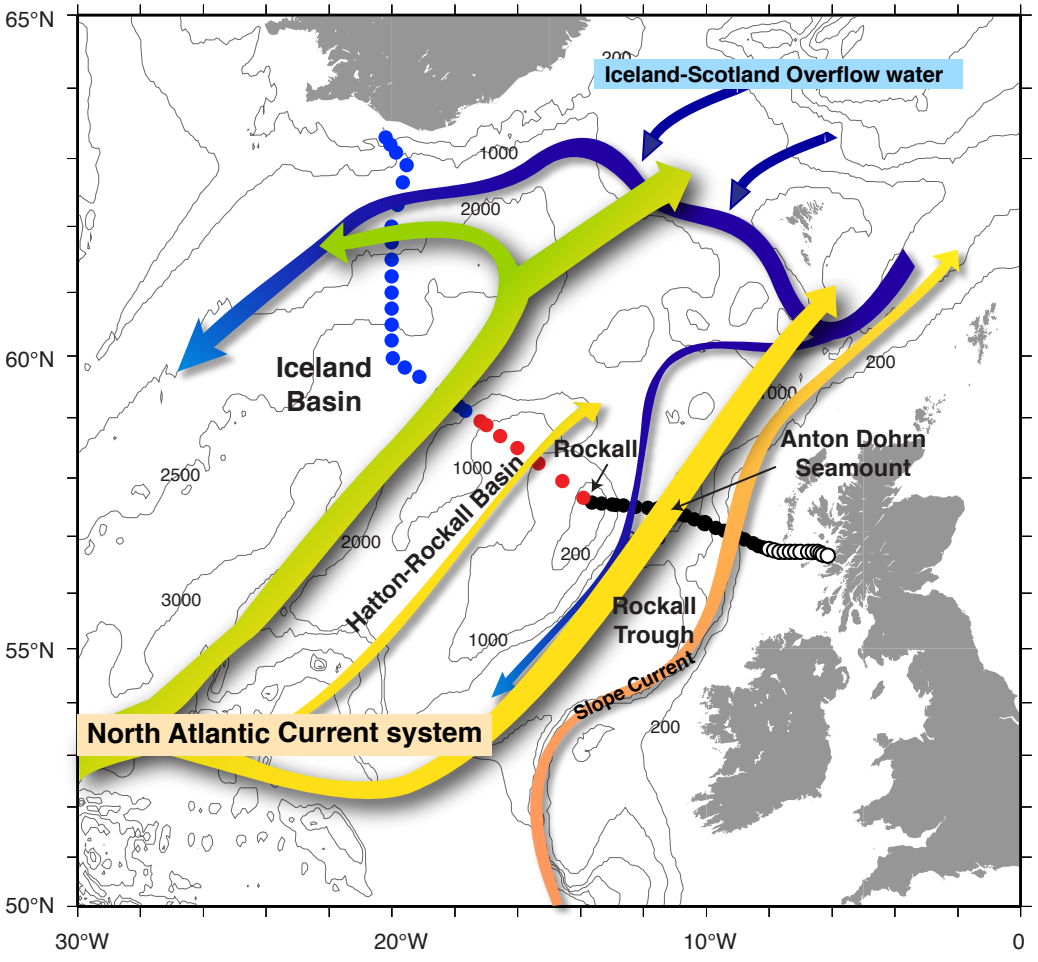

FIGURE 59. Circulation schematic for the Rockall Trough, Hatton-Rockall Basin, and Iceland Basin. Green, yellow, and orange colours indicate the upper waters of the North Atlantic Current and the slope current. Dark blue arrows show the approximate locations of the main overflow currents.

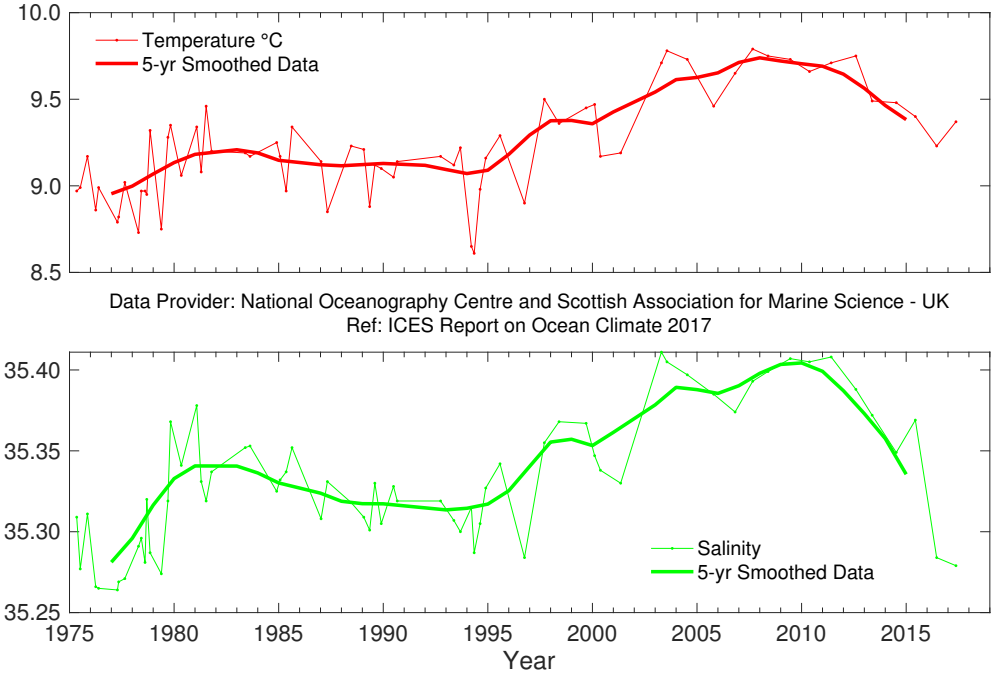

FIGURE 60.
Rockall Trough: Temperature (upper panel) and salinity (lower panel) for the upper ocean (potential density 27.2–27.50 kg m^{-3}, representing the top 800 m, but excluding the seasonally warmed surface layer).

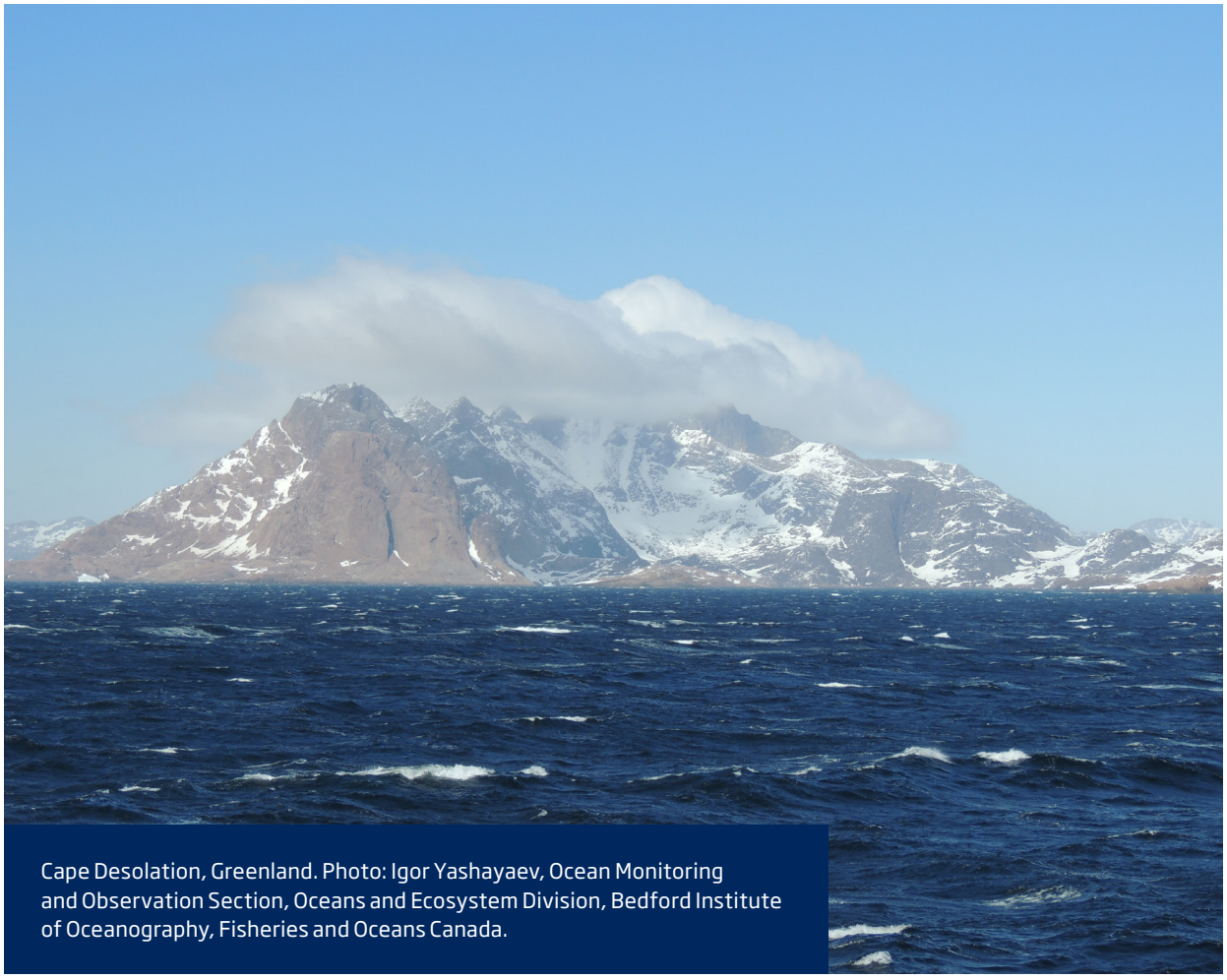

Cape Desolation, Greenland. Photo: Igor Yashayaev, Ocean Monitoring and Observation Section, Oceans and Ecosystem Division, Bedford Institute of Oceanography, Fisheries and Oceans Canada.

4.13 HATTON-ROCKALL BASIN

N. P. Holliday

The shallow Hatton-Rockall Basin (1000 m) lies between the Iceland Basin to the west and Rockall Trough to the east and is bounded by the Hatton and Rockall banks. The basin is filled with well-mixed subpolar-mode water (SPMW) moving northward as part of the North Atlantic Current (NAC) complex. Winter mixing reaches 800-1000 m here. Temperature and salinity vary considerably depending on the type of NAC water that enters the basin. The region is in the transition zone between cold, fresh, central subpolar water and warm, saline, eastern subpolar water.

The range in basin mean temperature and salinity in the upper 1000 m is more than 1°C and 0.1 psu, higher than the Iceland Basin to the west and Rockall Trough to the east. The lowest values were seen at the start of the time-series in 1996, followed by a steady rise to maximum values in the late 2000s. Since 2010, there has been a decrease in temperature and salinity; in 2017, salinity was lower than the 1996–2010 average, but the temperature has risen since 2016 to a value close to the long-term mean (Figure 61).

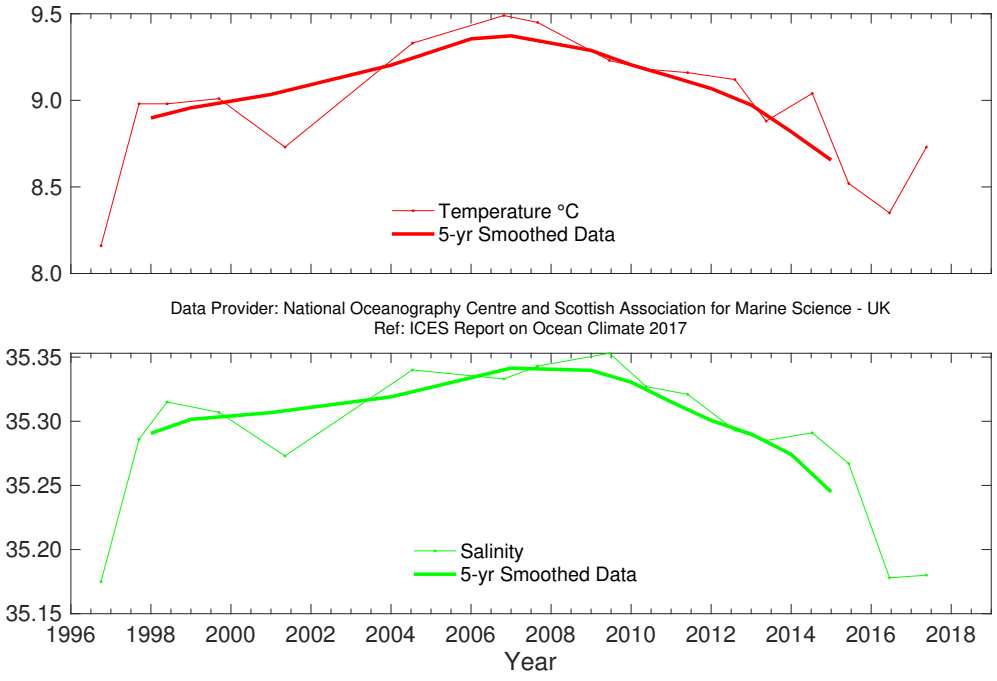

FIGURE 61.
Hatton-Rockall Basin: Temperature (upper panel) and salinity (lower panel) for the upper ocean (potential density 27.20-27.50 kg m^{-3}), representing the top 600 m and excluding the seasonally warmed surface layer.

4.14 ICELAND BASIN

N. P. Holliday

A major part of the NAC flows into the Iceland Basin, adjacent to the shallow Hatton Bank on the southeast side of the basin (Figure 59). The NAC typically consists of one or two fronts between warmer, more saline water in the east and colder, fresher water to the north and west. The region is rich in eddy activity, and the water properties are quite variable in time and space. Most of the water entering the Iceland Basin from the south flows through into the Norwegian Sea over the Iceland-Scotland Ridge. A smaller fraction of NAC water recirculates south of Iceland in the boundary currents of the main anticlockwise circulation of the Subpolar Gyre.

Temperature and salinity of the upper ocean (ca. upper 500–600 m) vary from year to year, but also exhibit multiyear changes. From 1996 to the late 2000s, both temperature and salinity were increasing, but have since been decreasing (Holliday *et al.*, 2015). In 2017, temperature and salinity values were the lowest recorded since 1996 (Figure 62). The freshening since 2010 implies that the basin is receiving more water originating in the west and central subpolar region and less warm, saline water from the eastern intergyre regions. Superimposed on that multiyear trend is rapid cooling observed between 2014 and 2015, caused by a high flux of heat from the ocean to the atmosphere (Duchez *et al.*, 2016) and rapid freshening in 2015–2017, which has, as yet, unidentified origins.

Record low salinity observed in the Iceland Basin upper ocean.

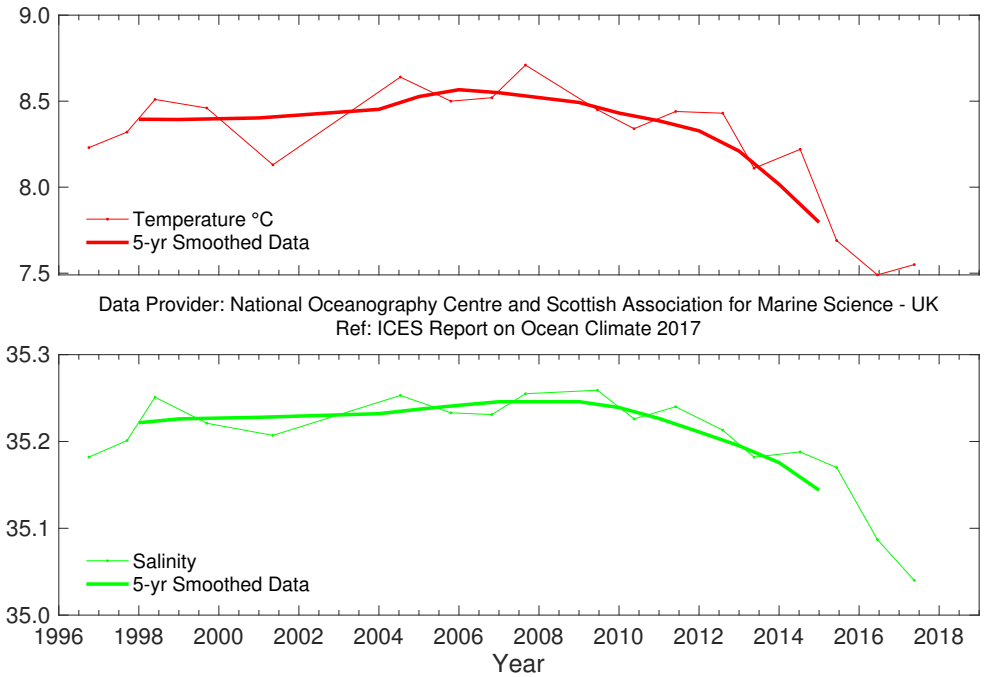

FIGURE 62.
Iceland Basin: Temperature (upper panel) and salinity (lower panel) for the upper ocean (potential density 27.20–27.50 kg m^{-3}, representing the top 500 m and excluding the seasonally warmed surface layer).

4.15 IRMINGER SEA

L. de Steur and F. de Jong

The Irminger Sea is the ocean basin between southern Greenland, the Reykjanes Ridge, and Iceland. This area forms part of the North Atlantic Subarctic cyclonic gyre. Due to this gyre, the exchange of water between the Irminger and Labrador seas proceeds relatively fast. In the bottom layers of the Irminger Sea, cold water originating in the subarctic seas flows from Denmark Strait southward over the continental slope of Greenland.

In 2004, SPMW in the central Irminger Sea (200–400 dbar) reached the highest recorded temperature and salinity levels since 1991. Since then, temperature has exhibited well-correlated interannual variations, suggesting that variations in wind-driven circulation were the main cause of this hydrographic variability.

Since 2014, a negative trend has been observed in temperature, but not in salinity until 2016. The temperature of the SPMW in the central Irminger Sea was nearly 0.4°C below the long-term mean, while salinity was 0.015 above the mean.

Deep convection occurred in winter 2014/2015 until the end of April leading to mixed layers as deep as 1400 m. Deep mixed layers were again seen in winter 2015/2016. Both winters were leading up to the cold anomaly observed in the Irminger Sea. While the time-series at Station FX9 in the northern Irminger Sea was updated, the trends in temperature and salinity are unclear in the central Irminger Sea as there were no hydrographic cruises in 2017, and the time-series could not be extended.

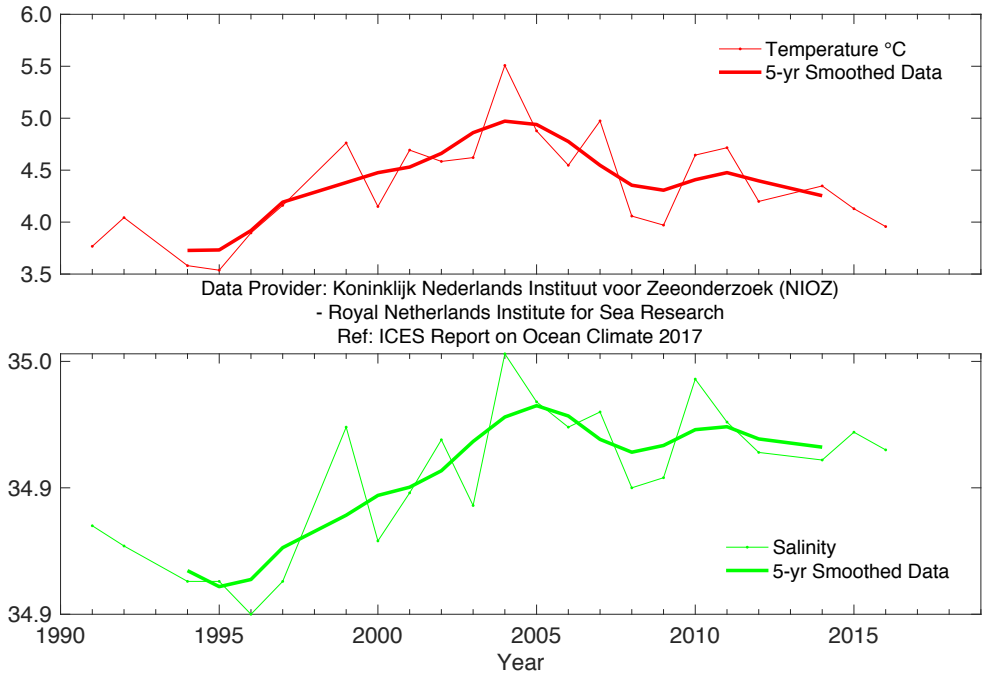

FIGURE 63.
Irminger Sea: Temperature (upper panel) and salinity (lower panel) of Subpolar Mode Water (SPMW) in the central Irminger Sea (averaged over 200–400 m). Data until 2016.

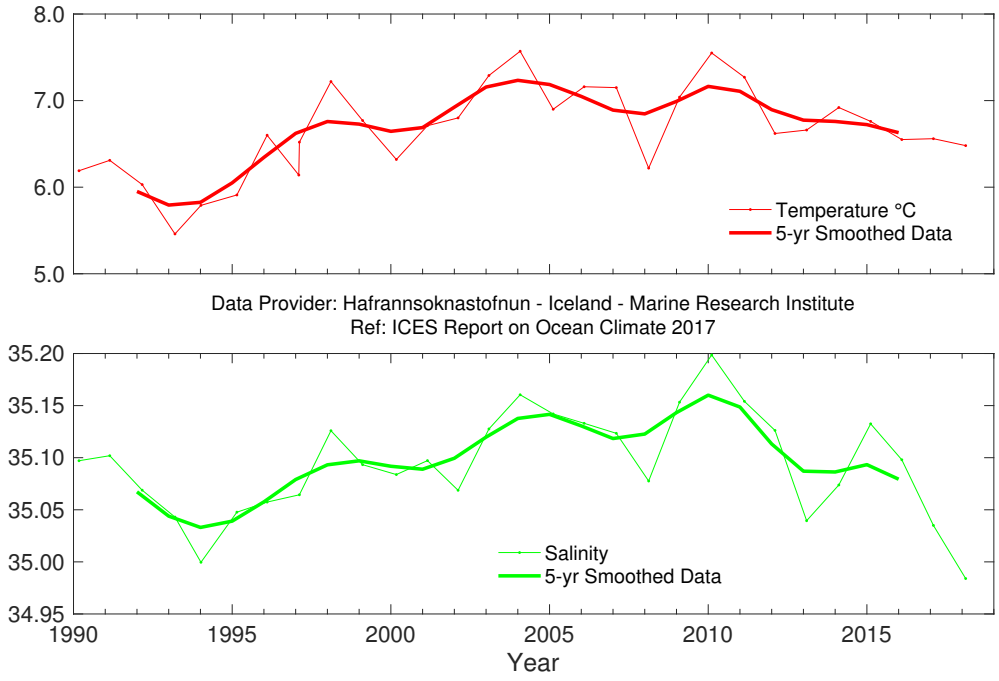

FIGURE 64.
Irminger Sea: Temperature (upper panel) and salinity (lower panel) of Subpolar Mode Water in the northern Irminger Sea (Station FX9, 64.33°N 28°W), from winter observations averaged over 200–500 m).

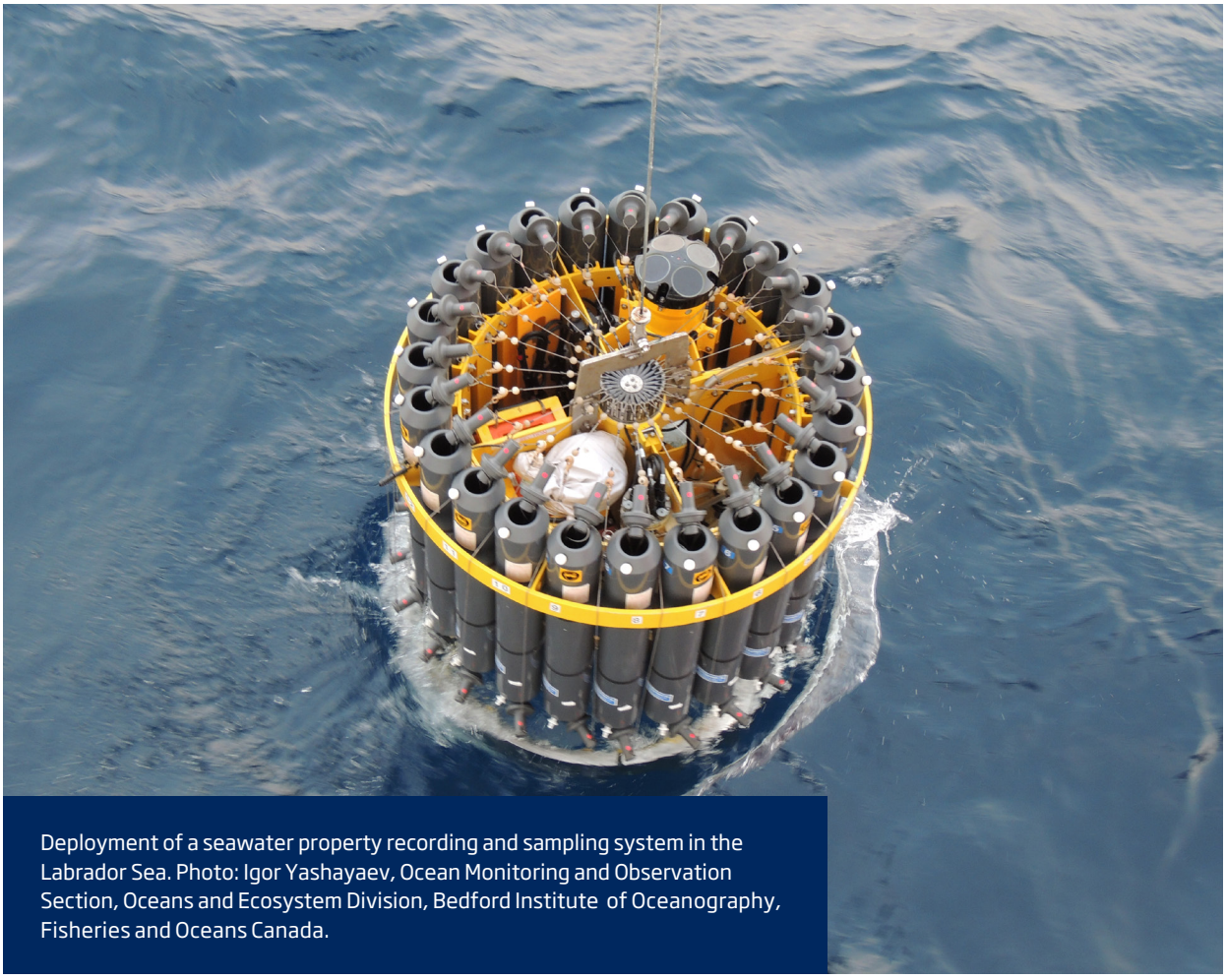

Deployment of a seawater property recording and sampling system in the Labrador Sea. Photo: Igor Yashayaev, Ocean Monitoring and Observation Section, Oceans and Ecosystem Division, Bedford Institute of Oceanography, Fisheries and Oceans Canada.

4.16 FAROESE WATERS AND THE FAROE-SHETLAND CHANNEL

K. M. H. Larsen, B. Berx, and J. Hindson

Data from the Faroese ecoregion are grouped together with data from the Faroe-Shetland Channel. This small region sits at the boundary between the Celtic Seas, North Sea, and Norwegian Sea ecoregions and also the boundary between the North Atlantic and Nordic seas.

One branch of the NAC crosses the Greenland-Scotland ridge (Figure 65), flowing on either side of the Faroes. Its properties are sampled by the Faroe Bank Channel before it crosses the ridge, and by the Faroe Current after it crosses the ridge. Some of this water recirculates and is sampled within the Faroe-Shetland Channel as modified North Atlantic Water (MNAW).

Farther east, the continental slope current flows along the edge of the northwest European continental shelf; originating in the southern Rockall Trough, it carries warm, saline AW into the Faroe-Shetland Channel. A proportion of this AW crosses onto the shelf itself and enters the North Sea, where it is diluted with coastal water and eventually leaves in the Norwegian Coastal Current. The remainder enters the Norwegian Sea and joins the water coming from north of the Faroes to become the Norwegian Atlantic Current.

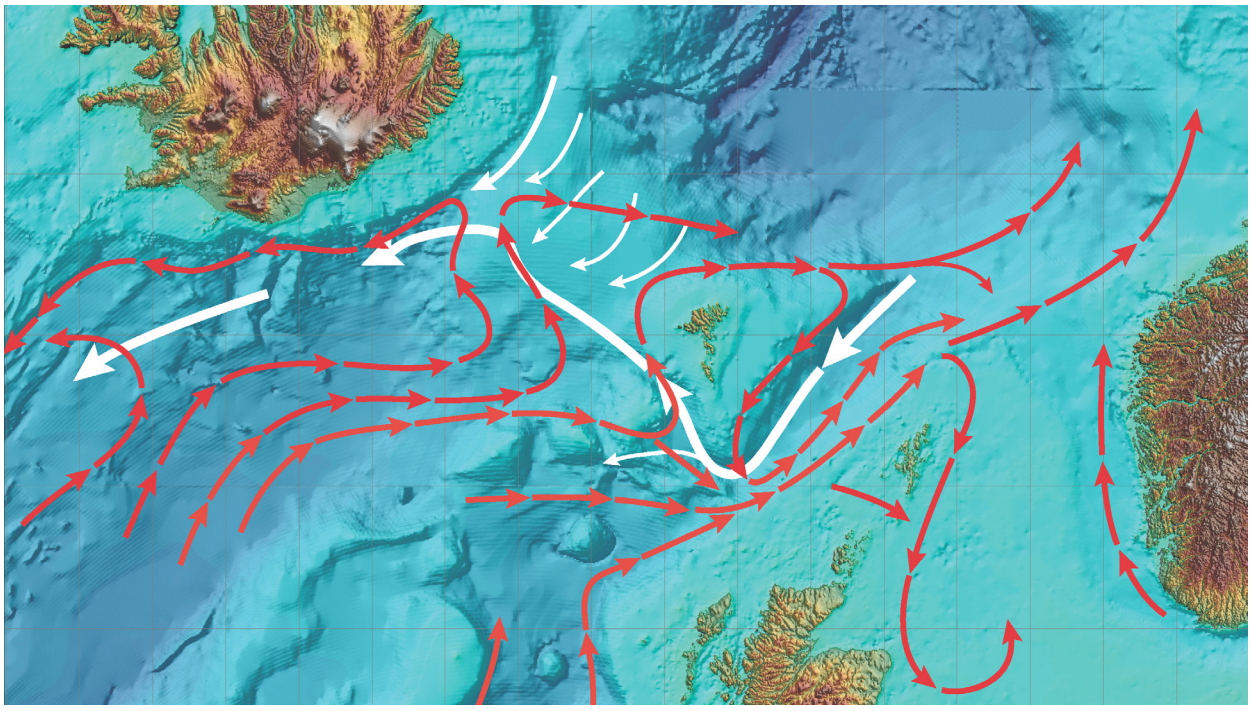

FIGURE 65.
Circulation schematic for the Faroes ecoregion and the Faroe-Shetland Channel. Red lines show the poleward movement of AW. Thick white lines show the return circulation (at depth) of waters from the Nordic seas.

Generally, both temperature and salinity in all upper-layer waters around the Faroes and the Faroe–Shetland Channel increased markedly during the 1990s and 2000s. Both temperature and salinity decreased during the first half of the 2010s.

After the record-high salinities observed in the Faroe Bank Channel (Figure 66) and the Faroe Current (Figure 67) in November 2009, salinities decreased at both locations. In the Faroe Bank Channel, salinities decreased from average values in 2015 to record-low

values in autumn 2016; record low values were observed in autumn 2017 in the Faroe Current.

Temperatures in the Faroe Bank Channel and the Faroe Current have been relatively high and stable since the mid-2000s and into the early 2010s. In 2012, they decreased and have been close to the long-term mean in the recent years; in 2017, they were somewhat above the long-term mean.

On the Faroe Shelf, the annual average temperature has been relatively high since the early 2000s, but in 2015, the annual average temperature was the lowest observed since 2000. In 2016 and 2017, temperature increased again; only December was below the monthly average in 2017 (Figure 68; left). The long-term trend in salinity on the Faroe Shelf follows the trend observed in off-shelf waters. Thus, salinities increased from the start of the observations in 1995 to record-high values in 2010. Since 2010, salinities have been decreasing, and the record-low values observed in the Faroe Bank Channel in autumn 2016 were already evident in the Faroe Shelf salinities in late summer 2016, and remained low for the rest of 2016 and throughout 2017 (Figure 68; right).

Temperature and salinity of the surface waters in the Faroe–Shetland Channel show a general increase since the early 1990s, although there has been a reduction in both parameters over the past seven years. MNAW on the western slopes of the channel experienced record-high temperatures in 2010 alongside the highest salinity recorded since 1950 (Figure 69). Temperature and salinity of AW masses on both sides of the Faroe–Shetland Channel have since decreased significantly (Figure 70): salinities are now lower than the long-term mean, and temperatures are close to the long-term mean.

Very low salinities were observed in the North Atlantic Water (NAW) and modified NAW (MNAW) around the Faroes and steep freshening was observed in the AW in the slope current. Temperatures in the whole region were close to or above the long-term mean.

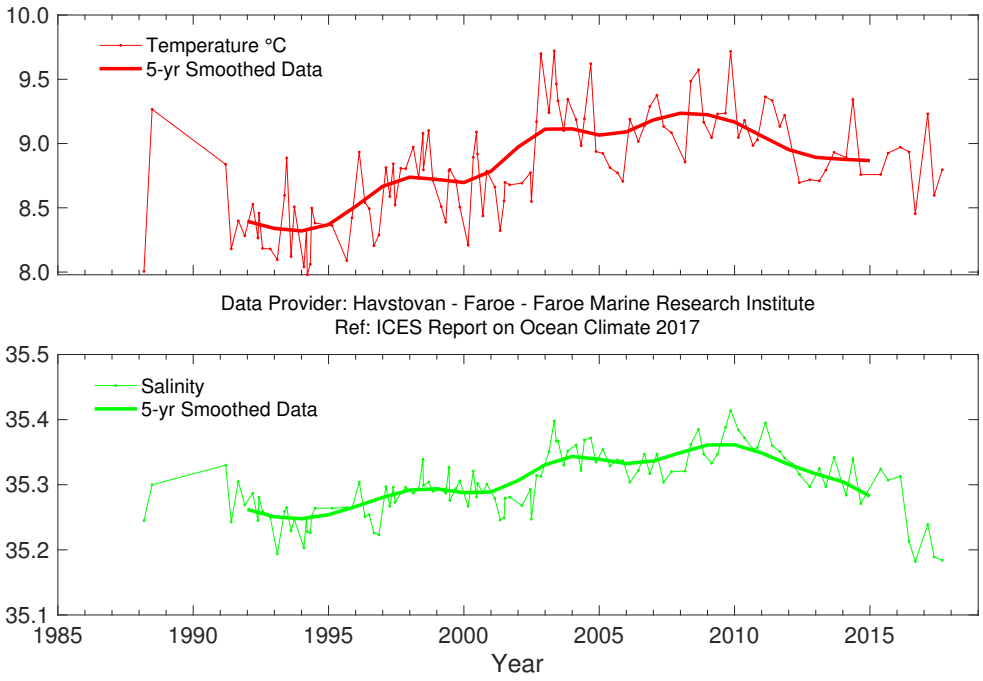

FIGURE 66.
Faroese waters. Temperature (upper panel) and salinity (lower panel) in the high salinity core of Atlantic water (AW) over the Faroe Bank Channel (maximum salinity averaged over a 50 m deep layer).

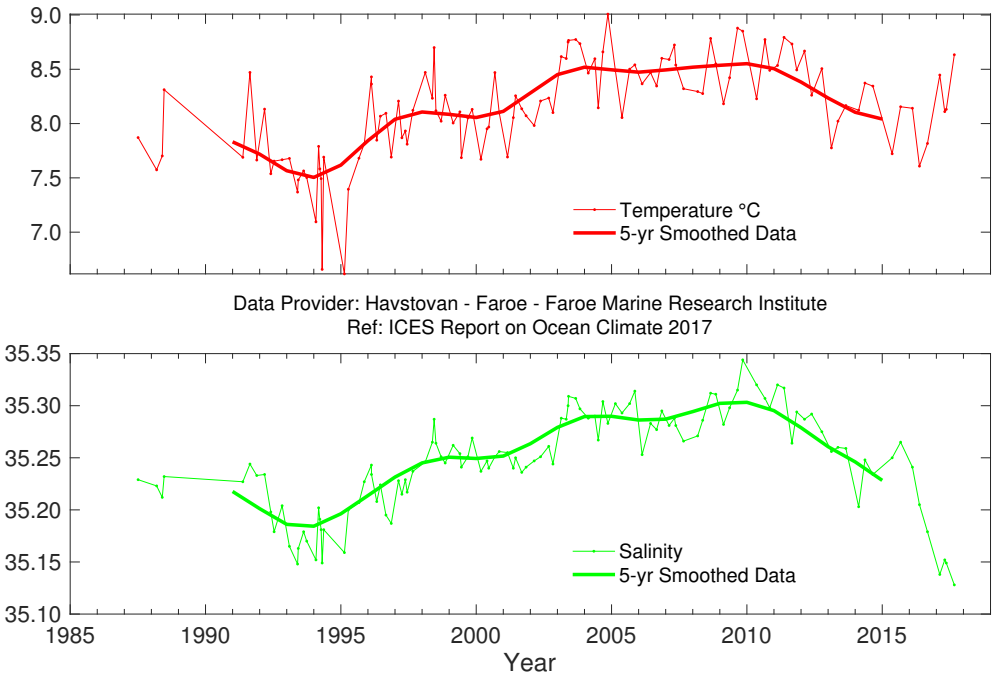

FIGURE 67.
Temperature (upper panel) and salinity (lower panel) in the high salinity core of the Faroe Current north of the Faroes (maximum salinity averaged over a 50 m deep layer).

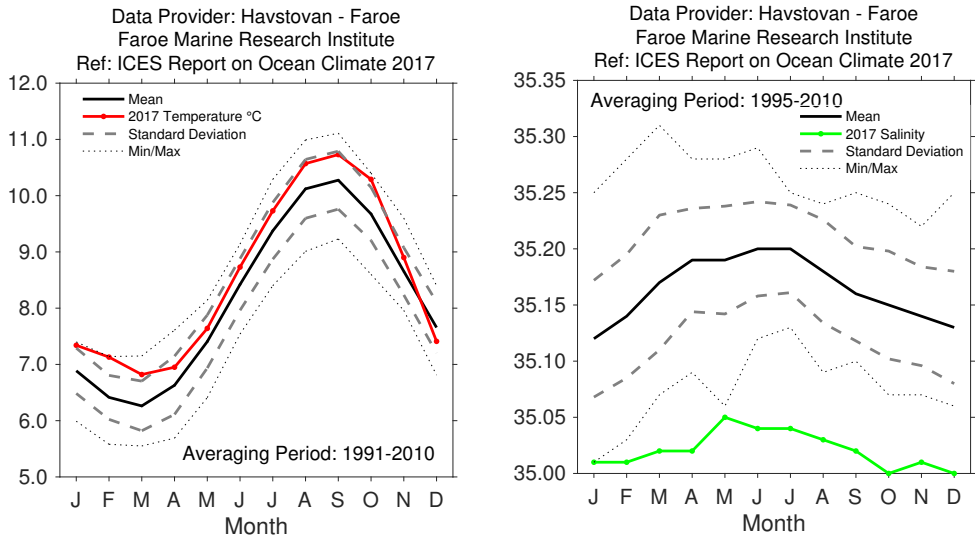

FIGURE 68.
Faroese waters. 2017 monthly temperature (left) from the Faroe coastal station at Oyrargjogv (62.12°N 7.17°W) and monthly salinity (right) from the Faroe coastal station at Skopun (61.91°N 6.88°W). Note the different averaging periods.

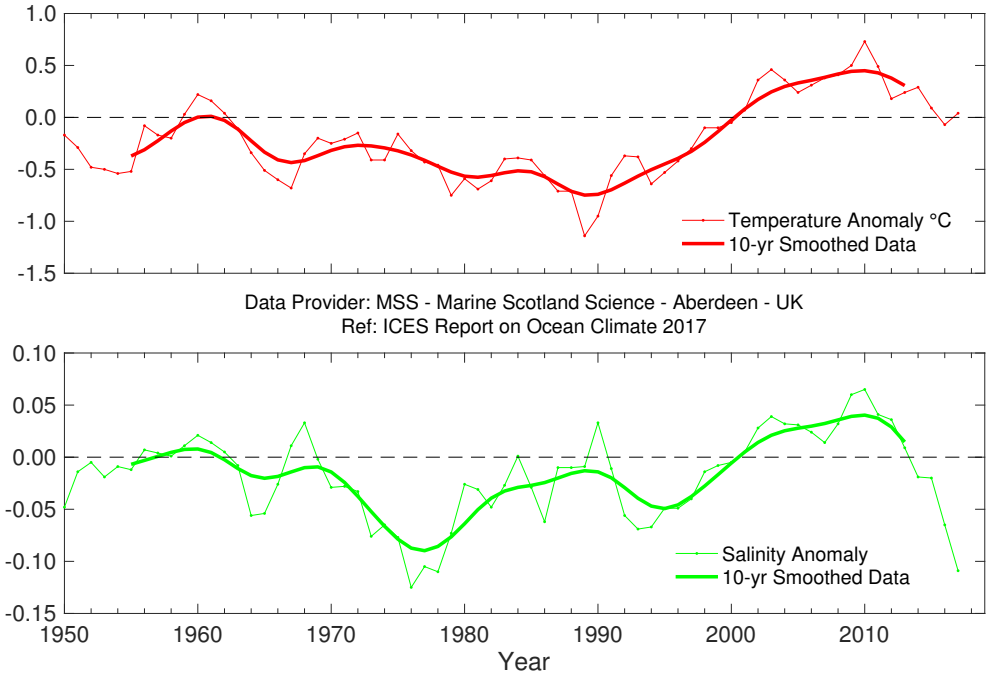

FIGURE 69.
Faroe–Shetland Channel. Temperature anomaly (upper panel) and salinity anomaly (lower panel) in the MNAW entering the Faroe–Shetland Channel from the north after circulating around the Faroes.

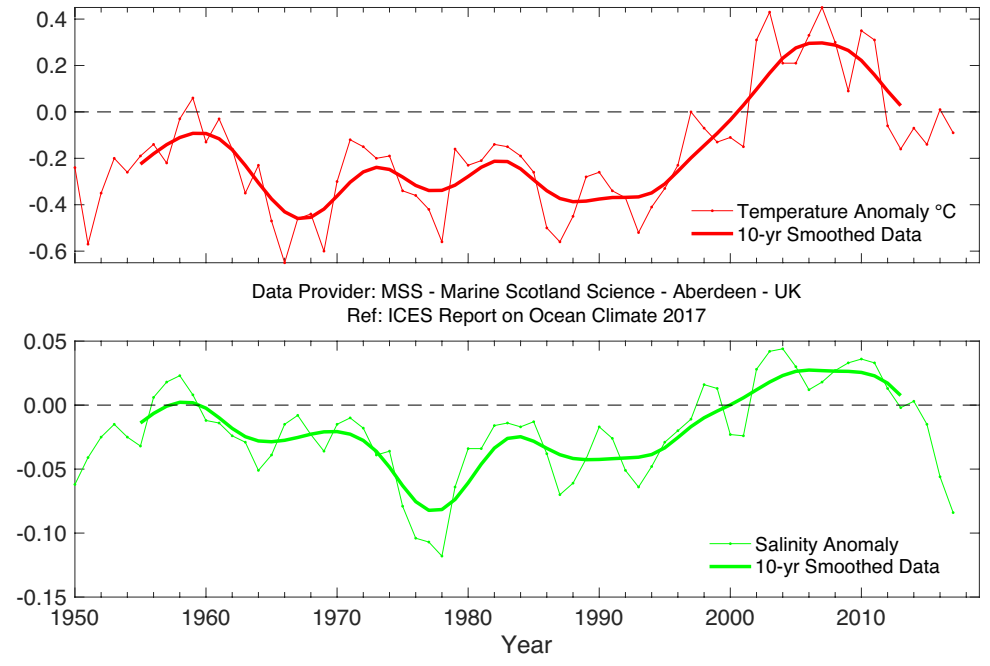

FIGURE 70.
Faroe–Shetland Channel. Temperature anomaly (upper panel) and salinity anomaly (lower panel) in the Atlantic water (AW) in the slope current.

4.17 NORTH SEA

H. Klein and P. Loewe

North Sea oceanographic conditions are determined by the inflow of saline AW (Figure 71) and the ocean–atmosphere heat exchange. The inflow through the northern entrances (and, to a lesser degree, through the English Channel) can be strongly influenced by the NAO. Numerical model simulations also demonstrate strong differences in North Sea circulation, depending on the state of the NAO. The AW mixes with river run-off and lower-salinity Baltic outflow along the Norwegian coast. A balance of tidal mixing and local heating forces the development of seasonal stratification from April/May to September in most parts of the North Sea.

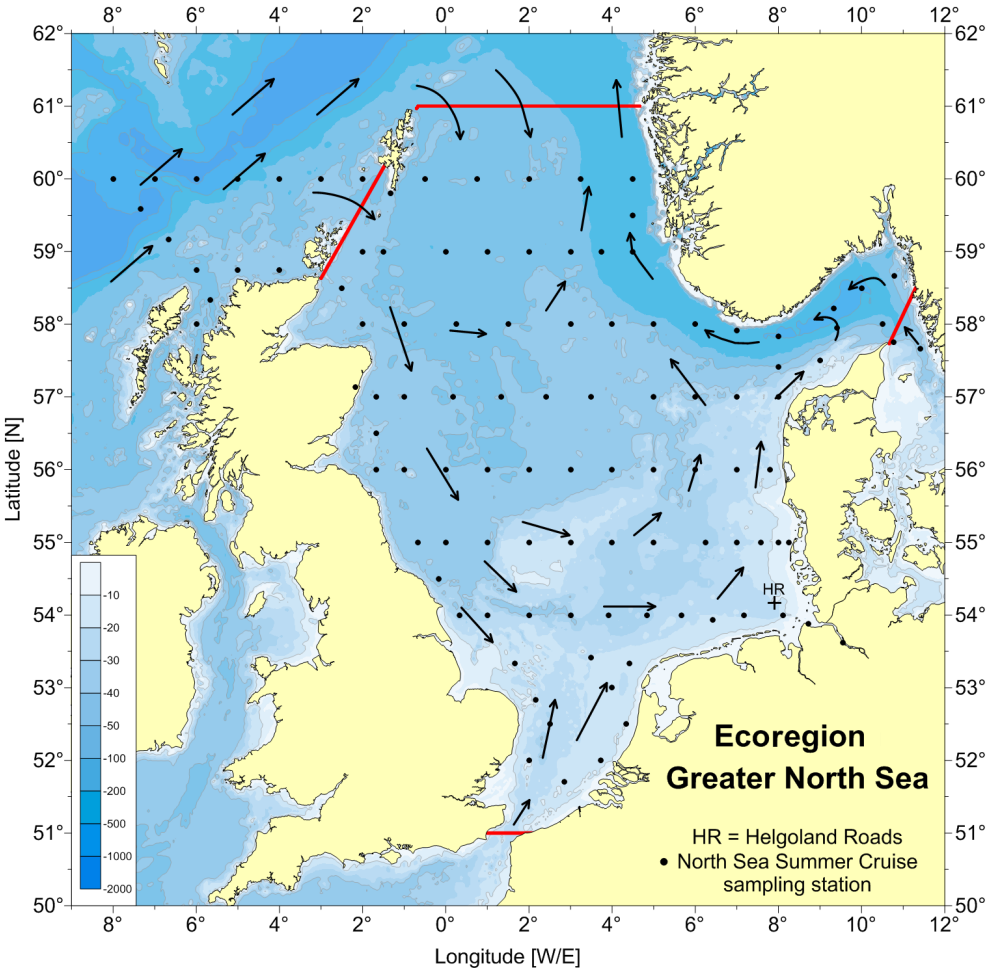

FIGURE 71. Circulation schematic for the North Sea. Red lines show the extent of the North Sea region. The sampling station at Helgoland Roads is marked with a HR+. Black arrows indicate mean residual circulation patterns. Black dots show the summer sampling undertaken in the North Sea by Bundesamt für Seeschifffahrt und Hydrographie (BSH), Germany.

In 2017, all monthly means of area-averaged North Sea SST are between 0.1°C (December) and 0.9°C (September) above the reference period 1981-2010. The seasonal SST maximum of 16.0°C in August was slightly below the 2016 maximum (16.2°C) which occurred in September. The annual mean of area-averaged North Sea SST in 2017 was 10.8°C, +0.6°C above the mean of the reference period. Besides the inflow of warmer AW at the northern boundary and through the English Channel, much of the North Sea SST variability is caused by local ocean–atmosphere heat flux (Figure 72).

During summer, surface temperatures in the southern North Sea exceeded the 10-year average (2000–2010) by 0.5–1.0°C. In the outer Firth of Forth estuary and over the Norwegian trench, surface temperatures were as much as 1°C below the 10-year average. Bottom

temperatures exceeded the 10-year average over large areas, with anomalies greater than +4°C over Dogger Bank and up to +3°C over Jyske Rev and west of Jutland.

The maximum vertical temperature gradient in the thermocline was 2.9°C m^{-1} on the 57°N section. The 54°N section was vertically mixed with vertical gradients < 0.5°C m^{-1}. Generally, the thermocline depth in the North Sea varied between 15 m on the 55°N section and 99 m over the Norwegian Trench. There was a strong thermocline in the central North Sea and a weakening of thermocline strength from south to north. Differences between surface and bottom temperature exceeded 8°C in the Norwegian Trench and in a small ribbon north of Dogger Bank. Compared with 2016, the total heat content increased slightly to 1.677×10^{21} J and exceeded the reference mean of 1.631×10^{21} J by 0.5 s.d.

The southern boundary of AW > 35 psu intruding from the north was located at about 58°N in the surface and at 57°N in the bottom layer. At the surface, as well as in the bottom layer, AW intruded along a broad front. The general special pattern in both layers showed only minor deviations from the 10-year average; over Viking–Bergen Bank, Utsiragrund, and at the southern tip of Norway, there were positive anomalies of up to 1 psu in the surface layer. Positive anomalies of the same order of magnitude were also observed in both layers in the inner German Bight. Compared to 2016, the total salt content increased slightly to 1.105×10^{12} t, which is still 1.6 s.d. below the 2000–2010 mean.

During the first month of 2017, all monthly Elbe River run-off volumes were below the reference period 1981–2000 and slightly above the reference period in November and December. The annual run-off volume of 18.2 km^3 was low compared to the long-term mean, but higher than in the previous three years.

Temperature and salinity in the northern North Sea illustrate conditions in the Atlantic inflow (Figures 73 and 74). There has been an increase in both salinities and temperatures since 2008.

Hydrographic works and mooring service in the Canary Basin.
Photo: Pedro Vélez-Belchi, Canaries Oceanographic Centre, Spanish Institute of Oceanography.

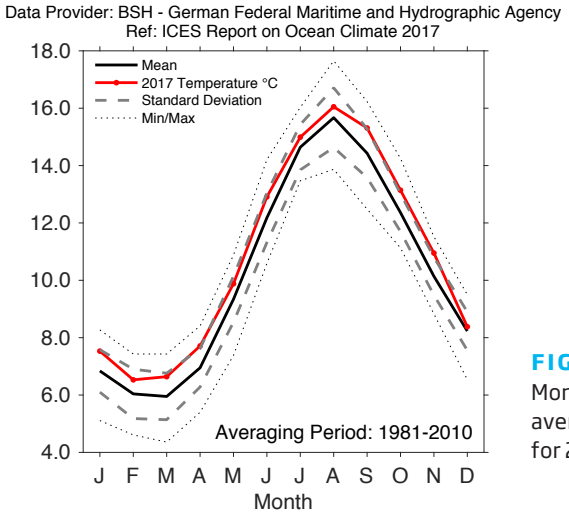

FIGURE 72.
Monthly means of area averaged North Sea SST for 2017.

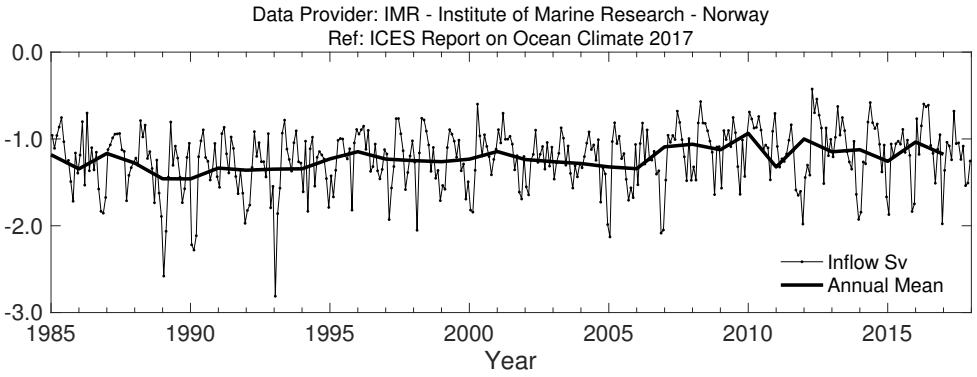

FIGURE 73.
Northern North Sea. Modelled annual mean (bold) and monthly mean volume transport of Atlantic Water (AW) into the northern and central North Sea southward between the Orkney Islands and Utsire, Norway.

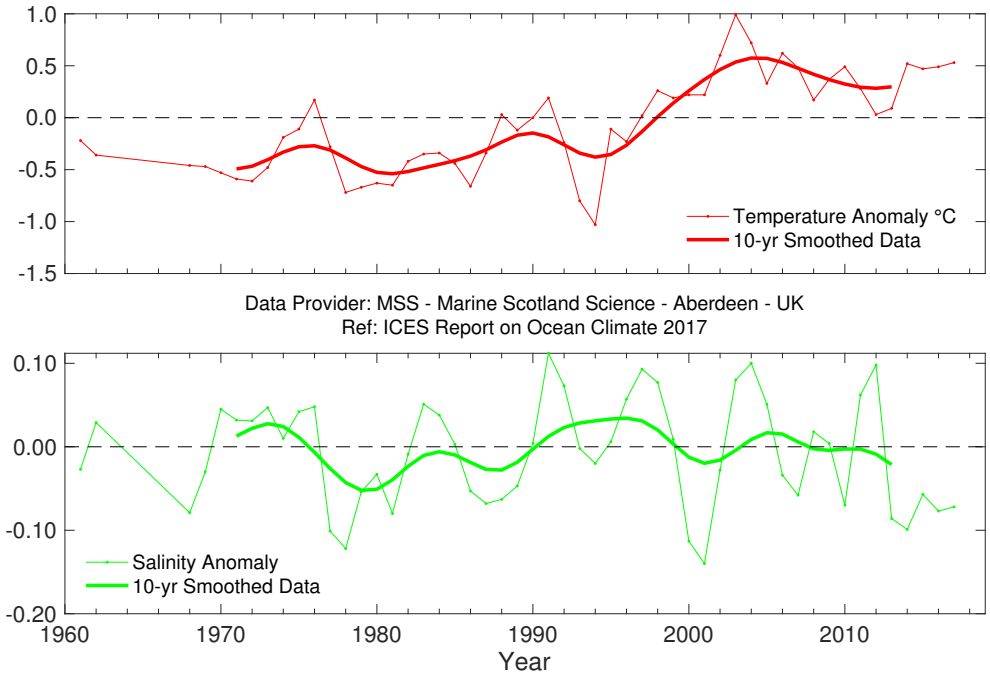

FIGURE 74.
Northern North Sea. Temperature anomaly (upper panel) and salinity anomaly (lower panel) in the Fair Isle Current entering the North Sea from the North Atlantic.

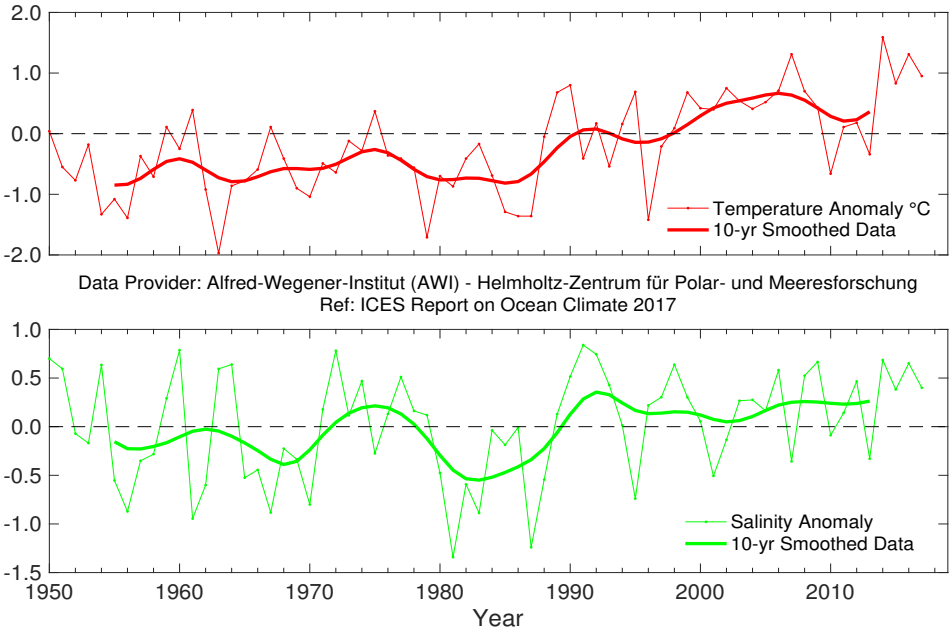

FIGURE 75.
Southern North Sea. Annual mean surface temperature anomaly (upper panel) and salinity anomaly (lower panel) at Station Helgoland Roads. Data until 2015.

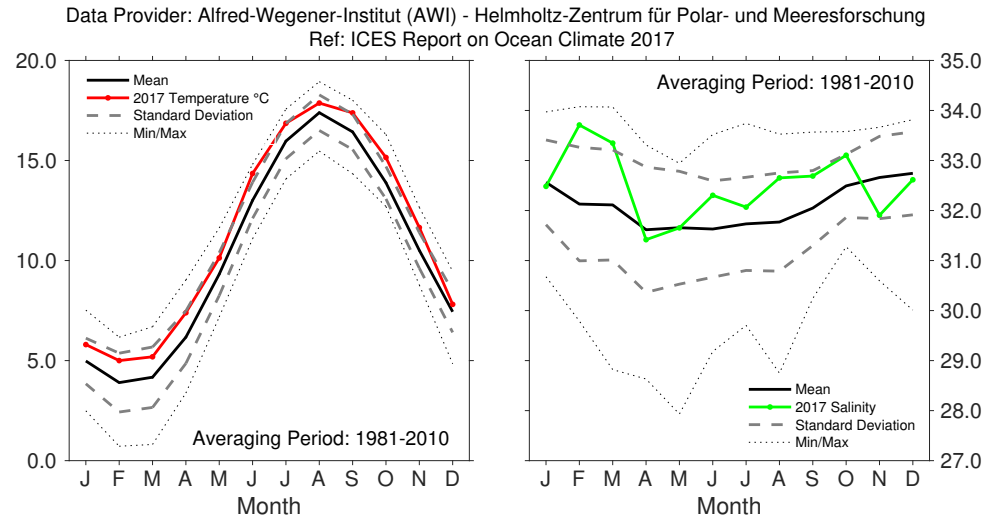

FIGURE 76.
Southern North Sea. Monthly surface temperature (left panel) and salinity (right panel) at Station Helgoland Roads.

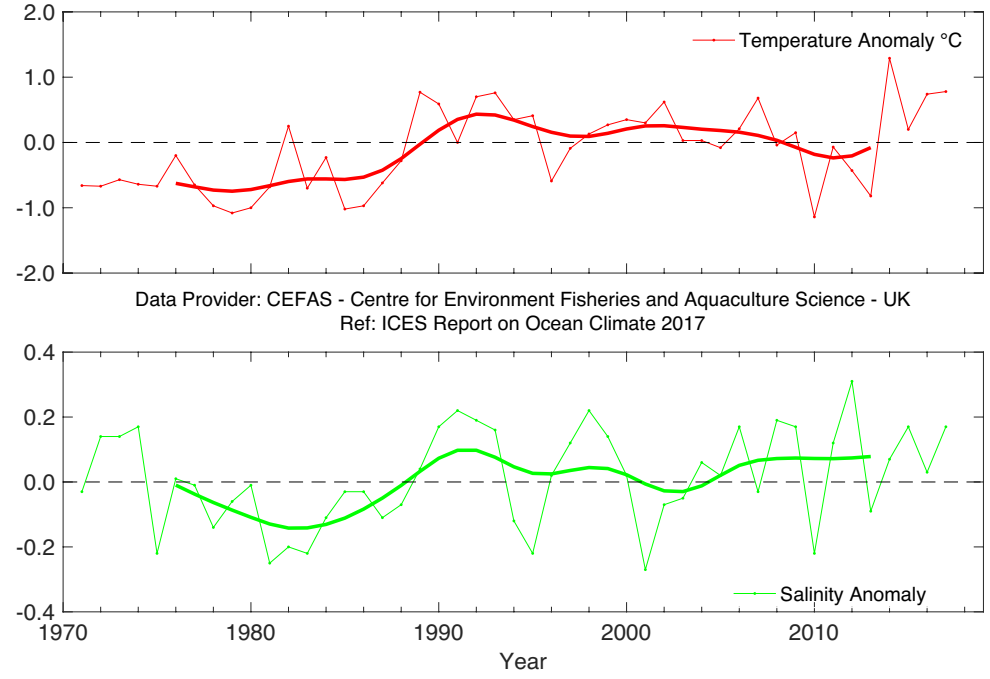

FIGURE 77.
Southern North Sea. Annual sea surface temperature (SST) anomaly (upper panel) and salinity anomaly (lower panel) relative to 1981–2010 from the merged Harwich Ferry Route and West Gabbard Smartbuoy time-series located at 52°N 003°E. Between 1971 and 2002, this was measured as part of a regular ferry route along 52°N between Harwich and Rotterdam. Data from 2002 are from the Cefas West Gabbard Smartbuoy site.

4.18 SKAGERRAK, KATTEGAT, AND THE BALTIC

J. Linders and T. Wodzinowski

The shallow seas of the Skagerrak, Kattegat, and the Baltic are characterized by large salinity variations. In the Skagerrak, water masses from different parts of the North Sea are present. The Kattegat is a transition area between the Baltic and the Skagerrak. The water is strongly stratified with a permanent halocline (sharp change in salinity at depth). The deep water in the Baltic Proper, which enters through the Belts and the Sound, can be stagnant for long periods in the inner basins. In the relatively shallow area in the southern Baltic, smaller inflows pass relatively quickly, and the conditions in the deep water are highly variable. Surface salinity is very low in the Baltic Proper and its gulfs. The Gulf of Bothnia and the Gulf of Finland have ice cover during winter.

The mean air temperature in Sweden was above normal in 2017; summer was a little colder than normal, but winter was warm and raised the mean air temperature. Owing to its central location relative to the Skagerrak, Kattegat, and Baltic, the weather in Sweden can be taken as representative for the area. Mean precipitation was higher than normal especially in the southern and northern parts of Sweden. The number of sun hours was close to normal in the north, otherwise above normal.

In the Skagerrak and Baltic, the year began with SST close to normal. In February, most of the stations in Skagerrak were colder than normal, but SST was close to or slightly below normal in both Skagerrak and in the Baltic for the rest of the year. Surface salinities were mostly above normal in the northern part of Skagerrak, but close to normal in the southern part and in the Kattegat, except for February when salinity was less than normal. In the southern Baltic, surface salinities were close to normal the entire year except in October and November when they were lower than normal. In the Gulf of Gdańsk, surface salinities were close to normal. The rest of the Baltic Proper showed surface salinities to be above normal, except during July and September when they were close to normal.

There was an inflow of more saline water to the Baltic in mid-February, which continues the period of higher frequency inflows that began in 2014. However, no major Baltic inflow was detected in 2017. A major Baltic inflow can significantly refresh the deep water along its route into the Baltic proper (Figure 78)

A warm year with continuing low oxygen conditions in the deep waters in the Baltic Proper and slightly higher surface salinity.

Despite a period of higher frequency inflows since 2014, ca. 18% of the bottom water in the Baltic Proper is anoxic and 28% is hypoxic. The inflows have lowered the concentration of hydrogen sulphide in the eastern and western Gotland basin. In 2017, though, a small increase in the concentration of hydrogen sulphide was observed.

The 2016/2017 ice season started in November and ended in May, which is close to normal. A cold period in February covered most of the Bay of Bothnia, the Quark, and the northern Bothnian Sea. Thin ice cover was present at that time in the Bay of Finland and in the Bay of Riga. Maximum ice extent of 101 000 km^2 was reached on 12 February. The ice season ended 29 May, about one week later than normal.

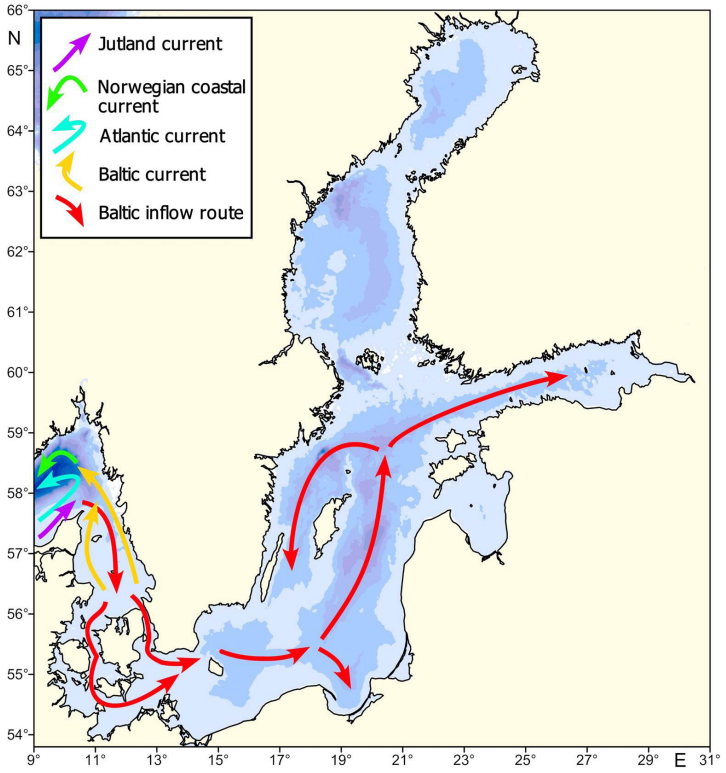

FIGURE 78.
Skagerrak, Kattegat, and the Baltic. Circulation map of water masses.

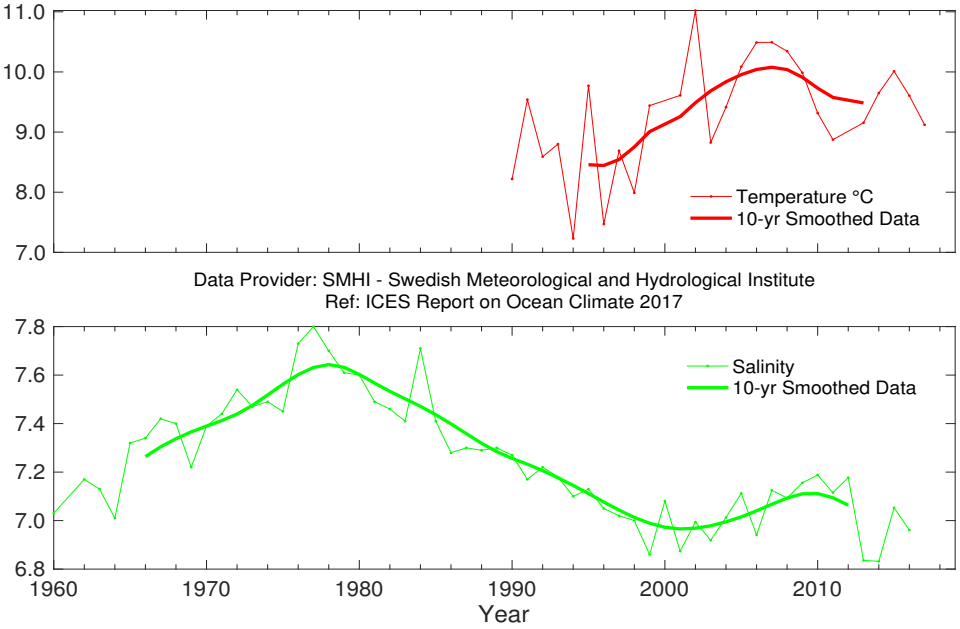

FIGURE 79.
Skagerrak, Kattegat, and the Baltic: Surface temperature, yearly mean (upper panel) and surface salinity, yearly mean (lower panel) at Station BY15 (east of Gotland) in the Baltic Proper.

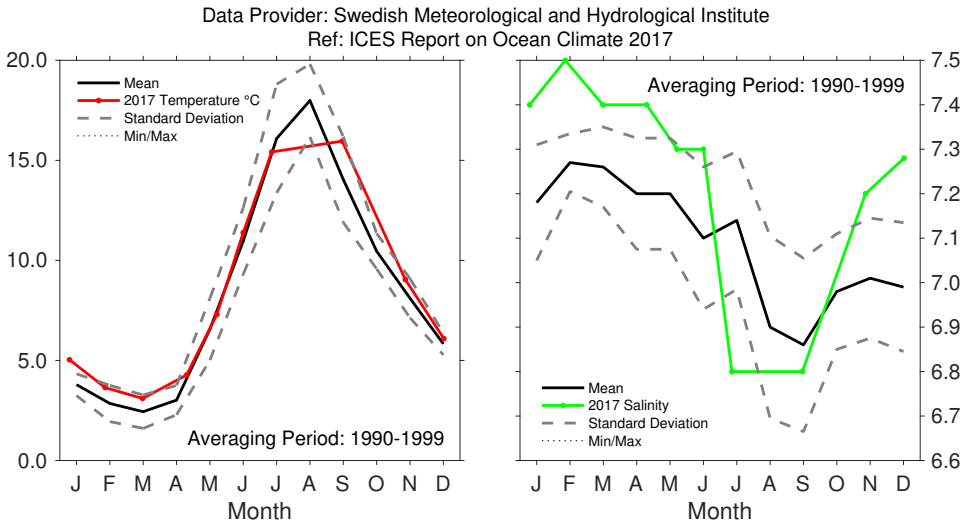

FIGURE 80.
Skagerrak, Kattegat, and the Baltic: Monthly surface temperature (left panel) and salinity (right panel) at Station BY15 (east of Gotland) in the Baltic proper.

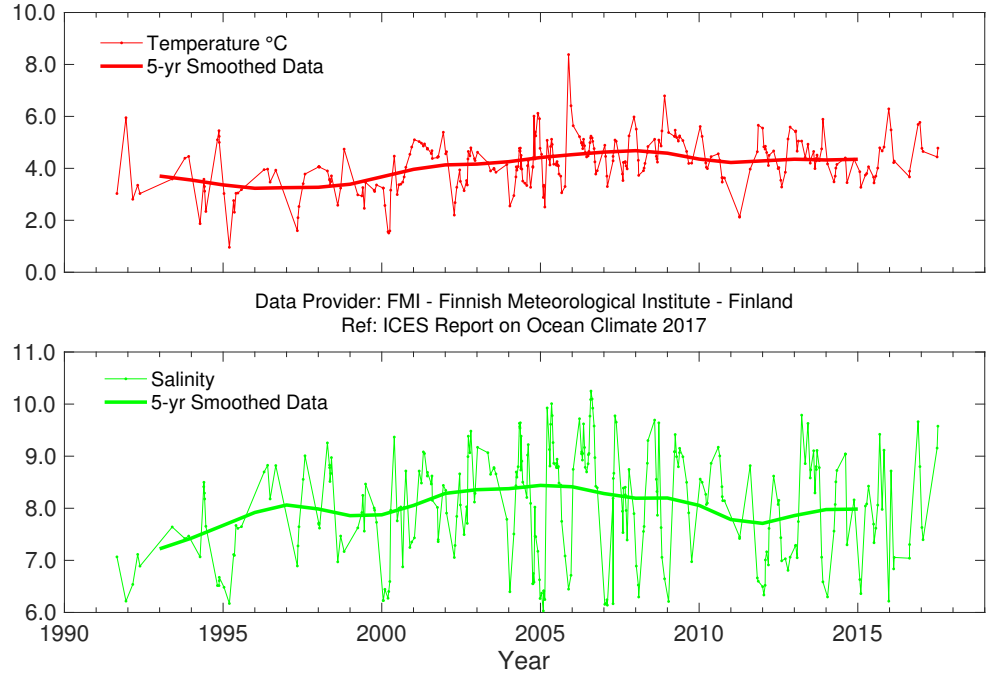

FIGURE 81.
Skagerrak, Kattegat, and the Baltic: Temperature (upper panel) and salinity (lower panel) at Station LL7 in the Gulf of Finland.

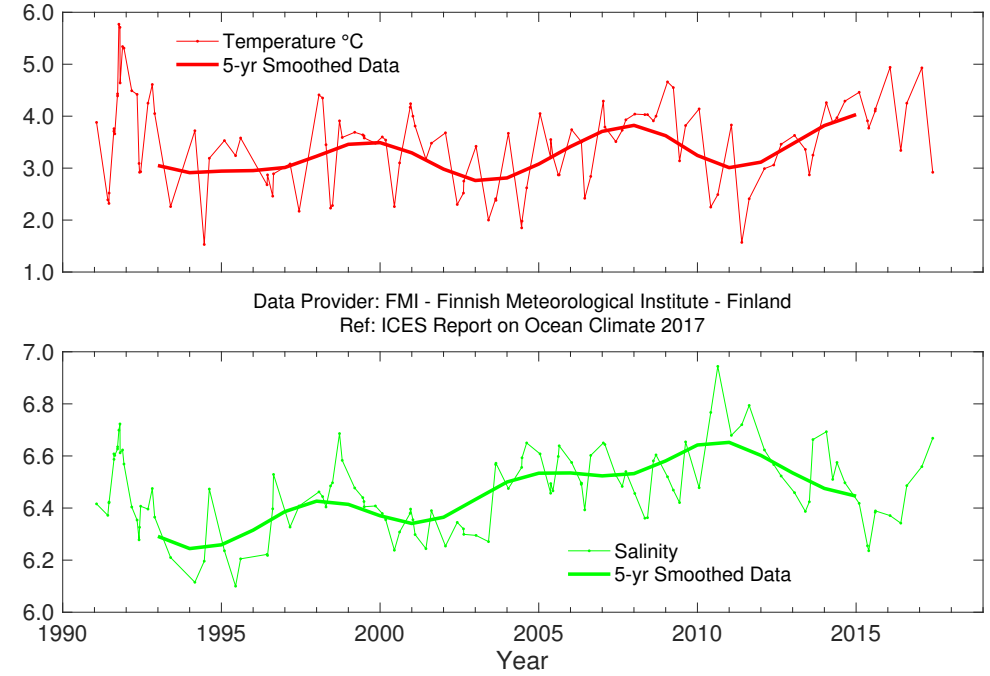

FIGURE 82.
Skagerrak, Kattegat, and the Baltic: Temperature (upper panel) and salinity (lower panel) at Station SR5 in the Bothnian Sea.

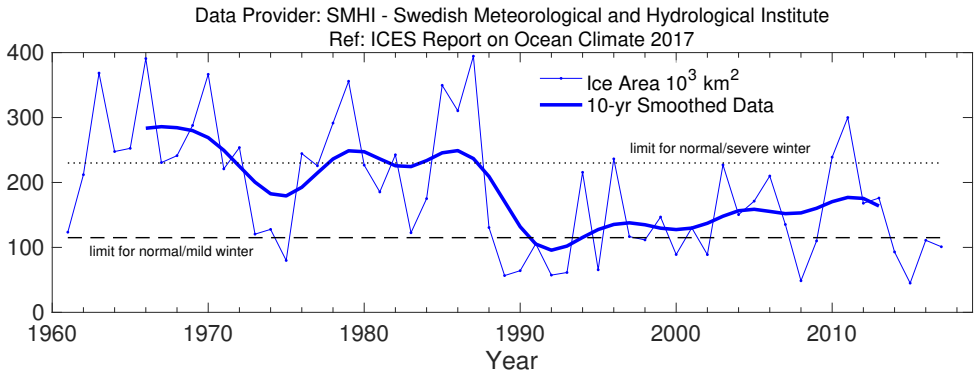

FIGURE 83.
Skagerrak, Kattegat, and the Baltic: The maximum ice extent in the Baltic, starting from 1957.

4.19 NORWEGIAN SEA

K. A. Mork and S. Østerhus

The Norwegian Sea is characterized by warm AW on the eastern side and cold Arctic water on the western side, separated by the Arctic front (Figure 84). AW enters the Norwegian Sea through the Faroe-Shetland Channel and between the Faroes and Iceland via the Faroe Front. A smaller branch, the North Icelandic Irminger Current, enters the Nordic seas on the western side of Iceland. AW flows north as the Norwegian Atlantic Current, which splits when it reaches northern Norway; some enters the Barents Sea, whereas the rest continues north into the Arctic Ocean as the West Spitsbergen Current.

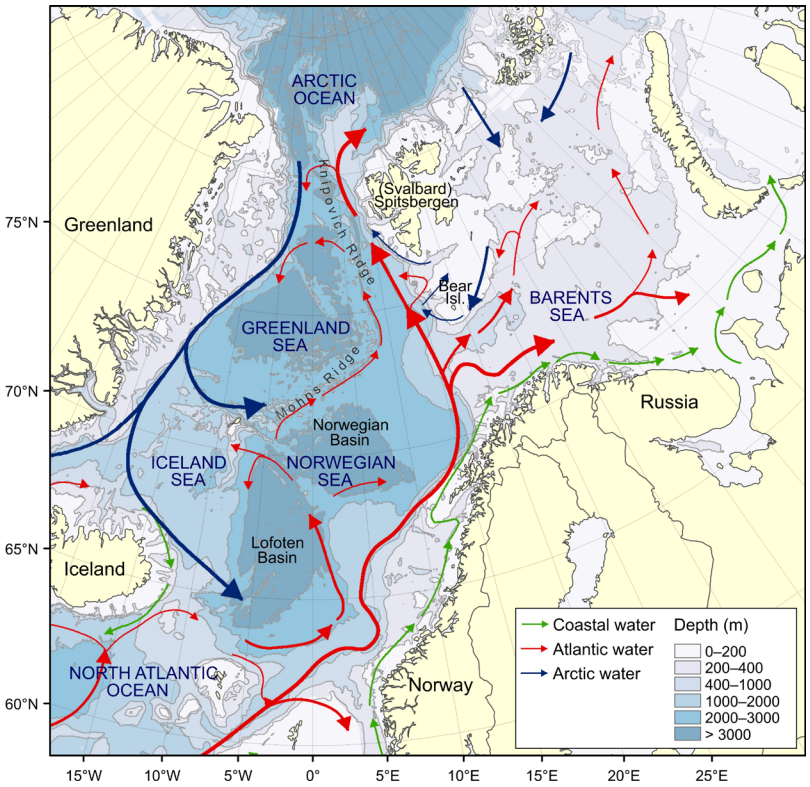

FIGURE 84.
Circulation schematic for the Norwegian Sea, Barents Sea and Fram Strait. Red lines show the poleward movement of Atlantic water (AW) Blue lines show the circulation of Arctic Water. Green lines show the circulation of coastal waters.

Record-high heat content and salinity decline in the Norwegian Sea.

Three sections from south to north in the eastern Norwegian Sea demonstrate the development of temperature and salinity in the core of the AW at Svinøy-NW (Figure 85), Gimsøy-NW (Figure 87), and Sørkapp-W (Figure 88). In general, there has been an increase in temperature and salinity in all three sections since the mid-1990s, except for the most recent years when both temperature and salinity declined at the Svinøy-NW and Gimsøy-NW sections. In the Svinøy-NW section, salinity decreased to the lowest value since the end of the 1970s (Figure 85). Temperatures were still higher than the long-term means for all three sections. Annual temperature averages in 2017 were 0.4°C above the long-term means at both the Svinøy-NW and Gimsøy-NW sections (Figures 85 and 87) and 1.4°C above the long-term mean at the Sørkapp-W section (Figure 88).

Annual salinity averages in 2017 were 0.09 and 0.05 below the long-term means at the Svinøy-NW and Gimsøy-NW sections, respectively, while the annual average salinity was 0.04 above the long-term mean in the Sørkapp-W section.

Ocean heat and freshwater content of AW using hydrographic data during spring from 1951 describe climate variability of the Norwegian Sea (Figure 89). Heat content in the Norwegian Sea has been above the long-term mean since 2000 and was a record-high in 2017. Freshwater content has increased since 2000 and was slightly above the long-term mean in 2017.

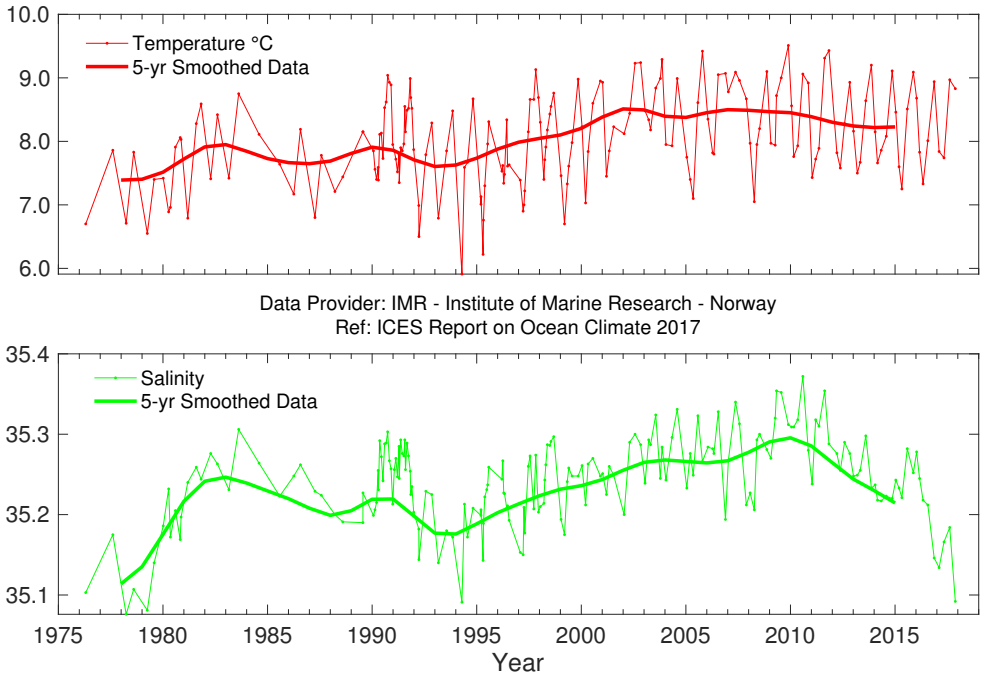

FIGURE 85.
Norwegian Sea: Temperature (upper panel) and salinity (lower panel) above the slope at Svinøy Section (63°N).

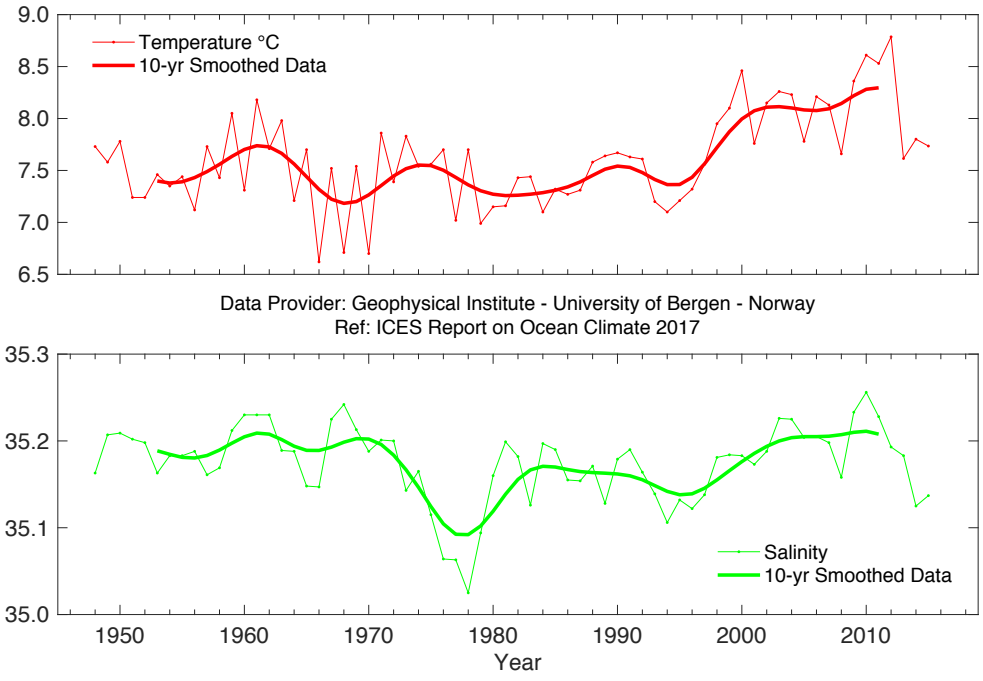

FIGURE 86.
Norwegian Sea: Temperature (upper panel) and salinity (lower panel) at 50 m at Ocean Weather Station "M" (66°N 2°E). Data until 2015.

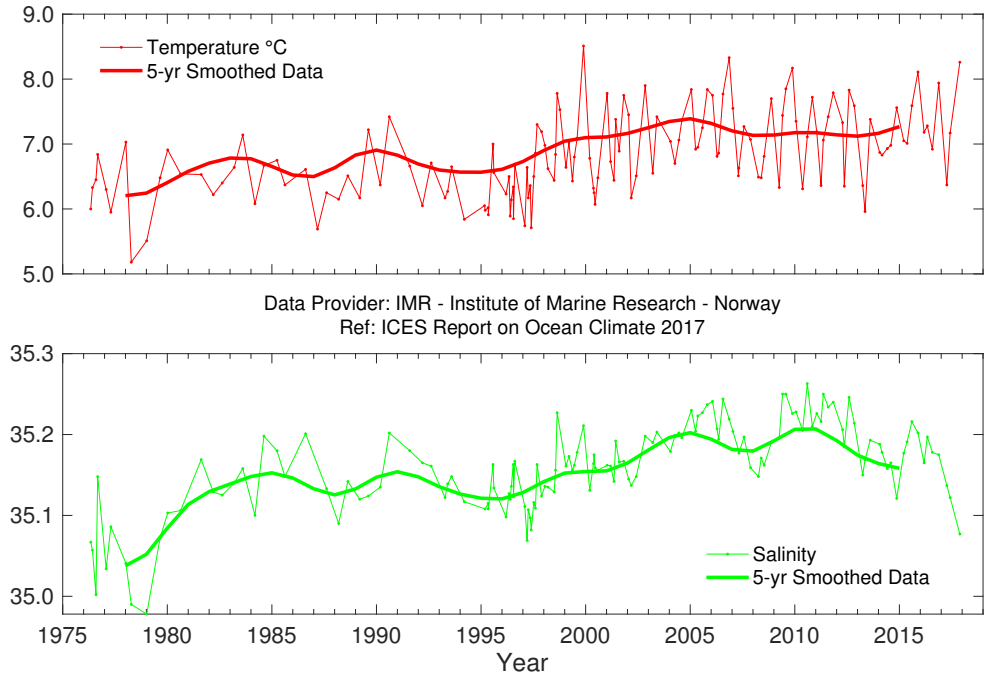

FIGURE 87.
Norwegian Sea: Temperature (upper panel) and salinity (lower panel) above the slope at Gimsøy Section (69°N).

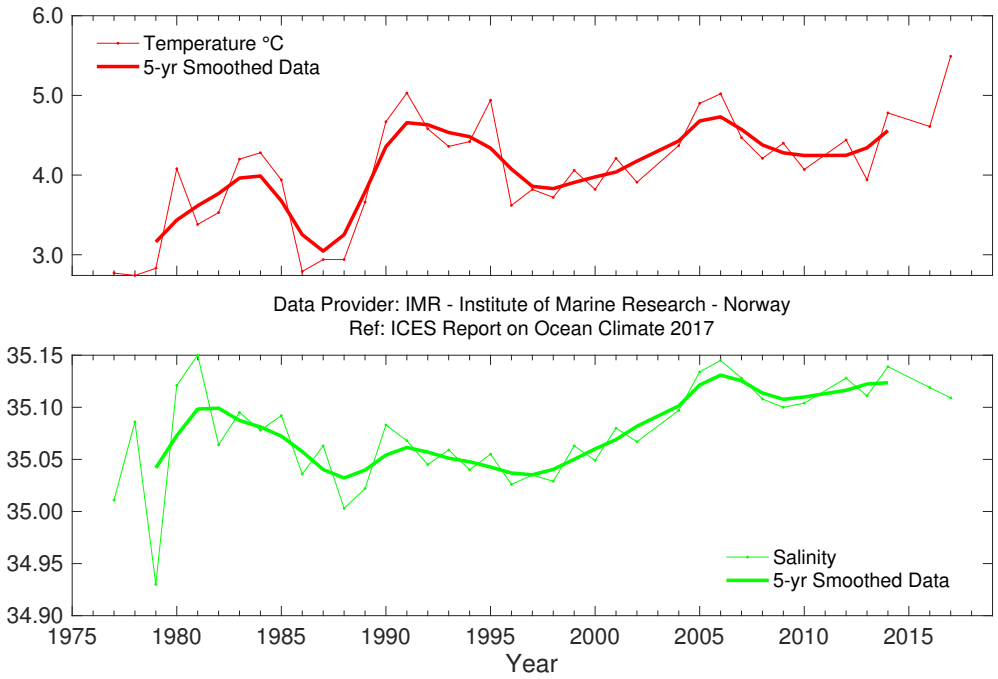

FIGURE 88.
Norwegian Sea: Temperature (upper panel) and salinity (lower panel) above the slope at Sørkapp Section (76°N).

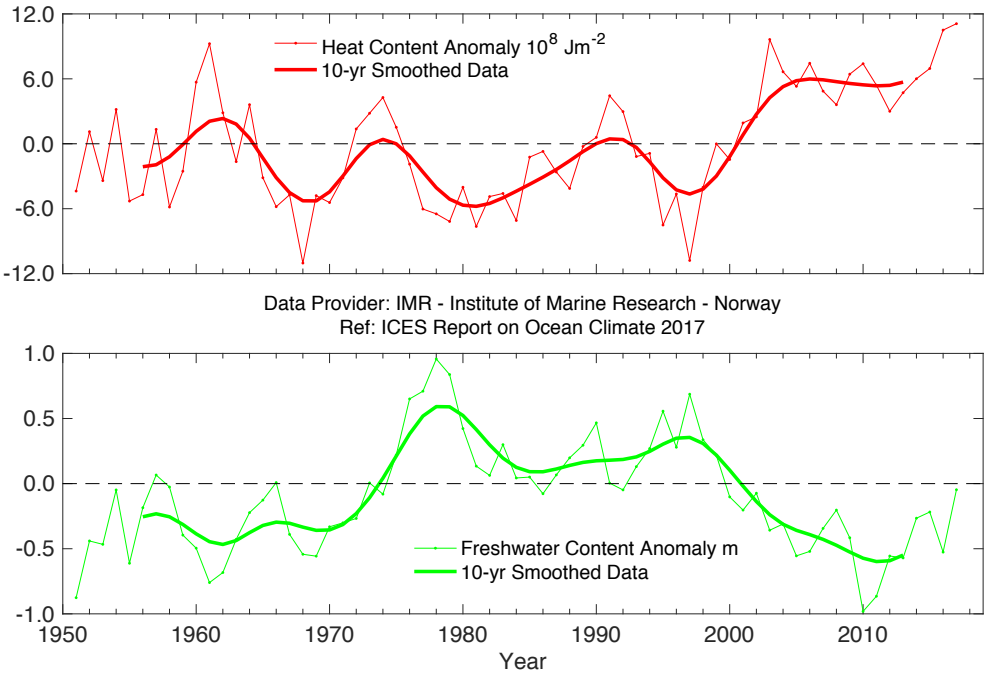

FIGURE 89.
Norwegian Sea: Heat (upper panel) and freshwater (lower panel) contents of Atlantic Water (AW) in the Norwegian Sea.

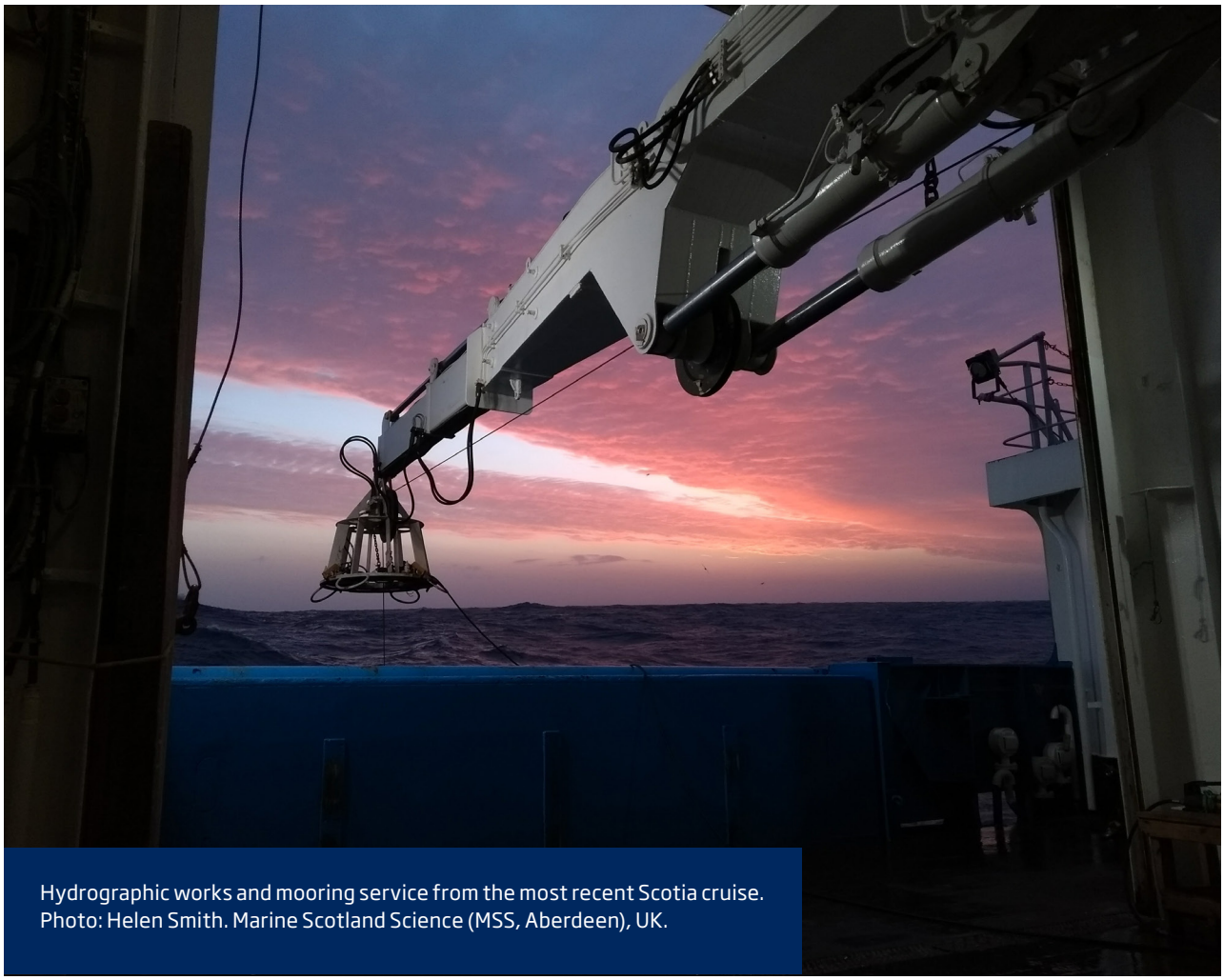

Hydrographic works and mooring service from the most recent Scotia cruise. Photo: Helen Smith. Marine Scotland Science (MSS, Aberdeen), UK.

4.20 BARENTS SEA

A. Trofimov and R. Ingvaldsen

The Barents Sea is a shelf sea that receives an inflow of warm AW from the west (Figure 84). This inflow demonstrates considerable seasonal and interannual fluctuations in volume and water-mass properties, causing high variability in heat content and ice coverage of the region.

In 1996 and 1997, after a period with high temperatures in the first half of the 1990s, temperatures in the Barents Sea dropped to values slightly below the long-term average. From March 1998, temperature in the western Barents Sea increased to just above average, whereas temperature in the eastern part remained below average during 1998. From the beginning of 1999, there was a rapid temperature increase in the western Barents Sea that spread to the eastern part. Since then, temperature has remained above average.

In 2017, air and water temperatures in the Barents Sea were still well above average, typical of warm and anomalously warm years, but lower than in 2016. In June 2017, observations along the Kola Section (Figure 91) were recommenced after a one-year gap. From June to December, AW (0–200 m) in the section was 0.6–1.1°C warmer than normal. In coastal waters, positive temperature anomalies were decreasing from June (0.6°C) to October (0.1°C). Due to weak seasonal cooling in November and December, the anomalies increased and exceeded 0.9°C in all parts of the section by the end of 2017, typical of anomalously warm years. Compared to the first half of 2016, when record-high positive temperature anomalies (1.0–1.3°C) were observed in the Kola Section, they decreased in the second half of 2017. From June until December 2017, coastal waters (inner part of the section) and AW (central part of the section) were slightly fresher than average, whereas AW salinity in the outer part of the section was close to average.

From August until October 2017, surface, deeper, and bottom waters were still much warmer (by 1.1, 0.9, and 1.1°C, respectively, on average over the surveyed area) than the long-term mean (1931–2010) in most of the Barents Sea. However, they were colder (by on average 1.0, 0.7 and 0.8°C, respectively) than in 2016 in most of the sea (more than 84% of the surveyed area), and negative anomalies were observed in the northern part of the sea at all depths and in its southwestern part at the surface. From August until October, surface waters were saltier (+0.3) than the long-term mean (1931–2010) in most of the Barents Sea, with the largest positive anomalies west of the Spitsbergen Archipelago as well as in the southeastern and northeastern parts of the sea. Negative salinity anomalies were mainly found in the southern and northern parts. Bottom salinity was close to average in most of the sea. In autumn 2017, the area covered by AW (> 3°C) was still rather large, but decreased compared to a record large value in 2016, whereas the areas covered by Arctic and cold bottom waters (< 0°C) were still rather small, but increased compared to record small values in 2016. In 2017, ice coverage in the Barents Sea was still well below average (1951–2010), but higher than in 2016. Its smallest value (1%) was observed in September, when ice was only found between islands of the Franz Josef Land Archipelago and east of the Spitsbergen Archipelago.

Well above-average temperatures and low ice coverage in the Barents Sea in 2017.

On average, the Atlantic current brings about 2 Sv of water and 50 TW (relative 0°C) of heat into the Barents Sea. The volume and heat flux vary with periods of several years and was significantly lower during 1997–2002 than during 2003–2006. After 2006, inflow was relatively low for several years before increasing during winter 2014/2015. Maximum annual inflow was in 2015 when comparing the full time-series 1997–2017, with volume and heat fluxes almost 1.5-fold higher (3 Sv and 72 TW, respectively) than the long-term mean. Inflow decreased again in 2016, making that year close to the long-term mean. The dataseries stopped in March 2017; thus no information about summer, autumn, or early winter 2017 is yet available.

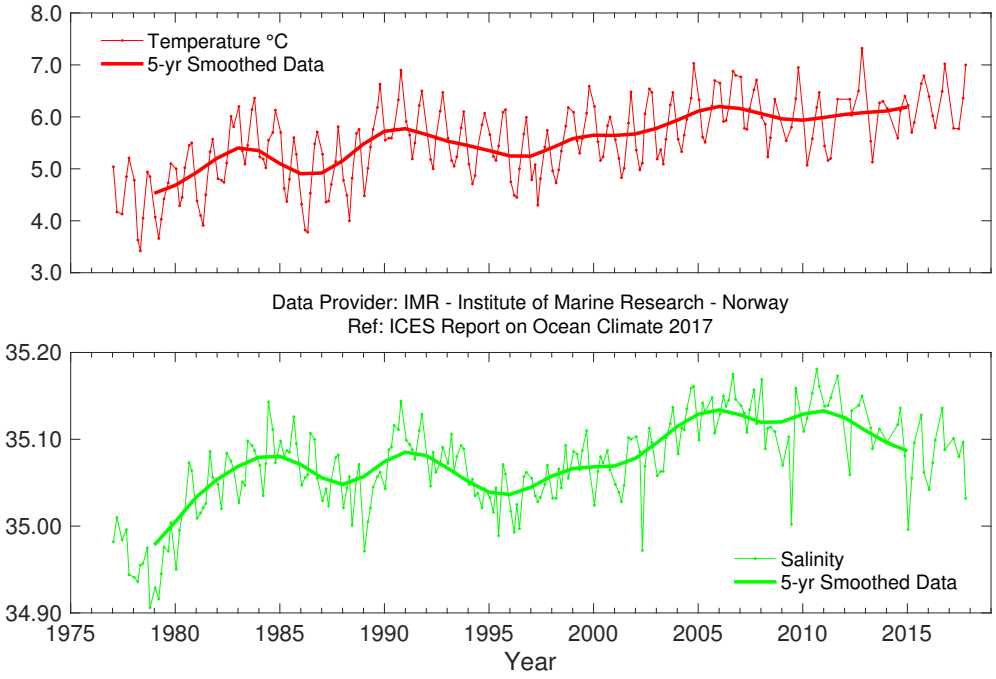

FIGURE 90.
Barents Sea. Temperature (upper panel) and salinity (lower panel) in the Fugløya–Bear Island Section.

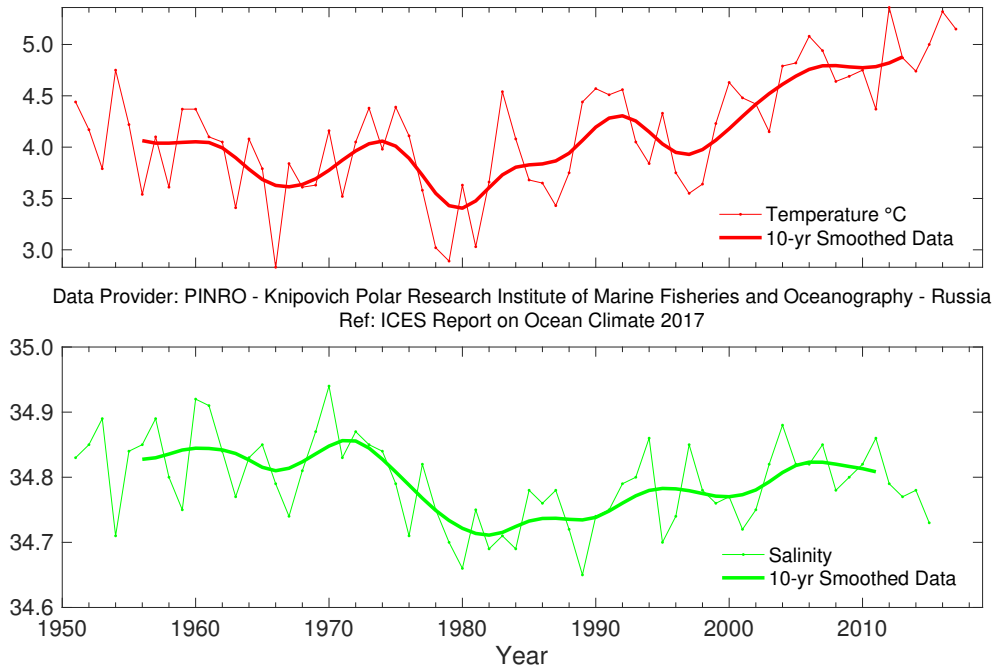

FIGURE 91.
Barents Sea. Temperature (upper panel) and salinity (lower panel) in the Kola Section (0–200 m). Salinity data until 2015.

4.21 GREENLAND SEA AND FRAM STRAIT

A. Beszczynska-Möller, W.J. von Appen, and G. Budeus.

The Fram Strait is the northern border of the Nordic Seas. It is the only deep passage connecting the Arctic to the rest of the world's oceans and one of the main routes whereby Atlantic Water (AW) enters the Arctic (the other is the Barents Sea). AW flows along the eastern rim of the Greenland Sea and in the Fram Strait is carried northwards by the West Spitsbergen Current. AW temperature, salinity, volume, and heat fluxes exhibit strong seasonal and interannual variations. A significant part of the AW also recirculates within Fram Strait and returns southwards (Return Atlantic Water). Polar Water from the Arctic Ocean flows south in the East Greenland Current and affects water masses in the Nordic Seas.

The temperature of Atlantic Water (AW) at the eastern rim of the Greenland Sea (along the 75°N section, between 10° and 13°E) reached its highest value in 2005–2007 with a peak in 2006. After this period, AW temperature decreased significantly in 2008–2009 and remained below its long-term mean value until 2011. Over the following three years (2012–2014), the temperature of AW in the eastern Greenland Sea increased and remained relatively stable with its values slightly exceeding its long-term mean (by 0.3°C). In 2015, the AW temperature increased further and reached 5.09°C (0.55°C warmer than average), the highest value recorded in the last decade. A slight cooling followed in 2016 and 2017 but AW remained about 0.4°C warmer than its long-term average. A significant increase in the salinity of AW in the eastern Greenland Sea was observed in 2005–2006, with a maximum of 35.16 recorded in 2006 (exceeding the long-term average by 0.07). This peak was followed by a sharp decrease in 2007 and a further slow descent until 2009, when AW salinity returned to its long-term average. In 2010, salinity began to rise again and reached another peak in 2012 (0.06 above its long-term mean). Between 2013 and 2017, it has been decreasing slowly except a slight rise found in 2014. Since 2004, the salinity of AW in the eastern Greenland Sea has been above its long-term average (except 2009 when it levelled out).However, a decreasing tendency in recent years, saw AW salinity in 2017 drop 0.03 from the 2016 figure and was only slightly more saline (0.02) than average.

The western and central areas of the Greenland Sea section at 75°N have not been measured since 2010. The temperature of Return Atlantic Water (RAW) at the western edge of the Greenland Sea reached it's maximum, 2.9°C, in 2006 and slowly decreased until the end of the observation period (2010). In 2008–2010, the RAW temperature was slightly lower than its long-term average. The high temperature in 2006 was accompanied by a strong peak in RAW salinity (0.13 above the long-term mean, more than 3 times higher than the standard deviation of RAW salinity). In 2007, the RAW salinity dropped again but remained slightly higher than its long-term average until 2008. In 2009 and 2010, further decreases brought salinity levels close to the long-term average.

In the southern Fram Strait, at the standard section along 76.50°N (at the level of 200 dbar, spatially averaged between 9° and 12°E), record-high summer temperatures for AW were observed in 2006 (maximum of 4.5°C, exceeding the long-term average by 1.3°C), accompanied by the highest AW salinity (35.13) in the observation period. Following this peak, the temperature and salinity decreased rapidly in 2007 and 2008, before increasing again in summers 2009–2012. In 2011–2015, AW temperature in the southern Fram Strait remained relatively constant (3.7–3.8°C, exceeding its average by approx. 0.6°C) except in summer 2013 when it dropped to 3.22°C and levelled out with its long-term mean value. A moderate increase has been observed since 2015 and in 2017, AW temperature reached its decadal maximum of 4.1°C, the second highest value after the 2006 maximum of 4.5°C. In 2011, 2012, and 2014, AW salinity levels in the southern Fram Strait were similar to those experienced during the 2006 maximum (35.13), exceeding the long-term mean by 0.07. Salinity slightly dropped in 2013 and 2015 but, since 2004, the salinity of AW has remained higher than its long-term mean value. After recovering from a drop in 2015, AW salinity has remained constant in 2016 and 2017 (about one standard deviation, i.e. 0.04, above its long-term mean of 35.06).

In the northern Fram Strait, at the standard section along 78.83°N, three characteristic areas can be distinguished in relation to the main flows: the West Spitsbergen Current (WSC) between the shelf edge

and 5°E, the Return Atlantic Current (RAC) between 3°W and 5°E, and the Polar Water in the East Greenland Current (EGC) between 3°W and the Greenland Shelf.

The spatially-averaged mean temperature of the upper 500 m layer in the WSC reached its peak in 2006 (4.54°C) and then decreased, varying in 2007–2011 within the range of ±0.4°C of the long-term average. In 2012–2013, the temperature in the WSC dropped further, reaching 0.7–0.8°C below its long-term mean. Since 2014, it has been rising again and, in 2015, reached the second highest value in the observation period (4.24°C, exceeding the long-term mean by 1.13°C). After a drop of about 0.7°C in 2016, temperature in the WSC returned to a high value of 4.05°C in 2017, exceeding its long-term average by 0.94°C. The highest salinity in the upper 500 m in the WSC was observed in 2006 (35.11), followed by a decrease to the long-term average in 2007–2008. Since 2009, salinity in the WSC increased again, reaching 0.5 above the long-term mean in 2011. After a slight decrease in 2012–2013, salinity in the WSC reached its second maximum (35.09) in 2014, followed by slightly lower values in 2015 and 2016. In 2017, AW salinity in the WSC increased again to 35.07, below the 2014 maximum but 0.05 above the long-term average.

In 2017, the AW at the standard section along 78.83°N occupied the core of the WSC deeper than in 2016. In 2016, the isotherm of 2°C reached a depth of 700–800 m in the WSC core located over the upper shelf slope, while one year earlier it was found at 500–600 m. In the offshore branch of the WSC, located over the lower shelf slope, the AW layer in 2017 was only slightly deeper and occupied by slightly warmer and more saline AW than in 2016. The low salinity surface water covered the upper 20–30 m layer over the WSC core in 2017 (opposite to 2016 when it was absent in the WSC).

The RAC and EGC domains were not measured in 2017. The RAC temperature in 2016 remained close to the previous year and a temperature difference between the Atlantic water in the WSC and that recirculating in the RAC was only a half of the 2015 value (0.7°C in 2016 as compared to 1.5°C). The highest temperature in the RAC was observed in 2005 (3°C) and in 2009–2010 (slightly above 2.9°C) while since 2011 it remained close to the long-term average of 2.2°C. Since 2013 the RAC temperature has increased slowly and reached 2.8°C in 2016. The maximum salinity in the RAC was observed in 2010 and in the following years (2011, 2012, and 2014) it exceeded its long-term mean by about 0.05, but leveled out in 2015 and increased again in 2016.

The temperature of the Atlantic inflow in the eastern Greenland Sea and Fram Strait has slowly increased 2012–2017 and was slightly higher in 2017 than in 2016. Over the last decade, it has remained below the 2006 maximum. In 2017, the salinity of the Atlantic inflow entering Fram Strait slightly decreased compared with 2016 but it has consistently stayed above its long-term average over the last decade.

In the EGC domain temperature reached its peak in 2007 (1.9°C), decreased significantly to 0.3°C in 2008 and since then has remained relatively stable (within ±0.3°C from its long-term mean) with a slight decrease to 0.3°C in 2014 and return to 1.0°C in 2015. In 2016 the EGC temperature was slightly higher than in the previous year. The salinity in the EGC was highest in 2007 (34.90) and dropped afterwards below its long-term average except of the intermediate peak (34.72) in 2011. In 2008 and 2014, the EGC salinity reached the lowest value during the last decade (34.50 as compared to the record low minimum of 34.45 observed in 2000 and 2002). Since 2014 salinity has steadily increased and in 2016 was slightly above its long-term mean.

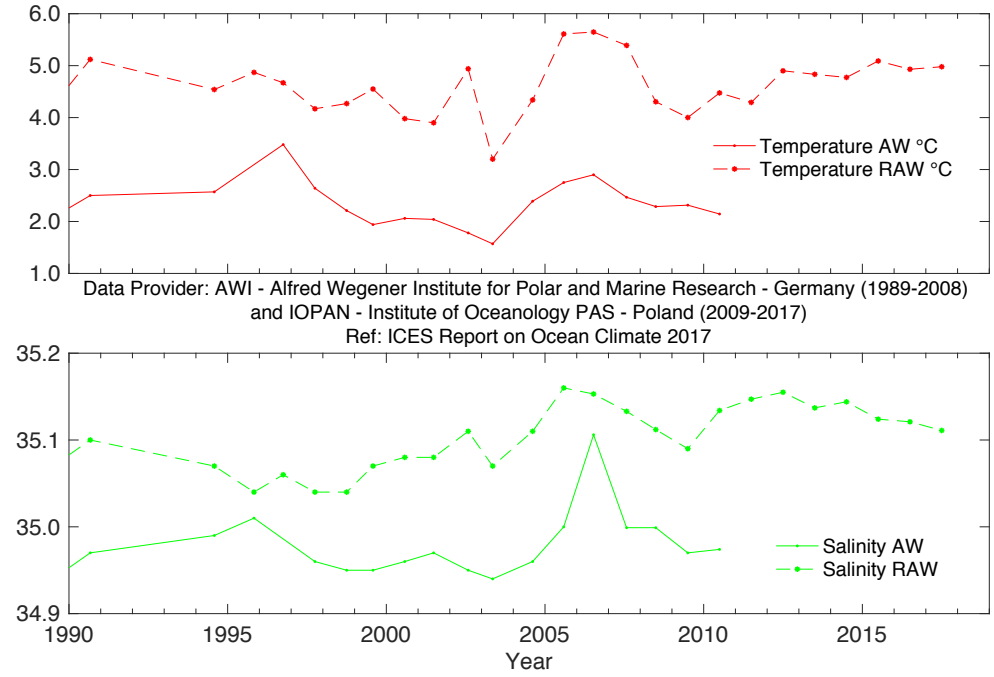

FIGURE 92.
Greenland Sea and Fram Strait. Temperature (upper panel) and salinity (lower panel) of Atlantic Water (AW) and Return Atlantic Water (RAW) in the Greenland Sea Section at 75°N. AW properties are 50–150 m averages at 10–13°E. The RAW is characterized by temperature and salinity maxima below 50 m averaged over three stations west of 11.5°W (not updated after 2010).

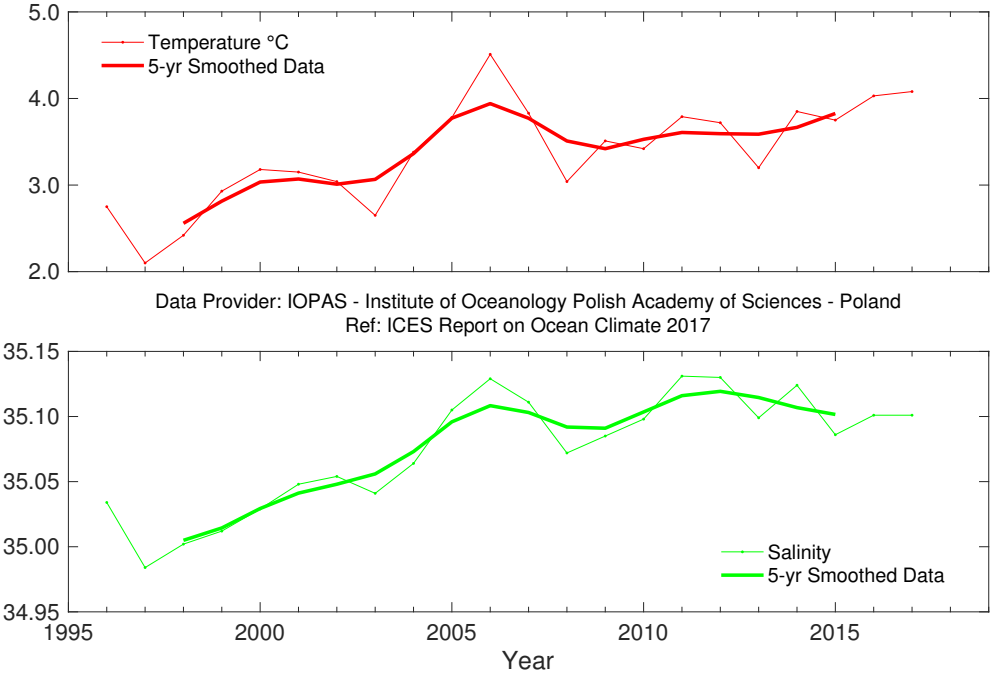

FIGURE 93.
Greenland Sea and Fram Strait. Temperature (upper panel) and salinity (lower panel) at 200 dbar in the southern Spitsbergen Section (76.50°N).

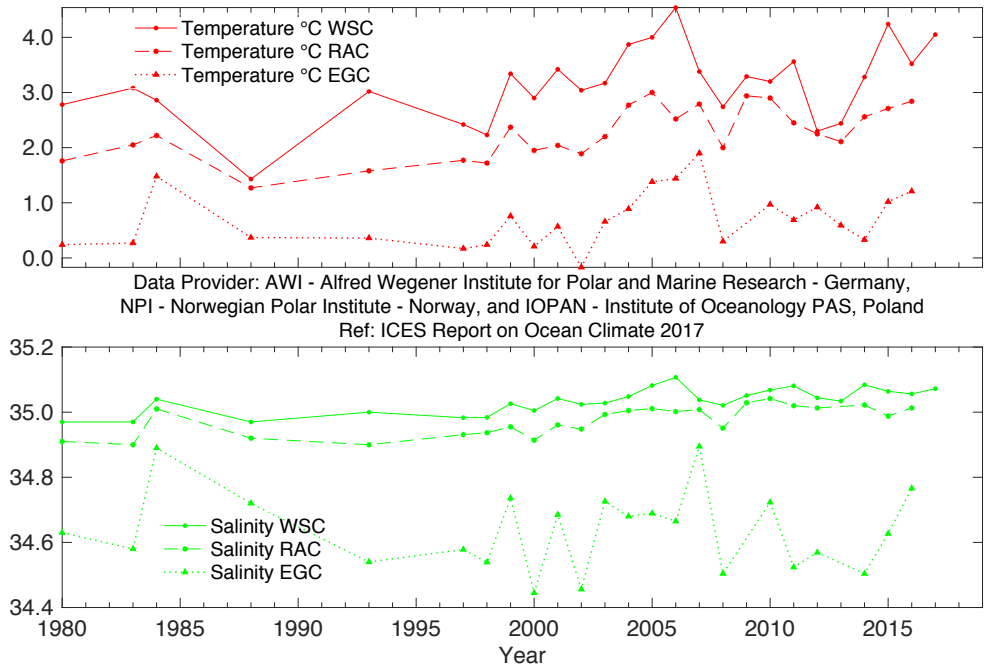

FIGURE 94.
Greenland Sea and Fram Strait. Temperature (upper panel) and salinity (lower panel) in Fram Strait (78.83°N) at 50–500 m: in Atlantic Water (AW) in the West Spitsbergen Current (WSC; between the shelf edge and 5°E), in the Return Atlantic Current (RAC; between 3°W and 5°E, not updated in 2017), and in the polar water in the East Greenland Current (EGC; between 3°W and the Greenland Shelf, not updated in 2017).

Pilot whales.
Photo: Penny Holliday, National Oceanography Centre, UK.

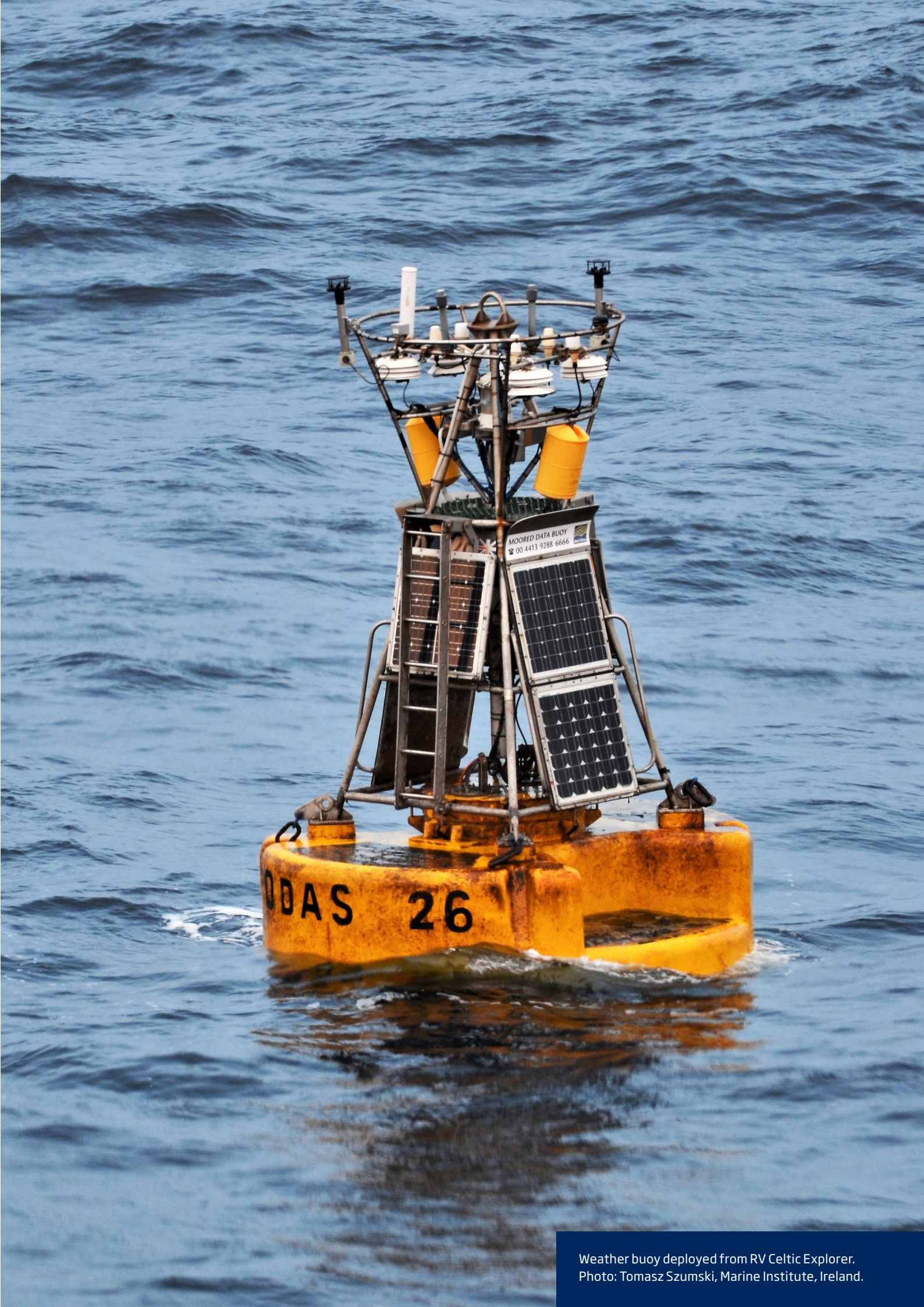

Weather buoy deployed from RV Celtic Explorer.
Photo: Tomasz Szumski, Marine Institute, Ireland.

Attaching a microcat to a mooring line on RRS Discovery
Photo: Penny Holliday, National Oceanography Centre, UK.

5. DETAILED AREA DESCRIPTIONS, PART II: DEEP OCEAN

INTRODUCTION

In this section, we focus on the deeper waters of the Nordic seas and the North Atlantic, typically below 1000 m. The general circulation scheme and dominant water masses are given in Figure 95.

At the northern boundary of our region of interest, the cold and dense outflow from the Arctic Ocean enters Fram Strait along its western side and reaches the Greenland Sea. The outflow is a mixture of Eurasian Basin and Canadian Basin deep waters and upper polar deep water (UPDW). The Eurasian deep water feeds the densest water of all Nordic seas: the Greenland Sea bottom water. The Canadian Basin deep water and UPDW supply the Arctic Intermediate Water in the Greenland Sea, and the UPDW also includes products of winter convection. The deep southward outflow from the North Atlantic in the deep western boundary current is fed by cold and dense overflow waters. The deepest and densest is the Denmark Strait overflow water (DSOW). This water mass originates in the Arctic intermediate water produced in the Greenland and Iceland seas by winter convection and mixing with surrounding water masses. The DSOW sinks to the bottom as it passes over the Denmark Strait sill, vigorously entraining ambient water. Downstream, it is overlain by an intermediate water mass, that of LSW, formed by deep winter con-vection in the Labrador Sea. The middle layer of the deep, cold-water export in the deep western boundary current is supplied by the Iceland–Scotland Overflow Water, originating in water masses formed in the Norwegian Sea (Arctic Intermediate Water and Norwegian Sea Deep Water). Passing through the Iceland Basin, the Iceland–Scotland Overflow Water also entrains upper ocean water and LSW. Deep Antarctic Bottom Water enters the North Atlantic on the western side, but its signature is also present in eastern Atlantic abyssal basins. At intermediate levels, MW originates from vigorous mixing of Atlantic central waters and Mediterranean outflow waters at the Gulf of Cadiz. This water mass spreads at a depth of ca. 1000 m in all directions, with a main vein progressing northward along the European margin. Around the Canaries, MW encounters the northern limit of Antarctic Intermediate Waters.

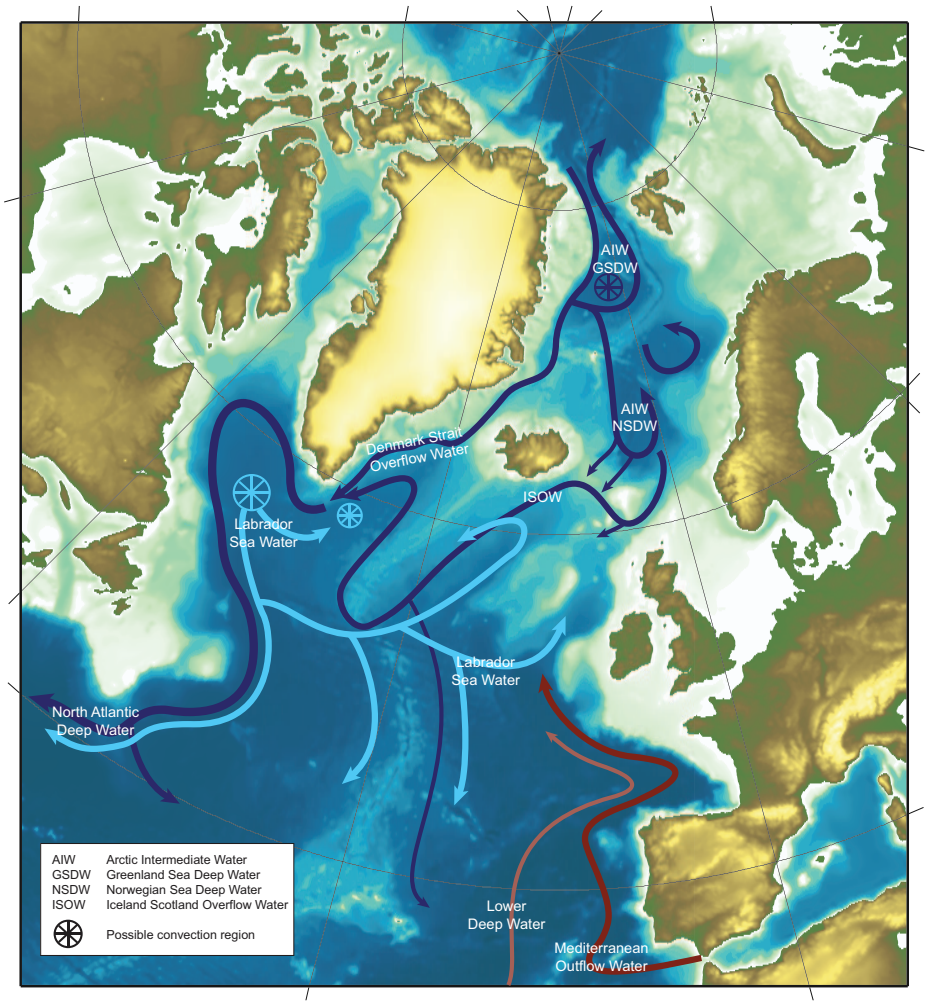

FIGURE 95.
Schematic circulation of the intermediate to deep waters in the Nordic seas and North Atlantic.

5.1 NORDIC SEAS

Deep waters of the Greenland, Iceland, and Norwegian seas are all warming. The source of the warming is the deep outflow from the Arctic Ocean, a south-flowing current of the Eurasian and Canadian Basin deep waters and the UPDW found on the western side of Fram Strait at ca. 2000 m depth. The Greenland Sea deep water (GSDW) is warming fastest owing to its direct contact with this Arctic outflow, whereas the Iceland and Norwegian seas are warming more slowly because they are products of the mixing of their own ambient waters with GSDW and Arctic outflow water.

5.1.1 Greenland Sea

A. Beszczynska-Möller and G. Budeus

Continuous warming has been observed in the Greenland Sea deep layer at 3000 m, both in the Greenland Sea Gyre (not measured since 2011) and in the eastern part of the deep basin (5°E). The temperature of Greenland Sea deep water (GSDW) is similar in both locations where a relatively steady increase of temperature from −1.18°C to −0.88°C was observed between 1993 and 2017. The largest temperature increase of 0.03°C was found between 2010 and 2011 while in the recent period its year-to-year changes were lower (between 0 and 0.02°C). Between 2016 and 2017, the deep water in the eastern Greenland Sea warmed by 0.01°C. For the entire observing period (1993–2017) the average warming rate in the deep Greenland Sea can be estimated on 0.12°C per decade.

The warming of deep waters in the Greenland Sea is accompanied by an increase in salinity, albeit its interannual variability differs between the central Greenland Sea Gyre (observed in 1993–2010) and the eastern Greenland Sea (measured since 2001). A relatively steady increase of salinity from 34.901 in 1993 to 34.916 in 2010 was observed in the Greenland Sea Gyre. In the eastern part of the deep Greenland Sea, the year-to-year changes are much larger than in the central gyre but the overall trend in 2001–2017 is positive and similar to that in the central basin. The salinity increase is of the order of 0.01 per decade. The maximum salinity, 34.919, was found in the eastern Greenland Sea in 2015 and 2017, with a slight drop in 2016.

After a cessation of deep convection, a two-layered water mass arrangement has replaced the doming structure in the Greenland Sea Gyre. During the measurement period 1993–2010, the winter convection depth has varied between 700 and 1600 m and has only been significantly deeper in small-scale convective eddies. In winter 2007/2008, the maximum convection depth was estimated to be 1700 m, deeper than the previous year (1200 m) and similar to the maxima observed during 2001/2002 and 2002/2003. The import of warm and saline Atlantic Water (AW) to the Greenland Sea is not balanced by an import of cool and fresh Polar Water from the north. The AW dominates changes in the upper ocean: it tends to prevent ice formation and vertically homogenize the waters ventilated by convective processes. The GSDW formerly included a small admixture of surface freshwater through the convective process and, therefore, had a lower salinity than the Arctic outflow waters. The observed increase in GSDW salinity may be the result of an adjustment to the Arctic outflow in the continued absence of deep convection and an increased presence of AW in the upper layer.

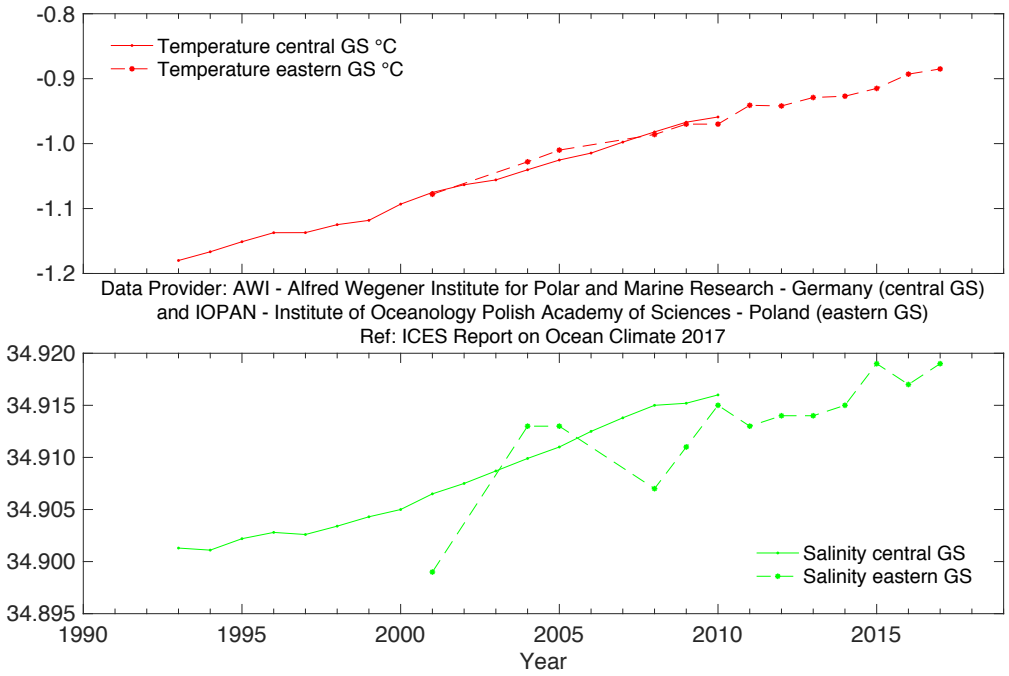

FIGURE 96.
Greenland Sea and Fram Strait. Temperature (upper panel) and salinity (lower panel) at 3000 m in the Greenland Sea Section at 75°N (solid line in the central Greenland Sea Gyre, dashed line in the eastern Greenland Sea at 5°E).

5.1.2 Norwegian Sea

S. Østerhus

The longest time-series in the Nordic seas is from Ocean Weather Station M in the Norwegian Sea. It reveals warming from the mid-1980s; however, a slight decrease in temperature occurred in 2010/2011 and again in 2014/2015 (Figure 97). Preliminary data from 2016 and 2017 are limited, but they indicate that the temperature at 2000 m increased to −0.78°C (same value for both years), which is in line with the warming trend over the last several decades. The long-term warming rate for the most recent decade is 0.08°C, similar to that in the Iceland Sea, but lower than in the Greenland Sea.

It is unclear whether there has been any corresponding salinity trend in the Norwegian Sea deep waters in recent decades. After a slight decrease in the early 1990s, salinity in the Norwegian Sea deep basins has remained relatively stable over the 2000s and until 2017, but with a record-low value in 2012 (Figure 97).

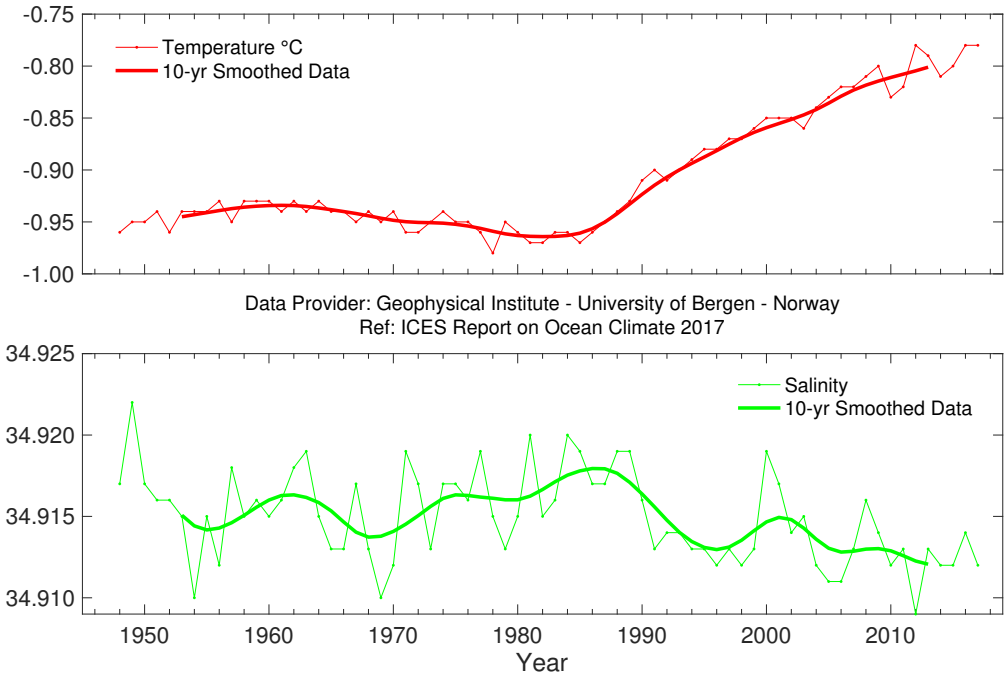

FIGURE 97.
Norwegian Sea. Temperature (upper panel) and salinity (lower panel) at 2000 m at Ocean Weather Station M (66°N 2°E).

Dissolved oxygen sample taken from CTD at GO-SHIP transatlantic survey 2017. Photo: Tomasz Szumski, Marine Institute, Ireland.

5.1.3 Iceland Sea

H. Valdimarsson

In the Iceland Sea, an increase in temperature in the depth range 1500–1800 m has been observed almost continuously since the beginning of the time-series (early 1990s), and the temperature continued to rise slowly until the end of 2017 (Figure 98). The long-term warming rate for the last decade is 0.063°C.

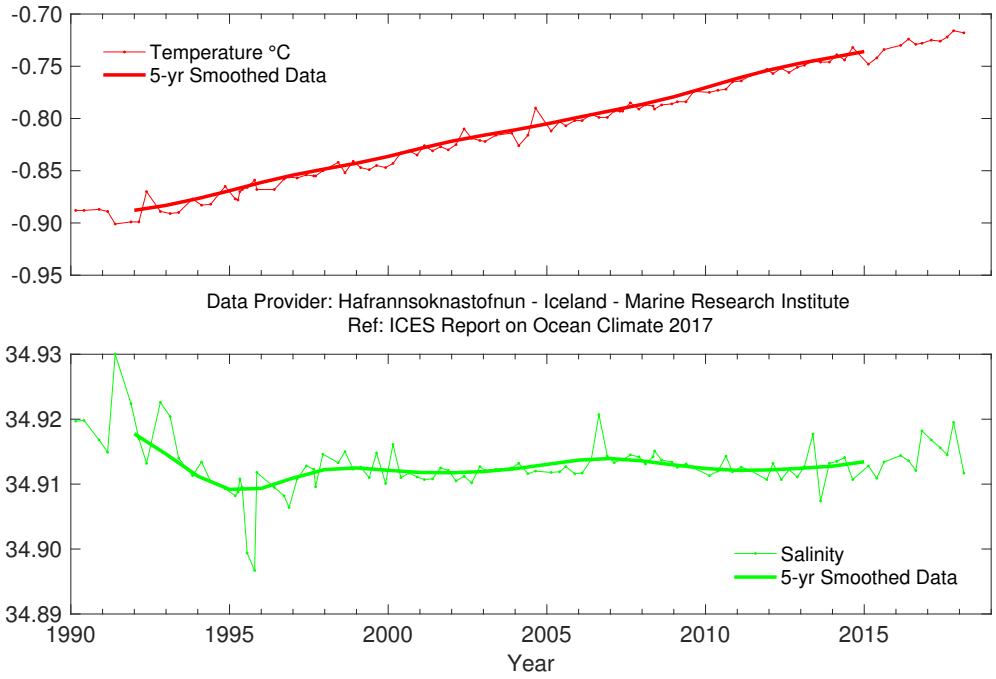

FIGURE 98.
Icelandic waters. Temperature (upper panel) and salinity (lower panel) at 1500-1800 m in the Iceland Sea (68.00°N 12.67°W).

Hydrographic works and mooring service from the most recent Scotia cruise. Photo: Helen Smith. Marine Scotland Science (MSS, Aberdeen), UK.

5.2 NORTH ATLANTIC

5.2.1 Greenland–Scotland Ridge overflow waters

B. Berx and J. Hindson

In the deep layers of the Faroe–Shetland Channel, the properties at 800 m are the same as those of Norwegian Sea deep water as it passes through the Channel back into the North Atlantic.

The temperature at this depth has relatively strong variability, but the overall trend is of decreasing temperature from the 1950s to the 1990s (Figure 99). Following some fluctuations with both increasing and decreasing temperatures, there has been an increasing trend from around 2000 until 2017, but the temperature still remains lower than the highest temperatures observed in the early 1980s. Relatively stable salinity in the first period of measurements (1950 until the mid-1970s) was followed by a slow decline. The lowest annual mean salinity values were observed in 1997; there has been a slow but gradual increase in salinity since then (Figure 99).

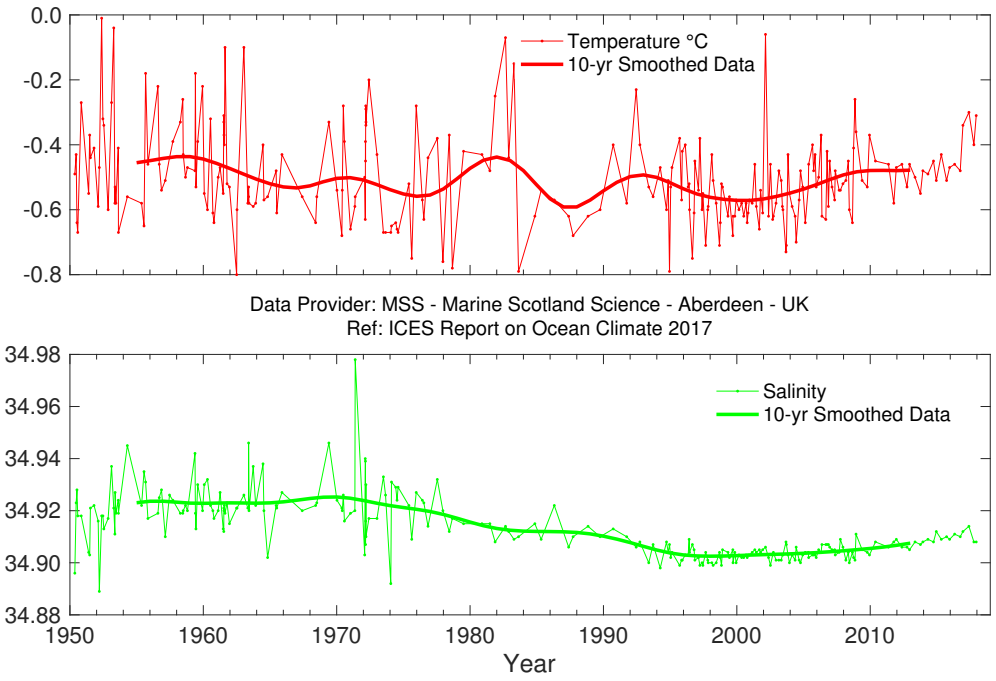

FIGURE 99.
Faroe-Shetland Channel. Temperature (upper panel) and salinity (lower panel) at 800 m.

5.2.2 Iceland Basin

N. P. Holliday

In the Iceland Basin, LSW is the dominant water mass below about 1000 m, evident as a large recirculating body of relatively fresh and low stratified water whose core lies between 1700 and 2000 m (Holliday *et al.*, 2015). In 2017, the LSW was similar in temperature and salinity to the preceding five years, and temperature and salinity were both slightly higher than the 1996–2010 means (Figure 100).

After the Norwegian Sea deep water flows through the Faroe–Shetland Channel and Faroe Bank Channel and into the Iceland Basin, it becomes known as Iceland–Scotland overflow water (ISOW; Figure 59). The dense water, supplemented by a small amount of additional flow over the sill between Iceland and the Faroes, mixes rapidly with upper ocean and intermediate water of the Iceland Basin, entraining the lighter water and increasing the volume of the overflow plume. Properties of the ISOW measured at 20°W in the Iceland Basin, therefore, become a product of the properties of the dense water at the sill and the entrained ambient water. ISOW temperature and salinity vary closely with the LSW and upper ocean water in the Iceland Basin; since 1996, the water has warmed and increased in salinity, although there has been a slight decrease in both since 2011 (Figure 101).

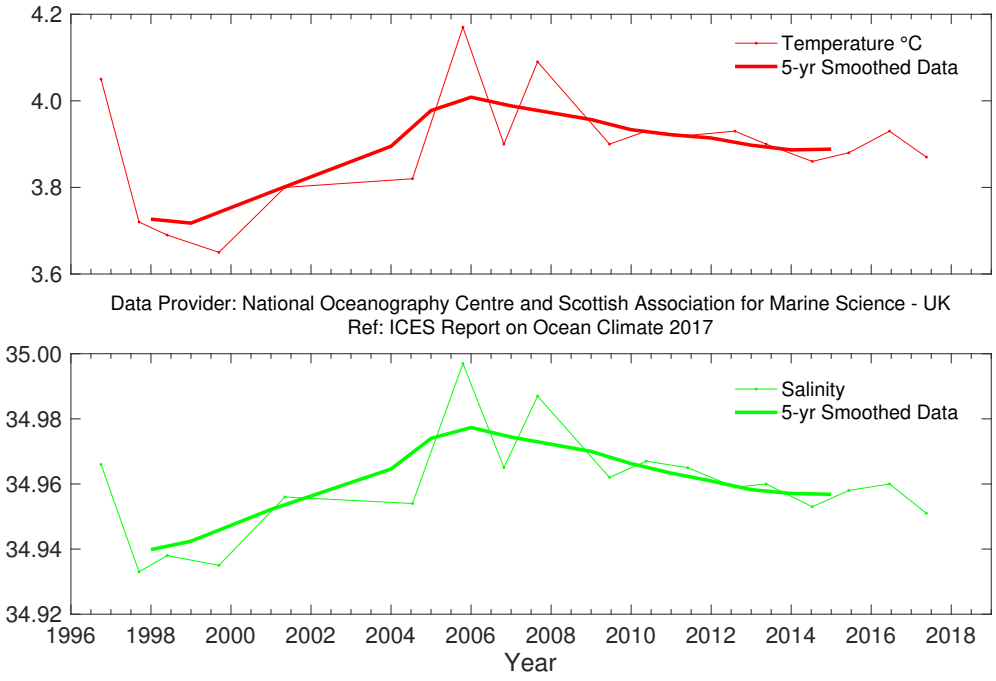

FIGURE 100.
Iceland Basin. Temperature (upper panel) and salinity (lower panel) of Labrador Sea water (LSW; 27.70 ≤ σθ ≤ 27.85 kg m^{-3}, ca. 1200–2000 m).

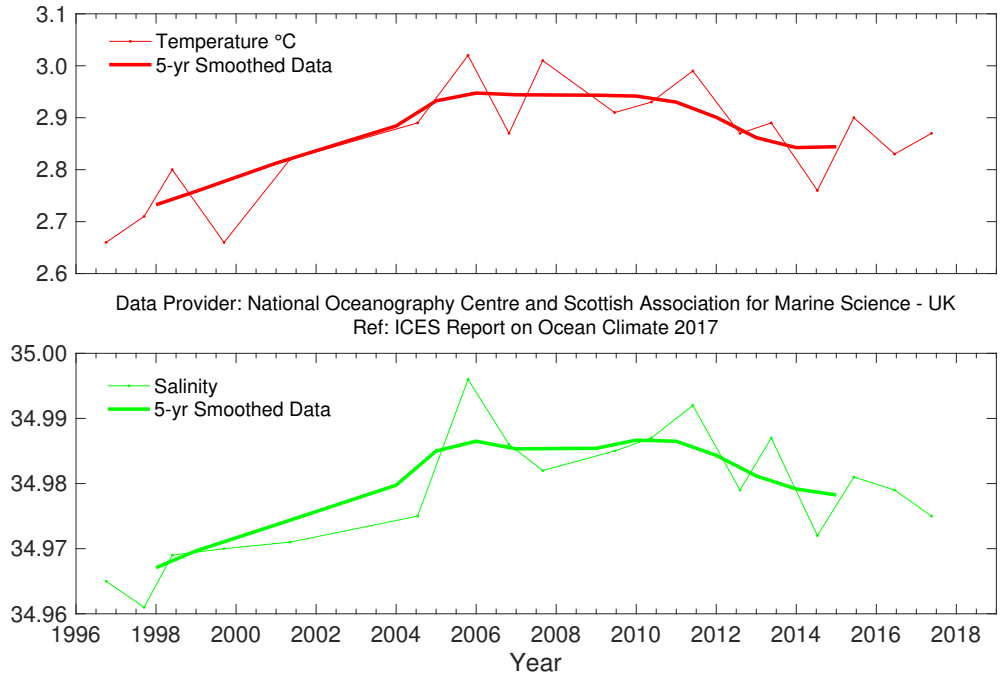

FIGURE 101.
Iceland Basin. Temperature (upper panel) and salinity (lower panel) of Iceland-Scotland Overflow Water (σθ > 27.85 kg m^{-3}, ca. 2000–2600 m).

5.2.3 Rockall Trough

N. P. Holliday

In Rockall Trough, LSW is the dominant water mass below about 1500 m, which usually has its maximum concentration between 1700 and 2000 m. East of the Anton Dohrn seamount, this peak tends to be characterized by a minimum in salinity and potential vorticity, although its patchy temporal distribution (possibly due to aliasing of mesoscale eddies) results in a noisy year-on-year signal.

Over the time-series, there is no significant trend. From 1975 to the mid-1990s, there was a cooling and freshening trend, which was followed by gradual warming and increasing salinity. In 2017, the LSW potential temperature and salinity were close to the long-term means (Figure 102).

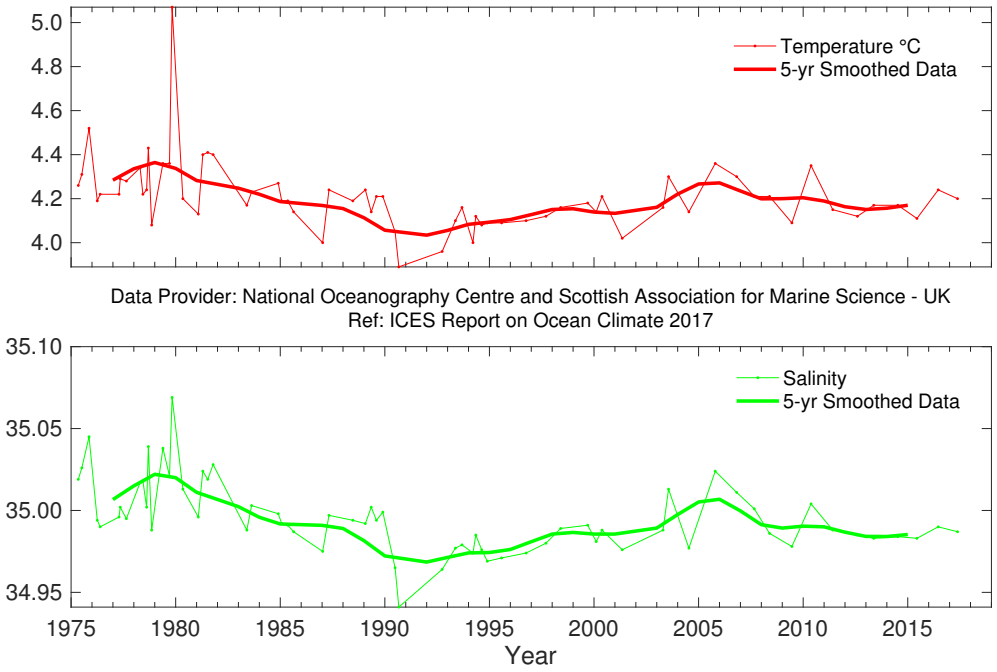

FIGURE 102.
Rockall Trough. Temperature (upper panel) and salinity (lower panel) of Labrador Sea water (LSW; $27.70 \leq \sigma\theta \leq 27.85$ kg m^{-3}, approx. 1500–2000 m).

5.2.4 Irminger Basin

L. de Steur

A cold and low-salinity core was observed between 1600 and 2000 m in the central Irminger Sea during the early 1990s (Figure 103). This was the result of the presence of deep LSW formed during 1988–1995. Since summer 1996, this LSW core has generally been increasing in temperature and salinity as it mixes with surrounding water masses. In 2012, temperature and salinity were only slightly below the long-term maximum observed in 2011. In 2014, the temperature of LSW in the Irminger Sea had continued to decline relative to 2011. Salinity, however, was higher than in 2011 and actually obtained the highest value since 1991. Until 2014, salinity continued to increase, but became stable in 2015 and 2016. Temperature in 2015 was only slightly higher than in 2014. A new maximum record in temperature was set in 2016, 0.314°C above the long-term mean. There is a clear increasing trend in temperature since 1996 at this depth. Deep convection occurred in the Irminger Sea in the cold winter 2014/2015 and produced a water mass with LSW properties down to 1400 m in the central Irminger Sea; however, this did not affect properties of LSW below 1400 m.

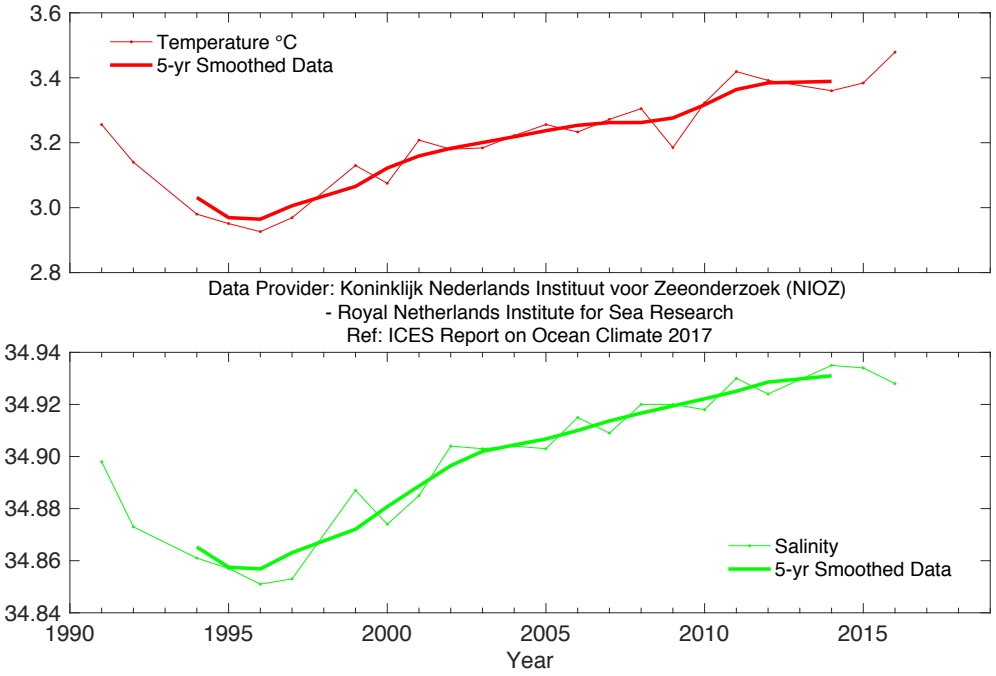

FIGURE 103.
Irminger Sea. Temperature (upper panel) and salinity (lower panel) of Labrador Sea water (LSW; averaged over 1600–2000 m).
No data available for 2017.

Salinity and potential temperature of the Denmark Strait overflow water (DSOW) near Cape Farewell showed correlated interannual variations between 1991 and 2007 (correlation = 0.75; Figure 104). However, since 2007, these variations in temperature and salinity of the DSOW have been less correlated. This continued to be the case in 2016. This implies that < 30% of the variance in salinity can be explained by the variance of the temperature variability. Density of the DSOW changes very little on long time-scales. Measurements with moored instrumentation have demonstrated that temperature and density mainly vary at an annual time-scale, possibly forced by wind-driven processes near Denmark Strait. In 2016, the DSOW temperature was 0.049°C below the long-term mean; however, salinity continued to increase and was 0.024 above the mean.

As there were no hydrographic cruises in the Irmingher Sea in 2017, neither time-series could not be extended, meaning that the trends in temperature and salinity are unclear at present.

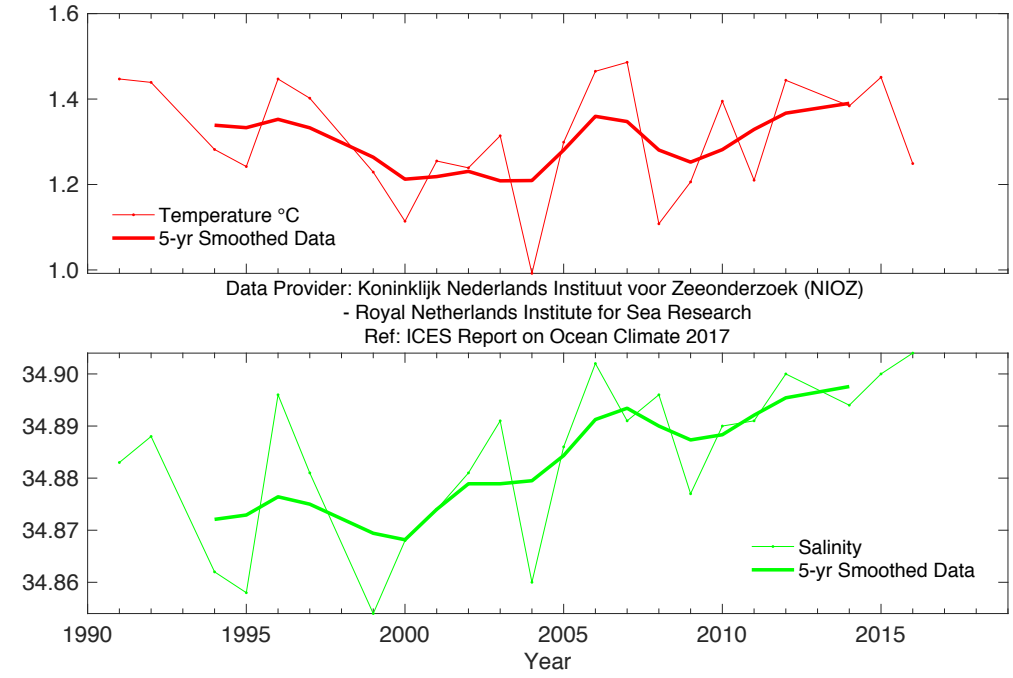

FIGURE 104.
Irminger Sea. Temperature (upper panel) and salinity (lower panel) in Denmark Strait Overflow Water (DSOW) on the East Greenland Slope.
No data available for 2017.

5.2.5 Labrador Basin

I. Yashayaev and B. Cisewski

In the Labrador Sea, average temperature and salinity of the deep intermediate layer (1000–1800 m) decreased between the beginning of the 1970s and the early 1990s by about 0.9°C and 0.09, respectively (Figure 105). In 2011, less than two decades after reaching its record minimum, temperature was as high as it was in 1970 when the previous maximum was observed, while salinity was also at its highest since 1971. These trends were interrupted in winter 2011/2012 by strong convection. Temperature of the deep intermediate layer (1000–1800 m) continued to decrease during subsequent years (2013–2017), while salinity decreased until 2016 and has increased from winter 2016/2017 onwards.

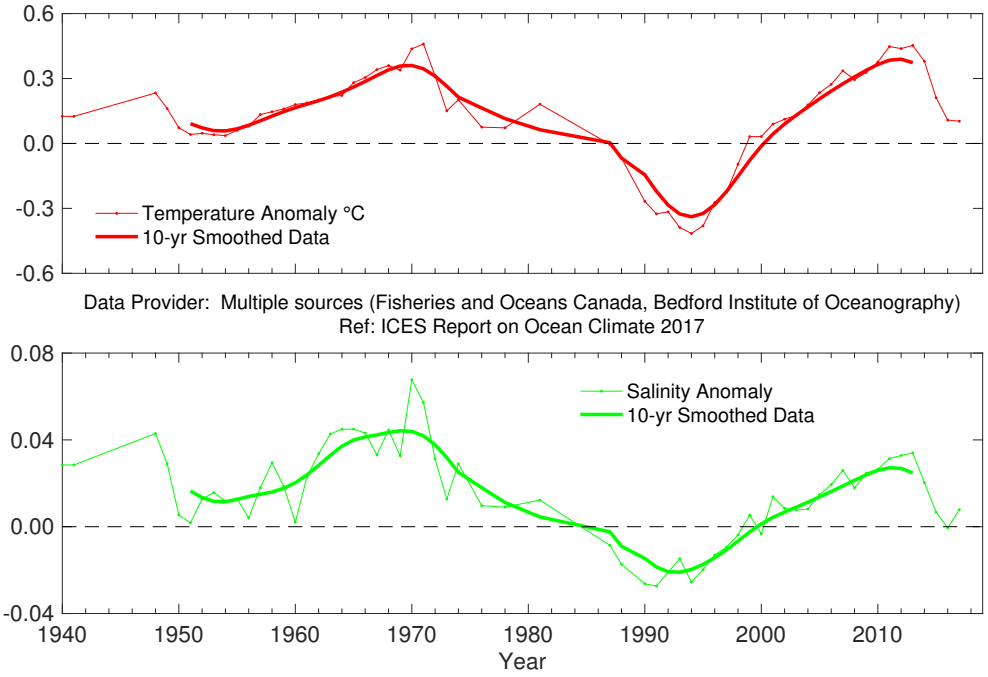

FIGURE 105.
Labrador Sea. Temperature (upper panel) and salinity (lower panel) anomalies in the deep intermediate layer of the Labrador Sea. Vertical profile data to 2017 were averaged over 1000–1800 m and then over calendar years.

Properties of the North Atlantic Deep Water (NADW) in the deep boundary current west of Greenland are monitored at 2000 m at Cape Desolation Station 3 (Figure 106). Temperature and salinity of this water mass underwent strong interannual variability during the 1980s. Since the beginning of the 1990s, both characteristics were decreasing and reached their minimum values in 1998 and 1997, respectively. After that, temperature of the NADW revealed a positive trend until 2014, whereas salinity rather stagnated between 2007 and 2014. However, in 2017, the Cape Desolation Section had to be abandoned due to severe weather conditions.

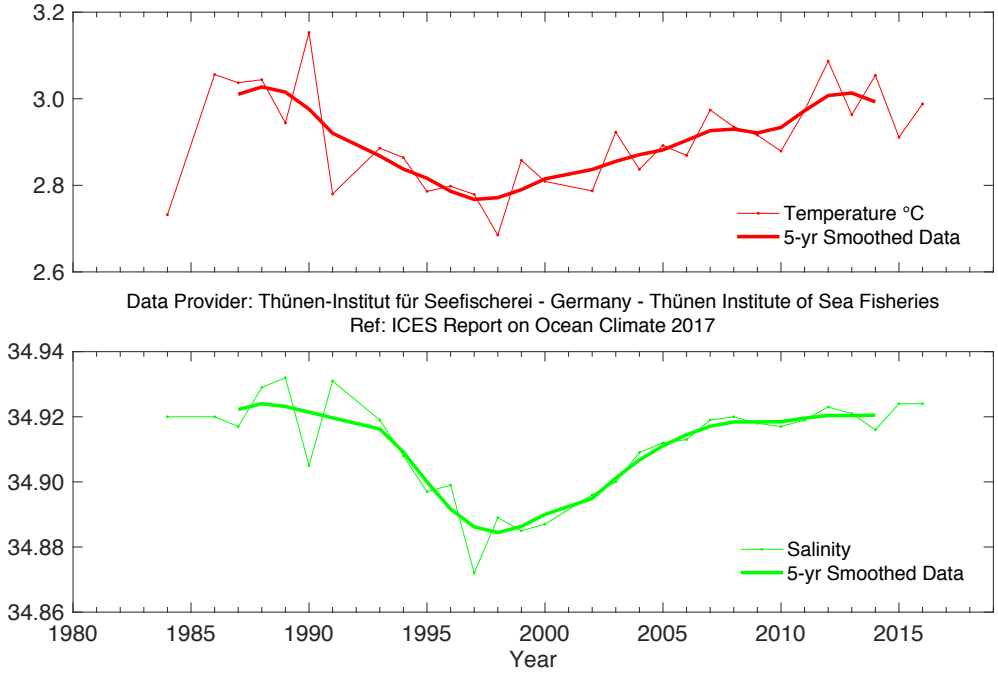

FIGURE 106.
West Greenland. Temperature (upper panel) and salinity (lower panel) at 2000 m water depth at Cape Desolation Station 3 (60.47°N 50.00°W). No data available for 2017.

5.2.6 Western Iberian Margin

C. González-Pola

The outer slope stations in Santander (Figure 45) have been sampling the entire water column down to 1000 m (core of MW) on a monthly basis since the early 1990s (González-Pola *et al.*, 2005). Overall warming for the previous 20 years is evident at most layers, corrtesponding to the ENACW (300–600 m; Figure 107) and upper MW (600–1000 m; Figure 108).

Evolution of the water masses is strongly influenced by a strong shift in salinity at lower ENACW (ca. 400 m) in 2005, after the occurrence of very strong winter mixing (Somavilla *et al.*, 2009). In 2014, upper central waters showed freshening and cooling for the first time in about a decade. In 2015, salinity values fell continuously, ending the year about 0.05 units lower than values observed in mid-2014. During 2016 and 2017, salinity remained at about the same level as in late 2015, i.e. fresher and colder than in recent years. Deeper, at the level of the MW, water masses have remained relatively stable since the mid-2000s, becoming progressively fresher at their core after peaking around 2007–2009.

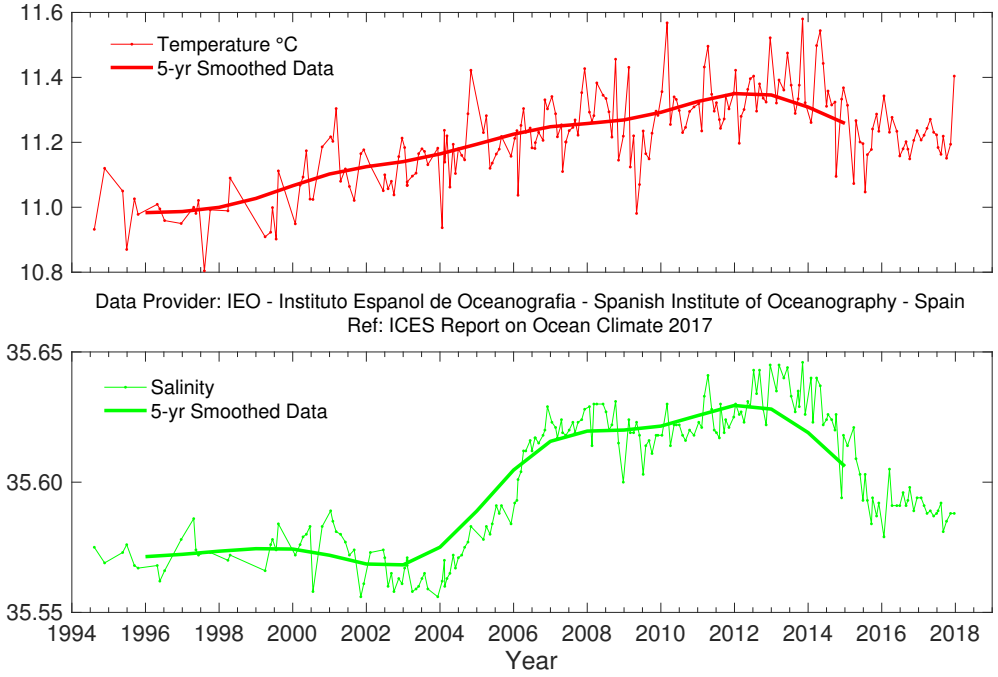

FIGURE 107.
Bay of Biscay. Potential temperature (upper panel) and salinity (lower panel) for the 300-600 m layer at Santander Station 7.

Since 2003, levels deeper than 1000 m have been monitored in the region and at the Western Iberian Margin for the entire water column (> 5500 m) by a repeated section programme that supplements the monthly monitoring of the upper ocean in the area (Prieto *et al.*, 2015). Cruises were carried out on a semi-annual basis 2003–2010 and annually after that. The Finisterre section, ca. 400 km, stretches from west of the Iberian Peninsula (43.0°N 9.3°W) to the centre of the Iberian Abyssal Plain (43.0°N 15.5°W).

The Finisterre section provides information about upper, intermediate, and deep waters. At 2000 m, it corresponds to the core of LSW and the base of the permanent thermocline; this is considered the limit of intermediate waters. From the core of MW to the core of LSW, there is a strong gradient and some coherence in variability, indicating the influence of large-scale atmospheric patterns. The main highlight of the series is the passage of a cold fresh anomaly between 2008 and 2010. After an upward swing in temperature and salinity in 2015, 2016, and 2017 reversed again towards colder and fresher values (Figure 109), consistent with positive NAO behaviour.

Abyssal waters in this basin are NADW (composed of a mixture of all Arctic water masses) and what is known as Lower Deep Water that presents a signature of waters with Antarctic origin. Interannual variability of these abyssal waters within the monitored period has been weak, with interannual swings below 0.1°C and 0.01 in salinity. No trends have been observed. Potential temperature in 2017 was near the long-term average, and salinity was slightly below (Figure 110).

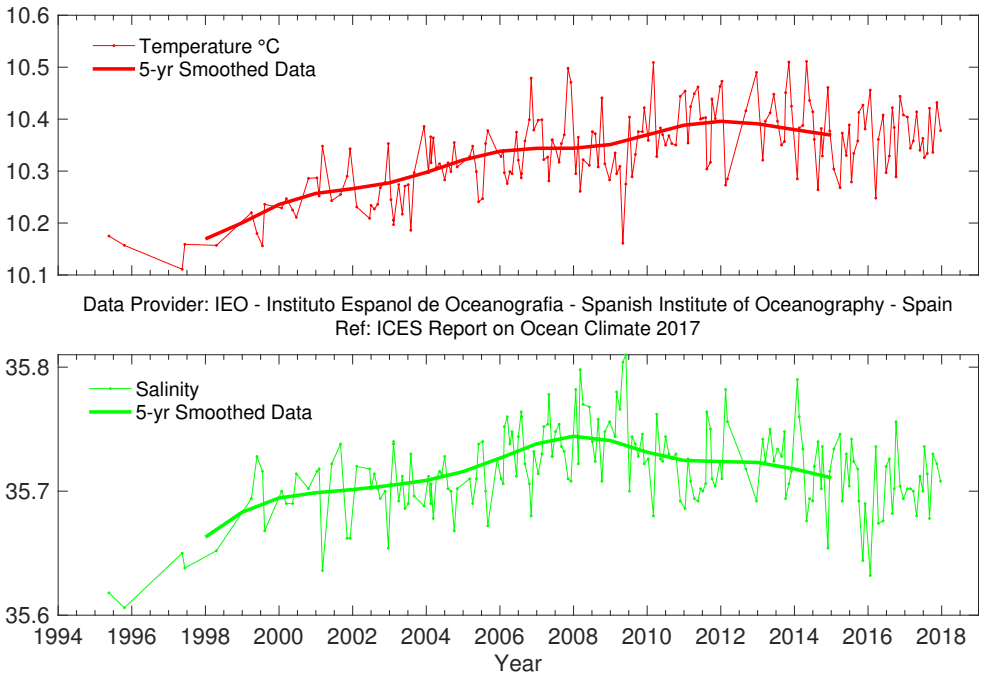

FIGURE 108.
Bay of Biscay. Potential temperature (upper panel) and salinity (lower panel) for the 600–1000 m layer at Santander Station 7.

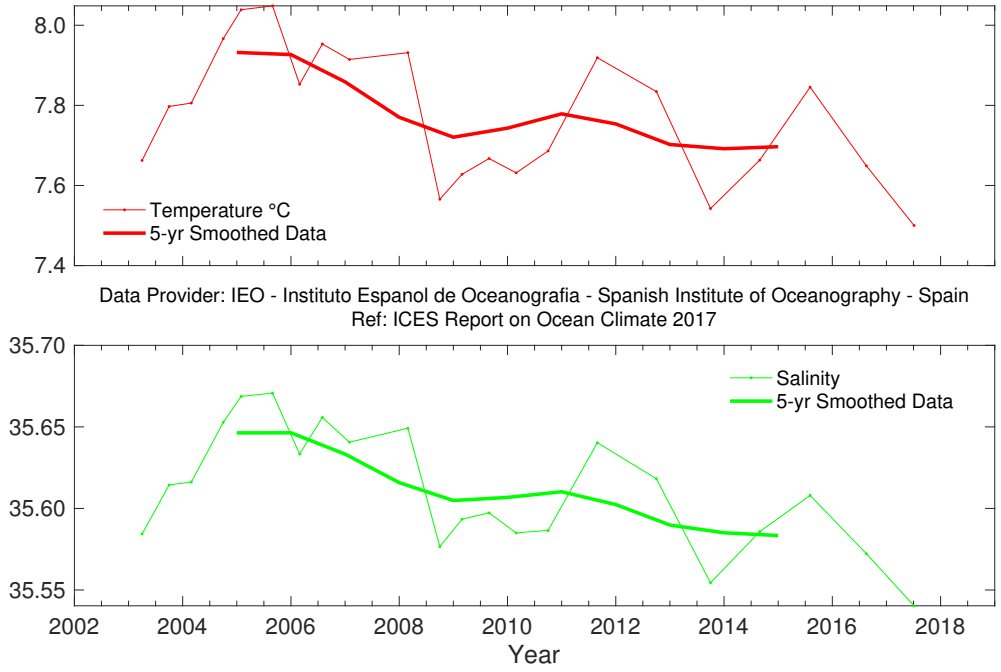

FIGURE 109.
Western Iberian Margin. Potential temperature (upper panel) and salinity (lower panel) for the 800–2000 m layer averaged across the Finisterre section.

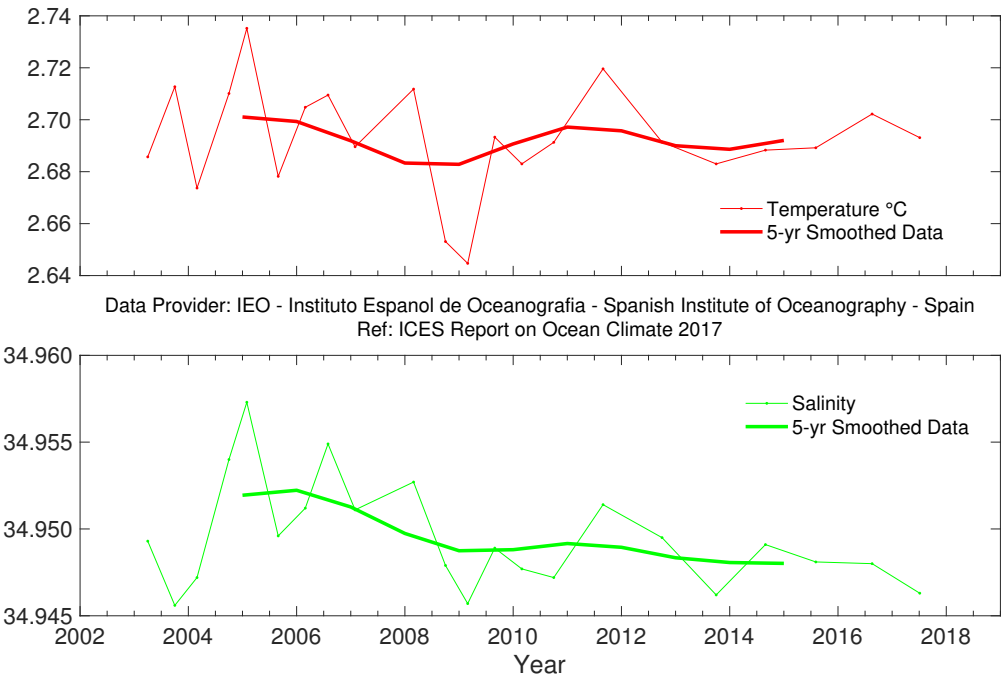

FIGURE 110.
Western Iberian Margin. Potential temperature (upper panel) and salinity (lower panel) for the 2000–5500 m layer averaged across the Finisterre section.

5.2.7 Canary Basin

P. Vélez-Belchí

In the stratum corresponding to the intermediate waters (800–1400 m), weak cooling and decreasing salinity has been observed since the 1990s; however, the changes are not statistically significantly different from zero in the oceanic region or in the CTZ. Both time-series show high variability due to two very different intermediate water masses present in the region, i.e. MW and AAIW.

In the layer corresponding to the upper NADW (1700–2600 m), there was weak warming and an increase in salinity that is not statistically significantly different from zero. However, in strata corresponding to the NADW (2600–3600 m), a marginally statistically significant cooling (−0.01 ± 0.01°C decade^{-1}) and freshening (−0.002 ± 0.002°C decade^{-1}) is observed (Figure 112).

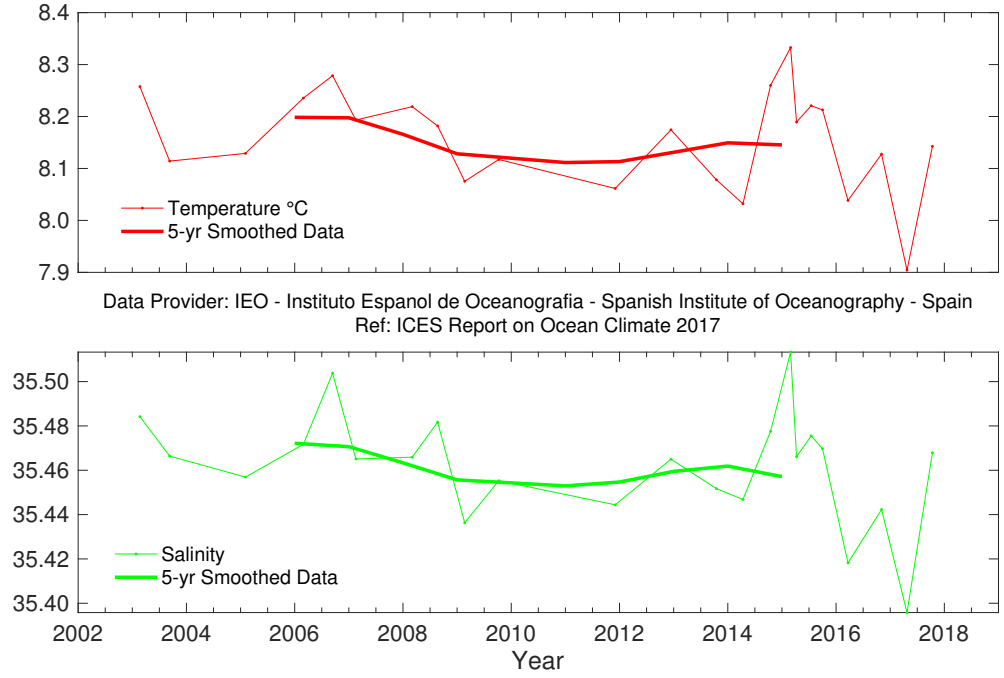

FIGURE 111.
Canary Basin. Potential temperature (upper panel) and salinity (lower panel) for the 800-1400 m layer.

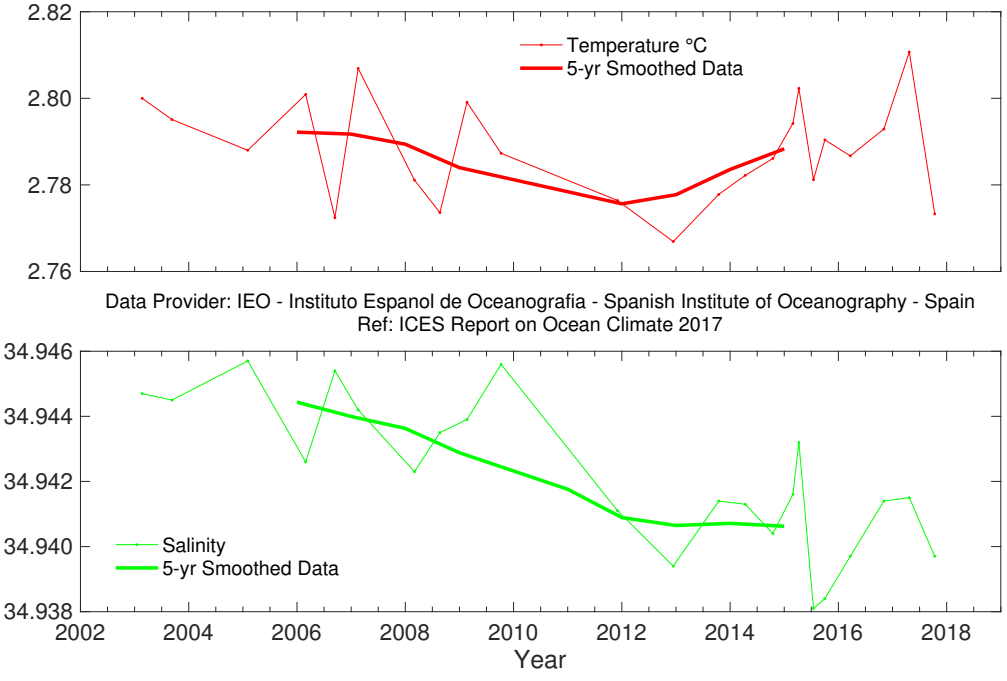

FIGURE 112.
Canary Basin. Potential temperature (upper panel) and salinity (lower panel) for the 2600-3600 m layer averaged across the Canaries section.

Sunset in the Irminger Sea.
Photo: Penny Holliday, National Oceanography Centre, UK.

REFERENCES

Berx, B., and Payne, M. R. 2017. The Sub-Polar Gyre Index–a community data set for application in fisheries and environment research. Earth System Science Data, 9: 259–266. https://doi.org/10.5194/essd-9-259-2017

Buckley, M. W., and Marshall, J. 2016. Observations, inferences, and mechanisms of the Atlantic Meridional Overturning Circulation: A review, Reviews of Geophysics, 54(1): 5–63. https://doi.org/10.1002/2015RG000493

Cappelen, J. 2018. Greenland-DMI Historical Climate Data Collection 1784–2017, DMI Report 18-04.118 pp. Delworth, T. L., Zeng, F., Vecchi, G. A., Yang, X., Zhang, L., and Zhang, R. 2016. The North Atlantic Oscillation as a driver of rapid climate change in the Northern Hemisphere, Nature Geoscience, 9: 502–512

Duchez, A., Frajka-Williams, E., Josey, S. A., Evans, D. G., Grist, J. P., Marsh, R., McCarthy, G. D., *et al*. 2016. Drivers of exceptionally cold North Atlantic Ocean temperatures and their link to the 2015 European heat wave. Environmental Research Letters, 11(7): 074004. https://doi.org/10.1088/1748-9326/11/7/074004

Dunstone, N., Smith, D., Scaife, A., Hermanson, L., Eade, R., Robinson, N., Andrews, M. *et al*. 2016. Skilful predictions of the winter North Atlantic Oscillation one year ahead, Nature Geoscience, 9(11): 809–814. https://doi.org/10.1038/ngeo2824

Gaillard, F., Reynaud, T., Thierry, V., Kolodziejczyk, N., and von Schuckmann, K. 2016. *In situ*–based reanalysis of the global ocean temperature and salinity with ISAS: variability of the heat content and steric height, Journal of Climate, 29(4): 1305–1323. https://doi.org/10.1175/jcli-d-15-0028.1

González-Pola, C., Lavín, A., and Vargas-Yáñez, M. 2005. Intense warming and salinity modification of intermediate water masses in the southeastern corner of the Bay of Biscay for the period 1992–2003. Journal of Geophysical Research, 110: C05020. https://doi.org/10.1029/2004JC002367

Häkkinen, S., and Rhines, P. B. 2004. Decline of subpolar North Atlantic circulation during the 1990s. Science, 304 (5670): 555–559. https://doi.org/10.1126/science.1094917

Hátún, H., Azetsu-Scott, K., Somavilla, R., Rey, F., Johnson, C., Mathis, M. Mikolajewicz, U., *et al*. 2017. The subpolar gyre regulates silicate concentrations in the North Atlantic. Scientific Reports, 7: 14576. https://doi.org/10.1038/s41598-017-14837-4

Hátún, H., and Chafik, L. 2018. On the recent ambiguity of the North Atlantic subpolar tyre index. Journal of Geophysical Research: Oceans, 123. https://doi.org/10.1029/2018JC014101.

Hátún, H., Lohmann, K., Matei, D., Jungclaus, J. H., Pacariz, S., Bersch, M. Gislason, A., *et al*. 2016. An inflated subpolar gyre blows life toward the northeastern Atlantic. Progress in Oceanography, 147: 49–66. https://doi.org/10.1016/j.pocean.2016.07.009

Hátún, H., Payne, M., Beaugrand, G., Reid, P., Sandø, A., Drange, H., Hansen, B., *et al*. 2009. Large bio-geographical shifts in the north-eastern Atlantic Ocean: From the subpolar gyre, via plankton, to blue whiting and pilot whales. Progress in Oceanography, 80(3): 149–162. https://doi.org/10.1016/j.pocean.2009.03.001

Hátún, H., Sandø, A. B., Drange, H., Hansen, B., and Valdimarsson, H. 2005. Influence of the Atlantic Subpolar Gyre on the thermohaline circulation. Science, 309 (5742): 1841–1844. https://doi.org/10.1126/science.1114777

Hernández-Guerra, A., Espino-Falcón, E., Vélez-Belchí, P., Pérez-Hernández, M. D., Martínez- Marrero, A., and Cana, L. 2017. Recirculation of the Canary Current in fall 2014. Journal of Marine Systems, 174: 25–39. https://doi.org/10.1016/j.jmarsys.2017.04.002

Holliday, N. P., Cunningham, S. A., Johnson, C., Gary, S. F., Griffiths, C., Read, J. F., and Sherwin T. 2015. Multidecadal variability of potential temperature, salinity, and transport in the eastern subpolar North Atlantic. Journal of Geophysical Research: Oceans, 120: 5945–5967. https://doi.org/10.1002/2015jc010762

Hurrell, J. W., and Deser, C. 2010. North Atlantic climate variability: the role of the North Atlantic Oscillation. Journal of Marine Systems, 79: 231–244. https://doi.org/10.1016/j.jmarsys.2009.11.002

Hurrell, J. W., Kushnir, Y., Ottersen, G., and Visbeck, M. 2013. An overview of the North Atlantic oscillation In The North Atlantic Oscillation: Climatic Significance and Environmental Impact Ed. by J. W. Hurrell, Y. Kushnir, G. Ottersen, and M. Visbeck. Wiley Online Library. https://doi.org/10.1029/134GM01

Hurrell, J., and National Center for Atmospheric Research Staff (Eds). 2017. Climate Data Guide: Hurrell North Atlantic Oscillation (NAO) Index (station-based). https://climatedataguide.ucar.edu/climate-data/ hurrell-north-atlantic-oscillation-nao-index-station-based, last modified 07 Jul 2017, accessed 25 September 2017.

Kalnay, E., Kanamitsu, M., Kistler, R., Collins, W., Deaven, D., Gandin, L., Iredell, M., *et al*. 1996. The NCEP/NCAR 40-Year Reanalysis Project, Bulletin of the American Meteorological Society, 77: 437–471. https://doi.org/10.1175/1520-0477(1996)077<0437:TNYRP>2.0.CO;2

Moffa-Sánchez, P., and Hall, I. R. 2017. North Atlantic variability and its links to European climate over the last 3000 years. Nature Communications, 8: 1726. https://doi.org/10.1038/s41467-017-01884-8

Mountain, D. 2012. Labrador slope water entering the Gulf of Maine–response to the North Atlantic Oscillation. Continental Shelf Research, 47: 150–155. https://doi.org/10.1016/j.csr.2012.07.008

Paillet, J., and Mercier, H. 1997. An inverse model of the eastern North Atlantic general circulation and thermocline ventilation, Deep Sea Research Part I: Oceanographic Research Papers, 44(8): 1293–1328. https://doi.org/10.1016/s0967-0637(97)00019-8

Pingree, R. D. 1993. Flow of surface waters to the west of the British Isles and in the Bay of Biscay. Deep Sea Research Part II: Topical Studies in Oceanography, 40(1–2): 369–388. https://doi.org/10.1016/0967-0645(93)90022-f

Pingree, R. D., and Le Cann, B. 1990. Structure, strength and seasonality of the slope currents in the Bay of Biscay region. Journal of the Marine Biological Association of the United Kingdom, 70(4): 857–885. https://doi.org/10.1017/s0025315400059117

Prieto, E., González-Pola, C., Lavín, A., and Holliday, N. P. 2015. Interannual variability of the northwestern Iberia deep ocean: Response to large-scale North Atlantic forcing. Journal of Geophysical Research: Oceans, 120: 832–847. https://doi.org/10.1002/2014jc010436

Pujol, M. I., Faugère, Y., Taburet, G., Dupuy, S., Pelloquin, C., Ablain, M., and Picot, N. 2016. DUACS DT2014: the new multi-mission altimeter data set reprocessed over 20 years. Ocean Science, 12: 1067–1090. https://doi.org/10.5194/os-12-1067-201

Scaife, A. A., Arribas, A., Blockley, E., Brookshaw, A., Clark, R. T., Dunstone, N. Eade, R., *et al*. 2014. Skillful long-range prediction of European and North American winters. Geophysical Research Letters, 41: 2514–2519. https://doi.org/10.1002/2014gl059637

Scaife, A. A., Karpechko, A. Y., Baldwin, M. P., Brookshaw, A., Butler, A. H., Eade, R., Gordon, M., *et al*. 2015. Seasonal winter forecasts and the stratosphere. Atmospheric Science Letters, 17: 51–56. https://doi.org/10.1002/asl.598

Somavilla, R., Gonzalez-Pola, C., Rodriguez, C., Josey, S. A., Sanchez, R. F., and Lavin, A. 2009. Large changes in the hydrographic structure of the Bay of Biscay after the extreme mixing of winter 2005. Journal of Geophysical Research: Oceans, 114 (C1). https://doi.org/10.1029/2008jc004974

Tel, E., Balbin, R., Cabanas, J., Garcia, M., García-Martínez, M., González-Pola, C., Lavín, A., *et al*. 2016. IEOOS: The Spanish Institute of Oceanography Observing System. Ocean Science, 12: 345–353.

van Aken, H. M. 2002. Surface currents in the Bay of Biscay as observed with drifters between 1995 and 1999. Deep Sea Research Part I: Oceanographic Research Papers, 49(6): 1071–1086. https://doi.org/10.1016/s0967-0637(02)00017-1

Vélez-Belchí, P., González-Carballo, M., Pérez Hernández, M. D., and Hernández Guerra, A. 2015. Open ocean temperature and salinity trends in the Canary Current Large Marine Ecosystem. In Oceanographic and biological features in the Canary Current Large Marine Ecosystem, pp. 201–213. Ed. by L. Valdés, and I. Déniz González. IOC Technical Series, No. 115. IOC UNESCO, Paris. 383 pp.

Vélez-Belchí, P., Pérez Hernández, M. D., Casanova Masjoan, M., Cana, L., and Hernández Guerra, A. 2017. On the seasonal variability of the Canary Current and the Atlantic Me-ridional Overturning Circulation. Journal of Geophysical Research: Oceans, 122(6): 4518–4538. https://doi.org/10.1002/2017jc012774

Yashayaev, I., and Loder, J. W. 2017. Further intensification of deep convection in the Labrador Sea in 2016. Geophysical Research Letters, 44(3): 1429–1438. https://doi.org/10.1002/2016gl071668

CONTACT INFORMATION: DATASET PROVIDERS

AREA	SECTION	FIGURES	TIME-SERIES	CONTACT	INSTITUTE
West Greenland	4.1	19	Nuuk – air temperature	Boris Cisewski boris.cisewski@thuenen.de	Danish Meteorological Institute, Copenhagen, Denmark
West Greenland	4.1, 5.2.5	20, 21, 106	Fylla section and Cape Desolation section	Boris Cisewski boris.cisewski@thuenen.de	Thünen-Institut für Seefischerei (Thünen Institute of Sea Fisheries), Germany
Northwest Atlantic	4.4	27, 28, 29, 30	Cabot Strait sea ice, Sable Island air temperature, Misaine Bank, Emerald Bank	David Hebert David.Hebert@dfo-mpo.gc.ca Roger Pettipas Roger.Pettipas@dfo-mpo.gc.ca	Ocean Monitoring and Observation Section, Oceans and Ecosystem Division, Bedford Institute of Oceanography, Fisheries and Oceans Canada
Northwest Atlantic	4.3	23, 24, 25, 26	Newfoundland and Labrador sea ice, Cartwright air temperature, Station 27 temperature and salinity	Eugene Colbourne eugene.colbourne@ dfo-mpo.gc.ca	Northwest Atlantic Fisheries Centre, Canada
Labrador Sea	4.2, 5.2.5	22, 105	Section AR7W	Igor Yashayaev Igor.Yashayaev@dfo-mpo.gc.ca	Northwest Atlantic Fisheries Centre, Canada
Northeast US continental shelf	4.5	33, 34, 35, 36, 37, 38, 39	MAB, Gulf of Maine, Georges Bank, Northeast Channel	Paula Fratantoni paula.fratantoni@noaa.gov	NOAA Fisheries, NEFSC, Oceans and Climate Branch, USA
Icelandic waters	4.6, 5.1.3	41, 42, 43, 44, 98	Reykjavik and Akureyri air temperature, Siglunes Stations 2–4, Stations 2–4, Selvogsbanki Station 5, Langanes Stations 2–6, Icelandic deep water (1800 m)	Hedinn Valdimarsson hedinn.valdimarsson@hafogvatn.is	Hafrannsóknastofnun (Marine & Freshwater Research Institute), Iceland
Bay of Biscay	4.7	46, 47	San Sebastian air and water temperature	Almudena Fontán afontan@azti.es	AZTI, Aquarium of San Sebastian (SOG) and Igeldo Meteorological Observatory (INM) in San Sebastian, Spain
Bay of Biscay and western Iberian margin	4.7, 5.2.6	48, 49, 107, 108, 109, 110	Santander and Finisterre sections	César González-Pola cesar.pola@ieo.es	Instituto Español de Oceanografía (IEO, Spanish Institute of Oceanography), Spain
Gulf of Cadiz	4.8	51	STOCA Station SP6 – Gulf of Cadiz time-series	Ricardo F. Sánchez-Leal rleal@ieo.es	Instituto Español de Oceanografía (IEO, Spanish Institute of Oceanography), Spain
Canary Basin	4.9, 5.2.7	53, 111, 112	Canary Basin oceanic waters section	Pedro Vélez-Belchí pedro.velez@ieo.es	Instituto Español de Oceanografía (IEO, Spanish Institute of Oceanography), Spain
NW European continental shelf	4.10	56, ??	Astan section, Point 33	Pascal Morin pmorin@sb-roscoff.fr	CNRS–UPMC, Observatoire Oceanologique de Roscoff, France
NW European continental shelf	4.10	54, 55	Western Channel Observatory, Station E1	Tim J. Smyth tjsm@pml.ac.uk	Marine Biological Association and Plymouth Marine Laboratory, UK
NW European continental shelf	4.11	57, 58	Malin Head Weather Station, M3 Weather Buoy	Caroline Cusack Caroline.Cusack@Marine.ie	Marine Institute/Met Eireann, Ireland
Rockall Trough and Iceland Basin	4.12 4.13, 4.14, 5.2.2, 5.2.3	60,61,62 100, 101, 102	Ellett Line	N. Penny Holliday nph@noc.soton.ac.uk	National Oceanography Centre, Southampton and Scottish Association for Marine Science, UK
Irminger Sea	4.15	64	Station FX9 (64.33°N 8°W)	Hedinn Valdimarsson hedinn.valdimarsson@hafogvatn.is	Hafrannsóknastofnun (Marine & Freshwater Research Institute), Iceland
Irminger Sea	4.15, 5.2.4	63, 103, 104	Central Irminger Sea, East Greenland slope	Laura de Steur Laura.de.Steur@nioz.nl Femke de Jong Femke.de.Jong@nioz.nl	Koninklijk Nederlands, Instituut voor Zeeonderzoek (NIOZ, Royal Netherlands Institute for Sea Research), Netherlands
Faroe Bank Channel	4.16	66, 67, 68	Faroe Bank Channel–West Faroe Islands, Faroe Current – North Faroe Islands, Faroe Shelf	Karin Margretha H. Larsen KarinL@hav.fo	Havstovan (Faroe Marine Research Institute), Faroe Islands
Faroe–Shetland Channel	4.16 5.2.1	69, 70, 99	Faroe–Shetland Channel, Faroe Shelf and Shetland Shelf, deep waters (800 m)	Barbara Berx B.Berx@MARLAB.AC.UK	Marine Scotland Science (MSS, Aberdeen), UK
North Sea	4.17	73	North Sea Utsira, modelled North Sea inflow	Jon Albretsen jon.albretsen@imr.no Solfrid Hjollo solfrids@imr.no	Institute of Marine Research (IMR), Norway
North Sea	4.17	74	Fair Isle Current water	Barbara Berx B.Berx@ marlab.ac.uk	Marine Scotland Science (MSS, Aberdeen), UK
North Sea	4.17	75, 76	Helgoland Roads – coastal waters – German Bight, North Sea	Karen Wiltshire Karen.Wiltshire@awi.de	Alfred Wegener Institute for Polar and Marine Research (AWI)/Biologische Anstalt Helgoland (BAH), Germany
North Sea	4.17	77	Felixstowe–Rotterdam section average (52°N)	Stephen Dye stephen.dye@cefas.co.uk	Centre for Environment, Fisheries and Aquaculture Science (CEFAS), UK
Baltic Sea	4.18	79, 80, 83	Station BY15, Baltic Proper, east of Gotland, and observed ice extent	Johanna Linders johanna.linders@smhi.se	Swedish Meteorological and Hydrological Institute (SMHI), Sweden
Baltic Sea	4.18	81,82	Stations LL7 and SR5	Pekka Alenius pekka.alenius@fimr.fi	Finnish Institute of Marine Research (FIMR), Finland

AREA	SECTION	FIGURES	TIME-SERIES	CONTACT	INSTITUTE
Norwegian Sea	4.19	85, 87, 88	Svinøy, Gimsøy, and Sørkapp sections	Kjell Arne Mork kjell.arne.mork@imr.no	Institute of Marine Research (IMR), Norway
Norwegian Sea	4.19, 5.1.2	86, 97	Ocean Weather Station Mike (50 and 2000 m)	Svein Østerhus Svein.Osterhus@gfi.uib.no	Geophysical Institute, University of Bergen, Norway
Barents Sea	4.20	90	Fugløya – Bear Island section, Western Barents Sea	Randi Ingvaldsen randi.ingvaldsen@imr.no	Institute of Marine Research (IMR), Norway
Barents Sea	4.20	91	Kola section, Eastern Barents Sea	Oleg V. Titov titov@pinro.ru	Knipovich Polar Research Institute of Marine Fisheries and Oceanography (PINRO), Russian Federation
Greenland Sea and Fram Strait	4.21	94	Greenland Sea section N, west of Spitsbergen (76.5°N)	Agnieszka Beszczynska-Möller abesz@iopan.gda.pl	Institute of Oceanology, Polish Academy of Sciences (IOPAN), Poland
Greenland Sea and Fram Strait	4.21, 5.1.1	92, 96	Greenland Sea section 75°N, Greenland Gyre convection depth and deep waters (3000 m)	Gereon Budeus Gereon.Budeus@awi.de	Alfred Wegener Institute, Helmholtz Centre for Polar and Marine Research (AWI), Germany
Greenland Sea and Fram Strait	4.21	93	Fram Strait (78.83°N), West Spitsbergen Current and East Greenland Current	Wilken-Jon von Appen Wilken-Jon.von.Appen@awi.de	Alfred Wegener Institute, Helmholtz Centre for Polar and Marine Research (AWI), Germany

CONTACT INFORMATION: AUTHORS

AREA	SECTION	AUTHORS	INSTITUTE
Sea surface temperature	2.2	All WGOH members	
Gridded temperature and salinity fields	2.3	Nicolas Kolodziejczyk Nicolas.Kolodziejczyk@univ-brest.fr	University of Brest, CNRS, IRD, Ifremer, Laboratoire d'Océanographie Physique et Spatiale (LOPS, Laboratory for Ocean Physics and Satellite remote sensing), Brest, France
		Damien Desbruyères	
		Gilles Reverdin	Sorbonne University-CNRS-IRD-MNHN, LOCEAN Laboratory, Paris, France
Subpolar Gyre Index	2.4	Léon Chafik leon.chafik@misu.su.se	Department of Meteorology, Stockholm University, Stockholm, Sweden
		Hjalmar Hátún	Faroe Marine Research Institute, Torshavn, Faroe Islands
		Barbara Berx	Marine Scotland Science (MSS, Aberdeen), UK
The North Atlantic atmosphere	3	Stephen Dye stephen.dye@cefas.co.uk	Centre for Environment, Fisheries and Aquaculture Science (Cefas), Lowestoft, UK
West Greenland	4.1	Boris Cisewski boris.cisewski@thuenen.de	Thünen-Institut für Seefischerei (Thünen Institute of Sea Fisheries), Bremerhaven, Germany
Labrador Sea	4.2	Igor Yashayaev Igor.Yashayaev@dfo-mpo.gc.ca	Oceans and Ecosystem Division, Bedford Institute of Oceanography, Fisheries and Oceans, Bedford, Canada
Newfoundland Labrador Shelf	4.3	Eugene Coulborne Eugene.Colbourne@dfo-mpo.gc.ca	Northwest Atlantic Fisheries Centre, St. John's, Newfoundland, Canada
Scotian Shelf	4.4	David Hebert David.Hebert@dfo-mpo.gc.ca	Ocean Monitoring and Observation Section, Oceans and Ecosystem Division, Bedford Institute of Oceanography, Fisheries and Oceans, Bedford, Canada
		Roger Pettipas	
Northeast US Continental Shelf	4.5	Paula Fratantoni paula.fratantoni@noaa.gov	NOAA Fisheries, NEFSC, Oceans and Climate Branch, Woods Hole, MA, USA
Icelandic Waters	4.6	Héðinn Valdimarsson hedinn.valdimarsson@hafogvatn.is	Hafrannsóknastofnun (Marine and Freshwater Research Institute), Reykjavík, Iceland
Bay of Biscay and West Iberia	4.7	Almudena Fontán afontan@azti.es	AZTI Investigación Marina (Marine Research), San Sebastian, Spain
		Victor Valencia	
		César González-Pola	Instituto Español de Oceanografía (IEO, Spanish Institute of Oceanography), Gijón Oceanographic Centre, Gijón, Spain
Gulf of Cadiz	4.8	Ricardo Sánchez-Leal rleal@ieo.es	Instituto Español de Oceanografía (IEO, Spanish Institute of Oceanography), Cádiz Oceanographic Centre, Cádiz, Spain
Canary Basin	4.9	Pedro Vélez-Belchí pedro.velez@ieo.es	Instituto Español de Oceanografía (IEO, Spanish Institute of Oceanography), Canary Islands Oceanographic Centre, Tenerife, Spain
Southwest Approaches	4.10	Tim Smyth TJSM@pml.ac.uk	Plymouth Marine Laboratory, Plymouth, UK
Celtic Seas	4.11	Kieran Lyons Kieran.lyons@Marine.ie	Marine Institute/Met Eireann, Galway, Ireland
		Caroline Cusack	
Rockall Trough	4.12	Naomi P. Holliday penny.holliday@noc.ac.uk	National Oceanography Centre, Southampton, UK

AREA	SECTION	AUTHORS	INSTITUTE
Hatton–Rockall Basin	4.13	Naomi P. Holliday penny.holliday@noc.ac.uk	National Oceanography Centre, Southampton, UK
Iceland Basin	4.14	Naomi P. Holliday penny.holliday@noc.ac.uk	National Oceanography Centre, Southampton, UK
Irminger Sea	4.15	Laura de Steur Laura.de.Steur@nioz.nl Femke de Jong	Koninklijk Nederlands, Instituut voor Zeeonderzoek (NIOZ, Royal Netherlands Institute for Sea Research), Texel, Netherlands
Faroese Waters and the Faroe–Shetland Channel	4.16	Karin M.H. Larsen karinl@hav.fo Barbara Berx B.Berx@MARLAB.AC.UK Jenny Hindson	Havstovan (Faroe Marine Research Institute), Tórshavn, Faroe Islands Marine Scotland Science (MSS), Aberdeen, UK
North Sea	4.17	Holger Klein Holger.Klein@bsh.de Peter Loewe	Bundesamt für Seeschifffahrt und Hydrographie (Federal Maritime & Hydrographic Agency, Hamburg, Germany
Skaggerak, Kattegat and the Baltic	4.18	Johanna Linders johanna.linders@smhi.se Tycjan Wodzinowski	Swedish Meteorological and Hydrological Institute (SMHI), Sweden National Marine Fisheries Research Institute, Gdynia, Poland
Norwegian Sea	4.19	Kjell-Arne Mork kjell.arne.mork@hi.no Svein Østerhus	Institute of Marine Research (IMR), Bergen, Norway Geophysical Institute, University of Bergen, Norway
Barents Sea	4.20	Alexander Trofimov trofimov@pinro.ru Randi Ingvaldsen	Knipovich Polar Research Institute of Marine Fisheries and Oceanography (PINRO), Murmansk, Russian Federation Institute of Marine Research (IMR), Bergen, Norway
Fram Strait	4.21	Agnieska Beszczynska-Möller abesz@iopan.gda.pl Wilken-Jon von AppenGereon Budeus	Institute of Oceanology, Polish Academy of Sciences (IOPAN), Sopot, Poland Alfred Wegener Institute (AWI), Bremerhaven, Germany
Greenland Sea deep waters	5.1.1	Agnieska Beszczynska-Möller abesz@iopan.gda.pl Gereon Budeus	Institute of Oceanology, Polish Academy of Sciences (IOPAN), Sopot, Poland Alfred Wegener Institute (AWI), Bremerhaven, Germany
Norwegian Sea deep waters	5.1.2	Svein Østerhus Svein.Osterhus@uib.no	Geophysical Institute, University of Bergen, Norway
Iceland Sea deep waters	5.1.3	Héðinn Valdimarsson hedinn.valdimarsson@hafogvatn.is	Hafrannsóknastofnun (Marine and Freshwater Research Institute), Reykjavík, Iceland
Greenland–Scotland Ridge overflow waters	5.2.1	Barbara Berx B.Berx@MARLAB.AC.UK Jenny Hindson	Marine Scotland Science (MSS), Aberdeen, UK
Iceland Basin deep waters	5.2.2	Naomi P. Holliday penny.holliday@noc.ac.uk	National Oceanography Centre, Southampton, UK
Rockall Trough intermediate waters	5.2.3	Naomi P. Holliday penny.holliday@noc.ac.uk	National Oceanography Centre, Southampton, UK

AREA	SECTION	AUTHORS	INSTITUTE
Irminger Basin deep waters	5.2.4	Laura de Steur Laura.de.Steur@nioz.nl	Koninklijk Nederlands, Instituut voor Zeeonderzoek (NIOZ, Royal Netherlands Institute for Sea Research), Texel, Netherlands
Labrador Basin deep waters	5.2.5	Igor Yashayaev Igor.Yashayaev@dfo-mpo.gc.ca Boris Cisewski	Oceans and Ecosystem Division, Bedford Institute of Oceanography, Fisheries and Oceans, Bedford, Canada Thünen-Institut für Seefischerei (Thünen Institute of Sea Fisheries), Bremerhaven, Germany
Western Iberian margin deep waters	5.2.6	César González-Pola cesar.pola@ieo.es	Instituto Español de Oceanografía (IEO, Spanish Institute of Oceanography), Gijón Oceanographic Centre, Gijón, Spain
Canary Basin deep waters	5.2.7	Pedro Vélez-Belchí pedro.velez@ieo.es	Instituto Español de Oceanografía (IEO, Spanish Institute of Oceanography), Canary Islands Oceanographic Centre, Tenerife, Spain

ABBREVIATIONS AND ACRONYMS

AAIW	Antartic intermediate waters
AMOC	Atlantic meridional overturning circulation
AO	Arctic oscillation
Argo	Not an acronym, but the name of a type of instrument used to collect data. The name ARGO is a reference to Greek mythology.
AR7W	Atlantic Repeat 7 West
AW	Atlantic water
AZOMP	Atlantic Zone Off-Shelf Monitoring Program
BSH	Bundesamt für Seeschifffahrt und Hydrographie (German Federal Maritime and Hydrographic Agency)
CCLME	Canary Current Large Marine Ecosystem
CIL	Cold intermediate layer
CIRES	Cooperative Institute for Research in Environmental Sciences (USA)
CTD	Conductivity Temperature Depth
CTZ	Coastal Transition Zone
DJF(M)	December/January/February(March)
DSOW	Denmark Strait Overflow Water
GME	Gulf of Maine east
GMW	Gulf of Maine west
GSDW	Greenland Sea deep water
Ifremer	Institut français de recherche pour l'exploitation de la mer (French Research Institute for Exploitation of the Sea)
IROC	ICES Report on Ocean Climate
ISAS	*In Situ* Analysis System
ISOW	Iceland–Scotland overflow water
LME	Large Marine Ecosystem
MNAW	modified North Atlantic Water
NACW	North Atlantic Central Waters
MOW	Mediterranean Overflow Water
MLD	mixed-layer depths
NAO	North Atlantic Oscillation
NEC	Northeast Channel
NEUS	Northeast US continental shelf
NOAA	National Oceanic and Atmospheric Administration (USA)
NMAB	North Mid-Atlantic Bight
NWGB	Northwest Georges Bank
OISST.v2	Optimum Interpolation SST dataset version 2
SLP	sea level pressure
SMAB	South Mid-Atlantic Bight
SPMW	Subpolar mode water
SST	sea surface temperature
SSW	sudden stratospheric warming
STOCA	Series Temporales de datos Oceanográficos en el golfo de CAdiz
UPDW	upper polar deep water
WGC	West Greenland Current
WGOH	Working Group Oceanic Hydrography
WGWIDE	Working Group on Widely Distributed Stocks
WOA5	World Ocean Atlas 05